THE EVOLUTION OF AQUIFERS AND ARSENIC IN ASIA: A STUDY OF THE FLUVIO-DELTAIC PROCESSES LEADING TO AQUIFER FORMATION AND ARSENIC CYCLING AND HETEROGENEITY IN BANGLADESH, VIETNAM, AND NEPAL

By

BETH WEINMAN

Dissertation

Submitted to the Faculty of the

Graduate School of Vanderbilt University

in partial fulfillment of the requirements

for the degree of

DOCTOR OF PHILOSOPHY

in

Environmental Engineering

August, 2010

Nashville, Tennessee

Approved:

Professor Steven L. Goodbred, Jr.

Professor James Clarke

Professor Calvin Miller

Professor Florence Sanchez

Professor Ashok Singhvi

To all the people in need of safe drinking water…

ACKNOWLEDGEMENTS

This work would not have been possible without the financial support provided by the National Science Foundation (NSF) to Dr. Steve Goodbred of Vanderbilt University (EAR-0229600 and EAR-0345777), by the American Geophysical Union's Horton Award, and by the National Institute of Environmental Health Sciences (NIEHS) Superfund Basic Research Program grants made to Dr. Lex van Geen of Columbia University's Lamont-Doherty Earth Observatory. I am especially indebted to Lex van Geen and his "international OSL" and needle sampling team, as well as Dr. Ashok Singhvi and his Quaternary dating laboratory at Physical Research Laboratory in Ahmedabad India, for all of their generosity and patience in teaching a non-physicist like me the ins-and-outs of optical dating. Many thanks also go to Dr. Kaye Savage for all of her guidance while at Vanderbilt University, and to Dr. Yan Zheng of CUNY Queens College for her unwavering interest and support through the years—together, your teachings have carried me far beyond what I initially imagined.

For my research accomplishments at Vanderbilt, thanks to Steve Goodbred for taking me on as a student, Warner Cribb of Middle Tennessee State University and his student Jennifer Pickering for their interest and help with the XRF; Troi Rasbury of Stony Brook University for her time and generosity using her CL; David Hirschberg of SOMAS Stony Brook for his help with the C:N; Brendan Bream, Poojitha Matta, and Vanderbilt's Science Outreach for their help with the zircon dating; fellow student Aaron Covey for taking charge of the column experiments and his ever-present source of know-how (you can't say anything's impossible when Aaron's around); Karrie Radloff from Columbia University for being the best Oreo-provider in Vietnam, Cambodia, *and* Nepal; fellow student and roommate-extraordinaire Maria Takahashi for enabling me to give an award-winning talk at 2008 AGU; Eli Eiche from the University of Karlsruhe for sharing the Vietnam story; Michael Berg and the Swiss Federal Group of Aquatic Science and Technology EAWAG for giving me the opportunity to work in Vietnam; Laurent

Charlet, Stephane Gulliot, and their team from Grenoble University for the opportunity to work in Nepal, and all of the supporters who've gotten me where I needed to go: the American Geophysical Union's 2008-2009 Horton Award, AGU's Water in the Developing World Student Travel Grant, Lex van Geen, Kaye Savage, and Vanderbilt's Graduate School travel and graduate enhancement grants. Without their help this *work* and its *contribution* would not have been done: India (3x), San Francisco (3x), Chicago (2x), Cambodia, Bangladesh, Vietnam, Nepal, China, Switzerland, San Jose, Yucca Mountain, New Mexico, Las Vegas, Houston, Minneapolis, and to the Furbish-student sites in N. Carolina, Georgia, and Kentucky.

I would especially like to thank Dr. Jim Clarke and Dr. Florence Sanchez for giving a non-engineer like me some engineering skills as well as belated insight into the reactor modeling concepts of Stony Brook University's Dr. Bob Aller. Thank you also to our geology department's Teri Sparkman and Jewell Beasley for taking care of innumerable travel-expense forms, and for making sure that as a student, I was always well taken care of.

Most importantly, thanks to my great friends and family; I wouldn't be here if it wasn't for you: Mom and Dad; Mike, David, and Gail; Aunt Robbie and Uncle Stanley; Steven, Tamryn, Kenzy, and Stacey; Judit and Papszi; Happy; my 'Troublesome Trio' comrades Maria and Ches; SUNY's best: Kristal, Juliet, Bessie, Katie, Jennie, Jenni, Alex, and Penny; Needle-Sampler Extraordinaires, Zahid Aziz and Karrie Radloff; my Bellmore buddies Jen, Michelle, Ann, and Stephanie; the people who made Vanderbilt fun: Elise, Craig, Aaron, John, Lily, Roberta, Susan, Steven L., Yan Luo and Alyson; the graduate students who originally inspired me: CUNY's Yi He and Ratan Dhar; and the wonderful people at PRL who gave me lots and lots of Soan Papdi: Madhav, Yogesh, Anil, Gouri, Shilpy, Naveen, and Rabiul—really, thank you. I also need to thank a very patient Kyungsoo Yoo and Simon Mudd—without you guys, Asia's aquifers would be static and boring. I also would like to send my heartfelt thanks to Mavis, Sweetie, Harry, Kilowatt, Albino, Stinky, with some very special thanks to Bea Panigua and Jan Werner—without

their amazing coffee-making skills, this thesis would have killed me. Lastly, I wish to thank my husband Csaba Toth, for all of his love and support; you provide me with unending amounts of Smarties® and inspiration.

TABLE OF CONTENTS

Page

Appendix

LIST OF TABLES

Table Page

LIST OF FIGURES

Figure Page

LIST OF ABBREVIATIONS

α – alpha radiation

AMS – Atomic Mass Spectrometry

β – beta radiation

BGS - British Geological Survey

C – Incident Cosmic Dose (Gy)

^{14}C – Carbon-14

CL - Cathodoluminescence

C/N – Carbon Nitrogen Ratio

CRN – Cosmogenic Radionuclides

D_{β} – Beta Dose (Gy)

D_c – Corrected Cosmic Dose (Gy)

D_e – Dose Equivalent, also called 'Paleodose' (Gy)

D_{γ} – Gamma Dose (Gy)

D_0 – Dose Rate (Gy/kyr)

DPG – Detailed Planning Group

DPHE – Bangladesh's Department of Public Health Engineering

dR or ΔR – First Derivative Transform of Reflectance Spectra between 520 and 530nm

EAWAG - Swiss Federal Institute of Aquatic Science and Technology

Eh – reducing potential (mV)

EM – Electromagnetic Inductance

ENPHO – Environment and Public Health Organization (Nepal)

eV – Electron Volt $\approx \frac{1240}{\text{wavelength (nm)}}$

FeII/Fe-total – ratio of $Fe^{2+}/(Fe^{2+}+Fe^{3+})$

Gy – Gray, a unit of absorbed radiation dose

Gyr – 10^9 years

h – Altitude (km)

$^3H/^3He$ – Tritium Helium Groundwater Age

HR ICP-MS – High Resolution Inductively Coupled Mass Spectrometry

IBRD – the World Bank's International Bank for Reconstruction and Development

IODP – Integrated Ocean Drilling Program

IRSL – Infrared Stimulated Luminescence

JAM – West Bengal villages of Joypur, Ardivok and Moyna

K_d – Absorption Coefficient

Kyr – 10^3 years

λ – Geomagnetic Latitude

L – Liter

$\frac{L}{T}$ – Sample Luminescence Relative to a Test Dose

LA ICP-MS – Laser Ablation Inductively Coupled Mass Spectrometry

LDEO – Columbia University's Lamont Doherty Earth Observatory

LED – Light Emitting Diode

LGM – Last Glacial Maximum

LGMP – Last Glacial Maximum Paleosol

LOI – Loss on Ignition

m - Meter

mbgl – Meters Below Ground Level

mCi – 10^{-3} Curie

MIT – Massachusetts Institute of Technology

Myr – 10^6 years

N – Natural Dose (Gy)

NASC – National Arsenic Steering Committee (Nepal)

NCF – Natural Correction Factor

NOSAMS - National Ocean Sciences Accelerator Mass Spectrometry

OM – Organic Matter (also referred to as SOM or NOM: sedimentary or natural OM)

OSL – Optically Stimulated Luminescence

P-ext As – Phosphate Extractable Arsenic (mg/kg)

pH – $-\log[H^+]$

ø - Longitude

PRL – Physical Research Laboratory, Ahmedabad India

REE – Rare Earth Elements

ρ_B – Bulk Density (g/cm^3)

Ph – Preheat

s - Seconds

SAR – Single Aliquot Regeneration

SCM – Surface Complexation Model

SGC – Standard Growth Curve

T_D – Test Dose (Gy)

ϑ - Latitude

TL – Thermoluminescence

UK – United Kingdom

UNESCO – United Nations Educational Scientific and Cultural Organization

UNICEF – United Nations Children's Fund

UNDP – United Nations Development Project

UTAG – University of Tennessee's Department of Archaeology and Geochronology

W - Watt

WHO – World Health Organization

XRF – X-ray Fluorescence

ya – Years Ago

CHAPTER I

INTRODUCTION

"By 2015, reduce by half the proportion of people without sustainable access to safe drinking water."
- United Nations Millennium Development Goals

1. Overview

Arsenic is a natural constituent of Earth's waters. It weathers from the crust into the hydrosphere, where, if dissolved at high enough levels, it can pose a natural hazard to our supply of drinking water. Despite its ubiquitous nature (i.e., Saunders et al., 2005, Figure 1), nowhere is this hazard more evident than in the Asian and South East Asian aquifer systems, where it is estimated that millions of people are at risk of ingesting arsenic-laden groundwater (BGS-DPHE 2001; Yu et al., 2003; Zhang et al., 2003; Agusa et al., 2005; World Bank 2005; Berg et al., 2008). While there is still much uncertainty about the consequences of what has been dubbed one of the world's 'worst calamities on record' (Chakraborti et al., 2002), ***known*** effects of drinking water high in arsenic include skin lesions (Lindberg et al., 2008), bladder cancers (Lamm et al., 2003), respiratory illnesses (Parvez et al., 2008), developmental delays (Wasserman et al., 2008) and childhood morbidity (Mazumder et al., 2007). For the Asian region, these effects are particularly punctuated, since nutritional limitations (Kordas et al., 2007; Vahter et al., 2007) and the want for rapid development (GWSP, 2006) make it even more necessary to have good quality water.

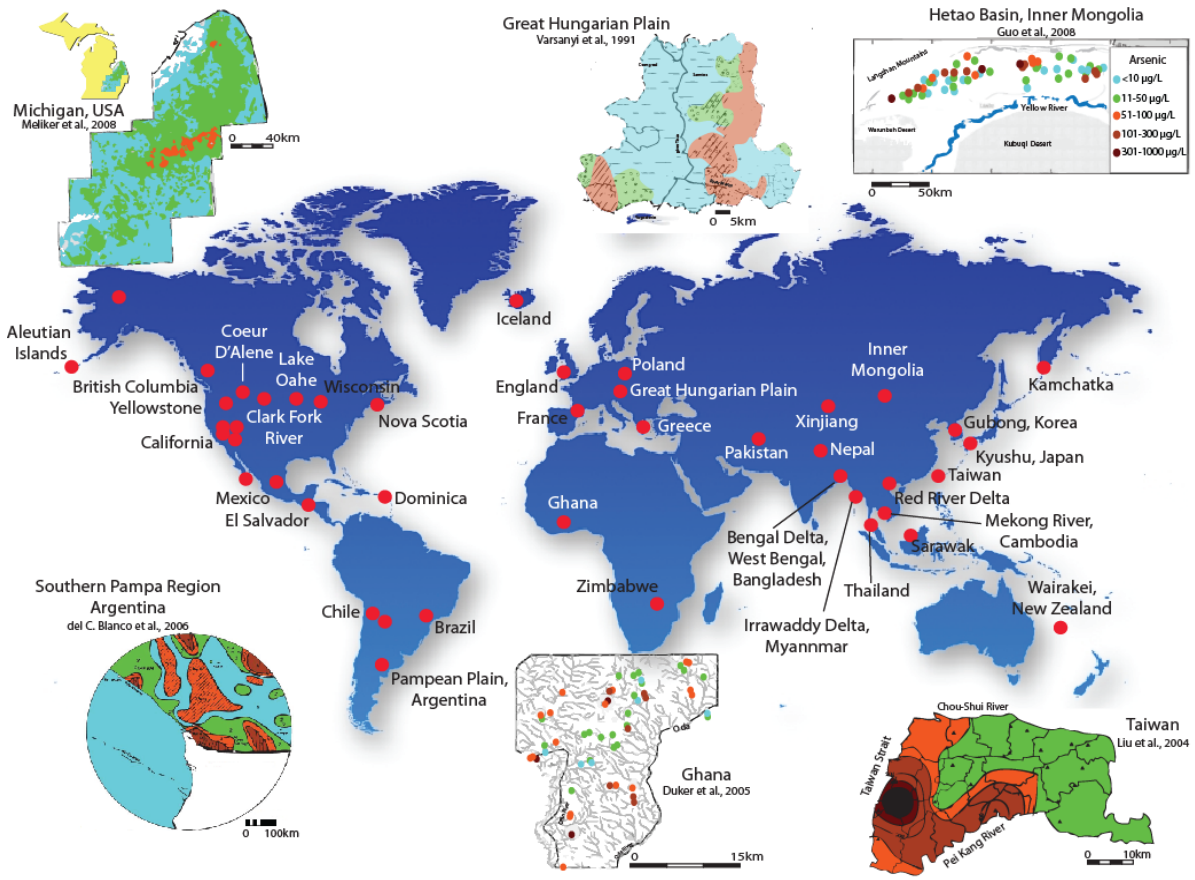

Figure 1. A world map compilation showing some of the more well-documented cases (red dots) of groundwater arsenic contamination. Zoomed in areas of Mongolia, Taiwan, Ghana, Hungary, Argentina, and Michigan are colored to denote how arsenic spatially varies. The color legend for the different concentrations is in the upper right corner, in the map showing Inner Mongolia's groundwater arsenic distribution. The world map clipart is from http://randrcomputersandaudio.com/global_map.jpg overlain with worldwide arsenic sites from the IBRD 33757 April 2005 map.

But sourcing arsenic-free groundwater is not so easy. In fact, it is probably one of the most challenging issues facing the Asian region, today. This stems from the fact that it is common to find wells located only a few meters apart from one another, tapping the same depth, with incredibly different concentrations of dissolved arsenic (BGS-DPHE 2001; van Geen et al., 2003). This type of heterogeneity is shown as a worldwide problem in Figures 1 and 2, and this is what makes mitigation especially challenging. As best stated in one of the World Bank's more recent reports on the state of the arsenic problem (World Bank 2005), not much more can be said about the natural contamination other

than it occurs from '***certain***[1] hydrogeological processes.' While several significant geostatistical studies have been conducted to help make locating safe water more predictable (Yu et al., 2003; Meliker et al., 2008), it is still outside of our understanding ***why*** the heterogeneous patterns of arsenic happen. Why does arsenic accumulate in this region? Why does it occur in predominantly Holocene aquifers (Guillot et al., 2007)? And, why does it display such a high degree of spatial heterogeneity (Figures 1 and 2)? Is there a geologic framework, a depositional patterning that can explain the patterns we see in arsenic?

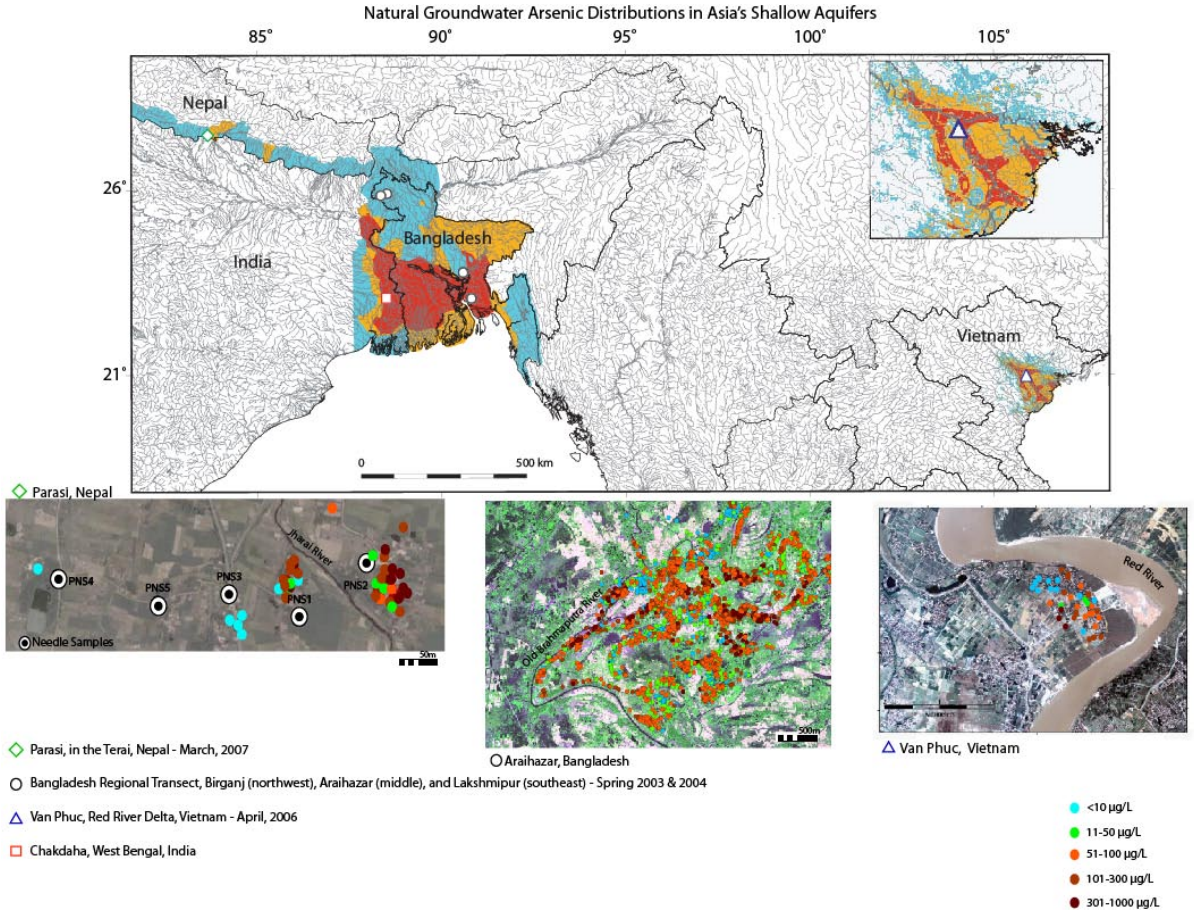

Figure 2, regional distributions of groundwater arsenic for South-Southeast Asia, and village-scale heterogeneity in Nepal, Bangladesh, and Vietnam. To investigate if sedimentary differences, such as age and geochemistry of aquifer material can account for arsenic's spatial patterns, field campaigns with collaborators from Columbia University, the University of Grenoble, and Swiss EAWAG were undertaken in Parasi, Araihazar, and Van Phuc villages.

[1] This is a very uncertain 'certain.'

There are still many questions regarding how groundwaters naturally develop high levels of arsenic. There are also many questions concerning how they will respond to increased pressures from human development. Since it is likely that sedimentary processes play a role in arsenic's complex distribution, it is likely that understanding how these aquifers form can help shed light on why arsenic is so spatially varied. The aquifer sediments—their textures, dimensions, and connectivities—tells us how dynamic the landscape is (Goodbred et al., 2003; Weinman et al., 2008), which then becomes a key factor in controlling the hydrogeology and geochemistry of these systems (Sharp Jr. et al., 2003). Without an evolutionary model for these settings, we have no idea how these aquifers form and what conditions we can expect for future generations. Were the aquifers always contaminated? Will they be contaminated well into the future? How long does it, or could it take, for deposits now contaminated to be flushed of arsenic? These are questions that we still don't have answers for, but which understanding the stratigraphy, geomorphology, and geochronology will help answer.

An emerging concept from previous investigations in Araihazar, Bangladesh is that much of the heterogeneous distribution of arsenic can be explained by differences in geomorphology (Weinman et al., 2008). The hypothesis for this scenario is that East Asian arsenic heterogeneity on scales 10-1000m can be explained by differences in aquifer facies. An alternation of sandy and fine facies deposited in response to natural changes in fluvial competency forms a shallow aquifer with a sedimentary architecture diverse enough to promote extreme heterogeneity of arsenic in the groundwater. Different facies along the surface of the fluvial plain affect the recharge capacity, and hence the flushing of the aquifer directly below, which ultimately controls the concentration of arsenic in the groundwater. In Bangladesh, this mechanism is consistent with observed patterns of arsenic distribution and thus, the overarching objective of this thesis is to understand how arsenic conforms to geomorphologies in other dynamic Asian fluvial settings—an important consideration for the applicability of findings from study sites in different regions: i.e., the London Arsenic Group's "JAM" site in West Bengal, the MIT or LDEO

sites in Bangladesh, EAWAG's site in Vietnam, and the Stanford site in Cambodia. Are similar aquifer evolutionary histories responsible for the groundwater heterogeneities we see in each of these countries? Or, are there different factors influencing arsenic distributions in the different regions? This is a key distinction in developing and maintaining water supplies—and meeting the much-needed Millennium Development Goals—for at least one billion people in the arsenic-prone reaches of our world.

2. Components of the Thesis

The following three chapters of this thesis are investigations focusing on sedimentological findings to better understand how Asia's aquifers develop such heterogeneous distributions of groundwater arsenic. Specifically, these chapters address the (presumably) main *geologic* pathways of evolving aquifers with such variable concentrations of groundwater arsenic: texture and age differences that impart a high degree of physical and chemical complexity over very small spatial scales (10-100m, Figure 3 and 4). My main goal is to record how architecturally diverse these aquifers are over small distances, and how the generation of these differences relate to arsenic. Facies, stratigraphic, and sedimentological differences noted in the aquifer sediments while in the field, coupled with subsequent laboratory analyses of grainsize, organic content (loss-on-ignition), bulk geochemistry (x-ray diffraction and x-ray fluorescence spectroscopy), and the ages of deposition (optically stimulate luminescence, or OSL) lend insight into how the architecture of aquifers evolve over 10s of meter distances—a distance that is highly significant at producing water at the village-scale.

The ***overarching goals*** of this work were to:

1. conduct high-resolution sediment and water sampling transects in Nepal and Vietnam to see if groundwater arsenic heterogeneity can be explained by aquifer sedimentology.

2. This was done by testing whether high arsenic areas are capped or isolated by more impermeable sediment facies (i.e., sediments controlling heterogeneity via physics),
3. and testing if high and low arsenic areas conform with different-aged aquifer units (i.e., sediments controlling heterogeneity via chemistry).
4. The final goal was to try to understand how different aged deposits could produce arsenic heterogeneity by testing if older sands weather slower than younger deposits.
5. Finally, the results from the new field sites were compared with my previous findings in Bangladesh to test whether there is a unifying theory that can explain most cases of arsenic heterogeneity.

In addressing these goals, Chapter 2 focuses on understanding the sedimentology and aquifer history of two new sites in Vietnam and Nepal. The chapter is divided into two parts, with Part 1 linking shallow groundwater arsenic with the evolution of aquifers in Van Phuc, Vietnam, and part two being a similar evolutionary study in Parasi, Nepal. These studies use ~1 km long, 20 m deep, high-resolution needle sampling transects of groundwater and sediment samples between high and low arsenic villages. In doing so, I explore how aquifer depositional histories impact groundwater arsenic.[i] Using optical luminescence dating of aquifer sands, I show that deposits of different ages can account for differences in dissolved arsenic. In both of the Nepal and Vietnam study sites, villages with low dissolved arsenic tap water in Pleistocene aquifers, while higher groundwater arsenic is typical of Holocene sands.

The findings from Chapter 2 are notably different than my previous surface-controlled findings in Araihazar, Bangladesh. In Araihazar, arsenic distributions differ in the upper 20m of aquifer due primarily to permeability differences in the upper 3m of sediments. The higher flushing of aquifers overlain by surficial sands can dilute and buffer groundwaters from accumulating high concentrations of arsenic. Unlike Araihazar, the Parasi and Van Phuc aquifers underlie a laterally continuous 10-20m-thick surface of muddy sediments. This means that surface-controlled differential flushing is unlikely causing arsenic heterogeneity in Parasi and Van Phuc. Instead, the dating of aquifer sands shows that different depositional ages account for the arsenic differences. Higher groundwater arsenic is found in aquifer

sands deposited since the Pleistocene-Holocene transition. While it is still unclear ***exactly*** why the different-aged sands have different vulnerabilities to arsenic, the significance of this chapter underscores the importance of realizing that there is not ***one*** scenario controlling heterogeneity in the different regions. Figure 5 shows a conceptual schematic of how these aquifer scenarios markedly differ:

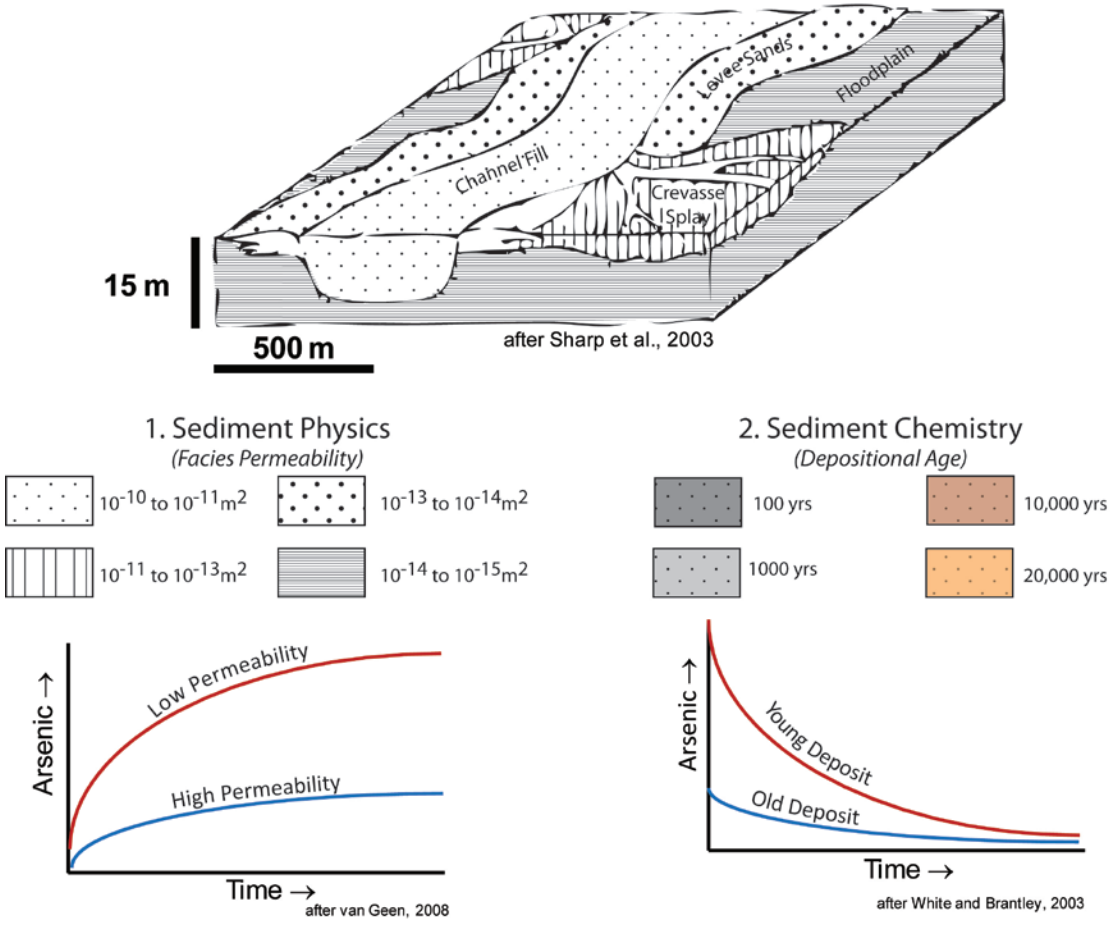

Figure 3 A schematic of how sedimentology can contribute to groundwater arsenic heterogeneity. The top is a cross-section showing how different fluvial deposits comprise the aquifer. Deposits vary over 10-100 m, which can explain groundwater heterogeneity occurring over these distances. Sediments can influence arsenic (1) physically and (2) chemically. Physically, the different facies have different permeabilities, which can help accumulate or dilute arsenic in the groundwater (lower left graph). Chemically, sediments of different ages can weather at different rates, meaning that more recent deposits can release higher amounts of arsenic to the groundwater (lowermost right graph).

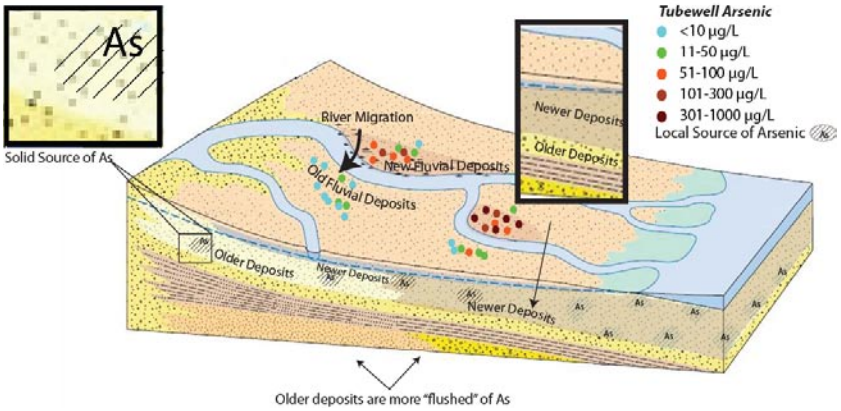

Figure 4 A contextual schematic showing how sedimentology, geochronology, and earth surface processes contribute to arsenic heterogeneity. In particular, this picture shows how the floodplains may produce tube-wells with different concentrations of arsenic, as seen in Figure 2.

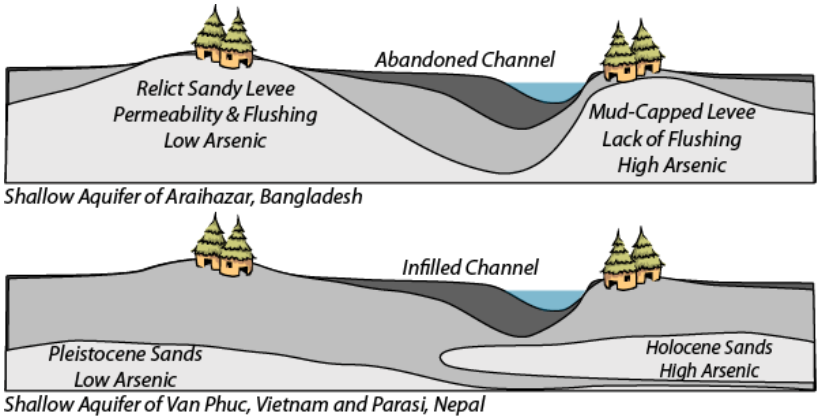

Figure 5. A conceptual schematic of the different aquifer evolution histories for our study sites in Bangladesh, Nepal, and Vietnam. In Araihazar, Bangladesh (top), shallow groundwater arsenic heterogeneity is controlled by the differences in surface sediments' facies and permeabilities.

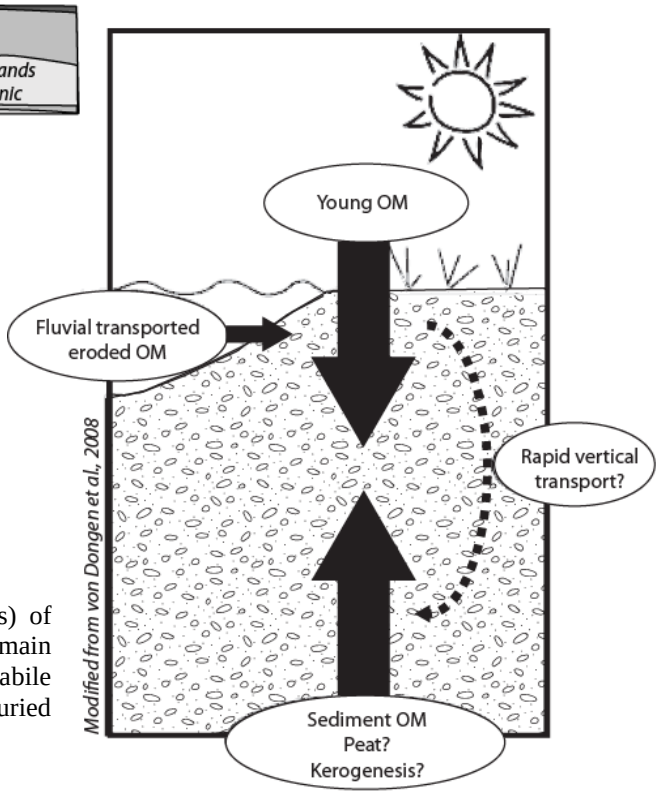

Figure 6, showing the competing ideas for the source(s) of organic matter in Asia's arsenic prone aquifers. Is the main reductant driving reducing conditions come from surface labile pools (sewage, riverine input, vegetation) or from older, buried organics, in the aquifer below?

The third chapter, entitled "Linking shallow groundwater arsenic heterogeneity with sediment age and sedimentary organic matter: leaching results from columns with sediments of different ages," tries to answer why sediment of different ages have different groundwater arsenic concentrations. The impetus for this chapter is based on the hypothesis that aquifer arsenic could be influenced by different weathering rates from sediments of different ages. First order kinetics should make younger Holocene deposits weather and produce arsenic faster than older Pleistocene deposits. Applying methods from previous weathering-rate work by White and Brantley (2003) to OSL dated aquifer samples, differential weathering rates were investigated. Surprisingly, instead of the expected simple correlation to sediment age, the weathering rates were more sensitive to the amount of sedimentary organic matter available in the sediment. While it is not what we expected in terms of sediment age and leaching, the fundamental finding of this chapter is that organic matter ***in*** the aquifer is indeed capable of driving weathering and the release of arsenic. So far, this has not been definitively shown, and there is a lot of debate about what drives aquifer reducing conditions: young or old carbon (Figure 6).

In following up on this question, Chapter 3 also explores the nature of organic matter present in the aquifer sediments. Knowing whether the 'primary' organic matter involved in arsenic's release is a young, labile source infiltrating from the surface (Harvey 2002; Polizzotto 2005; Sengputa 2008), or whether it is from another, more recalcitrant source, 'co-deposited' within the aquifer deposits themselves (McArthur 2004; Meharg 2006; McArthur 2008) is important, because it will help us understand how these aquifers actually become vulnerable to arsenic. Are the reductants responsible for arsenic's release found naturally in the aquifer? Or, is the organic matter something being loaded through human activity (Neumann et al., 2010)? This is an important distinction because we still do not know whether or not these aquifers were always affected.

Finally, a summary of how these three components may be synthesized and applied is presented in Chapter 4. This chapter also describes how I intend to apply the results of this work in my future investigations of sediment age and weathering.

References

Acharyya, S. K., S. Lahiri, B.C. Raymahashay, and A. Bhowmik (2000). "Arsenic toxicity of groundwater in parts of the Bengal basin in India and Bangladesh: the role of Quaternary stratigraphy and Holocene sea-level fluctuation." Environmental Geology **39**(10): 1127-1137.

Aggarwal, P. K., A.R. Basu, and K.M. Kulkarni (2003). "Comment on “Arsenic Mobility and Groundwater Extraction in Bangladesh” (I)." Science **300**: 584b.

Agusa, T., Takashi Kunito, Junko Fujihara, Reiji Kubota, Tu Binh Monh, Pham Thi Kim Trang, Hisato Iwata, Annamalai Subramanian, Pham Hung Viet, and Shinsuke Tanabe (2005). "Contamination by arsenic and other trace elements in tube-well water and its risk assessment to humans in Hanoi, Vietnam." Environmental Pollution.

Ahmed, K. M., Prosun Bhattacharya, M. Aziz Hasan, S. Humayun Akhter, S.M. Mahbub Alam, M.A. Hossain Bhuyian, M. Badrul Imam, Aftab A. Khan, and Ondra Sracek (2004). "Arsenic enrichment in groundwater of the alluvial aquifers in Bangladesh: an overview." Applied Geochemistry **19**: 181-200.

Aitken, M. J. (1985). Thermoluminescence Dating. London, Academic Press.

Aitken, M. J. (1998). An Introduction to Optical Dating. Oxford, Oxford University Press.

Ali, M. A. (2003). "Fate of Arsenic in the Environment, in M.F. Ahmed (Ed.)." Arsenic Contamination: Bangladesh Perspective: ITN, Bangladesh.

Aubert, D., A. Probst, and P. Stille (2004). "Distribution and origin of major and trace elements (particularly REE, U and Th) into labile and residual phases in an acid soil profile (Vosges Mountains, France)." Applied Geochemistry **19**: 899-916.

Aziz, Z., A. van Geen, R. Versteeg, A. Horneman, Y. Zheng, S. Goodbred, M. Steckler, M. Stute, B. Weinman, I. Gavrieli, M. Shamsudduha, M.A. Hoque, and K.M. Ahmed (2008). "Arsenic Concentrations in Shallow Groundwater and the Electromagnetic Conductivity of Soils in Bangladesh." Water Resources Research **in press**.

Berg, M., Caroline Stegel, Pham Thi Kim Trang, Phan Hung Viet, Mickey L. Sampson, Moniphea Leng, Sopheap Samreth, and David Fredericks (2008). "Magnitude of arsenic pollution in the Mekong and Red River Deltas--Cambodia and Vietnam." Science of the Total Environment **in press**.

Berg, M., Hong Con Tran, Thi Chuyen Nguyen, Hung Viet Pham, Roland Schertenleib, and Walt Giger (2001). "Arsenic contamination of groundwater and drinking water in Vietnam: A human health threat." Environmental Science & Technology **35**(13): 2621-2626.

BGS-DPHE, Ed. (2001). Arsenic contamination of groundwater in Bangladesh. British Geological Survey Technical report, WC/00/19, Keyworth.

Bibi, M. H., A. Faruque, and H. Ishiga (2008). "Mobility of arsenic and trace element inventories in sediment cores from Masuda City, southwestern Japan." Environ Geol **54**: 791-803.

Blundy, J. D., B.J. Wood, and A. Davies (1996). "Thermodynamics of rare earth element partitioning between clinopyroxene and melt in the system CaO - MgO - Al_2O_3 - SiO_2." Geochimica et Cosmochimica Acta **60**(2): 359-364.

Caldwell, B. K., John C. Caldwell, S.N. Mitra, and Wayne Smith (2003). "Searching for an optimum solution to the Bangladesh arsenic crisis." Social Science & Medicine **56**: 2089-2096.

Chakraborti, D., Mohammad M. Rahman, Kunal Paul, Uttam K. Chowdhury, Mrinal K. Sengputa, Dilip Lodh, Chitta R. Chanda, Kshitish C. Saha, and Subhash C. Mukherjee (2002). "Arsenic calamity in the Indian subcontinent. What lessons have been learned?" Talanta **58**: 3-22.

Chen-Wuing Liu, C.-S. J., and Chung-Min Liao (2004). "Evaluation of arsenic contamination potential using indicator kriging in the Yun-Lin aquifer (Taiwan)." Science of the Total Environment **321**(1-3): 173-188.

Cheng, Z., A. van Geen, A.A. Seddique., and K.M. Ahmed (2005). "Limited temporal variability of arsenic concentrations in 20 wells monitored for 3 years in Araihazar, Bangladesh" ENVIRONMENTAL SCIENCE & TECHNOLOGY **39**(13): 4759-4766.

Cheng, Z., Y. Zheng, R. Mortlock, and A. van Geen (2004). "Rapid multi-element analysis of groundwater by high-resolution inductively coupled plasma mass spectrometry." Analytical and Bioanalytical Chemistry **379**(3): 512-518.

Clairborne-Lowery, L. (2008). Substitution of Trace Elements into Zircon: Controls and Mechanisms, Vanderbilt University**:** *unpublished report for G. Gualda's Phase Transformations,* 7 pages.

Coleman, J. M. (1969). "Brahmaputra river: Channel processes and sedimentation." Sedimentary Geology **3**(2-3): 129-239.

Curtis, C. (2000). Mineralogy in long-term nuclear waste management. Environmental Mineralogy. D. Vaughan, and R. Wogelius, eds., European Mineralogical Union. **2:** p. 345.

Davis, J. A., S.B. Yabusaki, C.I. Steefel, J.M. Zachara, G.P. Curtis, G.D. Redden, L.J. Criscenti, and B.D. Honeyman (2004). "Assessing conceptual models for subsurface reactive transport of inorganic contaminants." Eos **85**(44): 449, 455.

de Mello, J. W. V., W.R. Roy, J.L. Talbott, and J.W. Stucki (2006). "Mineralogy and Arsenic Mobility in Arsenic-rich Brazilian Soils and Sediments." Journal of Soils & Sediments **6**(1): 9-19.

Deen, T. (2008). DEVELOPMENT: If There's No Rice, Let Them Eat Potatoes. IPS. **http://ipsnews.net/news.asp?idnews=42155**.

Dhar, R. K., Y. Zheng, M. Stute, A. van Geen, Z. Cheng, M. Shanewaz, M. Shamsudduha, M.A. Hoque, M.W. Rahman, and K.M. Ahmed (2008). "Temporal variability of groundwater chemistry in shallow and deep aquifers of Araihazar, Bangladesh." Journal of Contaminant Hydrology **99**(1-4): 97-111.

Dowling, C. B., R.J. Poreda, A.R. Basu, and S.L. Peters (2002). "Geochemical study of arsenic release mechanisms in the Bengal Basin groundwater." Water Resources Research **38**(9): 1173.

Doyle, M. (1994). "Crossing the Mekong: revitalizing Vietnam." Global Trade & Transportation **114**(1): 8.

Duller, G. A. T. (2004). "Luminescence dating of Quaternary sediments: recent advances." Journal of Quaternary Science **19**(2): 183-192.

Eiche, E., T. Neumann, M. Berg, B. Weinman, S. Norra, Z. Berner, A. van Geen, P.T.K. Trang, P.H. Viet, and D. Stüben (2008). "Geochemical processes underlying a sharp contrast in groundwater arsenic concentrations in a village on the Red River delta, Vietnam." Applied Geochemistry **in press**.

Fleet, A. J. (1984). Aqueous and Sedimentary Geochemistry of the Rare Earth Elements. Rare Earth Element Geochemistry. P. Henderson. New York, Elsevier. **2:** 343-373.

Goodbred, S. L., and S.A. Kuehl (2000). "The significance of large sediment supply, active tectonism, and eustasy on margin sequence development: Late Quaternary stratigraphy and evolution of the Ganges-Brahmaputra delta." Sedimentary Geology **133**: 227-248.

Goodbred, S. L., Steven A. Kuehl, Michael S. Steckler, and Maminul H. Sarker (2003). "Controls on facies distribution and stratigraphic preservation in the Ganges-Brahmaputra delta sequence." Sedimentary Geology **155**(3-4): 301-316.

Guillot, S., and L. Charlet (2007). "Bengal arsenic, an archive of Himalaya orogeny and paleohydrology." Journal of Environmental Science and Health Part A **42**: 1785-1794.

Gurung, J. K., H. Ishiga, and M.S. Khadka (2005). "Geological and geochemical examination of arsenic contamination in groundwater in the Holocene Terai Basin, Nepal." Environmental Geology **49**: 98-113.

GWSP (2006). Asian Network Meeting/Workshop. International Conference on Hydrological Sciences for Managing Water Resources in the Asian Developing World, Guangzhou, China.

Harrison, T. M., P.H. Leloup, F.J. Ryerson, P. Tapponnier, R. Lacassin, and C. Wenji (1996). Diachronous initiation of transtension along the Ailao-Shan-Red River shear zone, Yunnan and Vietnam. The Tectonic Evolution of Asia. A. Yin, and M. Harrison. Cambridge, Cambridge University Press**:** 208-226.

Harvey, C. F., C.H. Swartz, A.B.M. Badruzzaman, N. Keon-Blute, W. Yu, M.A. Ali, J. Jay, R. Beckie, V. Niedan, D. Brabander, P.M. Oates, K.N. Ashfaque, S. Islam, H.F. Hemond, M.F. Ahmed (2005). "Groundwater arsenic contamination on the Ganges Delta: biogeochemistry, hydrology, human perturbations, and human suffering on a large scale " Comptes Rendus Geoscience **337**(1-2): 285-296

Harvey, C. F., Christopher H. Swartz, A.B.M. Badruzzaman, Nicole Keon-Blute, Winston Yu, A. Ashraf Ali, Jenny Jay, Roger Beckie, Volker Niedan, Daniel Brabander, Peter M. Oates, Khandaker N. Ashfaque, Shariqul Islam, Harold F. Hemond, and M. Feroze Ahmed (2002). "Arsenic mobility and groundwater extraction in Bangladesh." Science **298**: 1602-1606.

Henderson, P., Ed. (1984). Rare Earth Element Geochemistry. Developments in Geochemistry. New York, Elsevier Science Publishing Company, Inc.

Hodgkinson, J., M.E. Cox, S. McLoughlin, and G.J. Huftile (2008). "Lithological heterogeneity in a back-barrier sand island: Implications for modeling hydrogeological frameworks." Sedimentary Geology **203**: 64-86.

Hoque, B. A., M.M. Hoque, T. Ahmed, S. Islam, A.K. Azad, N. Ali, M. Hossain, and M.S. Hossain (2004). "Demand-based water options for arsenic mitigation: an experience from rural Bangladesh." Public Health **118**(1): 70-77.

Horneman, A., A. van Geen, D. Kent, P.E. Mathe, Y. Zheng, R.K. Dhar, S. O'Connell, M.Hoque, Z. Aziz, M. Shamsudduha, A. Seddique, and K.M. Ahmed (2004). "Decoupling of arsenic and iron release to Bangladesh groundwater under reducing conditions. Part I: Evidence from sediment profiles." Geochim. Cosmochim. Acta. **68**(17): 3459-3473.

Hossain, M. F. (2006). "Arsenic contamination in Bangladesh--An overview." Agriculture, Ecosystems & Environment **113**(1-4): 1-16.

Itai, T., H. Masuda, A.A. Seddique, M. Mitamura, T. Maruoka, X.D. Li, M. Kusakabe, B.K. Dipak, A. Farooqi, T. Yamanaka, S. Nakaya, J. Matsuda, and K.M. Ahmed (2008). "Hydrological and geochemical constraints on the mechanism of formation of arsenic contaminated groundwater in Sonargaon, Bangladesh." Applied Geochemistry **23**(11): 3155-3176.

Jain, M., L. Botter-Jensen, and A.K. Singhvi (2003). "Dose evaluation using multiple-aliquot quartz OSL: test of methods and a new protocol for improved accuracy and precision." Radiation Measurements **37**(1): 67-80.

Jung, H. B. a. Y. Z. (2006). "Enhanced recovery of arsenite sorbed onto synthetic oxides by L-ascorbic acid addition to phosphate solution: calibrating a sequential leaching method for the speciation analysis of arsenic in natural samples." Water Research **40**: 2168-2180.

K.G. Stollenwerk, G. N. B., A.H. Welch, J.C. Yount, J.W. Whitney, A.L. Foster, M.N. Uddin, R.K. Majumder, and N. Ahmed (2007). "Arsenic attenuation by oxidized aquifer sediments in Bangladesh." Science of the Total Environment **379**: 133-150.

Keon, N. E., C.H. Swartz, D.J. Brabander, C. Harvey, and H.F. Hemond (2001). "Validation of an arsenic sequential extraction method for evaluating mobility in sediments." Environmental Science and Technology **35**: 2778-2784.

Ko, C. H., and M. Elimelech (2000). "The “Shadow Effect” in Colloid Transport and Deposition Dynamics in Granular Porous Media: Measurements and Mechanisms." Environ. Sci. Technol. **34**(17): 3681-3689.

Kordas, K., B. Lonnerdal, and R.J. Stoltzfuss (2007). "Interactions between nutrition and environmental exposures: Effects on health outcomes in women and children." Journal of Nutrition **137**(12): 2794-2797.

Kosson, D. S., H.A. van der Sloot, F. Sanchez, and A.C. Garrabrants (2002). "An integrated framework for evaluating leaching in waste management and utilization of secondary materials." Environmental Engineering Science **19**(3): 159-204.

Lamm, S. H., D.M. Byrd, M.B. Kruse, M. Feinleib, and S.H. Lai (2003). "Bladder cancer and arsenic exposure: Differences in the two populations enrolled in a study in southwest Taiwan." Biomedical and Environmental Sciences **16**(4): 355-368.

Lawrence, A. R., D.C. Gooddy, P. Kanatharana, W. Meesilp, and V. Ramnarong (2000). "Groundwater evolution beneath Hat Yai, a rapidly developing city in Thailand." Hydrogeology Journal **8**: 564-575.

Leleyter, L., J.L. Probst, P. Depetris, S. Haida, and J. Mortatti (1999). REE in river sediments: Partitioning into residual and labile fractions. Geochemistry of the Earth's Surface: Proceedings of the 5th

International Symposium on the Geochemistry of the Earth Surface. H. Armannsson. Reykjavik, Taylor and Francis**:** 574 pages.

Lindberg, A. L., M. Rahman, L.A. Persson, and M. Vahter (2008). "The risk of arsenic induced skin lesions in Bangladeshi men and women is affected by arsenic metabolism and the age at first exposure." Toxicology and Applied Pharmacology **230**(1): 9-16.

Liu, C.-W., Cheng-Shin Jang, and Ching-Min Liao (2004). "Evaluation of arsenic contamination potential using indicator kriging in the Yun-Lin aquifer (Taiwan)." Science of the Total Environment **321**: 173-188.

Lopez-Meza, S. (2005). Evaluation of the Impact of Environmental Conditions on Constituent Leaching from Granular Materials During Intermittent Infiltration. Environmental Engineering. Nashville, Vanderbilt. **Ph.D.:** 305 pages.

Maharjan, M., R.R. Shrestha, Sk.A. Ahmad, C. Watanabe, and R. Ohtsuka (2006). "Prevalence of Arsenicosis in *Terai*, Nepal." Journal of Health, Population, and Nutrition **24**(2): 246-252.

Mali, M. A. (2003). "Fate of Arsenic in the Environment, in M.F. Ahmed (Ed.)." Arsenic Contamination: Bangladesh Perspective: ITN, Bangladesh.

Mazumder, D. N. G. (2007). "Effect of drinking arsenic contaminated water in children." Indian Pediatrics **44**(12): 925-927.

McArthur, J. M., D.M. Banerjee, K.A. Hudson-Edwards, R. Mishra, R. Purohit, P. Ravenscroft, A. Cronin, R.J. Howarth, A. Chatterjee, T. Talukder, D. Lowry, S. Houghton, D.K. Chadha (2004). "Natural organic matter in sedimentary basins and its relation to arsenic in anoxic ground water: the example of West Bengal and its worldwide implications." Applied Geochemistry **19**: 1255-1293.

McMahon, P. B. (2001). "Aquifer/aquitard interfaces: mixing zones that enhance biogeochemical reactions." Hydrogeology Journal **9**: 34-43.

Meharg, A. A., C. Scrimgeour, S.A. Hossin, K. Fuller, K. Cruickshank, P.N. Williams, and D.G. Kinniburgh (2006). "Codeposition of organic carbon and arsenic in Bengal Delta Aquifers." Environ. Sci. Technol. **40**: 4928-4935.

Meliker, J. R., G.A. AvRuskin, M.J. Slotnick, P. Goovaerts, D. Schottenfeld, G.M. Jacquez, and J.O. Nriagu (2008). "Validity of spatial models of arsenic concentrations in private well water." Environmental Research **106**: 42-50.

Metral, J., L. Charlet, S. Bureau, S.B. Mallik, S. Chakraborty, K.M. Ahmed, M.W. Rahman, Z. Cheng, and A. van Geen (2008). "Comparison of dissolved and particulate arsenic distributions in shallow aquifers of

Chakdaha, India, and Araihazar, Bangladesh." Geochemical Transactions **9**(1): DOI 10.1186/1467-4866-9-1

Meza, S. L. (2006). Evaluation of the impact of environmental conditions on constituent leaching from granular material during intermittent infiltration. Environmental Engineering. Nashville, Vanderbilt University. **Ph.D.:** 284.

Mukherjee, A., A.E. Fryarb, and W.A Thomas (2008). "Geologic, geomorphic and hydrologic framework and evolution of the Bengal basin, India and Bangladesh " Journal of Asian Earth Sciences **34**(3): 227-244.

Muller, K., B. Daus, P. Morgenstern, and R. Wennrich (2007). "Mobilization of antimony and arsenic in soil and sediment samples--evaluation of different leaching procedures." Water Air Soil Pollution **183**: 427-436.

NASC/ENPHO (2004). The State of Arsenic in Nepal - 2003. B. R. Shrestha, J.W. Whitney, and K.B. Shrestha, (Editors), USGS**:** 100 pages.

Nickson, R. T., J.M. McArthur, P. Ravenscroft, W.G. Burgess and K.M. Ahmed (2000). "Mechanism of arsenic release to groundwater, Bangladesh and West Bengal." Applied Geochemistry **15**: 403-413.

Neumann, R. B., K. N. Ashfaque, et al. (2010). "Anthropogenic influences on groundwater arsenic concentrations in Bangladesh." Nature Geosci 3(1): 46-52.

Opar, A., A. Pfaff, et al. (2007). "Responses of 6500 households to arsenic mitigation in Araihazar, Bangladesh." Health and Place **13**(1): 164-172.

Parvez, F., Y. Chen, P.W. Brandt-Rauf, A. Bernard, X. Dumont, V. Slavkovich, M. Argos, J. D'Armiento, R. Foronjy, M.R. Hasan, H.E.M.M. Eunus, J.H. Graziano, and H. Ahsan (2008). "Nonmalignant respiratory effects of chronic arsenic exposure from drinking water among never-smokers in Bangladesh." Environmental Health Perspectives **116**(2): 190-195.

Piovano, E. L., F.E. Larizzatti, D.I.T. Favaro, S.M.B. Oliveira, S.R. Damatto, B.P. Mazzilli, and D. Ariztegui (2004). "Geochemical response of a closed-lake basin to 20th century recurring droughts/wet intervals in the subtropical Pampean Plains of South America." J. Limnol. **63**(1): 21-32.

Polizzotto, M. L., C.F. Harvey, S.R. Sutton, and S. Fendorf (2005). "Processes conducive to the release and transport of arsenic into aquifers of Bangladesh." PNAS **102**(52).

Prasad, S. a. E. A. K. (2005). "Gandak Fan--A macro Quaternary feature of Middle Ganga Plain, Uttar Pradesh and Bihar." Journal Geological Society of India **65**: 597-608.

Prescott, J. R., and J.T. Hutton (1988). "Cosmic ray and gamma ray dosimetry for TL and ESR." Nuclear Tracks and Radiation Measurements **14**: 223-227.

Prescott, J. R., and J.T. Hutton (1994). "Cosmic ray contributions to dose rates for luminescence and ESR dating: large depths and long-term variations." Radiation Measurements **23**(2/3): 497-500.

Randall, G. L. a. J. M. S. (1992). "On the relationship between river-basin geomorphology, aquifer hydraulics, and ground-water flow direction in alluvial aquifers." Geological Society of America Bulletin **104**(12): 1608-1620.

Ritter, D. F., R.C. Kochel, and J.R. Miller (2002). Process Geomorphology. Boston, McGraw Hill.

Rodnight, H., G.A.T. Duller, S. Tooth and A.G. Wintle (2005). "Optical dating of a scroll-bar sequence on the Klip River, South Africa, to derive the lateral migration rate of a meander bend." The Holocene **15**(6): 802-811.

Rowland, J. C., K. Lepper, W.E. Dietrich, C.J. Wilson, and R. Sheldon (2005). "Tie Channel sedimentation rates, oxbow formation age, and channel migration rate from optically stimulated luminescence (OSL) analysis of floodplain deposits." Earth Surface Processes and Landforms **30**: 1161-1179.

Rykken, R. (2001). "How Long Until Tomorrow." Global Business **17**(1): 59-60.

Samanta, G., and D.A. Clifford (2005). "Preservations of inorganic arsenic species in groundwater." Environ. Sci. Technol. **39**(22): 8877-8882.

Sampson, M. L., B. Bostick, et al. (2008). "Arsenicosis in Cambodia: Case studies and policy response." Applied Geochemistry **23**: 2977-2986.

Saunders, J. A., M.K. Lee, A. Uddin, S. Mohammad, Richard T. Wilkin, Mostafa Fayek, and Nic E. Korte (2005). "Natural arsenic contamination of Holocene alluvial aquifers by linked tectonic, weathering, and microbial processes." Geochemistry Geophysics Geosystems **6**(4): 1-7.

Sengputa, S., J.M. Mcarthur, A. Sarkar, M.J. Leng, P. Ravenscroft, R.J. Howarth, and D.M. Banerjee (2008). "Do ponds cause arsenic-pollution of groundwater in the Bengal Basin? An answer from West Bengal." Environ. Sci. Technol. **42**: 5156-5164.

Sengputa, S., P.K. Mukherjee, T. Pal, and S. Shome (2004). "Nature and origin of arsenic carriers in shallow aquifer sediments of Bengal Delta, India." Environmental Geology **45**: 1071-1081.

Shannon, W. M. a. S. A. W. (2005). "The analysis of picogram quantities of rare earth elements in natural waters." In Rare Earth Elements in Groundwater Flow Systems, K.H. Johannesson, ed: 1-37.

Sharp Jr., J. M., Mingjuan Shi, and William E. Galloway (2003). "Heterogeneity of fluvial systems--control on density-driven flow and transport." Environmental Engineering and Geoscience **IX**(1): 5-17.

Sholkovitz, E. R., E.A. Boyle, and N.B. Price (1978). "The removal of dissolved humic acids and iron during estuarine mixing." Earth and Planetary Science Letters **40**(1): 130-136.

Smedley, P. L., M. Zhang, G. Zhang, and Z. Luo (2003). "Mobilization of arsenic and other trace metals in fluviolacustrine aquifers of the Huhhot Basin, Inner Mongolia." Applied Geochemistry **18**: 1453-1477.

Sneddon, I. R., H. Garelick, and E. Valsami-Jones (2005). "An investigation into arsenic(V) removal from aqueous solutions by hydroxylapatite and bone-char." Mineralogical Magazine **69**(5): 769-780.

Stewart, B. W., R.C. Capo, and O.A. Chadwick (2001). "Effects of rainfall on weathering rate, base cation provenance, and Sr isotope composition of Hawaiian soils." Geochim. Cosmochim. Acta **65**(7): 1087-1099.

Stokstad, E. (2002). "Agricultural Pumping Linked to Arsenic." Science **298**: 1535-1536.

Stute, M., Y. Zheng, P. Schlosser, A. Horneman, R.K. Dhar, M. A. Hoque, A. A. Seddique, M. Shamsudduha, K. M. Ahmed, and A. van Geen (2007). "Hydrological control of As concentrations in Bangladesh groundwater." Water Resources Research **43**: W09417.

Sullivan, K. A. a. R. C. A. (1996). "Diagenetic cycling of arsenic in Amazon shelf sediments." Geochim. Cosmochim. Acta **60**: 1465-1477.

Tanabe, S., K. Hori, Y. Saito, S. Haruyama, L.Q. Doanh, Y. Sato, and S. Hiraide (2003). "Sedimentary facies and radiocarbon dates of the Nam Dinh-1 core from the Song Hong (Red River) delta, Vietnam." Journal of Asian Earth Sciences **21**: 503-513.

Taylor, A., and J.D. Blum (1995). "Relation between soil age and silicate weathering rates determined from the chemical evolution of a glacial chronosequence." Geology **23**(11): 979-982.

USDA (2005). Grain: World Markets and Trade. C. a. M. P. The Grain and Feed Division, Foreign Agricultural Service, Circular Series FG10-05.

Vahter, M. E. (2007). "Interactions between arsenic-induced toxicity and nutrition in early life." Journal of Nutrition **115**(12): 2798-2804.

van Geen, A., K. Radloff, Z. Aziz, Z. Cheng, M.R. Huq, K.M. Ahmed, B. Weinman, S. Goodbred, M. Berg, P.T.K. Trang, L Charlet, J. Metral, D. Tisserand, S. Guillot, S. Chakraborty, A.P. Gajurel, and B.N. Upreti (2008). "Comparison of arsenic concentrations in simultaneously-collected groundwater and aquifer particles from Bangladesh, India, Vietnam, and Nepal." Applied Geochemistry **in press**.

van Geen, A., K.M. Ahmed, A.A. Seddique, and M. Shamsudduha (2003). "Community wells to mitigate the arsenic crisis in Bangladesh." Bulletin of the World Health Organization **81**(9): 632-638.

van Geen, A., T. Protus, Z. Cheng, A. Horneman, A.A. Seddique, M.A. Hoque, and .M. Ahmed (2004). "Testing groundwater for arsenic in Bangladesh before installing a well." Environmental Science & Technology **38**(24): 6783-6789.

van Geen, A., Y. Zheng, M. Stute, and K.M. Ahmed (2003). "Comment on "Arsenic Mobility and Groundwater Extraction in Bangladesh" (II)." Science **300**: 584c.

van Geen, A., Y. Zheng, R. Versteeg, M. Stute, A. Horneman, R. Dhar, M. Steckler, A. Gelman, C. Small, H. Ahsan, J. H. Graziano, I. Hussain, and K. M. Ahmed (2003). "Spatial variability of arsenic in 6000 tube wells in a 25 km^2 area of Bangladesh." Water Resources Research **39**(5): 1140.

van Geen, A., Y. Zheng, S. Goodbred, A. Horneman, Z. Aziz, Z. Cheng, M. Stute, B. Mailloux, B. Weinman, S.H. Chowdhury, and K. M. Ahmed (2008). "Flushing history as a hydrogeological control on the regional distribution of arsenic in shallow groundwater of the Bengal Basin." Environ. Sci. Technol. **42**(7): 2283-2288.

Van Wagoner, J. C., R. M. Mitchum, K.M. Campion, and V.D. Rahmanian (1990). Siliclastic sequence stratigraphy in well logs, cores, and outcrops; concepts for high-resolution correlation of time and facies. American Association of Petroleum Geologists Methods in Exploration Series, no. 7**:** 55 p.

Vaniman, D. T. a. S. J. C. (1996). "Paleotransport of lanthanides and strontium recorded in calcite compositions from tuffs at Yucca Mountain, Nevada, USA." Geochim. Cosmochim. Acta **60**(22): 4417-4433.

Wasserman, G. A., X.H. Liu, P. Factor-Litvak, J.M. Gardner, J.H. Graziano (2008). "Developmental impacts of heavy metals and undernutrition." Basic & Clinical Pharmacology & Toxicology **102**(2): 212-217.

WB (2005). Towards a More Effective Operational Response: Arsenic Contamination of Groundwater in South and East Asian Countries. Volume 1: Policy Report, World Bank.

Weinman, B., S.L. Goodbred, Y. Zheng, A. van Geen, Z. Aziz, A. Singhvi, and M. Steckler (2008). "Controls of Floodplain Evolution on Shallow Aquifer Development and the Resulting Distribution of Groundwater Arsenic: Araihazar, Bangladesh." GSA Bulletin **120**(11/12): 1567-1580.

Weinman, B., Y. Zheng, S.L. Goodbred, A. Horneman, Z. Cheng, Z. Aziz, M. Stute, and A. van Geen (in prep). "Young Sediments and Aquifer Arsenic in Araihazar, Bangladesh: the affect of sedimentary facies on recharge and arsenic evolution in the shallow aquifer of the Old Brahmaputra floodplain." Applied Geochemistry.

White, A. F., and S.L. Brantley (2003). "The effect of time on the weathering of silicate minerals: why do weathering rates differ in the laboratory and the field?" Chemical Geology **202**: 479-506.

WHO (1997). Arsenic and drinking water and resulting arsenic toxicity in India and Bangladesh: report of a regional consultation, New Delhi, India, 29 April - 1 May 1997 New Delhi WHO Regional Office for South-East Asia **SEA-EH-507** 1-24.

Williams, P. N., A .H . Price, A. Raab, S.A . Hossain, J. Feldmann, and A.A. Meharg (2005). "Variation in Arsenic Speciation and Concentration in Paddy Rice Related to Dietary Exposure." Environ. Sci. Technol. **39**: 5531-5540.

Wintle, A. G. a. A. S. M. (2006). "A review of quartz optically stimulated luminescence characteristics and their relevance in single-aliquot regeneration dating protocols." Radiation Measurements **41**: 361-391.

Yu, W. H., Charles M. Harvey, and Charles F. Harvey (2003). "Arsenic in groundwater in Bangladesh: A geostatistical and epidemiological framework for evaluating health effects and potential remedies." Water Resources Research **39**(6): 1146.

Zeng, H., M. Arashiro and D.E. Giammar (2008). "Effects of water chemistry and flow rate on arsenate removal by adsorption to an iron oxide-based sorbent." Water Research **48**(18): 4629-4636.

Zhang J.J., P. P., and L.P. Wu (2003). "Arsenic risk assessment in Ronphibun District, Thailand (abstract)." Toxicology **191**(1): 62.

Zheng, Y., A. van Geen, M. Stute, R. Dhar, Z. Mo, Z. Cheng, A. Horneman, I. Gavrieli, H.J. Simpson, R. Versteeg, M. Steckler, A. Grazioli-Venier, S. Goodbred, M. Shahnewaz, M. Shamsudduha, M. Hoque and K. M. Ahmed (2005). "Geochemical and hydrogeological contrasts between shallow and deeper aquifers in two villages of Araihazar, Bangladesh: Implications for deeper aquifers as drinking water sources." Geochim. Cosmochim. Acta. **69**(22): 5203-5218.

Zheng, Y., M. Stute, A. van Geen, I. Gavrieli, R. Dhar, J.H. Simpson, P. Schlosser, and K.M. Ahmed (2004). "Redox control of arsenic mobilization in Bangladesh groundwater." Applied Geochemistry **19**(2): 201-214.

CHAPTER I

PART I: THE CO-EVOLUTION OF ARSENIC AND AQUIFERS: LINKING SHALLOW GROUNDWATER ARSENIC HETEROGENEITY WITH THE EVOLUTION OF AQUIFERS IN VAN PHUC, VIETNAM

Abstract

Shallow aquifer groundwater arsenic heterogeneity is well documented in many of the fluvial regions of Asia. To this day, the cause for the heterogeneity remains poorly understood in part because of the heterogeneity of sediment properties inherent to a young floodplain depositional environment. In April 2006, a simple device, the needle-sampler, was used to obtain depth profiles of precisely-matched samples of both sediment and groundwater to map this heterogeneity in Van Phuc village, located within a bend of the Red River 12.5 km south of Hanoi. The transect of profiles extends to ~30 m depth and over a distance of 1.5 km from one portion of the village characterized by low-As concentrations in groundwater to another area where most existing tube-wells are elevated in As. Sediment color and measurements of the Fe(II)/Fe ratio in the acid-leachable fraction of the sediment indicate consistently less reducing conditions in the low-As aquifers of Van Phuc compared to the high-As aquifers. Optically Stimulated Luminescence (OSL) dating of the two distinct formations also indicate markedly different ages of 17,000 ± 2000 and 700 ± 100 years, respectively. ^{3}H-^{3}He dating of the groundwater indicates the shallow aquifers groundwater is >55 years old in the older, less reducing formation, and only 10-30 years ago in the younger deposit. The observations demonstrate that the history of floodplain formation exerts an important control on the distribution of arsenic in relatively shallow reducing aquifers of Vietnam. A better understanding of the vulnerability of deposits underlying Van Phuc village to changes in redox conditions is likely to have implications for other regions affected by arsenic.

1. Introduction

Following the findings of arsenic in Bangladesh's groundwater, other countries in Southeast Asia have found similar problems. Dr. Chakraborti, perhaps one of the most active people in drawing attention to the extent of this problem, has noted:

> *"…despite years of research…additional…villages are identified by virtually every new survey. We feel that…present research may be only the tip of the iceberg representing the full extent of arsenic contamination." (2003)*

As to how extensive the arsenic problem will grow remains uncertain, but with the continued emplacement of tube-wells to prevent sickness from unclean surface waters, more and more affected regions are being recognized. Since the first emplacement of wells by international donors in the 1970's, an increasing number of people within the developing world are inadvertently being exposed to high-arsenic groundwater with the continued and unregulated installation of tubewells (van Geen 2008; Polya and Charlet 2009; Rahman, Naidu et al. 2009).

As in the millions of hand-wells drilled throughout Bangladesh, Nepal, and India, it is now recognized that a similar, seemingly chaotic patterning of tube-well arsenic exists in Vietnam. While the aquifers and landforms in these different regions are not obviously connected, the river (and hence aquifer) histories in these regions do, in fact, impact one another. Inasmuch, recent reports by the Ocean Drilling Program's Detailed Planning Group indicate that the drainage evolution affecting the Brahmaputra's headwaters has (and can) impacted the drainage and river evolution of Vietnam (IODP DPG, http://www.iodp.org/dpg/, (IODP-DPG 2008)). While today the tectonic evolution of Eastern Tibetan rivers is much better known (Clark, Schoenbohm et al. 2004; Hori, Tanabe et al. 2004), it is unclear how these changes link to the evolution of *arsenic* in the same region.

Arsenic was first reported in Vietnam in 2001 by (Berg 2001) and a team of researchers from the Swiss Federal Institute of Aquatic Science and Technology (EAWAG), a world-leading aquatic institute allowed into the country to determine if its shallow sedimentary aquifers—like Bangladesh and India—

were also vulnerable to arsenic. Since that pioneering study in 2001, which confirmed the presence of arsenic, many wells in northern Vietnam have been tested, with their arsenic distributions displaying patterns of heterogeneity very similar to those in Bangladesh (Figure 1, (BGS-DPHE 2001; van Geen 2003; Agusa 2005; Eiche 2008)). Similar to the large-scale correlation of arsenic with the regional geology (Yu 2003; Ahmed 2004) and major rivers of Bangladesh (BGS-DPHE 2001), arsenic in northern Vietnam is also found to be elevated along the current corridors of today's rivers (Figure 1, top panel). While understanding regional patterns is important for identifying countries and regions where arsenic might be a concern, it does not explain the differences in arsenic between villages and individual wells (Figure 1 middle and bottom panels). Understanding these more local scales of heterogeneity is necessary, since it is at distances of 10s to 100s of meters that household wells and source water are spaced. This close spacing reveals that wells placed a only few meters away from one another and drilled to the same depth can have dramatically different concentrations of arsenic in the groundwater (Berg 2008), a pattern similar to that found in Bangladesh (van Geen et a., 2003).

An example of this local heterogeneity occurs in the Van Phuc village of Vietnam, the focused research site for this study. The village is predominantly agricultural and located ~10 km southeast of Hanoi. It is located on the inside of a large meander bend in today's Red River (Figures 1 and 2), extending ~2km along the river's edge. Following a southward trend of arsenic enrichment, Van Phuc's groundwater ranges from <1μg/L in the northern part of the bend to ≥300 μg/L in wells drilled in the bend's southern portion (Figure 1, bottom). Prior to fieldwork, it was thought that one of two end-member scenarios were likely responsible for Van Phuc's arsenic heterogeneity: one where a complex stratigraphy within the river bend was controlling the arsenic (i.e., there is more than one aquifer) and another where arsenic was being controlled by flushing horizontally. From our previous work in Araihazar, Bangladesh we know that shallow groundwater arsenic can vary over 10-100m distances due to different thicknesses of the floodplain's mud cap. The different thicknesses allow for differential

Regional, 10-100 km Heterogeneity

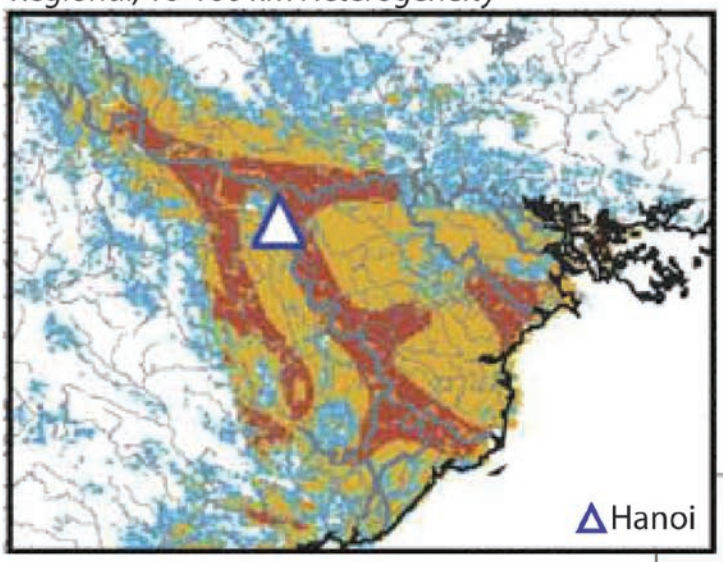

Figure 1. A progression of maps, zooming in to show the different length scales of arsenic heterogeneity in northern Vietnam. The first map, (*left*), is from van Geen et al. (2008), depicting the spatial patterns of grounwater arsenic for the entire Red River Delta, Vietnam.

(*Right, mid-panel, Berg 2001*) Zooming in to Hanoi's triangle from the regional arsenic map above, Hanoi's orange colored portion actually exhibits a lot more spatial complexity in arsenic on a 1-10km scale. This means that not every locality in the Hanoi region has 100-300µg/L arsenic in their groundwater. The patchiness shows that not all aquifers are necessarily unsuitable for drinking water.

1-10 km Heterogeneity

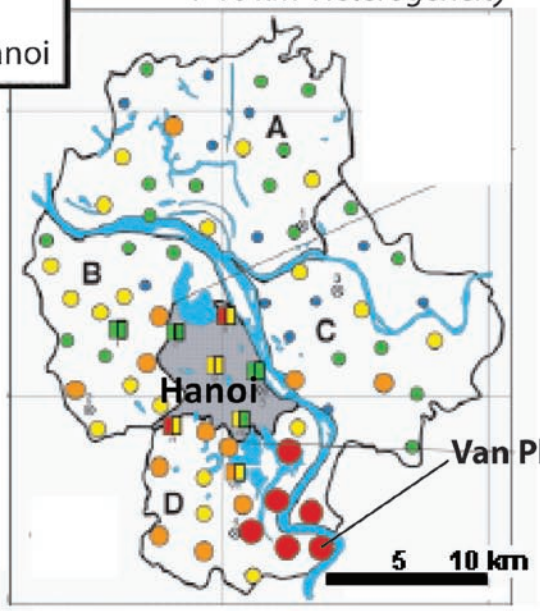

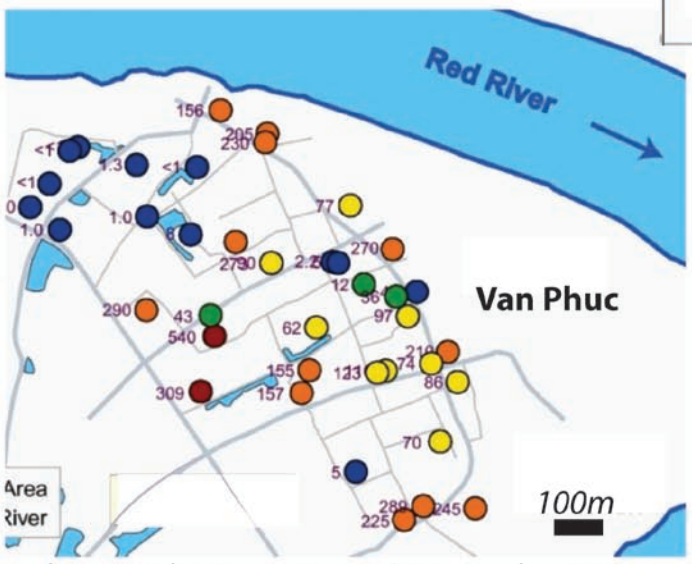

<1 km Local Heterogeneity (Berg et al., 2008)

(*Left*) Close up map of Van Phuc's river bend, ~10km south of Hanoi. In the 1-10km map, Van Phuc shows as tube-wells averaging >300µg/L. Zooming in to the river bend, however, shows (again) that not all of the groundwater is naturally contaminated. The northern part of Van Phuc's village has wells below the 10µg/L arsenic standard.

Arsenic µg/L
- <10
- 10-50
- 50-100
- 100-300
- >300

Figure 2. Google maps of the Van Phuc study site, ~10km southeast of Hanoi. This predominantly agricultural village exists on a modern point bar of today's Red River. While the river is a natural meander, human influence include dike and revetment building, as well as some sand mining. River water stage is also modified by damming upriver.

flushing of the aquifer below, which explains the different concentrations of arsenic in the groundwater (Stute 2007; Weinman 2008).

In Van Phuc, it was hypothesized that the same hydrological and stratigraphic controls could account for its differences in arsenic (Figure 3). In terms of hydrology, river height differences up- and downstream of the bend can setup a preferential flow path that evolves higher arsenic down flow, in the southern part of the bend (Figure 3, upper panel). Stratigraphically, downstream migration of the meander bend could also deposit younger fine-grained sediments towards the south that would prevent vertical flushing and allow for the accumulation of arsenic in groundwater within the southern part of the bend (Figure 3, lower panel). If the stratigraphy of this riverbend was found to be laterally homogenous, then the heterogeneity in arsenic documented at Van Phuc could serve as an ideal end-member model for how arsenic accumulated along a groundwater flow path. Alternatively, if we find that stratigraphic heterogeneity—such as differences in type and stacking of sedimentary facies—within the riverbend coincides with differences in arsenic, then results from Van Phuc could provide further evidence for a strong sedimentological control on groundwater chemistry (Papacostas, Bostick et al. 2008; Weinman 2008). This is a critical distinction because it reveals whether heterogeneity in the subsurface geology of this and other fluvial deltaic settings is a first order control on aquifer hydrology and chemistry, or whether these systems can be treated as a simple and uniform geomorphic unit, as is often done in hydrological modeling (Cardenas 2008).

1.1. Study Area

According to reports by the WHO/UNICEF Joint Monitoring Programme, groundwater arsenic in Vietnam is an emerging problem. As in the case of Bangladesh, Vietnam's groundwaters also display strong local heterogeneity (Figure 1 and (van Geen 2003)), in pH, Eh, and dissolved Fe and Mn,

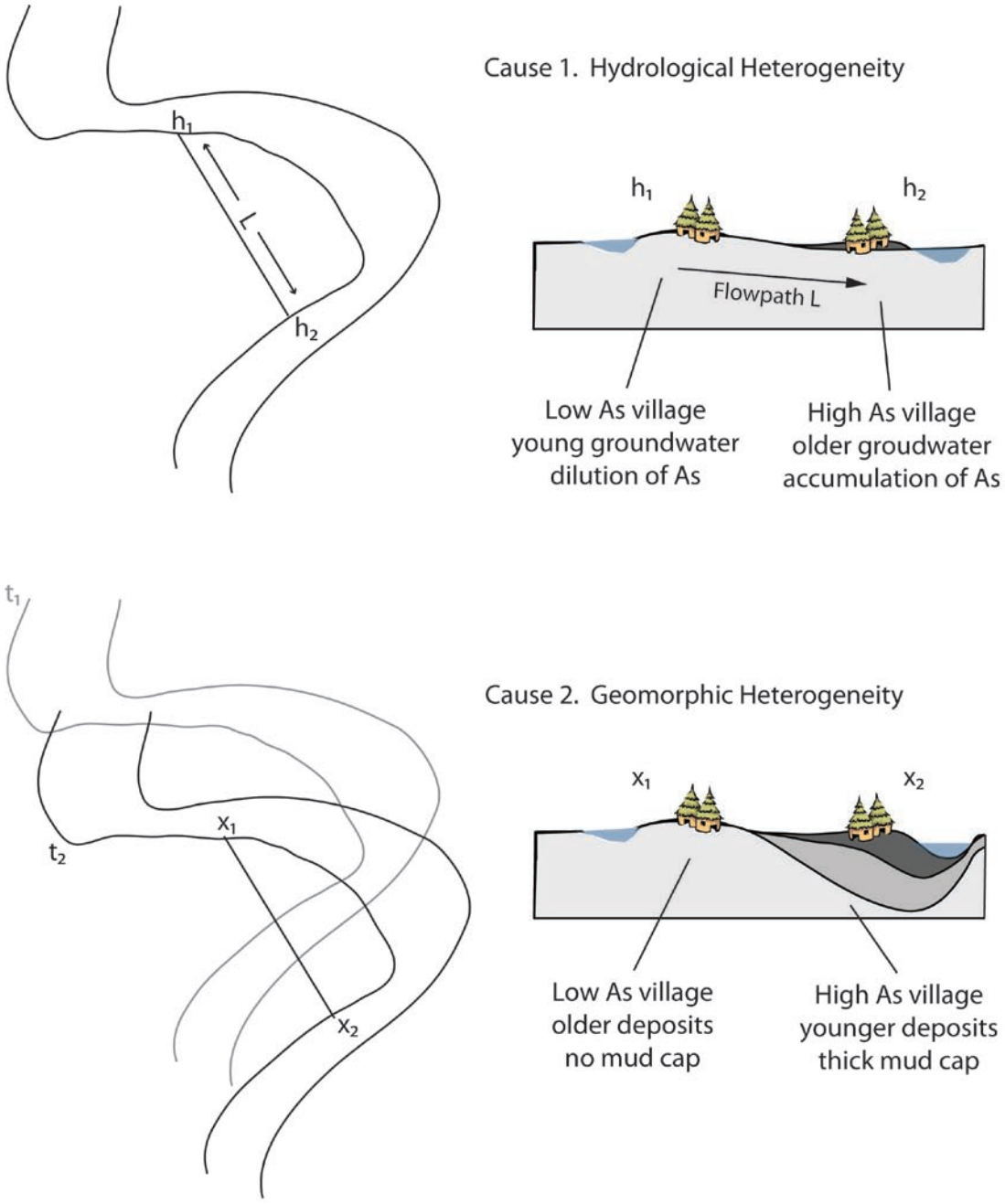

Figure 3. Prior to fieldwork, this schematic shows 2 scenarios we thought responsible for the arsenic heterogeneity in Van Phuc's river bend. The upper figure, "cause 1," shows how hydrological height differences of the river up- and downstream of the bend can setup a preferential flow path through the bend that evolves higher arsenic downflow, in the southern portion. The lower figure, "cause 2," was a hypothesis based on previous work in Araihazar, where we thought that downstream propagation of the river bend resulted in newer mud cappings in the southern portion of the bend, which prevented vertical flushing, allowing for the accumulation of arsenic the southern bend.

particularly in the Red River region—(Hug, Luepin et al. 2008; van Geen 2008). In addition, the vulnerable aquifers in both countries are comprised of deltaic alluvium sourced from the Himalayas. They also share a tremendous burden of arsenic: current estimates in the Red River Delta place over 11 million people at risk of ingesting water with >10 μg/L arsenic—the provisional compliance of the World Health Organization (Hug, Luepin et al. 2008).

The Red River (Song Hong) delta is one of largest deltas in Southeast Asia, draining a ~160,000 km^2 catchment that starts in the mountainous Yunnan Province of China (Allen, Gillespie et al. 1984; Li, Saito et al. 2006; Clift, Long et al. 2008). Its deltaic complex is made of sediments shed from the eastern Tibetan plateau from ongoing uplift, incision, and river reorganization since the Miocene's collision of India with Asia (Clarke et al., 2004). The river is a considered a stable, fault-controlled system, that has become increasingly smaller since ~50Myr due to the northern migration of the east Himalayan syntaxis (Clark, Schoenbohm et al. 2004). Developing along a NW-SE fault system that extends into the Gulf of Tonkin, the river is thought to have been depositing continuous sequences to the delta since the Eocene (Moores et al., 1997). Today, the Red River's catchment is limited to the proximal terrains surrounding the delta: the Yangtze and Indochina cratons. It flows ~1,200km southeastward into the Gulf of Tonkin (also known as the Gulf of Bac Bo), and is thought to have maintained its current course southward of Hanoi since 4kyr—after the delta's retrogadational period ((Tanabe, Saito et al. 2006), Figure 4).

In terms of basin size, the delta is ~500km long and 50–60km wide and filled with Neogene and Quaternary sediments, typically ≥3km thick (Li, Saito et al. 2006). The Quaternary sediments, which unconformably overlie the Neogene deposits, are composed mainly of sands and gravels with minor lenses of silt and clay. These sediments deposited since the last glacial maximum (LGM) comprise three main formations (Mathers and Zalasiewicz 1999; Tanabe, Hori et al. 2003; Li, Saito et al. 2006; Tanabe, Saito et al. 2006):

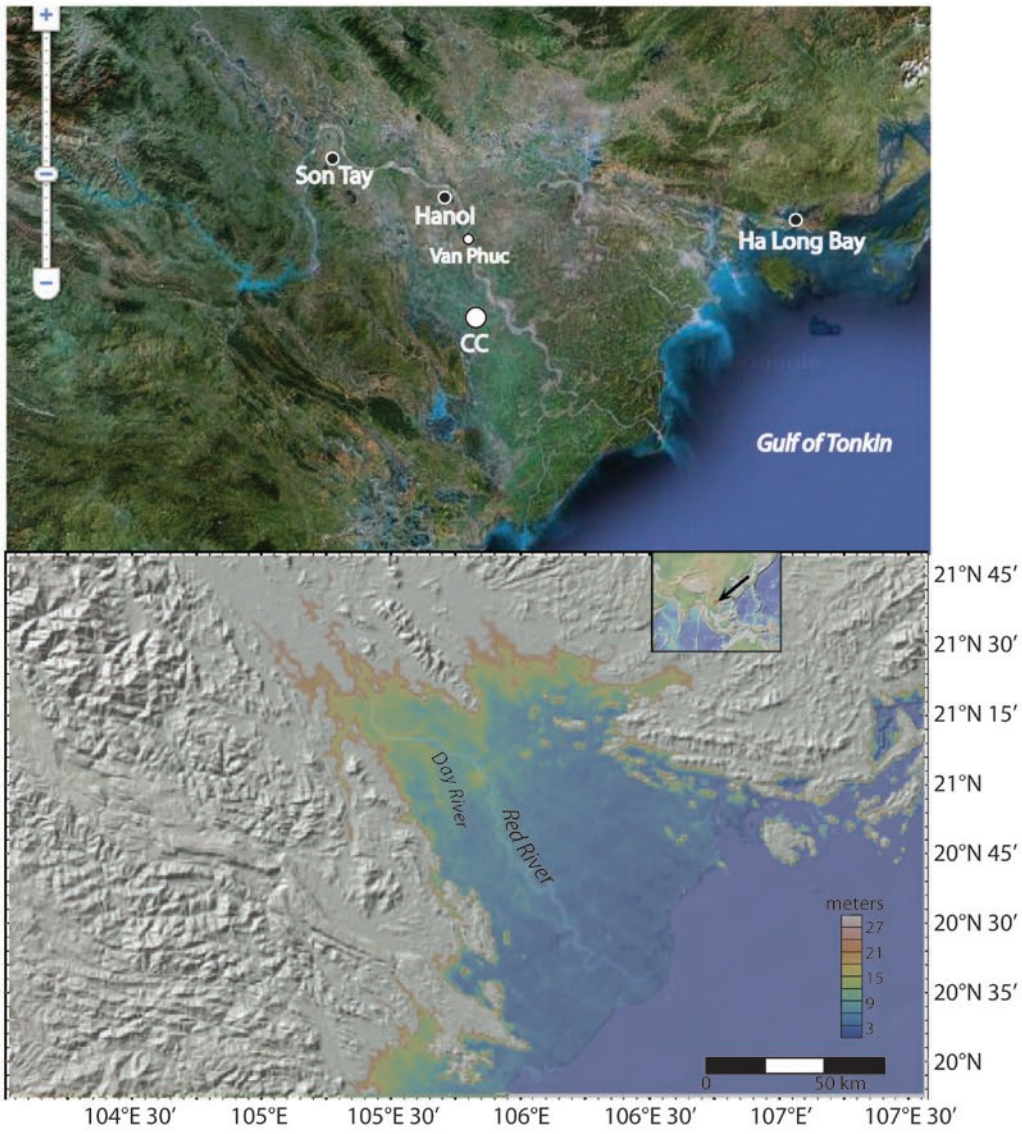

Figure 4. Google Earth (upper) and GeoMap App (lower) views of today's Red River (Song Hong) Delta in northern Vietnam. The delta is a complex of sediments being shed from the eastern Tibetan plateau due to ongoing uplift, incision, and river reorganization since the Miocene's collision of India with Asia (Clarke et al., 2004). Today, the Red River's catchment is limited to proximal terrains, surrounding the delta: the Yangtze and Indochina cratons. Developing along a NW-SE fault system that extends into the Gulf of Tonkin, the deposits to the delta have been continuous since the Eocene, with onshore thicknesses reaching up to 6000 meters (Moores et al., 1997). The location of core CC, a tidal influenced channel- and 2006), is shown in the upper panel.

1) the Vinphuc formation, a ~30m thick fluvial unit of upward-fining clays and gravels, dating from ~20-7kyr,

2) the Haihung formation, a ~30m thick estuarine unit comprised mainly sands deposited between 7 and 4kyr,

3) and the Thai Binh formation, a ~30m thick fluviodeltaic unit of upward-fining gravel, sands, and clays dating 4kyr to present.

Within the delta complex, Van Phuc's riverbend is located along the Red River, ~10km southeast of Hanoi (~N20.920810° E105.896130°, Figures 1 and 2). Previous drillings by EAWAG and BGS indicate the presence of both Holocene and Pleistocene deposits in the area, with both of the aquifer types recharged predominantly by Red River water, due in part from the large withdrawals supplying the city of Hanoi (Berg, Stengel et al. 2007; Berg 2008). Within this area is the Van Phuc village, which is located along a riverbend between the Red River and a dike that protects the southwestern parts of Hanoi from annual flooding (Figure 2). Unprotected by the dike, the village undergoes occasional floods during the rainy season. The village's annually flooded fields are planted with corn, medicinal plants, and cabbage (Eiche 2008). In the absence of the monsoon, the village fields are irrigated during the dry season either by water from ponds or, to a lesser extent, by groundwater from dug wells.

While not used extensively for irrigation, groundwater is, however, the main source of drinking water for the people in the village. During our field work, we learned that, while there was no specific treatment for arsenic, households were passing their groundwater through sand filters to make their water taste better by removing high concentrations of Fe and Mn. An ancillary benefit of this filtering is that it also lowers arsenic concentrations due to enough Fe in Red River delta groundwater—sufficient Fe co-precipitates arsenic, which is not as readily achieved in other arsenic-prone areas with lower Fe concentrations in the groundwater (i.e., Bangladesh and the Mekong River Delta, (Berg, Luzi et al.

2006)). Between the rainy and dry season, the depth of the water table varies widely in the aquifer (64 m) as well as in the Red River (7–10 m). The similar major ion composition of groundwater in Van Phuc and water from the Red River is consistent with a significant component of recharge originating from the river, as recently documented at different locations upstream (Postma, Larsen et al. 2007; Berg 2008).

2. Methods

2.1 Field Sampling

In April 2006, groundwater and sediments samples were collected along a needle sampling transect to resolve subsurface patterns of arsenic and sediment heterogeneity (Figures 5a and b). The needle-sampling device is an evacuated tube that can be lowered into a drill hole and used to obtain high resolution depth transects of both sediment and porewater samples (van Geen 2004). A preliminary account of the aquifer facies were characterized while drilling. Overall, a total of 10 depth profiles were sampled during the 2006 campaign, with 7 of the profiles extending along a ~1km transect across the riverbend (Figure 5a). The needle-sampling transect extends between (and beyond) two alternatively contaminated areas: sites with low and high arsenic (VPNS1 with <1µg/L arsenic, also called "Site L" in Eiche et al., 2008 and VPNS2 with ~300µg/L arsenic, also referred to as "Site H" in Eiche et al., 2008). At VPNS1 and 2, high resolution aquifer stratigraphy was obtained from two 55 m-long sediment cores that were recovered by rotary drilling (Figure 5b). This rotary drilling enables sediments to be recovered in 1.5m intervals, with the benefit of not disturbing the sediments as much as the wash boring drilling used during needle-sampling. In this way, we could get a better understanding of the undisturbed texture and more accurate grainsize measurements of the aquifer facies to use in our reconstruction (i.e., root castings, crossbeds, ripples, and unconformities).

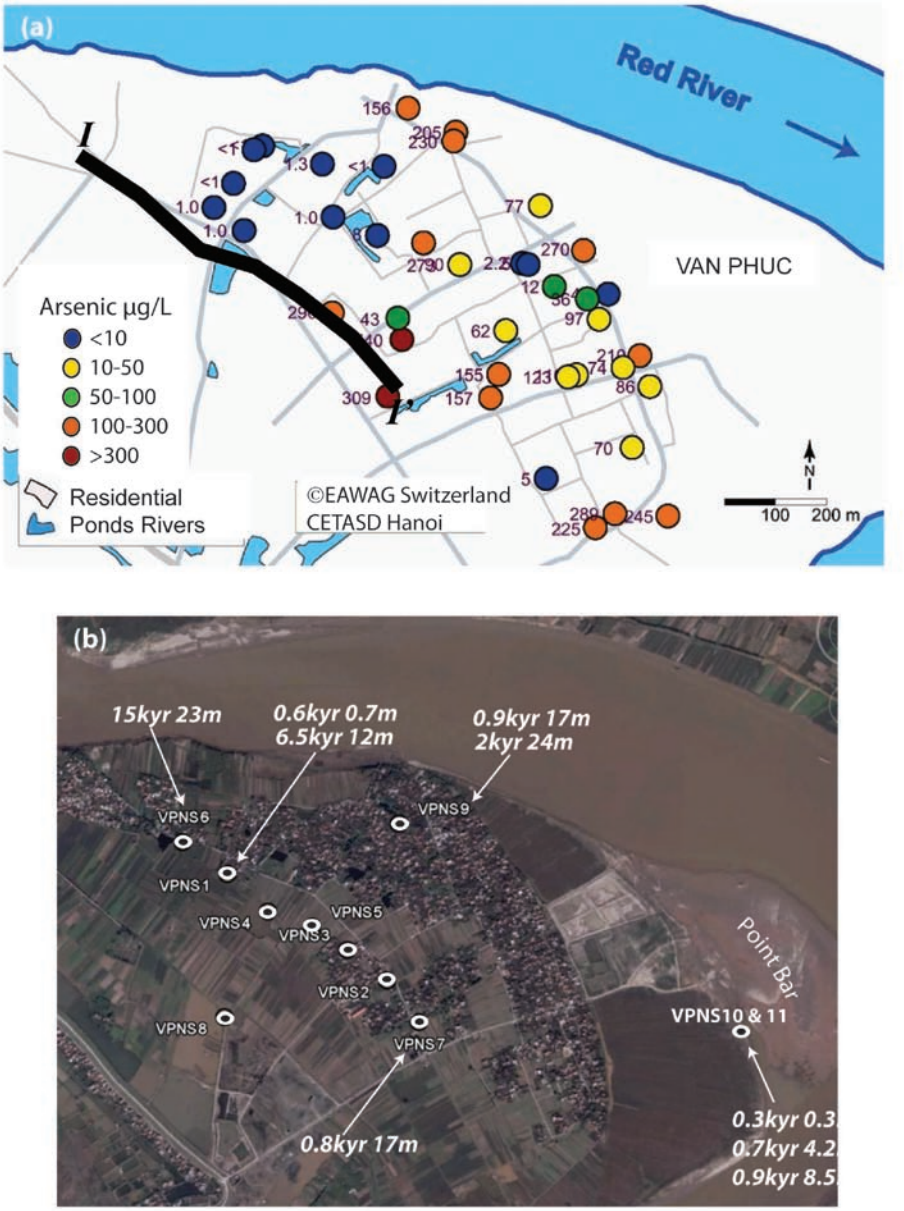

Figure 5a and b. Top panel (a), a close up view of the groundwater arsenic concentrations in the Van Phuc study area. The marked degree of heterogeneity from ~1 to 300 µg/L within hori1qzontal distances of 102 meters prompted the detailed sediment and water sampling conducted in this study. The dark black line follows the course of the high-resolution needle-sampling transect (I-I') conducted during a field campaign in April 2006. Bottom panel (b), locations of needle sample sites in the Van Phuc river bend, along the Red River. From northwest to southeast, a transect line was sampled for groundwater and aquifer sediments to depths generally ~25m deep. From the north-western low arsenic (<1µg/L) to the southeastern high arsenic site(~300µg/L) the needle samples are: VPNS63 VPNS1 (Site L)→ VPNS4 →VPNS5 → VPNS3 → VPNS2 (Site H) →VPNS7. SIte L and Site H areOere two 55m drillings took place (Eiche et al., 2008). Two additional needle samples were retrieved perpendicular to the transectrder to get a better three-dimensional understanding of the aquifer (VPNS8 and VPNS9), as well as to get an OSL sample to test zeroing in deposits along the modern river (VPNS10 & 11). The results of OSL and carbon-14 dating are indicated along the transe40ct and listed with the depth of each sample.

Needle sampling between and beyond the rotary cores was done approximately every 200m to obtain a good resolution of the aquifer's subsurface. Sediments and groundwaters were retrieved at ~3m intervals to as far as wash-drilling allowed--a very coarse and impenetrable gravel layer typically limited our needle sampling to depths of 40m. While sampling, sediment redox properties, including Fe(II)/Fe-total ratios as extracted by 1.2M HCl and diffuse spectral reflectance were obtained within a day of drilling (Horneman 2004). Groundwater for subsequent $^{3}H/^{3}He$ dating at EAWAG's Noble Gas Laboratory in Zurich was collected and measured from monitoring wells installed after bore-hole drilling and needle sampling. The wells ranged from 17 to 55 m deep and consist of PVC casings with a 1-m long sand trap at the bottom. To avoid infiltration of surface water, concrete pads surrounding the upper steel casing were installed and each well was capped with a steel screw cap. Waters from the wells and from needle sampling were filtered onsite and preserved for HR ICP-MS for dissolved arsenic and other elements at Lamont Doherty Earth Observatory (Cheng 2004). Aquifer samples for OSL (optically stimulated luminescence) dating were recovered using an AMS probe inserted into the needle-sampling hole with a steel or black-taped liner. The OSL samples were then wrapped in aluminum foil and protected from light until measurement at the Physical Research Laboratory (PRL) in Ahmedabad, India.

2.2. Aquifer Depositional Ages

Following the fieldwork, grainsize analysis was performed on borehole cores and wash-cuttings by laser diffraction at Vanderbilt University. Aquifer depositional ages were measured in India's PRL OSL dating laboratory on quartz separates of the aquifer and corroborated by ^{14}C done on organic fragments that were collected on pieces recovered from the rotary drilling at VPNS1. A piece of wood retrieved from the core at 10.8 m was sent for ^{14}C measurement using liquid scintillation counting by Dan Weinand at the University of Tennessee's Center for Archaeometry and Geochronology (UTAG ID UTCAG 07-012). A bivalve recovered from the same core at 5.9m, which was not suitable for the liquid

scintillation method, was sent to NOSAMS for AMS ^{14}C determination (NOSAMS ID OS-64758). The wood was calibrated using the typical intcal04.14c correction (http://calib.qub.ac.uk/calib/calib.html), while the shell was calibrated using the Marine/INTCA curve due to its identification as a subtidal marine bivalve (*Cyrenacea* suborder heterodont, Easton 1960).

Depositional ages by optical OSL were made using the standard SAR (single aliquot regeneration) protocol modified with a correction factor on the natural signal (SAR-NCF) to account for sensitivity changes during measurement (Nagar 2007). Briefly, OSL—which is also called 'electron trap dating'—utilizes the natural dosimeter properties of quartz to measure the amount of time since a grain has undergone burial. The age of the deposit is calculated using the equation (Aitken 1998):

$$OSL\ age = \frac{equivalent\ dose\ (Gy)}{dose\ rate\ (\frac{Gy}{yr})}$$

where luminescence is induced by the natural radioactive dosing from the local environment. The dosing displaces electrons into traps, or crystal defect states, at band-gap depths (eV) that can be voided by energies in the visible spectrum, i.e., photons and sunlight. The more time a quartz grain is buried and shielded away from the sun, the more electrons become trapped, ideally yielding a more and more intense natural luminosity.

2.2.1. OSL Sample Preparation & Measurement

In the laboratory, all of the Van Phuc samples were processed under red light conditions. The inner portions of the AMS liners were recovered and treated with 1N HCl to remove carbonate fractions. Upon no longer reacting with HCl, the sediment was washed with deionized water and then immersed in 30% H_2O_2 to remove any of the sample's organic matter. The sample was then washed again, left to dry, and then hand-sieved to separate the 90-150µm size fraction. Heavy minerals (>2.72 g/cm^3) were then removed using heavy liquid (sodium polytungstate) separations. The samples were then etched with

40% hydrofluoric (HF) acid for 30 minutes to further purify the quartz grains. The final quartz separates were mounted as mono-layers (approximately 5 mg per disc) on 5 mm diameter steel discs using viscosil oil. Each disc, or 'aliquot', was tested for feldspar contamination by infra-red light (IRSL) exposure prior to ensure the purity of the sample (Stokes 1992). If a sample showed an IRSL response, it was etched again in HF until the IRSL remained unresponsive.

A Risø TL/OSL DA-15 reader fitted with a blue diode array was used for OSL measurements (wavelength =470 nm, power =18 mW/cm^2) (Botter-Jensen, Mejdahl et al. 1999)). The reader uses a calibrated Sr^{90}/Y^{90} β radioactive source for generating dose response curves for interpolating natural paleodoses. All of the samples were pre-heated (Ph) at 240˚C for 10s prior to measurement. The luminescence signal emitted from the samples was measured with a photomultiplier (type 9235QA, series 101482) filtered with two corning U-340 glass filters (Nagar 2007). A typical sequence for one of the Van Phuc aquifer samples (VPNS6) using test does of 200 beta seconds (10% of the maximum dose point):

(1) Natural Dose and Correction:

$$\beta_{100s} \rightarrow TL_{200^\circ C} \rightarrow Ph_{240^\circ C} \rightarrow \beta_{100s} \rightarrow TL_{200^\circ C} \rightarrow OSL_{125^\circ C} \rightarrow TL_{200^\circ C} \rightarrow \beta_{100s} \rightarrow TL_{200^\circ C} \rightarrow \beta_{100} \rightarrow Ph_{240^\circ C} \rightarrow OSL_{125^\circ C} \rightarrow \text{Blue LED Bleach}_{100s}$$

(2) First Dose Point:

$$\beta_{1000s} \rightarrow Ph_{240^\circ C} \rightarrow OSL_{125^\circ C} \rightarrow \beta_{200s} \rightarrow TL_{240^\circ C} \rightarrow OSL_{125^\circ C} \rightarrow \text{Blue LED Bleach}_{100s}$$

(3) Second Dose Point:

$$\beta_{1500s} \rightarrow Ph_{240^\circ C} \rightarrow OSL_{125^\circ C} \rightarrow \beta_{200s} \rightarrow TL_{240^\circ C} \rightarrow OSL_{125^\circ C} \rightarrow \text{Blue LED Bleach}_{100s}$$

(4) Third Dose Point:

$$\beta_{2000s} \rightarrow Ph_{240^\circ C} \rightarrow OSL_{125^\circ C} \rightarrow \beta_{200s} \rightarrow TL_{240^\circ C} \rightarrow OSL_{125^\circ C} \rightarrow \text{Blue LED Bleach}_{100s}$$

(5) Recuperation/Thermal Transfer:

$$\beta_{0s} \rightarrow Ph_{240^\circ C} \rightarrow OSL_{125^\circ C} \rightarrow \beta_{200s} \rightarrow TL_{240^\circ C} \rightarrow OSL_{125^\circ C} \rightarrow \text{Blue LED Bleach}_{100s}$$

(6) Recycled Dose Point:

$$\beta_{1000s} \rightarrow Ph_{240^\circ C} \rightarrow OSL_{125^\circ C} \rightarrow \beta_{200s} \rightarrow TL_{240^\circ C} \rightarrow OSL_{125^\circ C} \rightarrow \text{Blue LED Bleach}_{100s}$$

This sequence modifies the standard SAR procedure by beginning with an additional TL step to measure changes in aliquot sensitivity during the sample's natural measurement. In between each of the irradiation, preheating and optical stimulation cycles, a test dose and TL measurement routine allows us to monitor measurement-induced sensitivity changes. By measuring the TL from 0-200°C between each step, we capture any changes in the quartz 110°C peak. This permits us to simultaneously construct a SAR growth curve and monitor sensitivity changes at each stage of its construction. After each measurement, the integrated TL counts between 90–120°C are used to "correct" for sensitivity changes imparted to the sample during measurement:

$$\left(\frac{L}{T}\right)_{nat,corr} = \left(\frac{L}{T}\right)_{nat} \times \frac{1}{NCF}$$

where NCF is the "natural correction factor." NCF is calculated by dividing the integrated TL counts between 90-120°C for the initial and last TL measurement of the "natural dose and correction sequence" (i.e., the integrals of the first and fourth TL step in sequence 1 above). Using NCF gives a corrected natural luminescence $\left(\frac{L}{T}\right)$, which can be then used to interpolate an "equivalent" paledose from typical SAR (Murray 2000).

2.2.2. Calculation of the in-situ Dose Rates

To assess the contribution of cosmic rays to dose rates (C) for aquifer sediments from Van Phuc (Vietnam), a modified procedure from Prescott and Hutton (1994) was used. To account for the attenuation of dose rates as a package of sediment undergoes burial (i.e., Lagrangian changes), an average contribution of cosmic radiation is used in the calculations. By using an average value between the surface and depth, and by assuming a constant rate of burial, an adjustment is made for cosmic contributions received when sediments were at shallower levels. Using this average, a dose rate is calculated, which is then further adjusted for variations from latitude, altitude, and time.

Since the sampling intervals cover a wide range of depths and since we are interested in cosmic contributions that are an average between these depths and the surface (i.e., 0-50m), all the cosmic dose rates are based on the full expression for cosmic attenuation with depth from (Barbouti 1983), where uncorrected cosmic dose rate (D_0) in Gy ka^{-1} is:

$$D_0 = \frac{C}{((x+d)^{\propto} + a)(x+H)} e^{-Bx}$$

with C = 6072, B = 5.50 x 10^{-4}, d = 11.6, α = 1.68, a = 75, H = 212, and x depth in hg cm^{-2}. A conversion to depth in meters can be made by assuming a representative density for unconsolidated sediments ($\rho_B \approx$ 2.0 g cm^{-3}, (Schaetzl 2005)). This relationship is valid for depths from the surface down to ~500 km, and can be further modified to reflect dosing received when deep sediments were at shallower levels (Nagar 2007) such that the average dose is:

$$\overline{D}_0 = \frac{\frac{C}{(d^{\propto} + a)(H)} + \frac{C}{((x+d)^{\propto} + a)(x+H)} e^{-Bx}}{2}$$

$$\overline{D}_0 = 0.105 + \frac{\frac{C}{((x+d)^{\propto} + a)(x+H)} e^{-Bx}}{2}$$

The cosmic rates based on this average between depths ($\overline{D}_0$) are listed in Table 1. According to Prescott and Hutton (1994), the uncertainty bracketing traditional cosmic values is on the order of ± 5%.

2.2.3. Correcting for latitude and elevation

Not only does the cosmic ionization vary as a function of depth, it also varies along Earth's surface. This is due to changes in the orientation of Earth's magnetic field, whereby ionizing particles absorbed at the surface and penetrating to depth vary as a function of elevation and latitude. Because Earth has a geomagnetic field, incoming radiation is deflected towards the poles, resulting in less incidence at the equator. Similarly, there is also a bias towards more intense radiation at higher elevations since the number of cosmic particles increases with altitude. This means that the D_0 portion of the OSL signal needs to be normalized for the latitudes and elevations from which they were sampled. The method typically used for this adjustment starts by converting a sample's geographic latitude θ and longitude ϕ into a geomagnetic latitude λ through the equation (Prescott 1994):

$$\sin\lambda = 0.203\cos\theta\cos(\phi - 291) + 0.989\sin\theta$$

The cosmic dose (D_c) rate at a given sample's location and altitude *h* (km) is then computed by modifying D_0:

$$D_c = D_0\left[F + Je^{\frac{h}{H}}\right]$$

with F, H, and J parameters read from a graph plotting them as a function of geomagnetic latitude λ. The geomagnetic latitudes, their associated parameters, and the modified dose rates for all of the sampling locations are listed in Table 1.

2.2.4. Correcting for long-term variability in Earth's magnetic field

Cyclic changes in solar ray intensity and in the strength of Earth's magnetic field can introduce variability in the rate at which cosmic rays produce trapped electrons for OSL dating. A similar concern is addressed in the case of cosmogenic radionuclides (CRN), such as ^{14}C, due to past differences in the amount of cosmic rays penetrating Earth's atmosphere. According to Prescott and Hutton, (1994), variability in cosmic radiation does not affect trapped electron production as much as CRN because the former is determined by muon intensities below ground level, which varies much less than the variability of muons in the upper atmosphere. This is because of thresholds in the energy required for muons to reach Earth's surface and in the relatively constant effects above of atmospheric absorption for latitudes higher than 40° (Aitken 1985). Additional observations from irony meteorites support the notion that cosmic ray contributions have remained relatively stable over the last 500kyr, altogether yielding correctional factors that are on the order of 1.00±0.02 times the altitude and latitude corrected dose rates. Correction factors for these time changes are available from Prescott and Hutton (1994), with the ones applicable for the samples in this study listed in Table 1.

2.3. Luminescence from the in-situ sedimentary matrix

While cosmogenic sources are important for luminescence dating, most of the radiation responsible for the luminescence signal comes from local sources, in the sediments. In particular, the majority of the defects needed for electron trapping are generated by the natural radioactive decay of ^{40}K, ^{232}Th, and ^{238}U in the sedimentary matrix. In 'typical' quartz sands, beta and gamma doses are responsible for 56% and 39% of the annual dose, respectively (Aitken 1985). Alpha components can be neglected since the portion affected by their radiation can be removed by HF-etching. This leaves only the annual dosing from cosmic, beta, and gamma to be determined, the first of which is already addressed in the previous section. For the beta and gamma contributions, thick source alpha counting

was used to measure the ppm concentrations of ^{232}Th and ^{238}U, and gamma spectroscopy was used to determine the percentage of ^{40}K. In calculating the dose contributions from the ^{40}K, ^{232}Th, and ^{238}U concentrations, we assume that radioactive equilibrium persists for all samples. The final in-situ dose rates were then calculated according to the standard method of (Aitken 1985) where dose rate (Gy/yr) equals:

$$Dose\ rate = 0.9D_{\beta} + D_{\gamma} + D_{c}$$

with D_{β} equal to the beta dosing from ^{40}K, ^{232}Th and ^{238}U; Dγ equal to the gamma dosing from ^{40}K, ^{232}Th and ^{238}U, and D_c the depth, latitude, and time corrected cosmic dose rates—all of which were also attenuated for the water content measured from drying a portion of each newly opened OSL sample (Aitken 1985). The ^{40}K, ^{232}Th and ^{238}U concentrations for the Van Phuc samples are listed in Table 2, with the final dose rates in Table 3.

3. Results

3.1. Van Phuc's Aquifer Stratigraphy – Sedimentary Units and Facies

The grainsize results and field descriptions show that the stratigraphy of Van Phuc is comprised of three main sedimentary facies: gravely sands, silty sands, and clayey silts. These facies relate to graded river channel sands, floodplain deposits, and estuarine muds deposited with the Quaternary progradation of the delta (Figure 6, bottom ternary diagram). The facies plot along a mixing line between pure sands and clayey silts, with a fit that is typical to the continuum of environments from channel to back swamps (Royse 1968; Figure 6). The silty muds and sands form the end-members of the distribution, which tends to follow a line of 3:1 silt and clay. Intermediate points between the end-

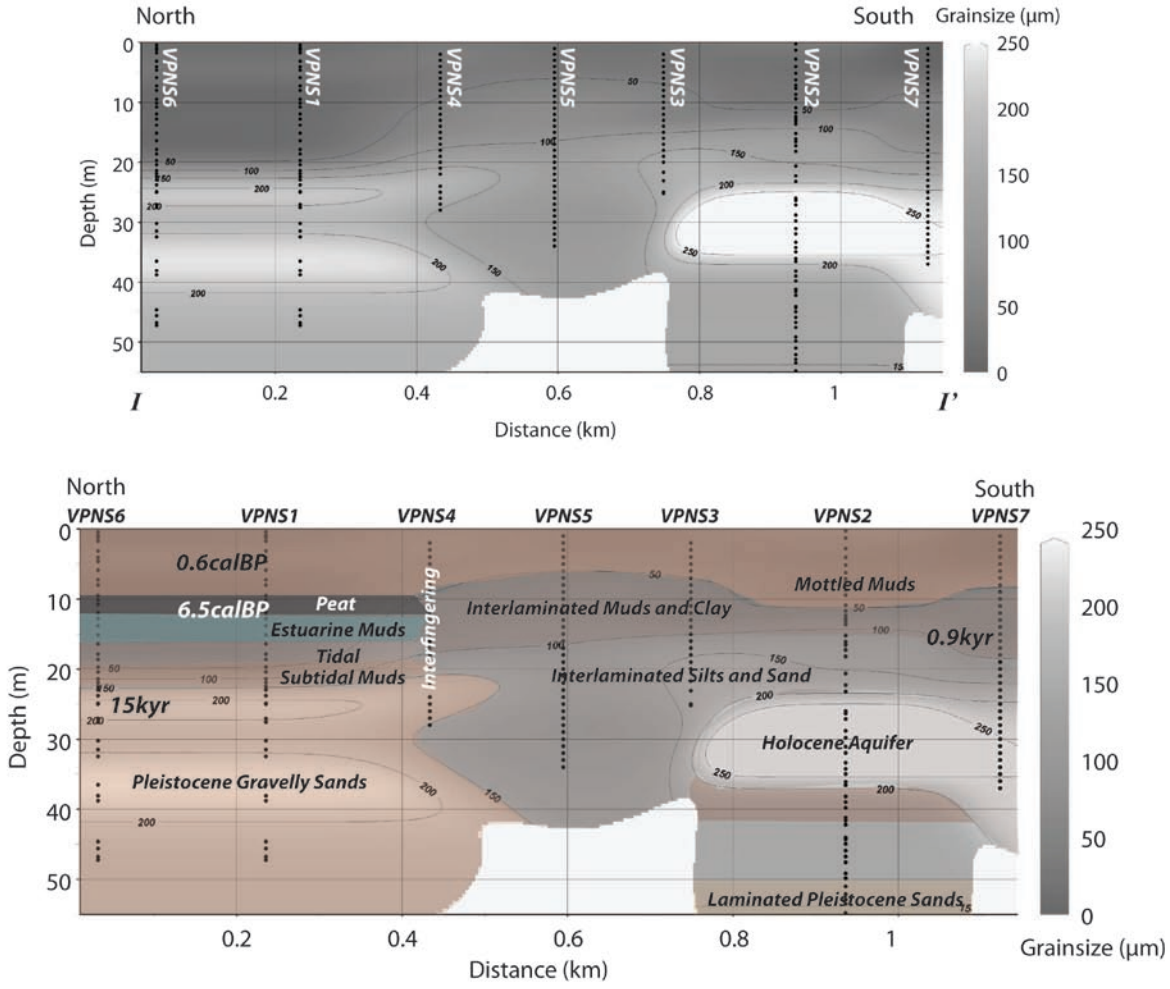

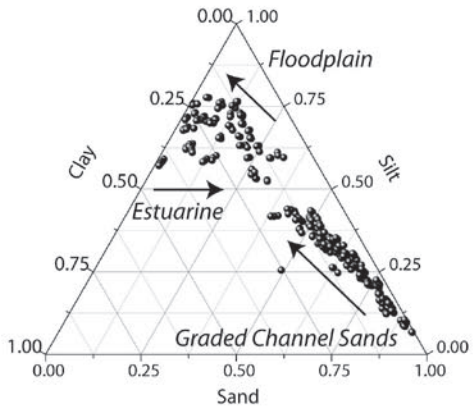

Figure 6. Grainsize and sedimentological profiles of the I-I' needle sampling transect across Van Phuc's Red River bend. The top panel shows the results of grainsize anaylsis for the aquifer sediments and the middle panel is the same, simply overlain with aquifer depositional ages and colored by our interpreted facies. The ternary diagram to the left shows the results of grainsize performed on samples from VPNS1 and VPNS2. Photographs of the actual sediments are archived for rotarty drillings at VPNS1 and VPNS2, and compliated into sediment logs in two picture supplementals: S1 and S2. More information about our grainsize methodology and the results can be found in Eiche et al., 2008.

members are mixed fluvial sediments, with a tighter grouping of the sandier facies around the mixing line—presumably from riverine suspension. The riverine sorting line of silty-sands, with coarser facies is interpreted as channel bedload with the siltier sands relating to finer substratum deposits. The mixing line gaps near the subequal sand-silt facies, indicating that there is a lack of a sandy-silt facies in the overall deposits. What exactly the break means can be attributed to a change from graded to uniform depositional conditions, or more likely, a lack of topstratum levee and crevasse-splay deposits. Given that the Red River has been so stably located since the Eocene (Moores and Fairbridge 1997), the absence of these meandering and avulsive fluvial facies is consistent with the expected, long-term conditions of the riverbend. A more divergent cluster picks up in the clayey-silt area of the plot, which are facies typical of floodplain and channel fill deposition, interspersed with finer, suspended estuarine muds (Royse 1968).

The stacking and architectural layout of these facies are shown in the sedimentological results of the Van Phuc transect (Figure 6, top and middle panels). Based on the grainsize results, along with the characterization methods of Tanabe et al., (2003 and 2006), the Van Phuc core sediments were divided into general sedimentary facies, characterized by lithology, color, textures, contacts, and subsequent ^{14}C and OSL ages. In profile, the stratigraphy shows the surface deposits comprised of a ~20m thick mud unit, with can be subdivided into 5 distinct facies (Figure 6). The first layer is a laterally continuous mottled mud facies, ~10m thick, which caps the profile. Underlying the mottled muds are several laterally discontinuous mud layers that interfinger with each other in the middle of the riverbend—in our transect, the interfingering occurs around the 0.4km mark, in the vicinity of VPNS4 (Figure 6). Underlying the mottled layer in the north is a ~1m thick peat layer, followed by a ~5m thick bluish mud and ~7m thick sequence of alternating red and grey muds (S1). This peat, blue, red and grey mud sequence was absent from the muds underlying the mottled unit in the southern drillings. There,

the underlying muds in the lower part of the riverbend were comprised of a ~10m thick interlaminated silt and clay sequence with grey, brown, and black cm-scaled bandings (S2).

Below the muddy layers, three types of sands were differentiated within the aquifer. In the northern part of the riverbend, a coarsening upwards sequence of gravelly orange sands was found between ~24 and 50 meters, bottoming out in an unconformable clean gravel (Figure 6 and S1). In the middle of the transect, the surface muds are underlain with a finer and greyer sandy facies, which are gradationally conformable with the overlying silt and clays, the only difference being that the unit is coarser, with less black organic banding (S2, 15-24m). Underlying the interlaminated sands in the south is a different grey sand facies, one which shows little to no lamination and more massive style bedding between ~25-40m (S2). The sands in the massive grey unit were often found to be disrupted periodically by grading into and out of a <1m thick muddy clay unit—probably caused by the periodic abandonment of a channel. Underlying these grey sands, were orange sands at depths ~50m, similar, though often not as gravelly, as the orange sands in the northern part of Van Phuc's bend.

Altogether, the sand and mud sequencing in Van Phuc is slightly different than sequence results recorded by Tanabe et al. (2006) in their coring of the delta. The most proximal of their cores, CC, lies 25km to the south of Van Phuc (Figure 4, (Hori, Tanabe et al. 2004; Tanabe, Saito et al. 2006)), from a similar, fluvially-dominated portion of the subaerial delta. Compared to the CC core, the Van Phuc sequences are more fluvially dominated and encompass more recent and ancient deposits over the same core-length (~30m). The stratigraphic resolution of CC over its depth records the progradation of a coastal, tide-influenced channel (Facies 2.1) to a more inland tide-influenced channel (Facies 3.1) during the emergence of the Red River's drowned valley between 9-7kyr. This sequence, occupying the depths between 3-30m in CC, is "abbreviated" or absent from the Van Phuc corings. In VPNS6 and VPNS1, these tidally influenced-channel facies are "abbreviated" in that they extend between ~12-20m, grading above into mangrove, abandoned channel, and floodplain deposits. Below 20m, the sequence is

truncated by orange-lateritic sediments matching descriptions of the late Pleistocene interfluves (Facies 0, (Tanabe, Saito et al. 2006)). In the meander's southern cores (VPNS4, VPNS5, VPNS3, VPNS2, and VPNS7), the transgressive-regressive estuarine and coastal-channel facies are absent from the sequence. Instead, the cores are comprised mostly of aggradational grey channel sands (~15-50m). Overlying the channel sands are abandoned channel fill and floodplain deposits, indicating the site is located on an older meander course of the modern Red River. Figure 7 shows the boundary of the paleo-channel valley that occupied Van Phuc, following the 20 to 55m deepening of the Pleistocene unconformity.

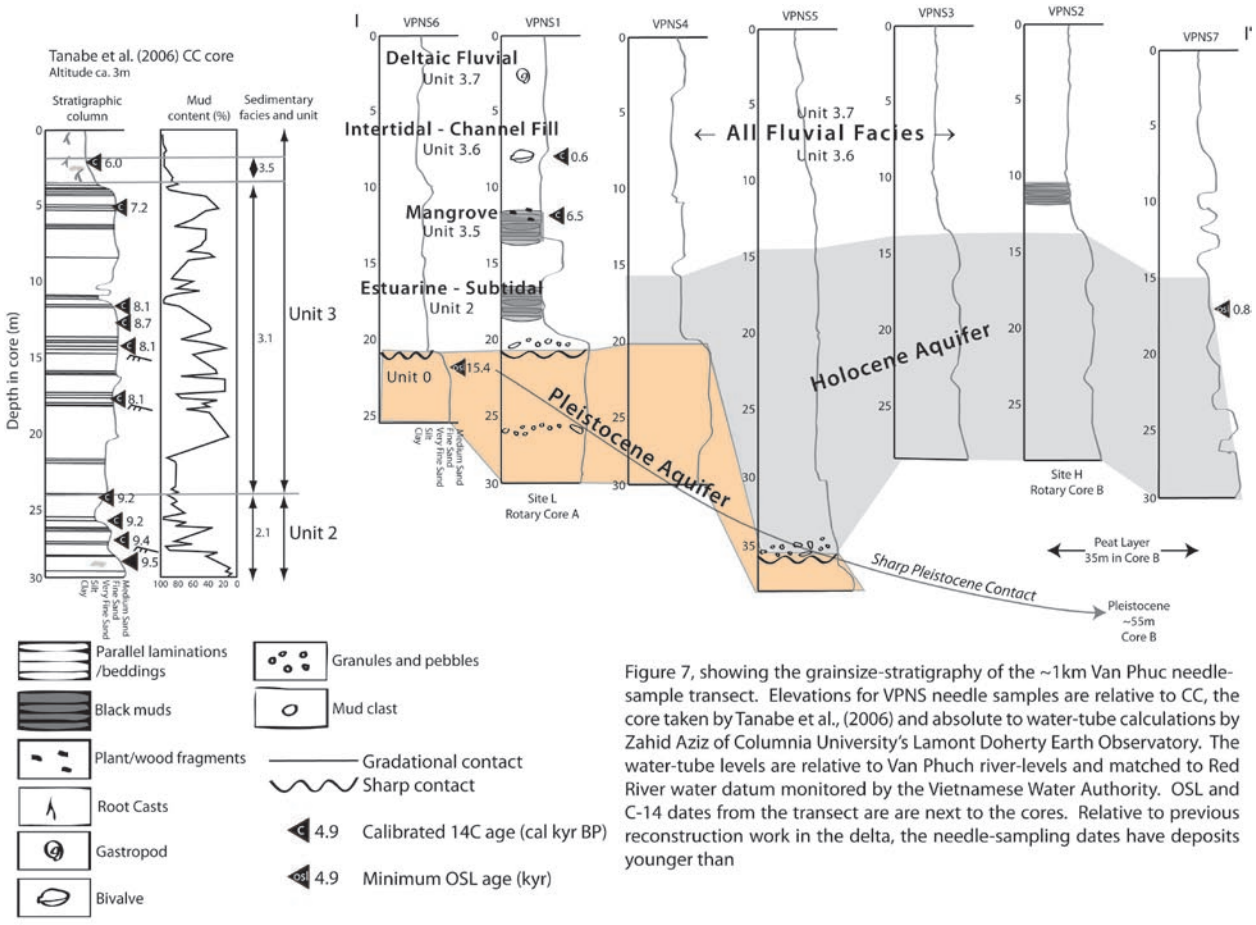

Figure 7, showing the grainsize-stratigraphy of the ~1km Van Phuc needle-sample transect. Elevations for VPNS needle samples are relative to CC, the core taken by Tanabe et al., (2006) and absolute to water-tube calculations by Zahid Aziz of Columnia University's Lamont Doherty Earth Observatory. The water-tube levels are relative to Van Phuch river-levels and matched to Red River water datum monitored by the Vietnamese Water Authority. OSL and C-14 dates from the transect are are next to the cores. Relative to previous reconstruction work in the delta, the needle-sampling dates have deposits younger than

3.2. Luminescence Dating

Similar to other samples from the Himalayas (e.g., Parasi, Nepal, Chapter 3 of this thesis and Araihazar, Bangladesh (Weinman 2008)), the luminescence sensitivity of quartz from the region was low (i.e., "dull"), with total counts varying only 100-2000 for vast age ranges from 300 to 130,000 years (Figures 8-15). Despite all of the samples being dull, the luminescence properties were otherwise well behaved with regeneration curves suitable for paleodose determinations. All of the samples showed no sign of IRSL or feldspar contamination, with the majority of aliquots having recycling ratios of 1 ± 0.1 and no recuperation. In assigning a final OSL age, we use each sample's dose histogram and radial distribution (Galbraith 1994) to help determine the most likely timing event of each deposit. Because of the likelihood for partial bleaching and the fact that we use a vertical needle sampling method to recover our samples, we expect all of our age distributions to have a certain degree of spreading. To assess how much of this spread is attributable to our sampling technique, we can approximate its effect using depositional rates typical to the active rivers of Southeast Asia—most likely this means accretion rates somewhere on the order of 1-5cm/yr ((Goodbred and Kuel 1998; Funabiki, Haruyama et al. 2007), Table 4). Since we use a ~0.3m vertical liner to recover a deposit, this translates into an expected ~300 year age-spread for a conformable unit. Add to that the fact that we subsample within the liner when processing our samples, we do not expect to see a spread effect more than 100 yr due to vertical sampling. This means that for the majority of the Pleistocene and Holocene ages we measured, the spread from vertical sampling in a conformable unit will be negligible, with the minimum age still corresponding to the most recent timing of the deposit. In other words, unlike partial bleaching, the spread in ages from sampling still yields *actual* burial ages, the minimum of which will still correspond to the most recent timing of the deposit.

3.2.1. Partial Bleaching in Van Phuc's Modern Deposits

Without a significant effect from vertical sampling, most of the age-spread then becomes attributable to partial bleaching. For sedimentary transport systems with short transport durations and/or where there is considerable attenuation of sunlight, the probability of perfect zeroing can decrease significantly (Singarayer, Bailey et al. 2005). This happens because, unlike eolian deposits, partial bleaching is typical of grains deposited in riverine settings, such as Van Phuc. The water column, its sediment load, and turbidity all help protect the grains from being totally bleached, which leaves behind a remnant OSL from a previous cycle. In terms of OSL ages, this causes an overestimation of the depositional age for a sample (Wallinga 2002). Being that Van Phuc is located on the actual bend of a river, partial bleaching of the aquifer grains is very likely. To test for partial bleaching in Van Phuc's sediments, we sought to determine whether there was any leftover OSL in the river bar's youngest samples. For this, sediments were collected from a depositional, point-bar site just downstream of the riverbend's apex (OSL samples VPNS10 and 11, Figure 5). At VPNS11, OSL samples were taken at the surface (0-0.3meters), 4.2 and 8.5 meters. A 'duplicate' sample was collected from VPNS10 at ~5m—a hole being drilled only a few meters away for a separate hyporheic zone study (Hun Bok Jung, UW Madison).

The bleaching-test results show that the majority of grains in the modern deposits are effectively being zeroed. This is shown by comparing our measured paleodoses to those that we'd expect to see throughout the VPNS10 and VPNS11 profile (Tables 5a-b). Going from the profile's top to bottom, the surface point-bar sands hold paleodose equivalents on the order of 1Gy (Figure 8A). This is on par with what we'd expect considering dosing rates between 2-4Gy/kyr and cm/yr rates of vertical accretion (Tables 5a-b). For a typical dose rate of 3Gy/kyr—which is similar to the surface's actual dosing (3.17Gy, Table 3)—sands at 0.3m would have an expected accumulated dose of 0.9Gy (Table 5a). This agrees well with VPNS11-1's actual paleodose of 1Gy (Figure 8A, Table 5b). Similar agreements

between expected and measured doses are found in the other VPNS11 and VPNS10 samples (Figures 9-11, Table 5b). For VPNS11-2, a dose rate between 2 and 3Gy/kyr (2.12 Gy/kyr, Table 3) yields an expected paleodose between 0.8-1.3Gy, which, again, agrees with the actual paleodose of 1.5Gy (Figure 9A, Table 5b). VPNS10, which is from a nearby hole at a similar depth to VPNS11-2, yields a result consistent with VPNS11-2, replicating the result of that sample (1.7Gy, Figure 10, Table 5b). The

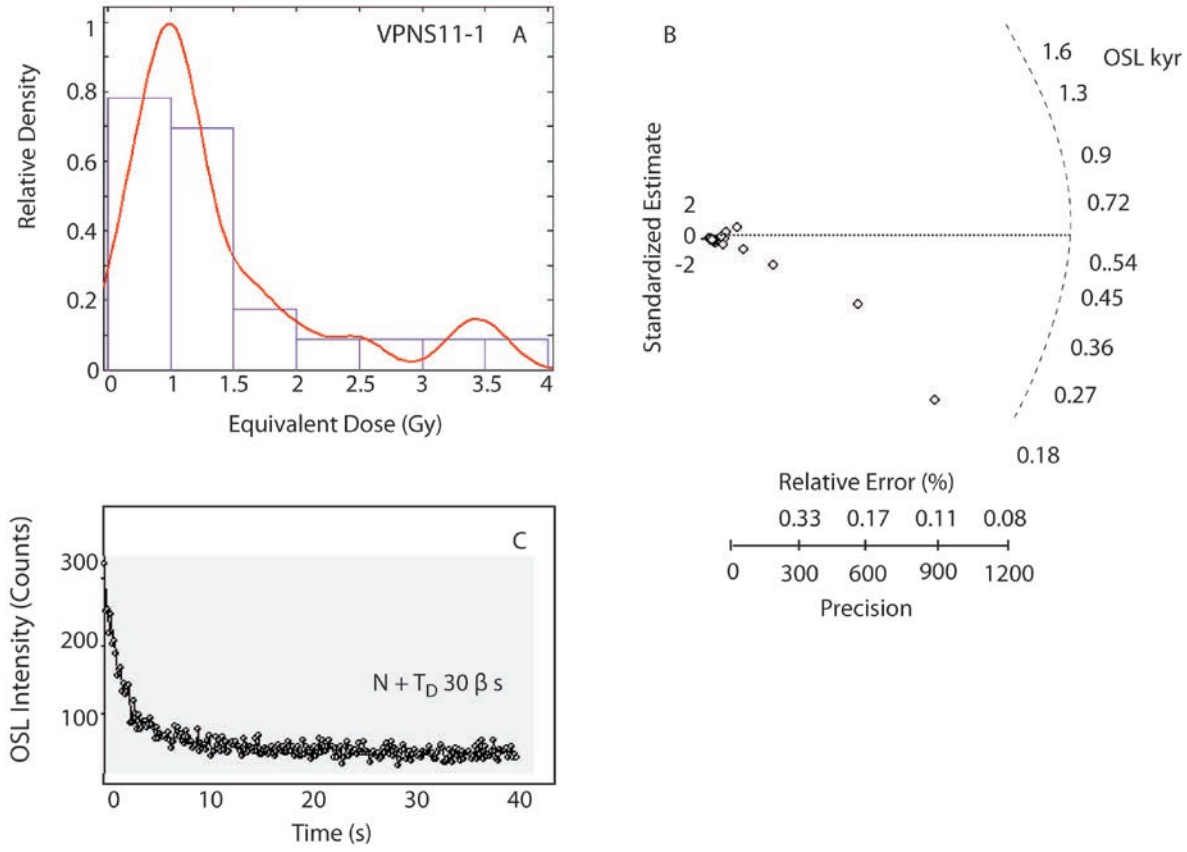

Figure 8 A-C, OSL results and shine down curves for Van Phuc aquifer sample VPNS11-1, which along with VPNS10 and the other VPNS11 samples, was taken to see if there is any remnant OSL in the modern sediments of the Red River. The relative density curve (A) plots a histogram of the dose equivalent results from OSL-SAR in Gy. Calculating the depositional ages by dividing each paleodose by the sample's dose rate (Table 3), OSL ages can be determined. The sample's age distribution for all of the aliquots measured are plotted in B, a radial plot that graphs standardized age estimates against reciprocals of standard measurement errors (Galbraith 1990). Shine down curves of the sample's natural luminosity with a test dose added to check for sensitivity changes during measurement are shown in C.

deepest sample from the point bar profile, VPNS11-3, also has a measured dose that agrees with its expected dose (2 vs. 1.7Gy, Figure 11, Table 5b), encouraging us to believe that the sediments being delivered to the point bar are bleached enough to produce high fidelity OSL ages.

While the comparison of expected versus measured doses indicates that the Red River sands are effectively being zeroed, the comparison also shows us that a small amount of grains in each sample do carry a latent luminescence. This is seen for all of the VPNS10 and 11 point bar samples, as well as in the aquifer samples. First, from the modern sediments, we see that the measured paleodoses show a subtle 0.1-0.3Gy difference between the expected and measured doses (Table 5b). This is consistent with Singarayer et al.'s, (2005), findings that modern fluvial samples typically carry latent signals less than 1Gy. Second, all of the dose distributions tend to have a tail, indicating that a small proportion of each sample contains grains that were ineffectively bleached before burial. Overall, these findings suggest that there is an incomplete resetting of OSL in each and every sand grain, which is what we would expect for Van Phuc's fluvial setting. This means that by neglecting the obvious partially-bleached paleodoses, the 0.1-0.3Gy latency in the *majority* of grains means that we should we should be able to date modern aquifer sediments within ~100 years using the youngest dose peak from each sample. This leaves us preferring paleodoses from each distribution's youngest paleodose peak, when determining the age for the rest of our samples.

3.2.2. The Depositional Ages of Van Phuc's Aquifer

Going north to the south along the Van Phuc transect (I-I'), the first OSL sample was successfully retrieved from the low arsenic site of VPNS6 at a depth of 23 meters. The typical response of VPNS6 to our protocol, along with the paleodoses and OSL ages, is plotted in Figure 12. The histogram of its OSL ages shows a high degree of positive skewing. This again indicates that the sample contains a small percentage of poorly bleached grains (Murray, Olley et al. 1995; Wallinga 2002). The sample also has an unusually large spread in depositional ages, ranging from 15-400kyr, with one aliquot even dating back

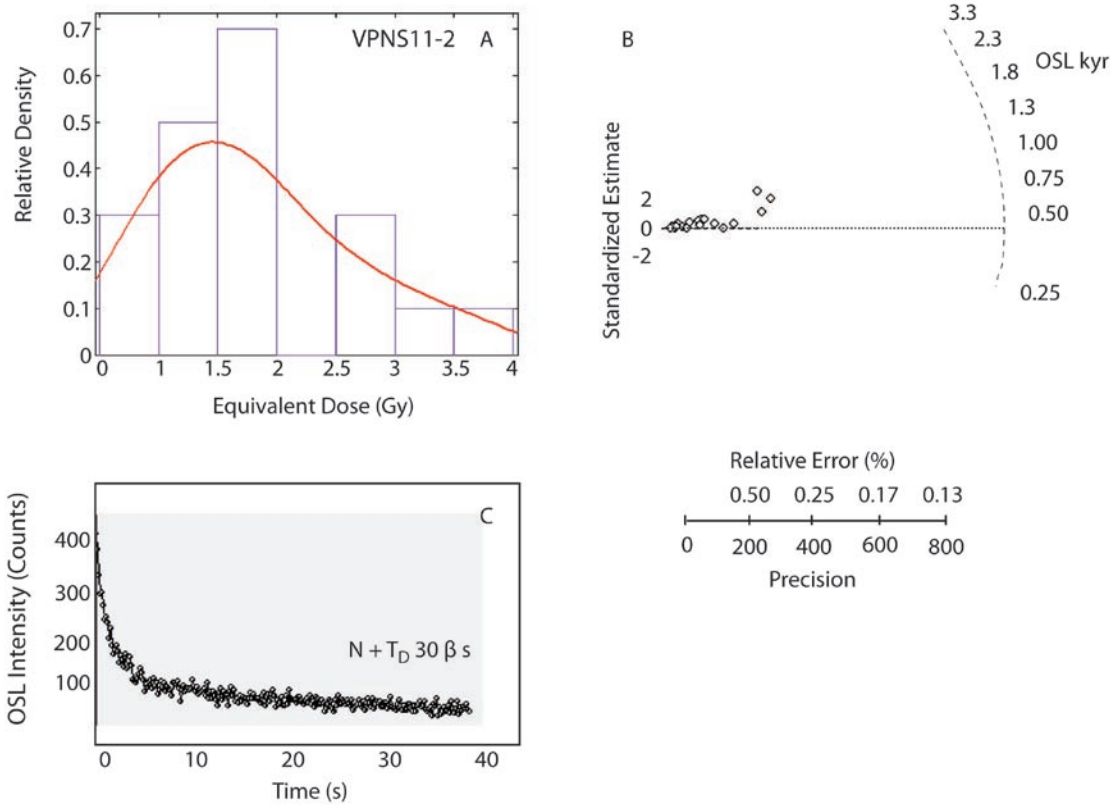

Figure 9 A-C, OSL results and shine down curves for Van Phuc aquifer sample VPNS11-2, which along with VPNS10 and the other VPNS11 samples, was taken to see the remnant dosing in modern sediments of the Red River. The relative density curve (A) plots a histogram of the dose equivalent results from OSL-SAR in Gy. Calculating the depositional ages by dividing each paleodose by the sample's dose rate (Table 3), OSL ages can be determined. The sample's age distribution for all of the aliquots measured are plotted in B, a radial plot that graphs standardized age estimates against reciprocals of standard measurement errors (Galbraith 1990). Shine down curves of the sample's natural luminosity with a test dose added to check for sensitivity changes during measurement are shown in C.

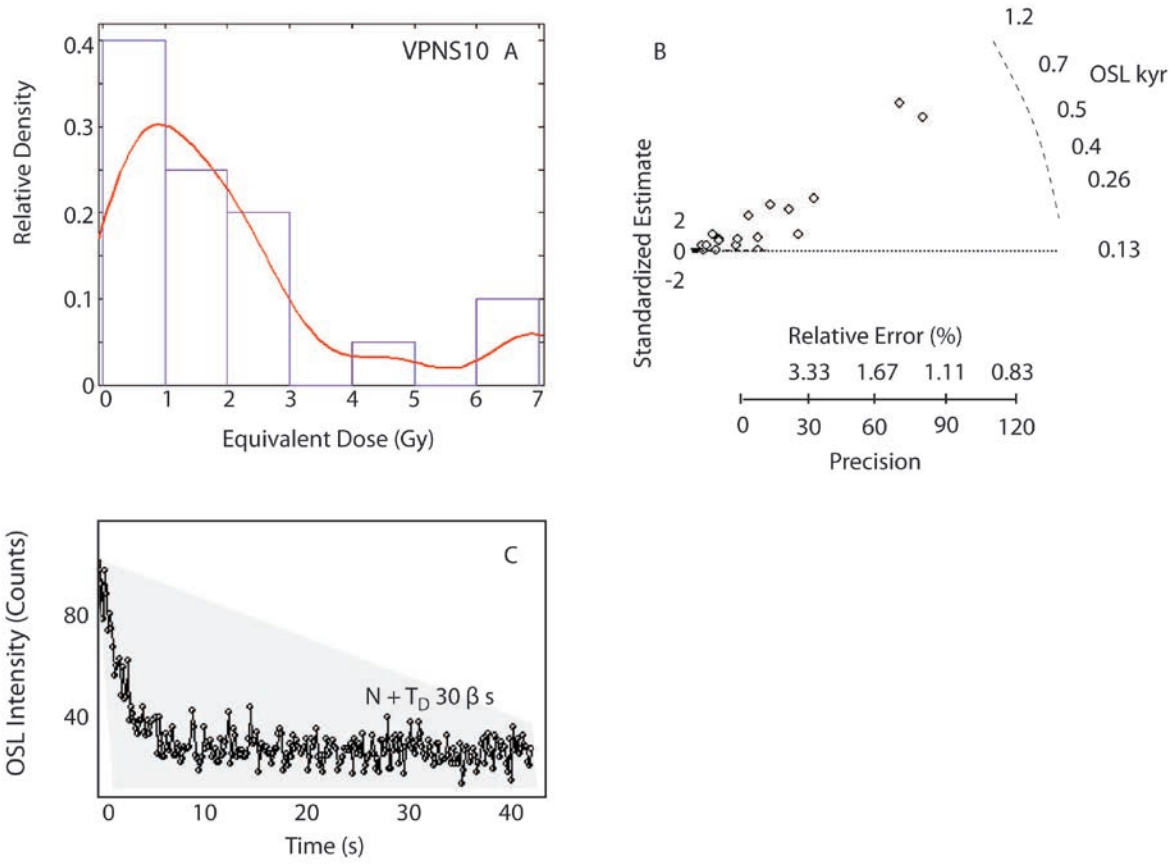

Figure 10 A-C, OSL results and shine down curves for Van Phuc aquifer sample VPNS10, a sample to test for evidence of partial bleaching. This sample is roughly at a similar depth horizon as VPNS11-2. Along with sample VPNS11, sample VPNS10 was taken in depositional setting downstream of Van Phuc's river bend apex to see if there was any remnant Gy in the modern samples. The relative density curve (A) plots a histogram of the dose equivalent results from OSL-SAR in Gy. Calculating the depositional ages by dividing each paleodose by the sample's dose rate (Table 3), OSL ages can be determined. The sample's age distribution for all of the aliquots measured are plotted in B, a radial plot that graphs standardized age estimates against reciprocals of standard measurement errors (Galbraith 1990). Shine down curves of the sample's natural luminosity with a test dose added to check for sensitivity changes during measurement are shown in C.

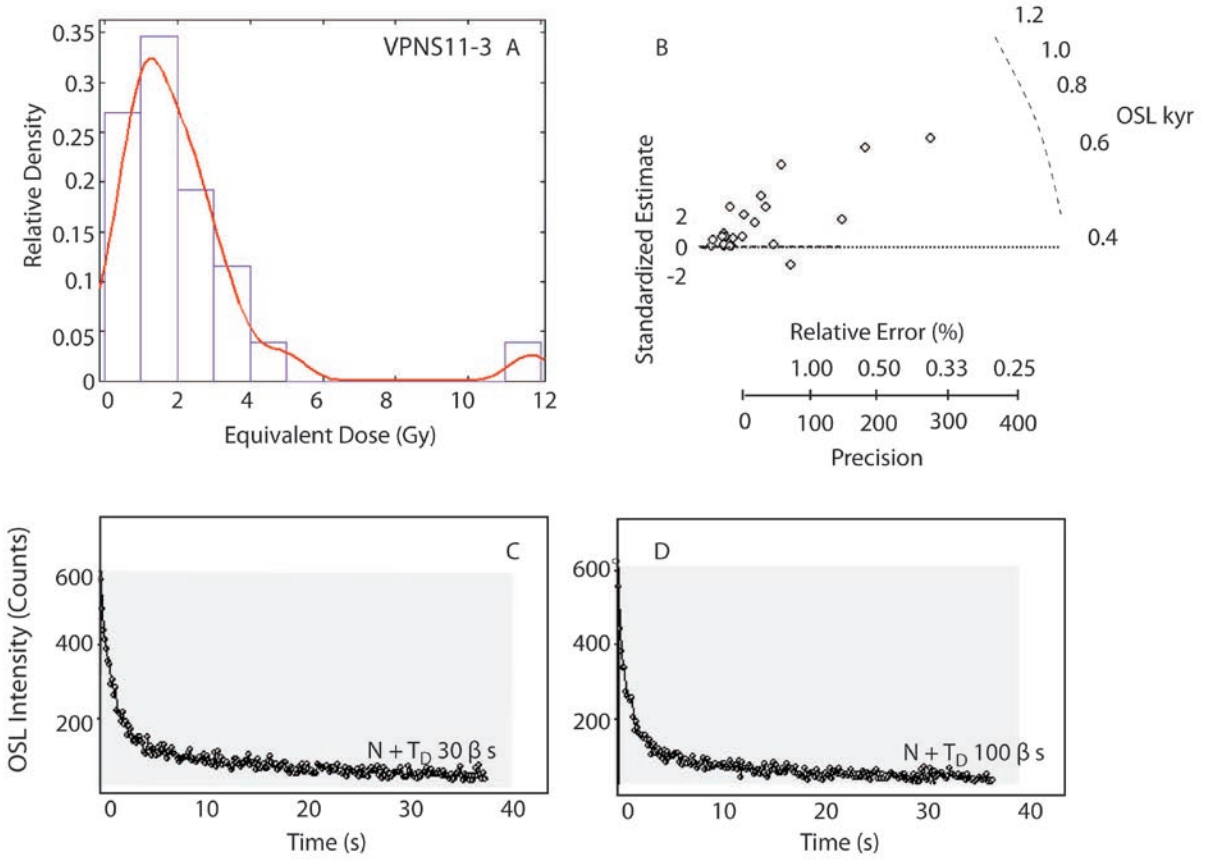

Figure 11 A-D, OSL results and shine down curves for Van Phuc aquifer sample VPNS11-3, which along with VPNS10 and the other VPNS11 samples, was taken to see the remnant dosing in modern sediments of the Red River. The relative density curve (A) plots a histogram of the dose equivalent results from OSL-SAR in Gy. Calculating the depositional ages by dividing each paleodose by the sample's dose rate (Table 3), OSL ages can be determined. The sample's age distribution for all of the aliquots measured are plotted in B, a radial plot that graphs standardized age estimates against reciprocals of standard measurement errors (Galbraith 1990). Shine down curves of the sample's natural luminosity with a test dose added to check for sensitivity changes during measurement are shown in C and D.

to 1300kyr. Since we aim at sampling the first sands we encounter in the aquifer—dating the last time a river was actively building the aquifer in that particular location—we typically pass through any major unconformities right before sampling. In the case of VPNS6, however, we think that the sample crosses a section that is *highly* unconformable, which explains the large range of OSL ages—in other words, this is different that the age span we'd get from sampling vertically through a conformable unit. A highly unconformable unit at this horizon was also seen in the rotary drilling nearby in VPNS1 (also called Site L and Core A), which also showed evidence of a ~0.2m indurated gradational sequence of coarse orange sands below a sharp contact with the overlying mud unit at 24m (i.e., see supplemental photo, S1). We take this 15kyr-1Myr age range as confirmation that this boundary is indeed a Pleistocene-Holocene surface, with the younger ages being the most likely timing event of the unit's last deposition: 15kyr (Table 3, Figure 6).

Southeastward, the next dated samples are the two ^{14}C ages from shell and wood samples collected from the borehole at VPNS1 (Site L, Eiche et al., 2008). In total, three samples were collected from this borehole, one of which was a littoral snail shell from 3.6m, which was too small and too diagentically altered for successful ^{14}C dating (Table 6). The other two samples collected from the borehole included a marine bivalve and some wood from a peaty deposit. The bivalve, identified as a *Cyrenacea* subtidal marine species (Moore, Lalicker et al. 1952; Tanabe, Saito et al. 2006), was in the middle of a continuous and massive brown mud deposit (~2.5 meters thick, between 5 and 7.5m), at 6.9m and yielded a calibrated ^{14}C age of 0.6kyrs (Figure 7, S1, and Table 6). The wood fragments were taken from a peaty deposit ~5m deeper down in the core, at 11.8m, at an unconformity between brown and grey mud facies (see supplemental photo, S1). The calibrated ^{14}C age of the wood in this unconformable layer dates to 6.5kyr, which gives the core the same type of time gap observed in other cores drilled in the region—Tanabe et al. typically find the upper 20m of their Red River cores with dates

ranging between 0.5-8kyr and with time gaps between 0.5-5kyr (Figure 7, Tanabe 2003; Hori, Tanabe et al. 2004; Tanabe, Saito et al. 2006).

The last OSL sample in the transect is from the high arsenic site, VPNS7, where the first sands encountered below the surface muds date to 0.9kyr (17m, Figure 6). Unlike the 15kyr sands at VPNS6, the sands at VPNS7 are a cleaner grey facies, more conformable with the overlying muds, and do not show obvious signs of diagenetic alteration and weathering (supplemental photos S2). The paleodose histogram for the grey sands shows a peak at ~2.5Gy, which agrees with the mode (2.6Gy) and the least 10% age of sample (0.8kyr, Figure 13). In seeing that we may be dealing with two different aged-aquifers while sampling, we wanted to corroborate the possibility of such different ages—the riverbend is a single geomorphic unit, and we expected a simple and laterally continuous stratigraphy. To corroborate our ages, we sampled from the same depths as VPNS6 and VPNS7 in another needle-sampling site, VPNS9, just a few meters northeast of the transect (Figure 5). Here, samples were collected from 17 and 24 meters, and as in VPNS7, the sands we encountered at both of these depths were grey, with no sharp or highly indurated surfaces. At 17m, the grey sands have one of the most Gaussian, unskewed dose distributions for all of our samples, indicating that its average modal age of 0.9kyr is the best representative age of the deposit (Figure 14, Table 3). This corroborates the timing of the 0.8kyr aquifer sands from VPNS7. The deeper grey sands from VPNS9 at 24 meters have a dose peak at 7Gy, which dates the deposit to 2kyr (Figure 15, Table 3). Otherwise, we found no evidence of the older, orange sands within the drillings at this site, with all of the sands consistently being grey and dating to the Holocene. To us, this means that the orange sands in the northern part of the bend are not just a chemically altered part of the southern grey deposit. Inasmuch, this “simple” riverbend is made of two differently-aged aquifer deposits (Figure 16). The grey sands are Holocene deposits, and the orange sands date to the Pleistocene. Overall, this indicates a lateral heterogeneity of sand ages in

the aquifer with the riverbend having a 15kyr unit in the north and a 1-2kyr aquifer underlying its southern portion (Figures 6, 7, and 16).

3.3. Geochemical Results of Van Phuc's Aquifer Needle-Sampling

Figure 17 is a compilation of the needle-sampling profile results of groundwater arsenic, sediment reflectance, sediment iron ratios, and $^{3}He/^{3}H$ groundwater ages. Since this contribution focuses more on the site specific patterns of arsenic in context with the riverbend's sedimentary and evolutionary history, the geochemistry is focused on elsewhere, in several of our other contributions (Berg, Trang et al. 2008; Eiche 2008; van Geen 2008). Relevant here, however, is how these geochemical distributions conform to the aquifer's internal facies, because we want to know how important aquifer sedimentology is in controlling local arsenic heterogeneity (Figure 17 and 18). Particularly relevant in our results is how all of the geochemical profiles follow the aquifer's sedimentary architecture (Figure 6). In each case, geochemistry remarkably conforms to Van Phuc's subsurface sedimentology (Figure 17 and 18). Following the profile's 0.4km interfingering of different facies, a similar interfingering can be seen in the aquifer's geochemical conditions (VPNS4, Figure 6 and 17). This is particularly observable in the distinction of groundwater arsenic between the riverbend's two main aquifer units: the orange Pleistocene sands and the grey Holocene sand facies. In the riverbend, groundwater needle-samples retrieved from the grey sand units measured between ~10µg/L and 500µg/L in dissolved arsenic, with an average of 200 ± 130µg/L (n=25, Figure 17, top panel). Contrasting this heterogeneity, the orange sands in the north are consistently low in groundwater arsenic—all 6 needle-samples from the indurated orange sand facies tested below the World Health Organization's drinking water standard of 10µg/L arsenic (VPNS6, VPNS1, and VPNS4).

As with the different concentrations of arsenic, the sediment reflectance and iron ratios, which are telling of the aquifer's sedimentary and aqueous redox conditions (Horneman 2004; van Geen,

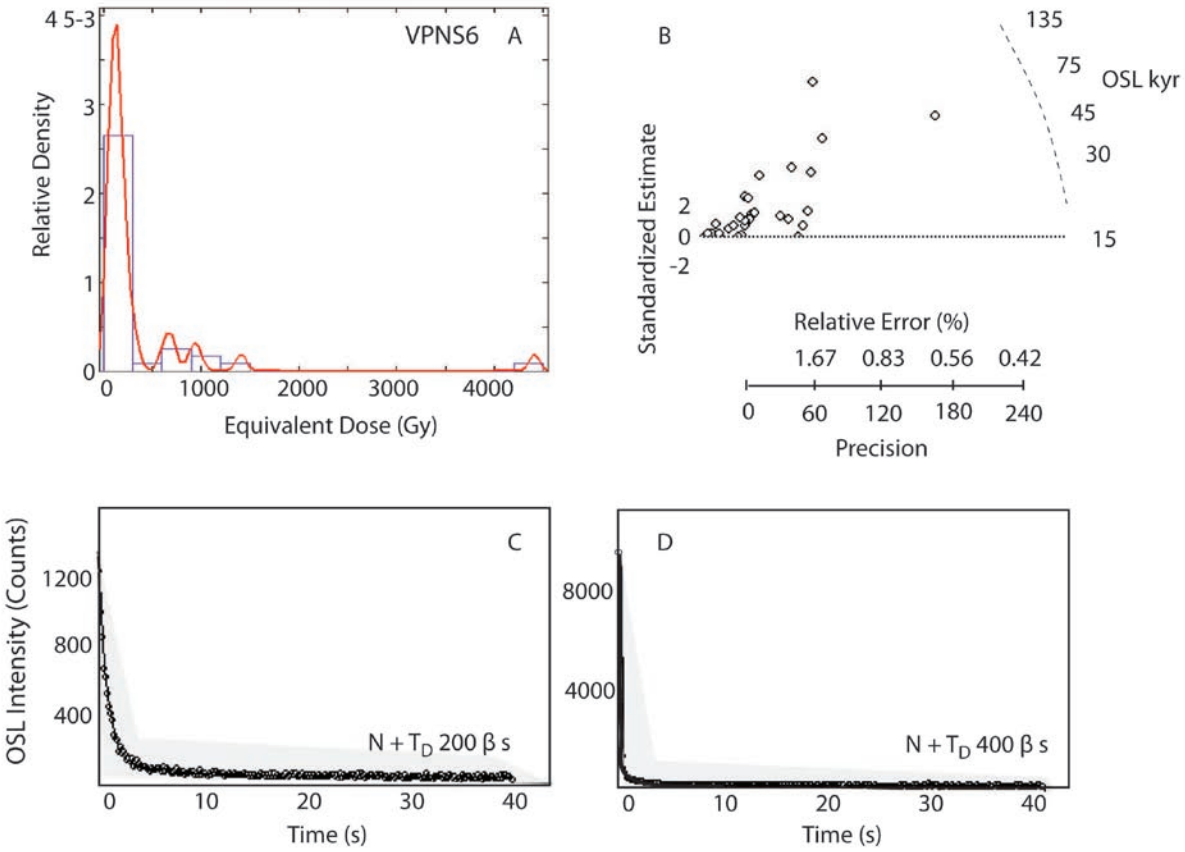

Figure 12 A-D, OSL results and shine down curves for Van Phuc aquifer sample VPNS-6. The relative density curve (A) plots a histogram of the dose equivalent results from OSL-SAR in Gy. Calculating the depositional ages by dividing each paleo-dose by the sample's dose rate (Table 3), OSL ages can be determined. The sample's age distribution for all of the aliquots measured are plotted in B, a radial plot that graphs standardized age estimates against reciprocals of standard measurement errors (Galbraith 1990). Shine down curves of the sample's natural luminosity with a test dose added to check for sensitivity changes during measurement are shown in C and D.

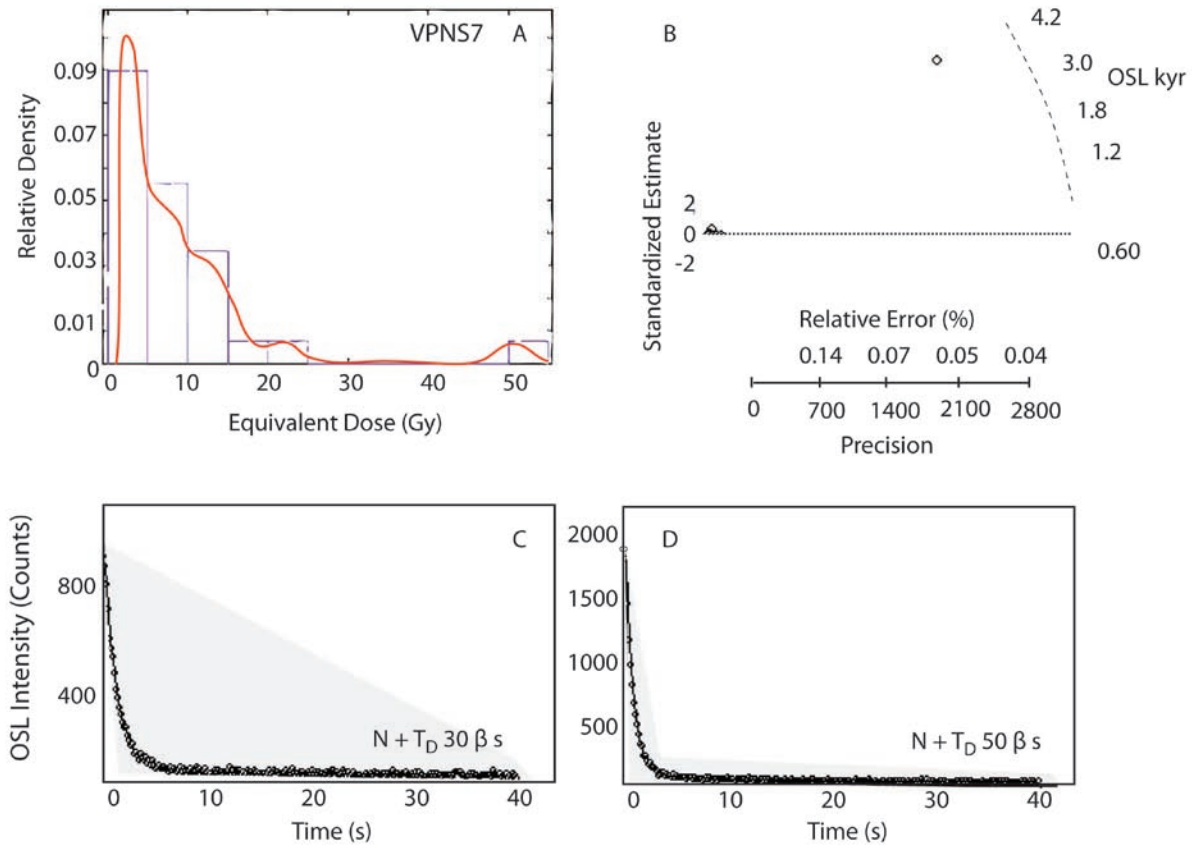

Figure 13 A-D, OSL results and shine down curves for Van Phuc aquifer sample VPNS-7. The relative density curve (A) plots a histogram of the dose equivalent results from OSL-SAR in Gy. Calculating the depositional ages by dividing each paleo-dose by the sample's dose rate (Table 3), OSL ages can be determined. The sample's age distribution for all of the aliquots measured are plotted in B, a radial plot that graphs standardized age estimates against reciprocals of standard measurement errors (Galbraith 1990). Shine down curves of the sample's natural luminosity with a test dose added to check for sensitivity changes during measurement are shown in C and D.

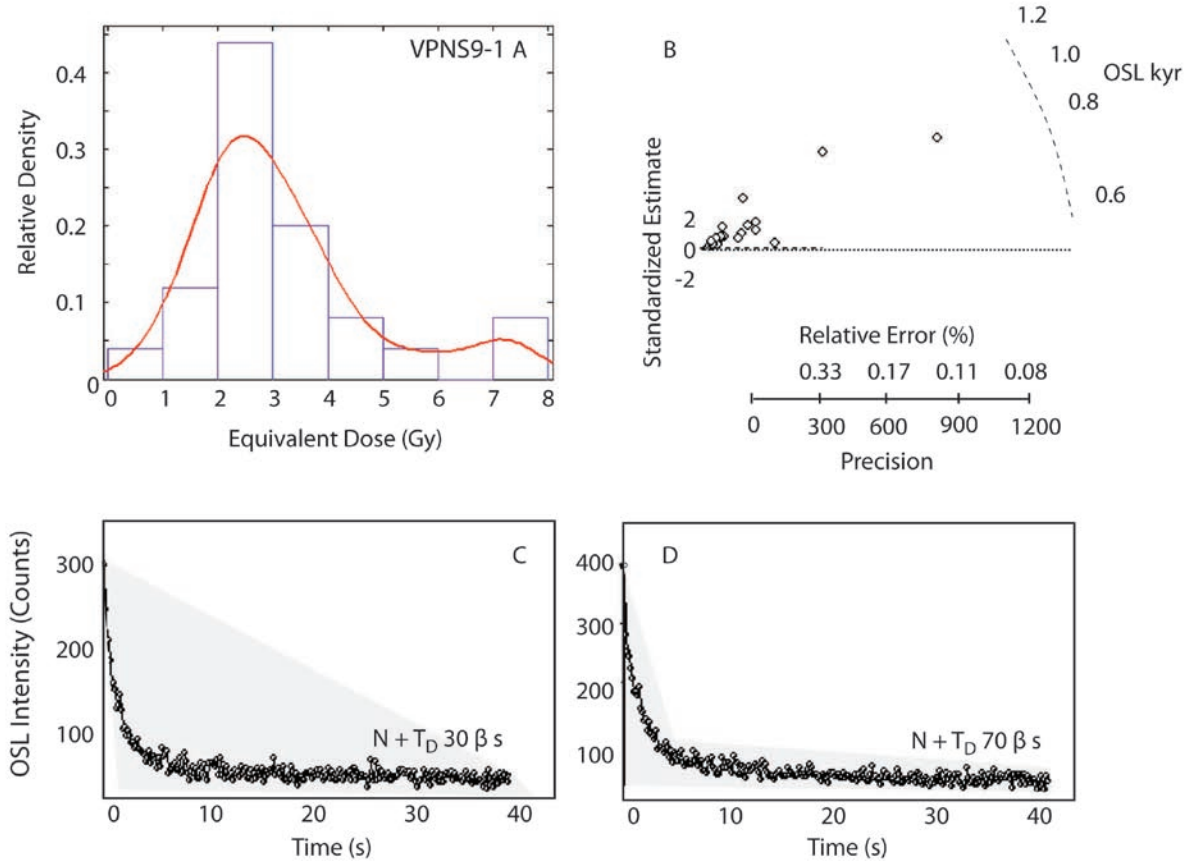

Figure 14 A-D, OSL results and shine down curves for Van Phuc aquifer sample VPNS9-1. The relative density curve (A) plots a histogram of the dose equivalent results from OSL-SAR in Gy. Calculating the depositional ages by dividing each paleo-dose by the sample's dose rate (Table 3), OSL ages can be determined. The sample's age distribution for all of the aliquots measured are plotted in B, a radial plot that graphs standardized age estimates against reciprocals of standard measurement errors (Galbraith 1990). Shine down curves of the sample's natural luminosity with a test dose added to check for sensitivity changes during measurement are shown in C and D.

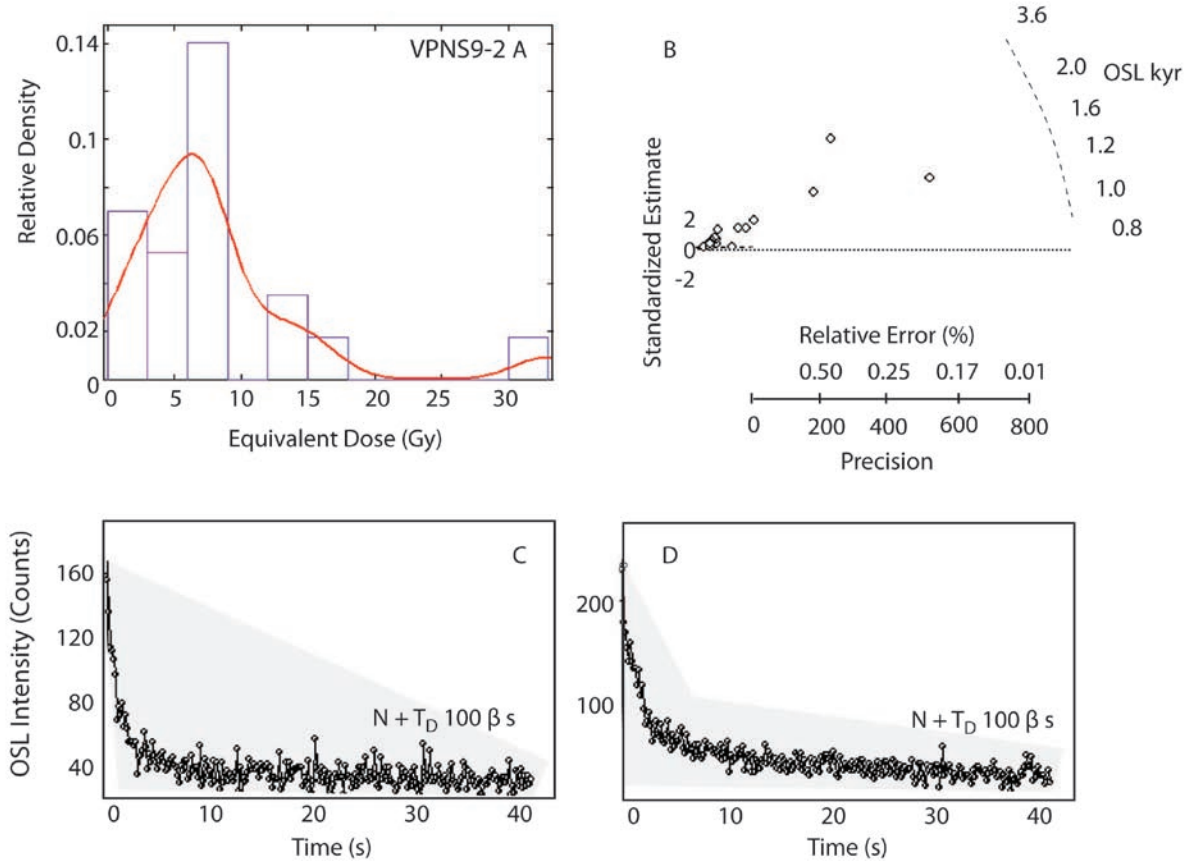

Figure 15 A-D, OSL results and shine down curves for Van Phuc aquifer sample VPNS9-2. The relative density curve (A) plots a histogram of the dose equivalent results from OSL-SAR in Gy. Calculating the depositional ages by dividing each paleo-dose by the sample's dose rate (Table 3), OSL ages can be determined. The sample's age distribution for all of the aliquots measured are plotted in B, a radial plot that graphs standardized age estimates against reciprocals of standard measurement errors (Galbraith 1990). Shine down curves of the sample's natural luminosity with a test dose added to check for sensitivity changes during measurement are shown in C and D.

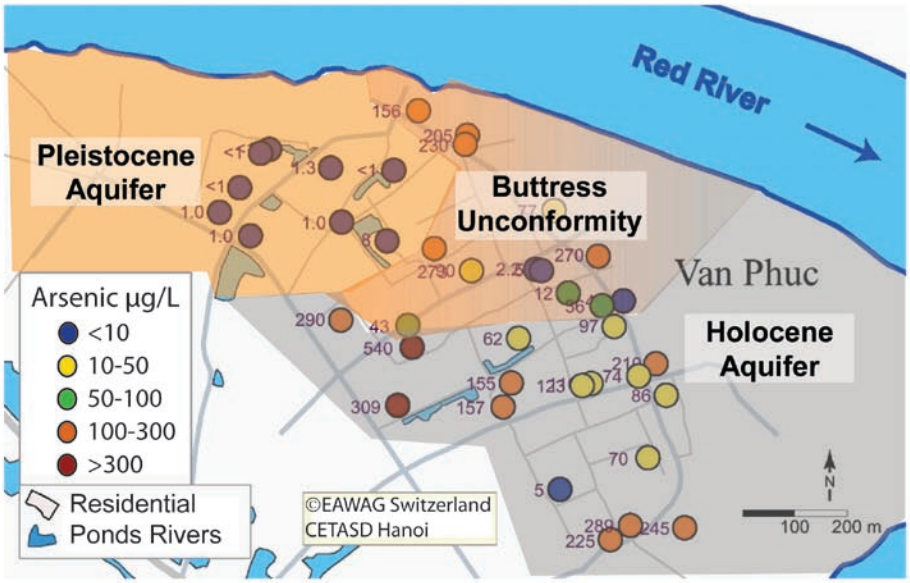

Figure 16 - The Van Phuc river bend shaded to show the different aged aquifers underlying the surface mud units (redrawn from Figure 5). Aquifer ages were determined using OSL quartz ages from samples collected along a needle-sampling transect, and corroborated by ^{14}C and replicate samplings. The results show that sediments in the same aquifer horizon have different depositional ages. When overlain with groundwater distributions, younger deposits appear more vulnerable to higher concentrations of dissolved arsenic.

As with the different concentrations of arsenic, the sediment reflectance and iron ratios, which are telling of the aquifer's sedimentary and aqueous redox conditions (Horneman 2004; van Geen, Zheng et al. 2006), also show a clear distinction between Van Phuc's orange and grey sand units. They also show distinct differences between the aquifers' overlying mud units. In the profiles, the grey sands have low reflectance values, consistently measuring below 0.2 (units of percent reflectance, between 10-40m). They are also capped by a mud unit that is a bit more reflective than the underlying sands, consistently measuring ~0.4. Alternatively, the orange sands in the northern bend, and their overlying muds, have a much larger dynamic range of reflectance values (<0.2-1). Opposite of the mud and sand trends in the southern portion of the bend, the muds here are less reflective and the sands are more reflective. Above the orange sandy aquifer, which is highly reflective (0.4-1%), the overlying muds (0-8m) measure <0.2-0.3 percent reflectance. The upper muds, between ~8-20m, show alternating 1-5m thick layers of different reflectance (i.e., a <0.2% reflectance mud between 10-12m, overlying a ~1% reflectance unit between 13-17m), presumably corresponding to a genetically different succession of muds than the more southern capping.

The leachable Fe(II)/Fe ratios along Van Phuc's profile span the 0.1-0.9 range, with, again, a stark distinction in iron ratios ~0.4km into the transect (Figure 17, third panel). Low Fe(II)/Fe ratios in the 0.1-0.4 range coincide with the orange sands, which are also values characteristic of older orange-brown sands associated with lower groundwater arsenic (<10 μg/L) in our other needle-sampling transects (van Geen 2008). Overall, the proportion of transect samples with Fe(II)/Fe <0.5 in Van Phuc (0.2) is between the proportion for transects in Balia Para, Bangladesh (0.05, (van Geen, Zheng et al. 2006)) and Chakdaha, India (0.4, (Metral 2008)), suggesting that Van Phuc's aquifer redox conditions are generally more reducing than Bangladesh but less reducing than India. Lower leachable Fe(II)/Fe ratios are in the upper, northern portion of the riverbend, corresponding to the more reflective orange sandy aquifer.

The estimated time elapsed since recharge into the aquifer, obtained by measuring both the ^{3}H and the concentrations of its stable daughter, the noble gas ^{3}He (Frei 2007; Stute 2007), range in the aquifer from 5 to >55 years, with >55 years ages assigned to pre-bomb water (Figure 17, lowermost panel). The $^{3}He/^{3}H$ results show recent recharge in both the northern and southern parts of the transect (VPNS6, VPNS3, and VPNS2), presumably from recent hyporheic exchange with the Red River. Thus have low reflectance values, consistently measuring below 0.2 (units of percent reflectance, between 10-40m). They are also capped by a mud unit that is a bit more reflective than the underlying sands, consistently measuring ~0.4. Alternatively, the orange sands in the northern bend, and their overlying muds, have a much larger dynamic range of reflectance values (<0.2-1). Opposite of the mud and sand trends in the southern portion of the bend, the muds here are less reflective and the sands are more reflective. Above the orange sandy aquifer, which is highly reflective (0.4-1%), the overlying muds (0-8m) measure <0.2-0.3 percent reflectance. The upper muds, between ~8-20m, show alternating 1-5m thick layers of different reflectance (i.e., a <0.2% reflectance mud between 10-12m, overlying a ~1% reflectance unit between 13-17m), presumably corresponding to a genetically different succession of muds than the more southern capping.

The leachable Fe(II)/Fe ratios along Van Phuc's profile span the 0.1-0.9 range, with, again, a stark distinction in iron ratios ~0.4km into the transect (Figure 17, third panel). Low Fe(II)/Fe ratios in the 0.1-0.4 range coincide with the orange sands, which are also values characteristic of older orange-brown sands associated with lower groundwater arsenic (<10 μg/L) in our other needle-sampling transects (van Geen 2008). Overall, the proportion of transect samples with Fe(II)/Fe <0.5 in Van Phuc (0.2) is between the proportion for transects in Balia Para, Bangladesh (0.05, (van Geen, Zheng et al. 2006)) and Chakdaha, India (0.4, (Metral 2008)), suggesting that Van Phuc's aquifer redox conditions are generally more reducing than Bangladesh but less reducing than India. Lower leachable Fe(II)/Fe ratios are in the upper, northern portion of the riverbend, corresponding to the more reflective orange sandy aquifer.

The estimated time elapsed since recharge into the aquifer, obtained by measuring both the ^{3}H and the concentrations of its stable daughter, the noble gas ^{3}He (Frei 2007; Stute 2007), range in the aquifer from 5 to >55 years, with >55 years ages assigned to pre-bomb water (Figure 17, lowermost panel). The $^{3}He/^{3}H$ results show recent recharge in both the northern and southern parts of the transect (VPNS6, VPNS3, and VPNS2), presumably from recent hyporheic exchange with the Red River. Thus, there's recent recharge into *both* of the orange and grey sand aquifers. Unlike the recent inputs, older groundwater underlies the middle portion of the aquifer (0.2-0.4km, VPNS1-VPNS4), which is made up primarily of orange sands. Older groundwater is also seen at the surface and at depth in the multi-wells at VPNS2, outlining a recharge plume flowing north and recharging the aquifer. Basically, this pattern shows inflow into the aquifer from the Red River.

Unbreached by any significant recent recharge, the older groundwaters of VPNS1 have $^{3}He/^{4}He$ ratios lower than atmospheric equilibrium. This suggests that the groundwaters in this orange sand section recharged well before the beginning of nuclear bomb testing (1955). It also suggests that the residence time of groundwater in VPNS1 and VPNS4 orange sands remained small enough that no significant amount of terrigenic ^{4}He was able to accumulate. Different than VPNS1, the groundwaters in the grey sands of VPNS2 (10-40m) have $^{3}He/^{4}He$ ratios greater than or equilibrated to the atmosphere, indicating accumulation of ^{3}He in the groundwater due recent recharge. In VPNS2's bottommost sample (46m), there are orange sands similar to VPNS1, with similar old groundwater. In comparison to the other geochemical profiles, the groundwater age patterns follow a similar interfingering ~0.4km into the transect, again conforming to the aquifer's orange and grey sand facies. The pattern, for the most part, conforms to younger groundwater in the more recent grey sands in the southern part of the bend, and older groundwater in the older orange sands shallowing in the north and underlying the grey sands in the south.

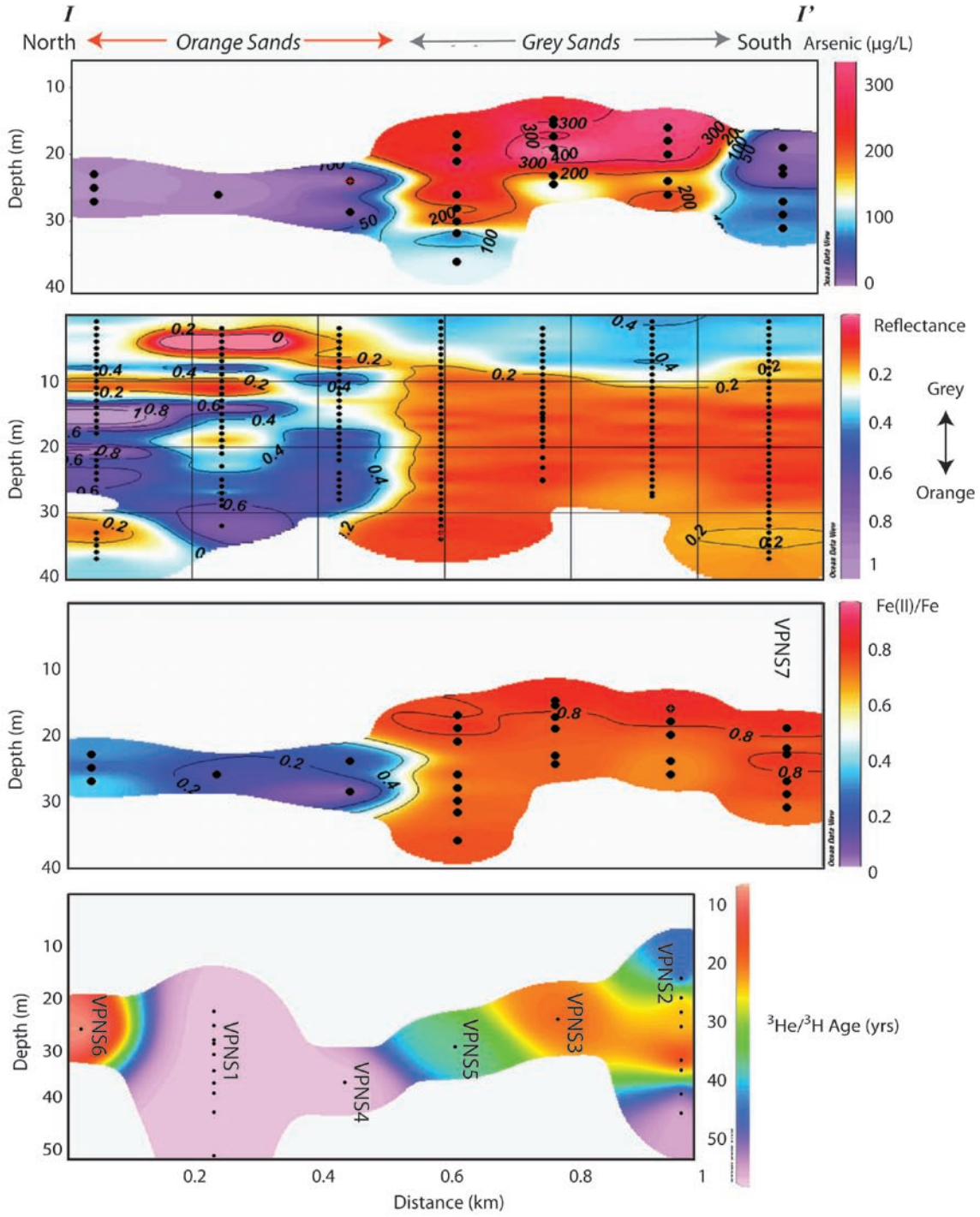

Figure 17. Profiles of the geochemical results of needle-sampling transect I-I', bisecting the Van Phuc village. From top to bottom, transects of groundwater arsenic, sediment reflectance, iron ratios, and groundwater ages. Groundwater ages were measured by Felix Frei at EAWAG. The sediment reflectance and iron ratios are notably different between the older (I) and younger (I') river bend areas, with lower reflectance (grey sands) and higher iron II/iron ratios (more reducing) in the younger, higher As sands (I'). Combined with sediment type and ages (Figure 16), the sands comprising the same ~20m depth horizon, in the upper, less contaminated aprt of the village have OSL ages of ~15kyr and older waters (>55yrs), while the lower, more contaminated part of the river bend is underlain by younger sands and waters, dating to ~800 and 10-30 years, resplectively.

4. Discussion

4.1 Support for the Geomorphic Control of Arsenic in the River Bend

Results from detailed transects across the Van Phuc riverbend show that the aquifer is comprised of both different aged water and sediments. The findings of different-aged water contributing to arsenic heterogeneity is not a new finding, and previous studies ($^3He/^3H$, time series, and OSL by ((Stute 2007), (Cheng 2005), and (Weinman 2005)) in Araihazar, Bangladesh converge on the idea that aquifers can continually weather and release arsenic at rates comparable to ~10-20μg L^{-1} yr^{-1}. That means that without adequate recharge and flushing, Araihazar's aquifers have the ability of becoming contaminated (relative to the WHO 10μg L^{-1} arsenic standard) within a year's time span. An interesting and important difference in the Van Phuc results is that, unlike Araihazar, there is less of a simple link between groundwater age and arsenic. This is important because it could mean that Van Phuc's aquifer (and other areas along the Red River) performs/behaves differently than Araihazar's in cycling its arsenic. This is a key finding because of the implications it has for extrapolating the vulnerabilities from one field site to another arsenic prone setting (including another field-site in the same country).

Considering that the recharge into Van Phuc's riverbend follows a horizontal gradient, with most of the recharge coming into the meander from the south (i.e., the flow gradient goes north towards Hanoi, instead of downriver, due to Hanoi's groundwater abstraction; Montagero, Anh et al. 2006), the highest groundwater arsenic should occur in the northern, upstream part of Van Phuc's meander according to the hydrological flow model (Cause 1, Figure 3). Instead, the highest occurrence of dissolved arsenic is in some of Van Phuc's youngest groundwaters. This is particularly true for the southern part of the meander. A comparison of groundwater age vs. dissolved arsenic shows VPNS1's oldest waters with the least amount of arsenic, although it does also support that some arsenic ingrowth

is occurring: the dissolved arsenic and groundwater ages from the Holocene aquifer shows that there is a modest ~4-5µg L^{-1} yr^{-1} release rate of arsenic in the recently deposited sand units (Figure 18). This is lower than the 10-20 µg L-1 yr-1 ingrowth seen in other shallow aquifers (Stute 2007; Larsen, Pham et al. 2008), but it does indicate that in the recently deposited sand units, there is probably an ongoing release of arsenic into the groundwater.

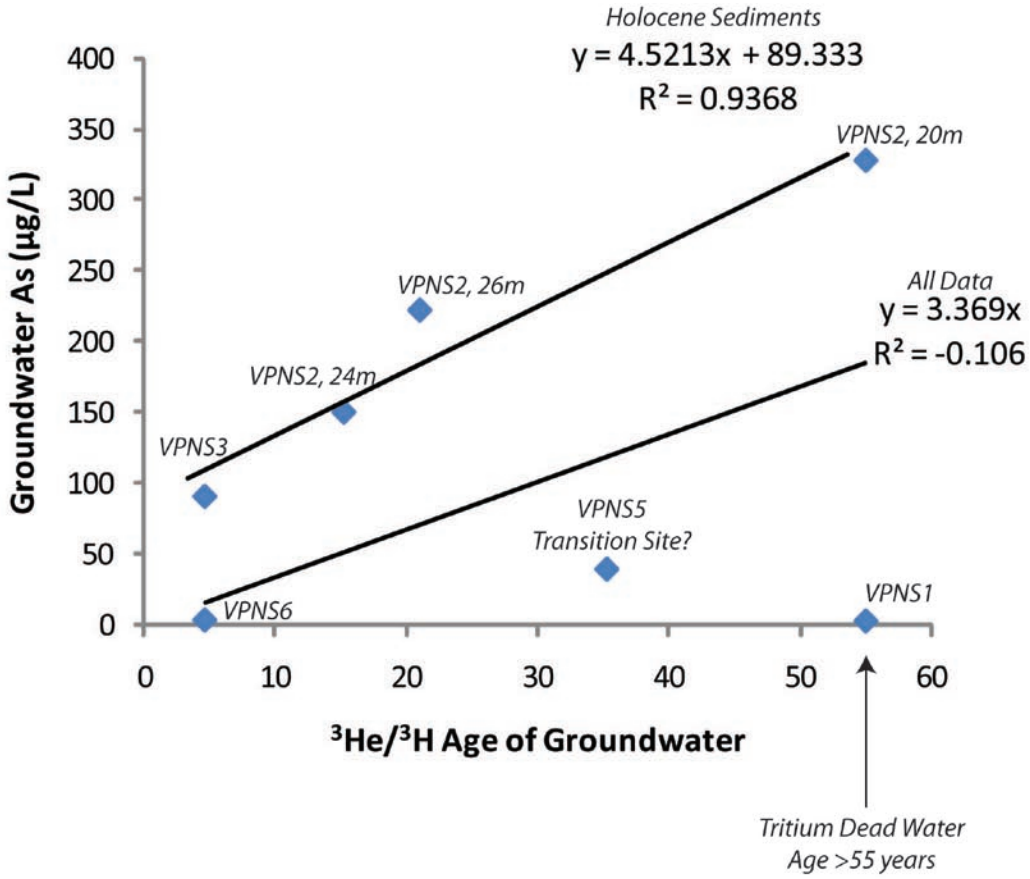

Figure 18, showing the correlation of groundwater ages to dissolved arenic concentrations in the needle-sampling transect of Van Phuc's aquifer. The helium-tritium groundwater ages were measured by F. Frei at EAWAG, and the arsenic concentrations were measured by L. van Geen at Lamont Doherty Earth Observatory after the 2006 field-sampling. Two trend lines are drawn for the data, the lower regression being for all of the data and the upper line regressing only samples from the higher-arsenic, Holocene aquifer (determined by OSL age-dating). The graph shows that for the entire set of samples, there is not as much of an arsenic-age trend than when only considering the higher-arsenic samples.

Unlike the Holocene unit, sands deposited during the Pleistocene do not show an ongoing release of arsenic. Groundwaters that were sampled for both groundwater age and dissolved arsenic in or near the Pleistocene units fall below the ~4-5µg L^{-1} yr^{-1} release rate seen for the Holocene unit (Figure 18). This indicates that the older units are not currently leaching arsenic into the groundwater. VPNS6 and VPNS1 are both located in the low-arsenic part of the riverbend (3-4µg/L), and VPNS5 is next to the buttressing unconformity of the Holocene and Pleistocene aquifer units (Figures 6 and 17). This is important because it indicates that as groundwater travels upstream through the Holocene sands and into the Pleistocene unit, reactive transport is likely taking place and removing arsenic out of the groundwater. Thus, the Pleistocene unit is probably acting like a natural filter, with the older, more indurated sands immobilizing arsenic in the surficial oxides imparted during the lowstand lateritic weathering, >15kya (i.e., the orange FeOOH phases). These more crystalline phases are more resistant to dissolution and weathering, and supported by the lower P-extractable phases measured from the older units—less than 0.3mg/kg As in the Pleistocene sands and 1-7mg/kg As in the Holocene sand unit (van Geen 2008).

The overall importance of Figure 18 is that it shows how hydrology and sedimentology can each explain Van Phuc's heterogeneity. The upper trend line explains a hydrologically produced heterogeneity within the young, Holocene aquifer, and the samples falling below the line show a strong sedimentological control. The fact that the Figure 18 shows groundwaters the same age with different arsenic concentrations suggests that all of the heterogeneity within the river bend *cannot* be primarily from hydrology (Cause 1, Figure 3). Without hydrology, and with such good visual correlations in the profiles of aquifer deposits and the aquifer geochemistry, Van Phuc's groundwater arsenic heterogeneity is also strongly controlled by differences in the meander's *sediment facies*. This would corroborate why the geochemical profiles of dissolved arsenic, reflectance, and Fe-ratios conform so

well to the aquifer sedimentology (Figures 6 and 17), meaning that how the riverbend evolved is an important aspect of understanding the arsenic distributions in today's groundwater.

4.2. The Evolution of Van Phuc's Aquifer and River Bend

Along with other stratigraphic work in the Red River (Tanabe, Saito et al. 2006; Larsen, Pham et al. 2008), the sedimentology and OSL dates recorded here indicate that the modern-day aquifer of Van Phuc evolved from an incised Pleistocene valley. The old valley fill has since been cut down by the Red River and infilled with modern channel and point bar sequences. These young deposits in Van Phuc are quite novel in that they record more recent and inland sediment accommodation taking place after 6kyr--a time that is typically gapped by other cores in the region (Tanabe 2003; Tanabe, Hori et al. 2003; Hori, Tanabe et al. 2004; Tanabe, Saito et al. 2006). The young deposits also overlie a Pleistocene sequence boundary at ~20m depth, which is substantially shallower than the surface in other corings (>40m). Given that more and more studies are showing Pleistocene aquifers in Asia's arsenic-prone regions as being somehow less vulnerable and/or free of arsenic in the drinking water (McArthur 2008; Michael and Voss 2008), mapping the depth of this boundary and the layout of the deposits is becoming increasingly important.

The youngest Pleistocene ages in the northern, low arsenic part Van Phuc have OSL ages dating to ~15kyr. This marks the sequence boundary unconformity between the Pleistocene and Holocene fluvial-estuarine-deltaic sediments (Figure 7, (Tanabe, Saito et al. 2006)). These ~15kyr orange sands suggest some active deposition occurred in the area during the Late Pleistocene, followed by a very Late-Pleistocene/Early Holocene period of emergence and lateritic weathering (<15-9kyr, a ~6-kyr period of weathering and non-deposition). This would explain the oxic and less reducing character of the Pleistocene sand facies, and why this portion of the aquifer may interact with arsenic differently than the southern more recent sand facies.

Following the 15-9kyr period of emergence and weathering, the Red River delta was progressively transgressed until ~9kyr (Li, Saito et al. 2006). During the transgression, areas southwest of Hanoi, along a former pathway of the Red River were extensively drowned in the Song Hong/Red River's Drowned River Valley (Figure 19, top left panel). This former corridor of the Red River followed a Mesozoic trough near the southwestern part of the Pleistocene drowned valley, which today comprises the Day estuary/river area near Ninh Binh (Figure 19, lower left panel, Luu, Garnier et al. 2010). As sea

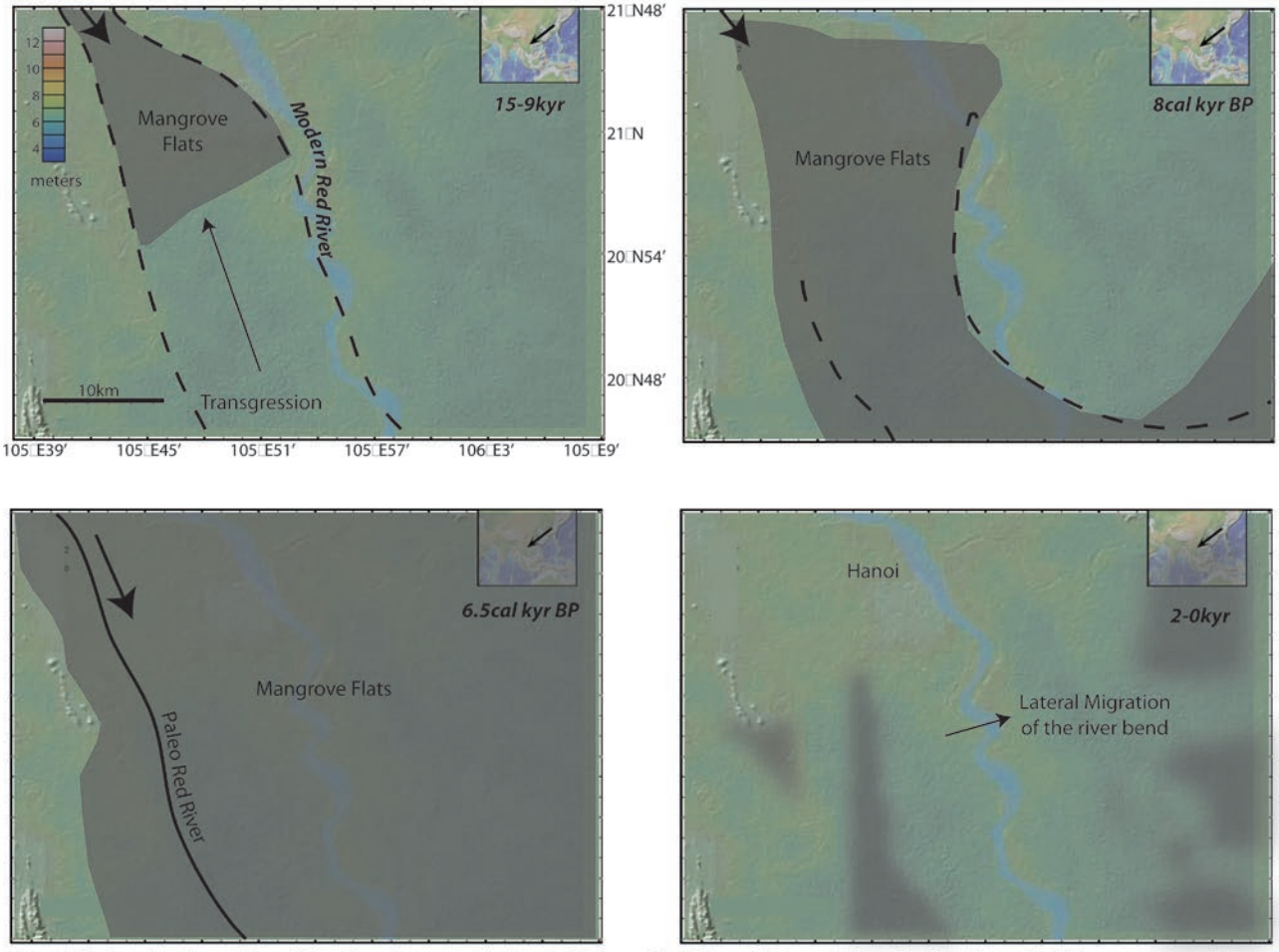

Figure 19, showing the setting of Van Phuc in context to the last 15kyr of Red River delta evolution. The locations of old river courses, paleo-shorelines, and mangrove flats are from Tanabe et al., 2006. Today's Global Multi Resolution Topography of the area is included in each panel to compare the modern setting with each of the previous environments picked up by the OSL and ^{14}C dated deposits.

level rapidly rose in the early Holocene, the drowned Red River valley aggraded ~25m between 8-10kyr (Tanabe, Hori et al. 2003), which we interpret correlative to the bluish-whitish estuarine and subtidal facies in Van Phuc's northern meander (Unit 2 , Figure 7; 12-19.5m, Supplemental 1). This timing coincides with the timing of the delta's maximum inundation period (Tanabe, Saito et al. 2006), indicating that the paleosea was able to transgress inshore of Van Phuc ~9kya—this is important because it enlarges the extent of the known inundated surface.

Between 9-6kyr, sea level stopped rising, letting the drowned valley infill during the Holocene highstand. During this time, the delta's shoreline migrated seaward with mangrove areas developing in marginal areas surrounding the mouth of the Red River (Tanabe, Saito et al. 2006). This retrogradation of the shoreline is recorded in Van Phuc by the presence of peaty mangrove clays (Unit 3.5; 10-12m Supplemental 1). In Van Phuc, this mangrove unit overlies the transgressive subtidal clays in the north part of the meander, with a ^{14}C peat age of 6.5 kcalBP (Figure 7, VPNS1, ~12m). This timing agrees with other ^{14}C ages from other cores where this unit is present (CC core ~3m), and places the history recorded in Tanabe et al.'s CC core (2006) equivalent to the deposition between 10-20m in VPNS1 facies (Figure 7). This means that while the entire 30m of the CC core is a high resolution account of the transition from an drowned estuary to a more stabilized delta, the Van Phuc river-bend transect gives a better account of what was happening before and after this 9-6kyr period. The limit of the CC core to the estuarine and old delta front makes sense given its more seaward location, and the inclusion of more recent fluvial facies in the stratigraphy of Van Phuc also makes sense because of its Red River proximity. Why the Pleistocene boundary is so shallow in Van Phuc and why there is such differential accommodation remains unclear, it is likely due to the rapid incision and fault activity along the Red River.

Overlying the early Holocene transgressive- estuarine (Unit 2) and the high-stand delta facies (Unit 3.5), there is not too much active deposition near Van Phuc until ~1kyr. Such a time gap between

6-1kyr is not uncommon, and typically attributed to the onset of delta progradation during the last phase of sea-level rise (6-7kyr, (Tanabe, Saito et al. 2006)). Basically, the sedimentation switched from vertical aggradation to a seaward progradation of the delta front. With the paleo-shoreline seaward of Van Phuc and at CC by 8kyr, the area by Van Phuc transitioned from a marine influenced setting to a terrestrial part of the subaerial delta. By 8kyr, Van Phuc was part of the lower delta plain, until a time after 6.5kyr, when it transitioned into an upper delta. This is recorded in the meander by an oxidized, less organic, and sandier unit ~10m in the northern meander (Figure 7 and Supplemental 1, Unit 3.6). The mangrove unit grades into this fining-upwards intertidal-channel facies ((~5-10m VPNS6 and 1, Figure 7), showing the initiation and takeover of fluvial dominance in this part of the delta. While we were unable to capture an OSL sample dating the initiation of incision of the Red River on this (eastern) side of the drowned river valley, Tanabe et al. place the Red River in its current drainage ~4kyr, which is close to the 3kyr timing of the Thai Bin/Duong River's faulted bisection and stabilization within the nearby Bac Ninh province (Sleeman 2000).

Once in Van Phuc, the Red River incised up to 55m below the surface, producing a sharp Pleistocene-Holocene contact grading from 20-55m deep over a lateral distance of only ~1km in the river bend (the slope is ~0.035). The earliest and only date of the Red River occupying Van Phuc dates to 0.8kyr using optical luminescence (VPNS7, 17m), inferring the stabilization of the Red River along its current corridor for the past ~4kyr. Within the last 1kyr, the OSL sample from VPNS7 suggests that Van Phuc underwent a change from a proper river channel into a point bar/ proximal scroll plain area. The facies that cap the Holocene Red River sands are comprised of abandoned channel-fill (Unit 3.6, ~5-10m) and floodplain surface soils (Unit 3.7, ~0-5m). The OSL age in VPNS1 suggests that the Red River started migrating away from Van Phuc ~600 years ago, meandering eastward to its present day location (Figure 19, bottom right panel).

4.3. The Evolution of Arsenic in the Groundwater of Van Phuc

While the sedimentology and OSL ages tell the story of Van Phuc's aquifer evolution and a persuasive connection between aquifer sedimentology and arsenic, it does not tell the full story of how its groundwater became contaminated with arsenic. Were these deposits always vulnerable to arsenic, or is vulnerability something that has developed recently, only after the onset of Holocene conditions? The $^{3}He/^{3}H$ ages help fulfill the story, although it is difficult to tell whether or not groundwater in the Pleistocene alluvium was ever as vulnerable to arsenic as the Holocene sands are today. The $^{3}He/^{3}H$ ages show that recharge is entering the riverbend laterally, recharging the bend horizontally through both the Pleistocene and Holocene deposits (Figure 17, bottom panel). With the water being sourced from both types of deposits, both can serve as weathering sources for accumulating arsenic along a flow path. Since arsenic is only elevated within the Holocene alluvium, and since the recharge flow direction travels mostly northwards from the Holocene and into the Pleistocene unit, it is therefore likely that arsenic is being sourced from weathering of the Holocene unit.

The natural weathering of arsenic from Holocene sands has been supported as a mechanism for arsenic release in Bangladesh by groundwater aging and column studies (Radloff, Cheng et al. 2007; Stute 2007). In Van Phuc, a weathering mechanism also can be inferred from mass-loss differences along the transect. High-resolution bulk geochemical studies of cores taken from the high and low arsenic regions (VPNS2 and VPNS1, respectively) show slightly higher arsenic concentrations in the Holocene sand unit (Eiche 2008). The Pleistocene sands (Unit 0) comprising the aquifer in the low arsenic site average ~2mg/kg As, while the remnant Red River channel sands making up the high arsenic site average between ~5mg/kg As (Figure 3 in Eiche et al., 2008). Estimating using a the 4µg L^{-1} yr^{-1} arsenic weathering rate (Figure 18), a particle density of 2.65g/cm^{3}, and an aquifer porosity of 0.25 (van Geen 2008), it would take ~8-13kyr to produce the mass loss difference in arsenic. This estimation is a reasonable approximation given the age of the units as well as their similar results in overall mineralogy

(Eiche 2008). It also gives us an idea about the minimum amount of time needed for the Holocene aquifer to weather-out its arsenic: with present conditions, it should take at least eight thousand years.

Because of the possibility that the Pleistocene sands underwent weathering during a previous depositional cycle, we cannot say for certain that Van Phuc's grey Holocene sands are the perfect unweathered analogue for the Pleistocene unit. The groundwater age results and aquifer sedimentology, however, do indicate that the Holocene aquifer is undergoing weathering. Because of the continuous interaction between groundwater and sediments, weathering is likely also still occurring in the Pleistocene unit, although it should be much slower than the Holocene aquifer. Older, weathered material tends to weather slower than fresh material (White 2003), and there are similar low total organic carbon contents in both sand units (<0.1%, (Eiche 2008)). In the low sedimentary organic content of the two units, the organics in the more recent, high arsenic deposits are presumably more labile, especially given the inferred lateritic degradation experienced during the older unit's oxic exposure during the Pleistocene lowstand (Hartog, Griffioen et al. 2002; Hartog, Griffioen et al. 2005).

Ultimately, the origin of the groundwater heterogeneity along the riverbend is controlled by the different deposits comprising the bend and their evolution. Two different-aged aquifer units persist in the river bend, each with different geochemical behaviors due to the different extent of weathering experienced by the units. Whereas we were previously unclear as to the origin of the redox contrast between the low and high arsenic sights (Eiche 2008), the facies and geochronological work here tells how the depositional history of Van Phuc's aquifer is responsible for the sedimentological and groundwater heterogeneity. The more recently deposited grey Holocene sands have low reflectance values, consistently measuring below 0.2 (units of percent reflectance), indicating the prevalence of more reduced iron phases in the matrix—the darker, Fe^{2+} minerals reflect less light during spectral analysis, resulting in lower reflectance measurements (Figure 17, second panel, (Horneman 2004)). An advanced state of reduction in the particulate phase as well as groundwater anoxia are further indicated

in the grey sands by their leachable Fe(II)/Fe ratios (van Geen 2008). This ratio, again, plots the prevalence of Fe^{2+} in the labile surficial phases of the sediments, with higher ratios equating to more reducing, less oxic aquifer conditions. Tending towards a steady state, higher ratios will favor the stability of more reduced iron phases, such as machinawite (FeS_{1-x}), greigite (Fe_3S_4), and FeS (Canfield, Raiswell et al. 1992; Wang and Morse 1996). As the grey sands have iron ratios >0.7, these portions of the aquifer are more reduced in their solid (and presumably aqueous) phase, which coincide with the profile's patterns of low reflectance (<0.2) and high groundwater arsenic (>200µg/L, Figure 17, first – third panels).

The lateritic Pleistocene sands, on the other hand, have much higher reflectance then the Holocene grey sands (>0.4, Figure 17), which is typical of sediments coated with iron-oxyhydroxides—rusty coatings that give sands an orange color. These phases are natural diagenetic alterations that occur, over time, due to the weathering of less stable primary mineral phases. More reactive primary iron minerals weather (Canfield, Raiswell et al. 1992) and coat the surfaces of the remaining, more recalcitrant minerals—typically quartz sands coated with oxic iron phases (Cotter-Howells and Paterson 2000; Nickson 2000; Postma, Larsen et al. 2007; Eiche 2008). For iron, the main oxidation product is ferrihydrite, which is also known as amorphous ferric (hydr)oxide, hydrous ferric oxide, or $Fe(OH)_3$ phases (Thamdrup 2000). The presence of these oxic iron phases are thought to govern the mobility of arsenic between sorbed and aqueous phases in these aquifer systems (Zhang and Selim, 2008). This is because the amorphous hydrous iron oxide phases have some of the highest arsenic adsorption values, with K_d's ranging from 10^3 to more than 10^6 L kg^{-1} for As(III) and As(V) (Smedley and Kinniburgh, 2002, and references therein; Berg et al., 2006). Compared to other more ordered iron oxide phases (10^2-10^4 L kg^{-1}), reactive iron sulfides (10^3 L kg^{-1}) and quartz (10^1 L kg^{-1}) (Smedley and Kinniburgh, 2002; Wolthers et al., 2005), the role of the amorphous iron phases in Asia's ubiquitously nearly neutral [pH] and reducing [Eh] groundwaters is the pivotal control on arsenic availability. Thus, the absence and

presence of FeOOH coatings on the aquifer sediments, which is a product of time, is what ultimately controls the partitioning of arsenic in the system: in aquifer deposits comprised of orange, FeOOH coated sediments, the arsenic left after thousands of years of oxic weathering is less mobilizable and better trapped within a "stickier," higher K_d aquifer sand facies.

4.4. Comparison to Evolution in other As-Prone Asian Countries

While a link between arsenic heterogeneity and sedimentology is not new, (McArthur 2008; van Geen 2008; Weinman 2008), the sedimentological cause of arsenic heterogeneity in the shallow aquifer of Van Phuc is different from our previous findings (van Geen 2008; Weinman 2008). In our previous studies, the cause of arsenic heterogeneity in Araihazar is due to differences in "flushing" due to the 10-100m scale differences in the thickness of surficial mud units. The overlying mud thickness depends on the presence or absence of a paleochannel, which differentially filled in the land when the main stem of the Brahmaputra River avulsed from its eastern channel ~200 years ago. Thick muds (3 - 12m) were left infilling Araihazar's aquifer portions where river courses used to be (i.e., the proper channel "valleys"), with muds thinning (0 - 3m) over floodplains and leveed parts of the paleochannel. This then explains the current 10 - 100m arsenic heterogeneity in Araihazar's shallow aquifer: accumulation of arsenic occurs in aquifer portions underlying thicker mud units where recharge is inhibited, while dilution can occur in parts where the surface muds are thin and flushing can prevent arsenic from accumulating in the groundwater. Thus, in Araihazar, arsenic in the aquifer depends on the transmissivity of the upper ~3m of sediments—a scenario we hypothesized could also explain the heterogeneity in the Van Phuc meander (Cause 2, Figure 3).

Surprisingly, however, we did not find the same sandy outcroppings and thin mud units overlying the low arsenic areas of Van Phuc's river bend. Instead, drilling in Van Phuc reveals a more uniformly thick surficial mud layer (~20m), which is quite different than the differential mud thicknesses

in Araihazar (0-13m). Additionally different, the surface muds overlying Van Phuc's low arsenic area are actually thicker than the muds overlying its higher arsenic area: the muds at the high-resolution, low arsenic core site in the north (VPNS1) are ~25m thick, while the muds in the higher arsenic core site to the south (VPNS2) are only 13m thick. This is opposite to the surficial mud thickness and arsenic trends we saw in Araihazar, where thicker muds overlie areas with higher groundwater arsenic (Aziz 2008; Weinman 2008).

The ubiquitously-thick surficial muds do not totally agree with our original geomorphic/sedimentological hypothesis for explaining the heterogeneity of arsenic within the river bend. As in Araihazar, we thought to find a scenario where Van Phuc's arsenic heterogeneity could be explained by differentially thick surface muds that were left as the Red River's meander migrated downriver (Cause 2, Figure 3). Abandoned portions of the meander would have infilled with muds, capping the aquifer, favoring arsenic accumulation in the southern part of the riverbend's groundwater. The sediment facies and OSL ages in the southern part of the river bend support a recent, ~1-2kya eastward migration of the meander (Figure 19), with the grey, reducing sands of the southern meander relating to a former thalweg of the Red River. The facies and OSL ages in the bend's northern aquifer, however, are much older, and they not conformable with the more recent Red River aquifer deposits (Figure 16). This means that, unlike the surficial-mud control of arsenic in Araihazar's shallow aquifer, heterogeneity in Van Phuc is controlled by a buttressing unconformity of two different types of shallow sandy deposits—a remnant low arsenic Pleistocene aquifer in the north and a higher arsenic Holocene aquifer in the southern meander.

So far, the only study are displaying a sedimentological control somewhat similar to Van Phuc is seen in the JAM site of West Bengal, India (McArthur 2001; McArthur 2004; McArthur 2008). A comparison of the aquifer facies from several field-sites shows that Van Phuc and JAM have the most similarity in both depositional type and timing (Table 7). From their work in JAM, McArthur et al. put

forth a model where extensive paleosols were deposited at the Last Glacial Maximum (LGM, ~20kyr), providing a hydrological barrier for arsenic drawdown vertically into the Pleistocene unit. Our findings from the Van Phuc transect show a horizontal transition from Holocene to Pleistocene sands, with no red-clay paleosol unit (LGMP) vertically preventing a "draw" or invasion of arsenic (and perhaps organic) into Van Phuc's older sand unit. The red clays deposited above the 15kyr Pleistocene sands in the northern, low arsenic part of the meander are part of Unit 2 (likely facies 2.2), an estuarine facies deposited after the Pleistocene-Holocene transition (Tanabe, Saito et al. 2006). This finding, along with the lack of a LGMP in other study sites (Table 7), supports more of a surface complexation-reactive transport process within the old sand, instead or too. So, the LGMP, while it functions as the authors suggest in their study site, may not explain the vulnerability of As-pollution worldwide (and hence, it may not be a worldwide datum).

In comparing our findings of arsenic heterogeneity in Van Phuc to other arsenic-prone regions, we only see this type of surprising arsenic- and aquifer-age similarity so far in the work we've done in Parasi, Nepal (next chapter). To qualify why this age trend was a surprise, it was because there was no surface expression or topographic indication of the Pleistocene-Holocene aquifers abutted adjacent to each other. In other words, unlike the more obvious uplifted Pleistocene terraces in Bangladesh, like the Dupi Tilla outcropping just north of Araihazar, there was no obvious surface geomorphology in Van Phuc that gives away the mud-capped Pleistocene surface. Pleistocene outcroppings in the Red River delta are typically thought to shallow north of Hanoi, and were beneath >20m of Holocene sands in Dan Phoung-Red River meander study (Dan Phoung is ~40 km northwest of Van Phuc and ~60km northwest of CC). Geomorphically speaking, this may mean that many low-arsenic aquifers cannot be identified from remote satellite imagery-type studies alone, emphasizing the importance of knowing the subsurface conditions in a local aquifer setting (i.e., 100m-scaled sedimentology, hydrology, and (bio)geochemistry).

5. Conclusion

The conformation of $^{3}He/^{3}H$, Fe-ratios, reflectance, and dissolved arsenic to the different deposits within the riverbend nevertheless support the idea that the sediments—the stratigraphy—are still the prime controls over the riverbend's arsenic availability. In the north part of the meander—the upper portion of the riverbend—old, Pleistocene sands comprise the aquifer deposits, while younger, Holocene sands are in the south. At the same ~20m depth horizon, the northern, less contaminated part of the village has OSL ages of ~15,000 years and older waters (>55 years), while the southern, more contaminated area is underlain by younger sands and waters, dating to ~800 and 10-30 years, respectively. Sediment reflectance and iron ratios are also notably different between the older and younger areas, with lower reflectance (grey sands) and higher iron II/iron total ratios (more reducing) in the younger, high-As sands. The 6500 ^{14}C age BP of wood collected from the mud capping at 11m by VPNS1 indicates the upper part of the riverbend stabilizing earlier than the lower, more recently in-filled areas.

The presence of such different-aged deposits comprising the lone geomorphic unit of the meander, along with younger water in the south having higher groundwater arsenic, means that horizontal recharge (arsenic ingrowing over a flow path) and vertical flushing (via differential thicknesses of surficial muds) is not as important as the actual aquifer sedimentology—the facies comprising the aquifer. Results from detailed transects across the Van Phuc riverbend that the different aged-sediments have different redox conditions as well as different concentrations of dissolved arsenic, indicating that aquifer history exerts a strong control over arsenic heterogeneity. OSL dates indicate that the modern-day aquifer evolved from an incised Pleistocene valley, that has since been filled with Holocene channel and point bar sequences. Thus, it appears that a simple geomorphic unit, such as a 1km bend of stable river, can contain a complex range of deposits and geochemistries, signifying the importance of detailed sampling where arsenic and other contaminants are a concern.

References

Agusa, T., Takashi Kunito, Junko Fujihara, Reiji Kubota, Tu Binh Monh, Pham Thi Kim Trang, Hisato Iwata, Annamalai Subramanian, Pham Hung Viet, and Shinsuke Tanabe (2005). "Contamination by arsenic and other trace elements in tube-well water and its risk assessment to humans in Hanoi, Vietnam." Environmental Pollution.

Ahmed, K. M., Prosun Bhattacharya, M. Aziz Hasan, S. Humayun Akhter, S.M. Mahbub Alam, M.A. Hossain Bhuyian, M. Badrul Imam, Aftab A. Khan, and Ondra Sracek (2004). "Arsenic enrichment in groundwater of the alluvial aquifers in Bangladesh: an overview." Applied Geochemistry **19**: 181-200.

Aitken, M. J. (1985). Thermoluminescence Dating. London, Academic Press.

Allen, C. R., A. R. Gillespie, et al. (1984). "Red River and Associated Faults, Yunnan Province, China - Quaternary Geology, Slip Rates, and Seismic Hazard." Geological Society of America Bulletin **95**(6): 686-700.

Aziz, Z., A. van Geen, R. Versteeg, A. Horneman, Y. Zheng, S. Goodbred, M. Steckler, M. Stute, B. Weinman, I. Gavrieli, M. Shamsudduha, M.A. Hoque, and K.M. Ahmed (2008). "Arsenic Concentrations in Shallow Groundwater and the Electromagnetic Conductivity of Soils in Bangladesh." Water Resources Research **44**(W07416): doi:10.1029/2007WR006000.

Barbouti, A. I., and B.C. Rastin (1983). "A study of the absolute intensity of muons at sea level and under various thicknesses of absorber." Journal of Physics G: Nuclear and Particle Physics **9**: 1577-1595.

Berg, M., Caroline Stegel, Pham Thi Kim Trang, Phan Hung Viet, Mickey L. Sampson, Moniphea Leng, Sopheap Samreth, and David Fredericks (2008). "Magnitude of arsenic pollution in the Mekong and Red River Deltas--Cambodia and Vietnam." Science of the Total Environment **in press**.

Berg, M., Hong Con Tran, Thi Chuyen Nguyen, Hung Viet Pham, Roland Schertenleib, and Walt Giger (2001). "Arsenic contamination of groundwater and drinking water in Vietnam: A human health threat." Environmental Science & Technology **35**(13): 2621-2626.

Berg, M., S. Luzi, et al. (2006). "Arsenic removal from groundwater by household sand filters: Comparative field study, model calculations, and health benefits." Environmental Science & Technology **40**(17): 5567-5573.

Berg, M., C. Stengel, et al. (2007). "Magnitude of arsenic pollution in the Mekong and Red River Deltas - Cambodia and Vietnam." Science of the Total Environment **372**(2-3): 413-425.

Berg, M., P. T. K. Trang, et al. (2008). "Hydrological and sedimentary controls leading to arsenic contamination of groundwater in the Hanoi Area, Vietnam: the impact of iron–arsenic ratios, peat, river bank deposits, and excessive groundwater abstraction." Chemical Geology **249**: 91–112

BGS-DPHE, Ed. (2001). Arsenic contamination of groundwater in Bangladesh. British Geological Survey Technical report, WC/00/19, Keyworth.

Botter-Jensen, L., V. Mejdahl, et al. (1999). "New light on OSL." Quaternary Science Reviews **18**(2): 303-309.

Canfield, D. E., R. Raiswell, et al. (1992). "The reactivity of sedimentary iron minerals toward sulfide." American Journal of Science **292**: 659-683.

Cardenas, M. B. (2008). "The effect of river bend morphology on flow and timescales of surface water-groundwater exchange across pointbars." Journal of Hydrology **362**(1-2): 134-141.

Cheng, Z., A. van Geen, A.A. Seddique., and K.M. Ahmed (2005). "Limited temporal variability of arsenic concentrations in 20 wells monitored for 3 years in Araihazar, Bangladesh " ENVIRONMENTAL SCIENCE & TECHNOLOGY **39**(13): 4759-4766.

Cheng, Z., Y. Zheng, R. Mortlock, and A. van Geen (2004). "Rapid multi-element analysis of groundwater by high-resolution inductively coupled plasma mass spectrometry." Analytical and Bioanalytical Chemistry **379**(3): 512-518.

Clark, M. K., L. M. Schoenbohm, et al. (2004). "Surface uplift, tectonics, and erosion of eastern Tibet from large-scale drainage patterns." Tectonics **23**.

Clift, P. D., H. V. Long, et al. (2008). "Evolving east Asian river systems reconstructed by trace element and Pb and Nd isotope variations in modern and ancient Red River-Song Hong sediments." Geochem. Geophys. Geosyst. **9**.

Cotter-Howells, J. D. and E. Paterson (2000). Minerals and Soil Development. Environmental Mineralogy. D. J. Vaughan and R. A. Wogelius. Budapest, Eotvos University Press. **2:** 91-124.

Easton, W. H. (1960). Invertebrate paleontology. New York, Harper.

Eiche, E., T. Neumann, M. Berg, B. Weinman, S. Norra, Z. Berner, A. van Geen, P.T.K. Trang, P.H. Viet, and D. Stüben (2008). "Geochemical processes underlying a sharp contrast in groundwater arsenic concentrations in a village on the Red River delta, Vietnam." Applied Geochemistry **in press**.

Frei, F. (2007). Groundwater Dynamics and Arsenic Mobilization near Hanoi (Vietnam) Assessed Using Noble Gases and Tritium. Department of Environmental Sciences. Zurich, Swiss Federal Instutite of Technology. **M.S.:** 78.

Funabiki, A., S. Haruyama, et al. (2007). "Holocene delta plain development in the Song Hong (Red River) delta, Vietnam." Journal of Asian Earth Sciences **30**(3-4): 518-529.

Galbraith, R. F. (1994). "Some applications of radial plots." Journal of the American Statistical Association **89**(428): 1232-1242.

Goodbred, S. L. and S. A. Kuel (1998). "Floodplain processes in the Bengal Basin and the storage of Ganges-Brahmaputra river sediment: an accretion study using ^{137}Cs and ^{210}Pb geochronology." Sedimentary Geology **121**: 239-258.

Hartog, N., J. Griffioen, et al. (2005). "Depositional and paleohydrogeological controls on the distribution of organic matter and other reactive reductants in aquifer sediments." Chemical Geology **216**(1-2): 113-131.

Hartog, N., J. Griffioen, et al. (2002). "Distribution and reactivity of O-2-reducing components in sediments from a layered aquifer." Environmental Science & Technology **36**(11): 2338-2344.

Hori, K., S. Tanabe, et al. (2004). "Delta initiation and Holocene sea-level change: example from the Song Hong (Red River) delta, Vietnam." Sedimentary Geology **164**: 237-249.

Horneman, A., A. van Geen, D. Kent, P.E. Mathe, Y. Zheng, R.K. Dhar, S. O'Connell, M.Hoque, Z. Aziz, M. Shamsudduha, A. Seddique, and K.M. Ahmed (2004). "Decoupling of arsenic and iron release to Bangladesh groundwater under reducing conditions. Part I: Evidence from sediment profiles." Geochim. Cosmochim. Acta. **68**(17): 3459-3473.

Hug, S. J., O. X. Luepin, et al. (2008). "Bangladesh and Vietnam: Different Groundwater Compositions Require Different Approaches to Arsenic Mitigation." Environ. Sci. Technol. **42**: 6318-6323.

IODP-DPG (2008). Asian Monsoon and Cenozoic Tectonic History: Report of the Detailed Planning Group. Chair David Rea. Washington D.C.**:** 47 pages.

Larsen, F., N. Q. Pham, et al. (2008). "Controlling geological and hydrogeological processes in an arsenic contaminated aquifer on the Red River flood plain, Vietnam." Applied Geochemistry **23**: 3099-3115.

Li, Z., Y. Saito, et al. (2006). "Climate change and human impact on the Song Hong (Red River) Delta, Vietnam, during the Holocene." Quaternary International **144**: 4-28.

Luu, T. N. M., J. Garnier, et al. (2010). "Hydrological regime and water budget of the Red River Delta (Northern Vietnam)." Journal of Asian Earth Sciences **37**(3): 219-228.

Mathers, S. and J. Zalasiewicz (1999). "Holocene sedimentary architecture of the Red River Delta, Vietnam." Journal of Coastal Research **15**(2): 314-325.

McArthur, J. M., D.M. Banerjee, K.A. Hudson-Edwards, R. Mishra, R. Purohit, P. Ravenscroft, A. Cronin, R.J. Howarth, A. Chatterjee, T. Talukder, D. Lowry, S. Houghton, D.K. Chadha (2004). "Natural organic matter in sedimentary basins and its relation to arsenic in anoxic ground water: the example of West Bengal and its worldwide implications." Applied Geochemistry **19**: 1255-1293.

McArthur, J. M., P. Ravenscroft, D.M. Banerjee, J. Milsom, K.A. Hudson-Edwards, S. Sengupta, C. Bristow, A. Sarkar, S. Tonkin, and R. Purohit (2008). "How paleosols influence groundwater flow and arsenic pollution: A model from the Bengal Basin and its worldwide implication." Water Resources Research **44**(11): W11411.

McArthur, J. M., P. Ravenscroft, S. Safiullah, and M.F. Thirlwall (2001). "Arsenic in groundwater: testing pollution mechanisms for aquifers in Bangladesh." Water Resources Research **37**: 109-117.

Metral, J., L. Charlet, S. Bureau, S.B. Mallik, S. Chakraborty, K.M. Ahmed, M.W. Rahman, Z. Cheng, and A. van Geen (2008). "Comparison of dissolved and particulate arsenic distributions in shallow aquifers of

Chakdaha, India, and Araihazar, Bangladesh." Geochemical Transactions **9**(1): DOI 10.1186/1467-4866-9-1

Michael, H. A. and C. I. Voss (2008). "Evaluation of the sustainability of deep groundwater as an arsenic-safe resource in the Bengal Basin." Proceedings of the National Academy of Sciences of the United States of America **105**(25): 8531-8536.

Montagero, A., N. V. Anh, et al. (2006). Building the Concept of Material Flow Analysis into the Household- Centered Environmental Sanitation Planning Approach. Proceedings of the Conference on Renewed Efforts to Plan for Sustainable Development, Germany, EAWAG.

Moore, R. C., C. G. Lalicker, et al. (1952). Invertebrate Fossils. New York, McGraw-Hill Book Company, Inc.

Moores, E. M. and R. W. Fairbridge (1997). Encyclopedia of European and Asian regional geology. London, Chapman & Hall.

Murray, A. S., J. M. Olley, et al. (1995). "Measurement of equivalent doses in quartz from contemporary water-lain sediments using optically stimulated luminescence." Quaternary Science Reviews **14**: 365-371.

Murray, A. S. a. A. G. W. (2000). "Luminescence dating of quartz using an improved single-aliquot regenerative-dose protocol." Radiation Measurements **32**: 57-73.

Nagar, Y. C. (2007). Methodological aspects of radiation dosimetry of natural radiation environment using luminescence techniques: New minerals and applications. Physical Research Laboratory. Ahmedabad, India, Gujurat University. **Ph.D. Thesis:** 162.

Nickson, R. T., J.M. McArthur, P. Ravenscroft, W.G. Burgess and K.M. Ahmed (2000). "Mechanism of arsenic release to groundwater, Bangladesh and West Bengal." Applied Geochemistry **15**: 403-413.

Papacostas, N. C., B. C. Bostick, et al. (2008). "Geomorphic controls on groundwater arsenic distribution in the Mekong River Delta, Cambodia." Geology **36**(11): 891-894.

Polya, D. and L. Charlet (2009). "Environmental science: Rising arsenic risk?" Nature Geosci **2**(6): 383-384.

Postma, D., F. Larsen, et al. (2007). "Arsenic in groundwater of the Red River floodplain, Vietnam: Controlling geochemical processes and reactive transport modeling." Geochimica et Cosmochimica Acta **71**(21): 5054-5071.

Prescott, J. R., and J.T. Hutton (1994). "Cosmic ray contributions to dose rates for luminescence and ESR dating: large depths and long-term variations." Radiation Measurements **23**(2/3): 497-500.

Radloff, K. A., Z. Cheng, et al. (2007). "Mobilization of arsenic during one-year incubations of gray aquifer sands from Araihazar, Bangladesh." Environ. Sci. Technol. **41**: 3639-3635.

Rahman, M. M., R. Naidu, et al. (2009). "Arsenic contamination in groundwater in the Southeast Asia region." Environmental Geochemistry and Health **31**: 9-12.

Royse, C. F. (1968). "Recognition of fluvial environments by particle-size characteristics." Journal of Sedimentary Research **38**(4): 1171-1178.

Schaetzl, R., and S. Anderson (2005). Soils: Genesis and Geomorphology. New York, Cambridge University Press.

Singarayer, J. S., R. M. Bailey, et al. (2005). "Assessing the completeness of optical resetting of quartz OSL in the natural environment." Radiation Measurements **40**: 13-25.

Sleeman, G. (2000). Holocene paleogeography of the Bac Ninh Province, Vietnam. Geological Society of America Annual Meeting, Reno NV, Geological Society of America.

Stokes, S. (1992). "Optical dating of young (modern sediments using quartz: Results from a selection of depositional environments." Quaternary Science Reviews **11**: 152-159.

Stute, M., Y. Zheng, P. Schlosser, A. Horneman, R.K. Dhar, M. A. Hoque, A. A. Seddique, M. Shamsudduha, K. M. Ahmed, and A. van Geen (2007). "Hydrological control of As concentrations in Bangladesh groundwater." Water Resources Research **43**: W09417.

Tanabe, S., K. Hori, et al. (2003). "Song Hong (Red River) delta evolution related to millennium-scale Holocene sea-level changes." Quaternary Science Reviews **22**: 2345-2361.

Tanabe, S., K. Hori, Y. Saito, S. Haruyama, L.Q. Doanh, Y. Sato, and S. Hiraide (2003). "Sedimentary facies and radiocarbon dates of the Nam Dinh-1 core from the Song Hong (Red River) delta, Vietnam." Journal of Asian Earth Sciences **21**: 503-513.

Tanabe, S., Y. Saito, et al. (2006). "Holocene evolution of the Song Hong (Red River) delta system, northern Vietnam." Sedimentary Geology **187**(1-2): 29-61.

Thamdrup, B. (2000). Bacterial manganese and iron reduction in aquatic sediments. Advances in Microbial Ecology, Vol 16. New York, Kluwer Academic / Plenum Publ. **16:** 41-84.

van Geen, A. (2008). "Environmental science - Arsenic meets dense populations." Nature Geoscience **1**(8): 494-496.

van Geen, A., K. Radloff, Z. Aziz, Z. Cheng, M.R. Huq, K.M. Ahmed, B. Weinman, S. Goodbred, M. Berg, P.T.K. Trang, L Charlet, J. Metral, D. Tisserand, S. Guillot, S. Chakraborty, A.P. Gajurel, and B.N. Upreti (2008). "Comparison of arsenic concentrations in simultaneously-collected groundwater and aquifer particles from Bangladesh, India, Vietnam, and Nepal." Applied Geochemistry **23**: 3244-3251.

van Geen, A., T. Protus, Z. Cheng, A. Horneman, A.A. Seddique, M.A. Hoque, and .M. Ahmed (2004). "Testing groundwater for arsenic in Bangladesh before installing a well." Environmental Science & Technology **38**(24): 6783-6789.

van Geen, A., Y. Zheng, R. Versteeg, M. Stute, A. Horneman, R. Dhar, M. Steckler, A. Gelman, C. Small, H. Ahsan, J. H. Graziano, I. Hussain, and K. M. Ahmed (2003). "Spatial variability of arsenic in 6000 tube wells in a 25 km^2 area of Bangladesh." Water Resources Research **39**(5): 1140.

van Geen, A., Y. Zheng, S. Goodbred, A. Horneman, Z. Aziz, Z. Cheng, M. Stute, B. Mailloux, B. Weinman, S.H. Chowdhury, and K. M. Ahmed (2008). "Flushing history as a hydrogeological control on the regional distribution of arsenic in shallow groundwater of the Bengal Basin." Environ. Sci. Technol. **42**(7): 2283-2288.

van Geen, A., Y. Zheng, et al. (2006). "A transect of groundwater and sediment properties in Araihazar, Bangladesh: Further evidence of decoupling between As and Fe mobilization." Chemical Geology **228**(1-3): 85-96.

Wallinga, J. (2002). "On the detection of OSL age overestimation using single-aliquot techniques." Geochronometria **21**: 17-26.

Wang, Q. and J. W. Morse (1996). "Pyrite formation under conditions approximating those in anoxic sediments I. Pathway and morphology." Marine Chemistry **52**(2): 99-121.

Weinman, B. (2005). Controls of Floodplain Sediments and Evolution on Shallow Aquifer Development and the Distribution of Groundwater Arsenic: Araihazar, Bangladesh. Marine and Atmospheric Sciences. Stony Brook, Stony Brook University. **M.S. Thesis:** 73.

Weinman, B., S.L. Goodbred, Y. Zheng, A. van Geen, Z. Aziz, A. Singhvi, and M. Steckler (2008). "Controls of Floodplain Evolution on Shallow Aquifer Development and the Resulting Distribution of Groundwater Arsenic: Araihazar, Bangladesh." GSA Bulletin **120**(11/12): 1567-1580.

White, A. F., and S.L. Brantley (2003). "The effect of time on the weathering of silicate minerals: why do weathering rates differ in the laboratory and the field?" Chemical Geology **202**: 479-506.

Yu, W. H., Charles M. Harvey, and Charles F. Harvey (2003). "Arsenic in groundwater in Bangladesh: A geostatistical and epidemiological framework for evaluating health effects and potential remedies." Water Resources Research **39**(6): 1146.

Table 1. Cosmic dose rate calculations for OSL samples from Vietnam

Sample	Depth (m)	Latitude □	Longitude □	Latitude □	[1,2]Altitude (m)	D_{AVG}(Gy/kya) Modified Barbouti & Rastin 1983	F Prescott & Hutton 1994 - Appendix	H Prescott & Hutton 1994 - Appendix	J Prescott & Hutton 1994 - Appendix	D Corrected for Alt. and Lat.	Time Correction	D Corrected for Time Variation
VPNS6	23	20.9243	105.8904	9	7.5	0.12	0.40	4.36	0.53	0.11	1.02	0.11
VPNS7	17	20.9185	105.8986	9	7.5	0.12	0.40	4.36	0.53	0.12	0.97	0.11
VPNS9-OSL1	16.5	20.9249	105.8979	9	7.5	0.12	0.40	4.36	0.53	0.12	0.97	0.11
VPNS9-OSL2	23.7	20.9249	105.8979	9	7.5	0.12	0.40	4.36	0.53	0.11	0.97	0.11
VPNS10	5	20.9179	105.9100	9	7.5	0.16	0.40	4.36	0.53	0.15	0.97	0.15
VPNS11-OSL1	0	20.9179	105.9100	9	7.5	0.21	0.40	4.36	0.53	0.20	0.97	0.19
VPNS11-OSL2	4.2	20.9179	105.9100	9	7.5	0.17	0.40	4.36	0.53	0.16	0.97	0.15
VPNS11-OSL3	8.5	20.9179	105.9100	9	7.5	0.14	0.40	4.36	0.53	0.13	0.97	0.13

[1]Van Phuc elevation is based on the 4/20/06 river elevation survey.

Table 2. Concentrations of the main in-situ dosing elements

Sample	%K	^{232}Th (ppm)	±	^{238}U (ppm)	±
VPNS6	2.51	7.9	0.2	2.4	0.1
VPNS7	2.02	10.2	0.3	3.1	0.1
VPNS9-OSL1	2.05	8.4	0.2	2.6	0.1
VPNS9-OSL2	2.03	10.8	0.4	3.3	0.1
VPNS10	2.11	10.0	0.3	3.0	0.1
VPNS11-OSL1	1.66	9.7	0.3	2.9	0.1
VPNS11-OSL2	1.64	6.0	0.2	1.8	0.1
VPNS11-OSL3	1.85	5.5	0.2	1.67	0.05

Table 3. OSL results for Van Phuc's aquifer

Sample	Latitude (N) and Longitude (E)		Location/Setting	Depth (m)	SAR-NCF OSL Aliqouts (n)	Dose rate (Gy/kyr)	±	Mean Age (kyr)	±	Least 10% Age (kyr)	±	Histogram & Radial Plot Age (kyr)	sed rate (cm/yr) Least 10%	sed rate (cm/yr) Mean
VPNS6	20.92429	105.89043	Upper portion of Van Phuc's river bend (*I*), in an area with low groundwater arsenic (<5ug/L).	23	39	3.4	0.1	104	121	15.4	0.6	15	0.15	0.02
VPNS7	20.91848	105.89861	Lower portion of Van Phuc's river bend (*I'*), in an area with high groundwater arsenic (>300ug/L).	17	29	2.9	0.2	3	3	0.8	0.2	0.9	2.14	0.57
VPNS9-1	20.92489	105.89791	Upper portion of Van Phuc's river bend, in an area with intermediate groundwater arsenic (200ug/L).	16.5	25	2.6	0.2	1.1	0.5	0.5	0.1	0.9	3.57	1.57
VPNS9-2	20.92489	105.89791	Upper portion of Van Phuc's river bend, in an area with intermediate groundwater arsenic (200ug/L).	23.7	19	3.1	0.2	3	2	0.7	0.08	2	3.39	0.79
VPNS10	20.917933	105.910017	Downstream of the river bend's apex, river-transect bar sands.	5	20	2.8	0.2	0.7	0.7	0.13	0.01	0.7	3.85	0.71
VPNS11-1	20.917933	105.910017	Downstream of the river bend's apex, river-transect bar sands.	0-0.3	23	3.17	0.04	0.4	0.3	0.19	0.01	0.3	0.16	0.08
VPNS11-2	20.917933	105.910017	Downstream of the river bend's apex, river-transect bar sands.	4.2	20	2.2	0.1	0.8	0.4	0.38	0.03	0.7	1.11	0.53
VPNS11-3	20.917933	105.910017	Downstream of the river bend's apex, river-transect bar sands.	8.5	26	2.3	0.1	1	1	0.39	0.03	0.9	2.18	0.85

Table 4. Vertical AMS soil probe[1] sampling effects on OSL ages

Sedimentation Rate (mm/yr)	Years	kyrs	Deposition Type
<0.1	>3048	>3	Non deposition, unconformity, and hiatus
1	305	0.3	Overbank muds and floodplain deposits
10	30	0.03	Channel sands and bedload deposits
1000	0.3	0.0003	High energy flooding and crevasse deposits

[1]the butyrate sampling liner is 1 x 12 inches long

Table 5a. Expected Gy paleodose in modern deposits of Van Phuc (VPNS11)

0.3m		4.2m			8.5m		
5cm/yr 60yrs	1cm/yr 300yrs	5cm/yr 84yrs	1cm/yr 420yrs	1mm/yr 4200yrs	5cm/yr 170yrs	1cm/yr 850yrs	1mm/yr 8500yrs
0.1	0.6	0.17	0.8	8	0.3	1.7	17
0.2	0.9	0.25	1.3	13	0.5	2.6	26
0.2	1.2	0.34	1.7	17	0.7	3.4	34

Shaded cells are the most likely outcomes given the actual dose rates and most probable rates of sedimentation

Table 5b. Comparisons of expected and measured Gy

Sample	Depth	Measured Paleodose	Expected Paleodose
VPNS11-1	0.3m	1Gy	0.9 Gy
VPNS11-2	4.2m	1.5 Gy	0.8-1.3 Gy
VPNS10	~5m	1.7 Gy	1.4 Gy
VPNS11-3	8.5m	2 Gy	1.7 Gy

Table 6. Samples collected for Carbon age dating from Van Phuc

Sample	Needle Sample or Core	Depth (m)	Description (LxWxH)	Dry Weight (g)	calBP	Measured by
I-8 120cm	Core A	11.79	Wood	4.3652	6673-6332	UTK UTAG C-14 Date
I-5 80cm	Core A	6.89	Cyrenacea suborder (heterodont) bivalve (subtidal marine, 3.6x3.1x1.1cm)	4.3073	605±30	NOSAMS (Lex)
VPNS7	VPNS7	35	Peat - Equivalent to ~37m black layer in Core B	0.4819	-	[1]Returned from UTAG
I-3 60cm	Core A	3.6	Hydrobia family gastropod, smooth littorinid shell (2x1.3cm)	0.9363	-	[1]Returned from UTAG

[1]Samples returned from UTAG were deemed not enough sample for the liquid scintillation method.

CC Core by Van Phuc had no Pleistocene "C Pleistocene only in coastal HV core

Moyna unit is undated, and Ardevok unit does not record LGM or equivalent hiatus

Age (cal. kyr BP)	Epoch	Van Phuc, Vietnam: Ref. in Li et al., (2006) and this study	Van Phuc, Vietnam: Sediment Character	JAM site, West Bengal: McArthur et al., (2007)	JAM site, West Bengal: Sediment Character	Dan Phuong site, Vietnam: Larsen et al., (2008)	Dan Phuong site, Vietnam: Sediment Character	Araihazar, Bangladesh: Zheng et al., (2005) and this study	Araihazar, Bangladesh: Sediment Character
0 warm-dry	Holocene	Thai Binh Fm (ca. 30m)	Sand-silt, clay transition facies, fluvial-lacustrine-marine	Hoogli Member	Organic-rich peaty silts	Red River and floodplain alluvium	Fluvial and alluvial gravels, sands and clays from braided and meandering rivers. All sequences are void of transgressive marine facies.	Old Brahmaputra Meghna Floodplain Alluvium	Ploughpan clays, muddy channel fill, silty flood deposits
0.1 cool-wet									
0.6 warm-dry									
1.5 cool-wet								Brahmaputra River Alluvium	Fine to medium channel, levee and crevasse sands. Little to no silt and clays preserved.
2 warm-dry									
3.3 cool-wet									
4 4.5 Neoglacial		Haihung Fm (ca. 30m)	Fluvial-marine transition facies with clay, silt and sand	Joypur Member or stays Hoogli if Joypur absent	Dark, micaceous grey sand				
7 8.2 kyr Event	9-5 kyr Hypsithermal								
8.5				Hiatus					
10 Younger Dryas									
12	Latest Pleistocene	OSL date from this study							
20 Last Glacial Maximum		Vinphuc Fm (ca. 30m)	Gravels and clay, lateric weathering	LGM Paleosol	Stiff brown clay				
				Ardevok or Moyna Member	Gray or Orange Sand				
				Sunti Fm	Clay overlying Sand				

Table 7. Comparative Late Pleistocene and Holocene stratigraphies for arsenic-study sites in Vietnam, West Bengal, and Bangladesh. References for the compilation are listed in the first row of the table.

Supplemental 1: Sediment Cores from Rotary Drilling at Site L, VPNS1
m
Section
0
I-1
0.4
1.5
I-2
2.5
3.0
I-3
Shells →
3.7
4.5
I-4
5.1
5.7
6.0
I-5
0.6kyr
Shells →
7.5
I-6
9.0
I-7
9.6
10.0
I-8
6.5kyr
Peat →
12.0
I-9
12.9
13.5
I-10
15.0
I-11
16.5
I-12
17.2
18.0
I-13
18.6
19.5
I-14
20.5
21.0
I-15
22.5
I-16
15kyr
24.0
I-17
24.5
27.0
I-19
27.4
31.5
I-22
32.4
34.5
I-24
35.2
36.0
I-25
36.5
37.5
I-26
40.0
I-28
41.5
I-29
42.5
43.5
45.0
I-31
46.5
I-32
47.4
48.0
I-33
49.5
I-34
51.0
Gravel→
I-35

Supplemental 2: Sediment Cores from Rotary Drilling at Site H, VPNS2
m
Section
0
0.4
1.5
2.3
3.0
4.5
II-1
II-2
II-3
4.5
II-4
5.3
6.0
II-5
6.6
7.5
II-6
8.6
9.0
II-7
9.4
9.5
II-7
10.4
10.5
II-8
12.3
II-9
13.5
II-10
15.0
II-11
15.9
18.0
II-13
19.2
19.5
II-14
20.2
21.0
II-15
21.6
22.5
II-16
22.8
25.5
II-18
26.4
28.5
II-20
28.8
34.5
II-24
35.5
36.0
II-25
36.5
37.5
II-26
38.2
39.0
II-27
39.9
40.5
II-28
41.4
42.0
II-29
42.7
43.5
II-30
44.3
45.0
II-31
46.3
46.5
II-32
47.5
48.0
II-33
48.6
49.5
II-34
50.1
52.5
II-35
51.5
52.8
II-36
53.5
54.0
II-37
55.4
55.5
II-38
55.8
57.0
II-39
57.3
57.4
II-39
58.0
58.5
II-40
59.9
60.0
II-41
60.0

PART 2: THE CO-EVOLUTION OF ARSENIC AND AQUIFERS: LINKING SHALLOW GROUNDWATER ARSENIC HETEROGENEITY WITH THE EVOLUTION OF AQUIFERS IN PARASI, NEPAL

Abstract

Like many regions of Asia afflicted by arsenic-contaminated groundwater, shallow aquifers in the Nepalese Terai display extremely high variance in the concentration and distribution of dissolved arsenic. To understand the geologic context of this localized heterogeneity, high resolution sediment and water sampling was conducted over a 1-km transect between two villages with contrasting concentrations of arsenic in Parasi, Nepal. Luminescence dating of aquifer sands show gradient-like trends in depositional age between villages, which corresponds to a similar 1-km gradient in well-water arsenic where sediments from 21,000 to 700 years encompass a 400 µg/L change in groundwater arsenic. Our findings in the alluvial Terai plains again show that sediments <10kyr are prone to groundwater arsenic values >10 µg/L, whereas groundwater in aquifers >5,000 yrs old support arsenic values <10 µg/L. These results are consistent with other works that find aquifer sediments that host elevated groundwater arsenic to have been deposited almost exclusively during the Holocene. One important distinction in this study, however, is that elevated groundwater arsenic is only found in sandy aquifers deposited between 10-5kyr—the Holocene climatic hypsithermal, when the regional water cycle was intensified under a strengthened Southwest Monsoon. In contrast, aquifer sands deposited after 5kyr maintain low concentrations of arsenic, which differs from heavily contaminated aquifers of the same age in Bangladesh and elsewhere. In this paper we demonstrate that this difference is primarily a function of sediment age *and* provenance, where the hypsithermal-age sediments with high-arsenic groundwaters were sourced from an older-course of the Narayani-Gandak river, which brought

to the Terai sediments derived principally from the higher Himalayan crystalline rocks. The younger, low-arsenic aquifer was deposited by the much smaller Jharai river, which drains more-highly weathered sedimentary strata of the Lesser Himalaya. This difference in origin and lithology is clearly defined by the ratio of zircon and titanite mineral separates collected from the aquifers, and independently corroborated by geochemical weathering work by Gulliot et al., (in submission). The unique provenance of the arsenic-contaminated aquifer sediments is further confirmed by characteristic U-Pb ages of the zircon and titanite separates. Altogether, our findings indicate that the age of aquifer formation alone may not account for observed heterogeneity in groundwater arsenic. Rather, climate-driven changes in erosional patterns and sediment source also play a role in the distribution of Asia's groundwater arsenic.

1. Introduction

Arsenic contamination in shallow groundwater is still a growing crisis in parts of South Asia, including areas of Nepal, Bangladesh, India, and Pakistan, where inhabitants living on the Himalayan forelands depend heavily on groundwater. Despite more than a decade's worth of research, one of the most striking features of the contamination remains poorly understood: the high degree of spatial heterogeneity in the groundwater arsenic. In countries like Bangladesh, Taiwan, and Nepal, it is common to find tube-wells with groundwater arsenic differing from 1 to 500μg/L over 10-100 meters (van Geen et al, 2005, Weinman et al., 2008, Shrestha et al. 2003). This makes locating arsenic-free water difficult in Asia's developing regions. Beyond finding arsenic-free water, we still do not know why some aquifers promote such high degrees of heterogeneity. Our understanding of how such heterogeneity develops in shallow aquifers is not only crucial for lessening exposure to arsenic, but for managing other groundwater issues—for instance new contaminants (i.e., DNAPL, agrochemicals, PERC, etc.) associated with rapid economic growth in the region. To address current contaminant issues and prepare for widespread emerging contaminants, we suggest that aquifer history is a key factor in

understanding and managing small-scale spatial heterogeneities associated with arsenic (Berg, 2007; BGS-DPHE, 2001; Chakraborti, 2004; Fendorf, 2009; Gurung, 2005; Harvey, 2005; McArthur, 2008; van Geen, 2008) and other contaminants (Hartley, 2010; Lawrence, 2000; Minh, 2006; Swati, 2008; Courdouan, 2004; Fung, 2005). For instance, our previous work in Bangladesh shows that 50-fold differences in groundwater arsenic across 10s of meters can be defined by the area's history of river channel dynamics, which control the age and character of local aquifer sediments. Currently, we do not know if groundwater arsenic and shallow aquifers in other regional settings evolve in the same way, and we need to know if aquifer formation is an important consideration in all cases where arsenic and other chemicals are a concern (Figure 1). For example, we ask if sediment depositional processes can be ignored such that aquifer sediments can be treated as passive or geochemically reactive matrixes. We also show that depositional history cannot be ignored, and further develop evidence for the important role that aquifer sedimentology play in defining groundwater heterogeneity.

To better understand how arsenic heterogeneity occurs over such local distances, and to see whether our sedimentological findings from Bangladesh (Weinman 2008) can be applied to the occurrence of arsenic in another one of Asia's arsenic prone regions, high-resolution aquifer sampling was undertaken between heterogeneously affected villages in Nawalparasi, Nepal. Using high-resolution needle-sampling (van Geen et al., 2004), we use traditional methods of facies characterization coupled with cutting-edge optically stimulated luminescence (OSL) age-dating to reconstruct the aquifer's sedimentological history. In doing so, we seek to better understand how Asian aquifers evolve such high degrees of groundwater heterogeneity, and to see whether the heterogeneity afflicting the Nepalese Terai evolves similarly to other arsenic-prone regions (i.e., ongoing study sites in Bangladesh, West Bengal, and Vietnam). This is important, because to date, we do not know if the arsenic heterogeneity in these aquifers evolves the same way, and/or if villages in different regions require different understandings of their aquifers to best mitigate and manage their groundwater. Specifically,

we seek to understand whether the sediments hosting different arsenic concentrations are partitioned within certain deposit types and/or ages to help explain and understand extreme arsenic heterogeneity.

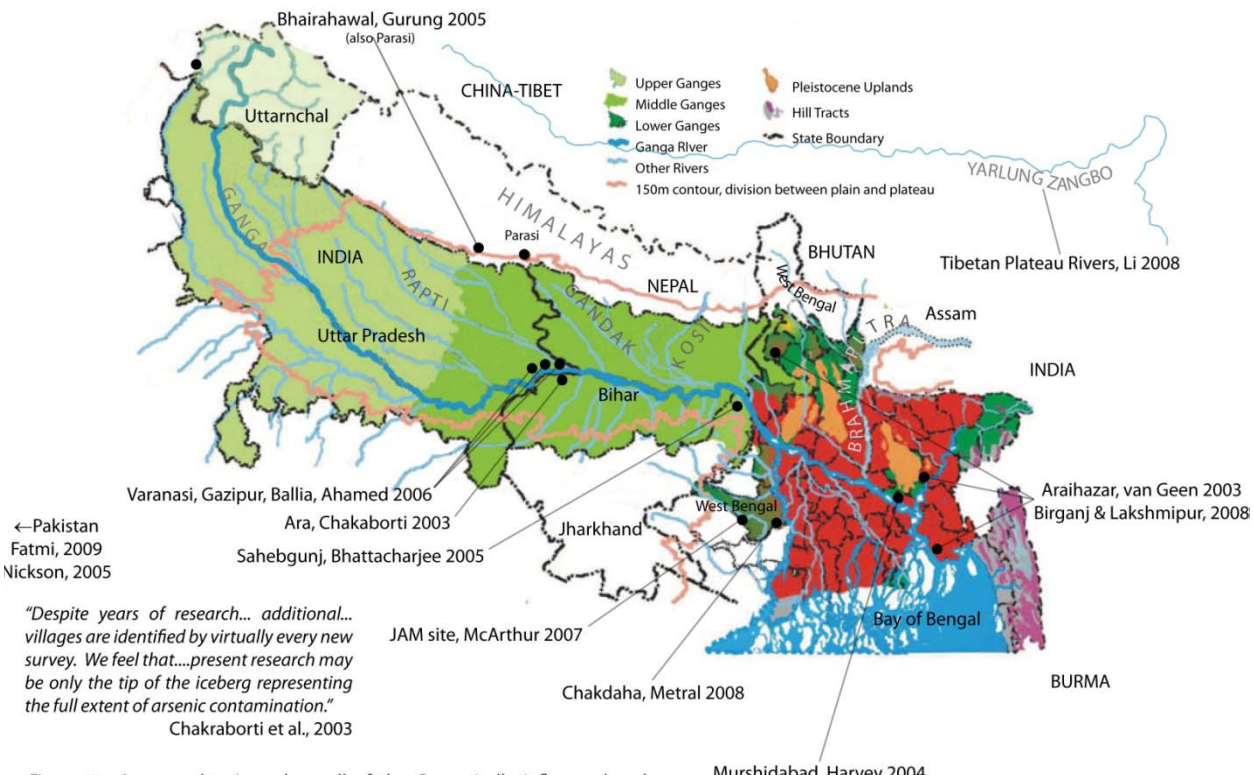

Figure 1. A map showing where all of the Gangetically influenced and arsenic-prone countries are in respect to each other. Modified from Chakaborti et al., 2003, circled locations are a complilation of the seminal and ongoing studies for Pakistan, Tibet, Nepal, India, and Bangladesh.

WHO update in 2006 had As listed as not a major concern--for the time--in Bhutan's groundwater, http://www.whobhutan.org/EN/Section4_26.htm

1.1 Study Area

Parasi is a town located in the Nawalparasi district of the Nepalese Terai, which is a low-lying region on the southern border of Nepal (Figures 2 and 3). Comprised mainly of Holocene alluvium from India's collision into Asia, the Terai runs east to west along the Indian-Nepal border, and it is bound to the north by the main frontal thrust of the Lesser Himalayas (NASC/ENPHO 2004). To the south of the Terai is India's Gangetic Plains, where Nawalparasi's main river, the Narayani, becomes India's Gandaki

River. The Jharai river, a smaller river in the Terai's Rapti- and Gandaki interfan region (Figures 3 and 4, (Gupta 1997)), bisects Parasi in a divisional area between the spring-fed stable-incised rivers of the eastern Terai and the hyper-avulsive, glacially- and monsoonal-driven rivers of the west. Being amid the Gandaki's dynamic instability, Parasi is prone to frequent flooding and river shifting (Dixit, Upadhya et al. 2007). Wells in Nawalparasi found that ~25% had >50 μg/L arsenic (NASC/ENPHO 2004), and preliminary work by Gurung et al. (2005) and Shrestha et al. (2004), indicate that village-scaled arsenic heterogeneity is likely controlled by differences in sediment facies.

The geology influencing the deposition in Parasi are the four major Himalayan units incised upstream by the Narayani: 1) the Tethys Himalaya, 2) the Higher Himalayan Crystallines, 3) the Lesser Himalaya, and 4) the Siwaliks (Gulliot et al., in submission). Together, these units span a wide range of different metamorphic, sedimentary, and igneous origins, making it possible for their differential erosion to account for some of the arsenic heterogeneity we see in Parasi. The provincial differences include a variety of metasedimentary rocks (limestones, calcschists, shales, quartzites) ranging from Cambrian to Jurassic in the Tethyan Himalayas (Colchen et al., 1986); the gneissic metamorphic stack of the Higher Himalayan Crystallines (Colchen et al., 1986); and the unfossiliferous metasediments of the Lesser Himalayas (Colchen et al., 1986)—the sediments shed from India and Asia into a foreland basin created by the uplift of the Himalayas (Mugnier et al., 1999; Huyghe et al., 2005). Today, the Lesser Himalayan Siwalik metasediments are divided into three units: 1) a lower unit of fluvial channel sandstones and calcareous paleosols, 2) a middle unit of very thick channel sandstones, and 3) an upper unit of gravely braided river deposits.

Just south of these units, the Indo-Gangetic foreland basin consists of a thick alluvial fill essentially of Quaternary age, which have accumulated in the peripheral foreland basin developed on the underthrusting Indian plate in response to thrust-belt loading in the Himalayas. Entering the Ganga Plain, the rivers tend to turn from their northern gridiron-type drainage to south-easterly directions

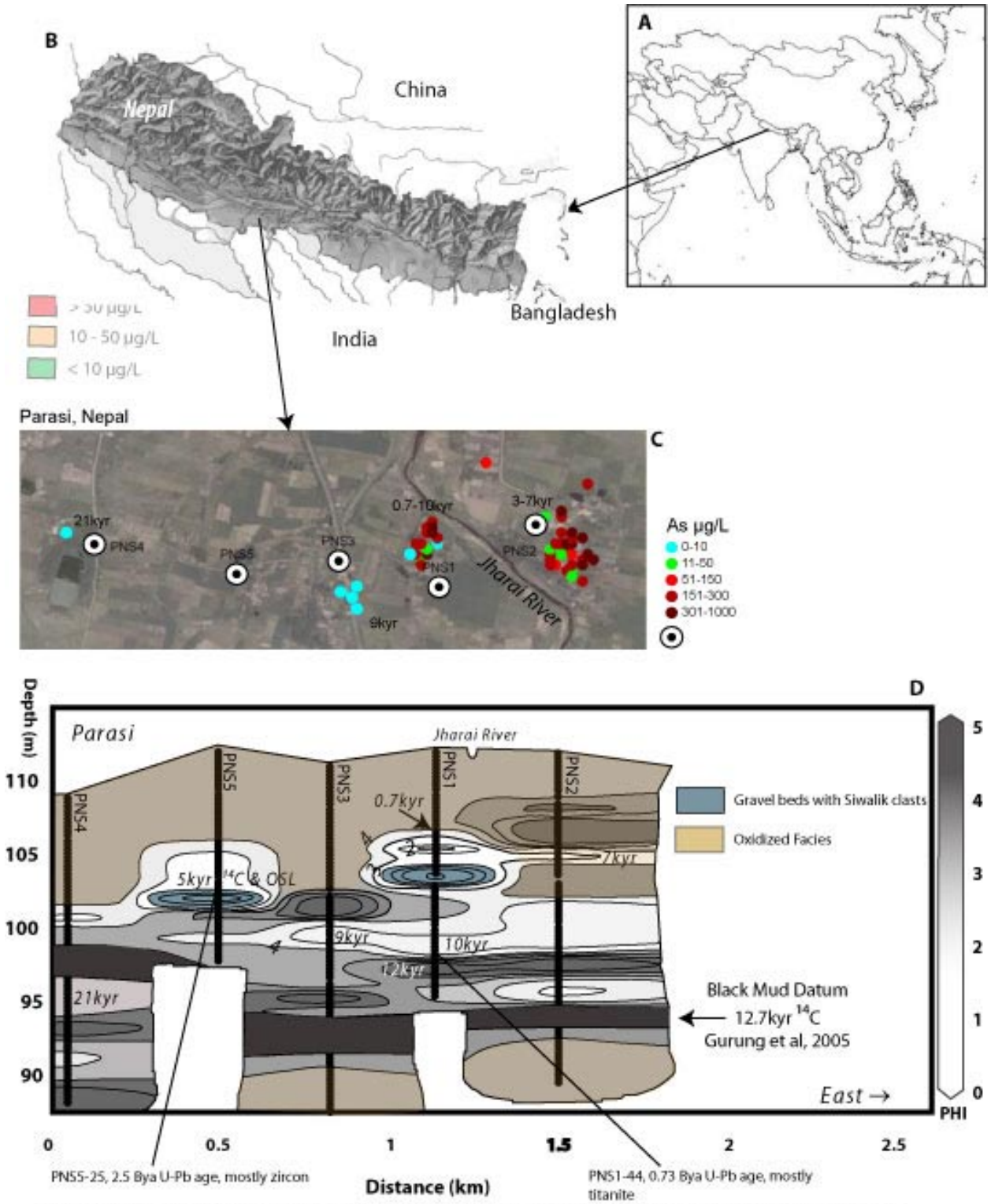

Figure 2. A-B are maps showing the locations of Nepal and Parasi in Asia, and C shows the ~1km groundwater and sediment sampling transect between differentl arsenic- contaminated villages. D is the cross-sectional depth results of aquifer sedimentology and OSL age dating.

(Gupta 1997; Chandra, Rhodes et al. 2007). In the northern part of the basin, the larger rivers have developed alluvial mega-fans or ridges: the Gandak and Kosi fans and the Ghanghra ridge, which date mostly to the Late Quaternary (Chandra, Rhodes et al. 2007). Amid the megafans, in an lowland interfluve between the Rapti and Gandak rivers is the heterogeneously affected village of Parasi, which has groundwater arsenic concentrations averaging 350±210 μg/L--the high deviation demarks the aquifer's high degree of arsenic heterogeneity (n=14, Gurung, 2005). Bounding Parasi are the foothill and mountain-fed rivers of the Tinau-Rapti and Narayani-Gandak, respectively, forming an interfluvial lowland south of the Churia range in the Terai's Northern Gangetic Plains. Located approximately 20km west of the Gandak megafan's westernmost limit, ~20km east of Tinau's Alluvial fan, Parasi sits in a ponded and forested part of the Rapti River basin. According to soil chronologies by Mohindra and Parkash (1992 and 1994), the Narayani-Gandak system has migrated slowly, yet significantly, 80km eastward in the last 5000 kyr, placing the current position of Parasi within the possible flow path of the Old Gandak-Narayani river.

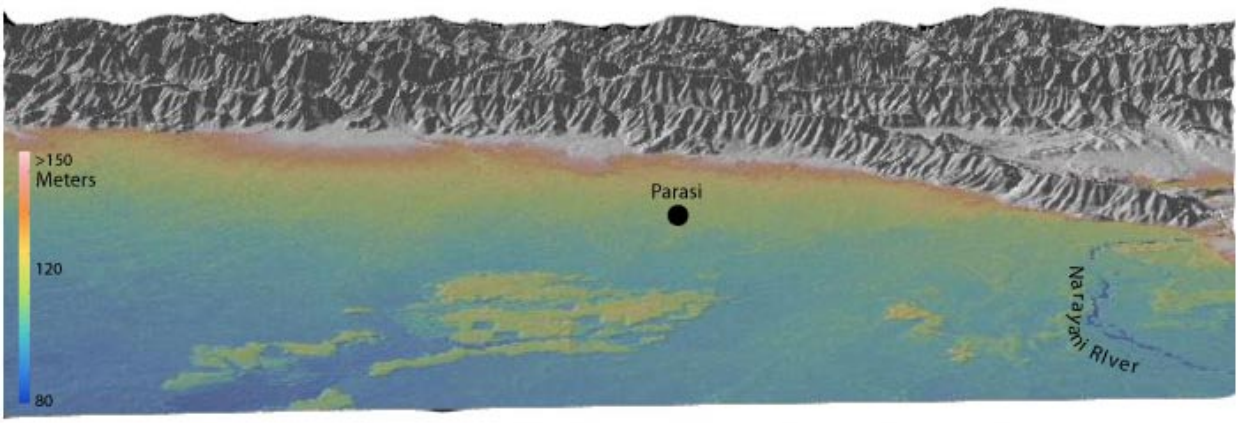

Figure 3, an elevation map showing Parasi's location in the Nepalese Terai, which is also known as the flat, depositional region just south of the Himalayan Siwaliks.

2. Methods

To resolve how aquifer evolution affects the accumulation of arsenic in a hyper-avulsive portion of the Terai floodplain, a needle-sampling device (van Geen 2004) was used to obtain depth transects of both sediment and pore-water samples. A transect was completed in May 2007 in Parasi, Nepal, which is an arsenic-affected site in the interfan region between today's Rapti and Gandaki River (Google Earth Coordinates 27°31'60.0"N, 83°40'0.0" E) (Figure 5). A total of 5 depth profiles were collected along a ~1km transect specifically chosen to span two villages differently affected by arsenic, from a low As cluster west of Sunwach (As <10μg/L) to a high As cluster just a few 100 of meters east, in Unwach village (As 300-500μg/L, Figure 2C, Table 1 (NASC/ENPHO 2004). To capture a good resolution of the aquifer's sedimentology, geochemistry, and history, the distance between sampling sites averaged ~200 to 300m horizontally with sediments and groundwater sampled at ~1-3 m intervals to a final depth ~20 m below the surface.

2.1. Sedimentology and Water Sampling

Samples of groundwater and aquifer sediments were collected using a drilling and needle-sampling method developed by van Geen et al. (2004). Briefly, the method obtains sediment and water via a needle-capped, evacuated tube that is plunged to a known depth within a drill hole. This way, simultaneous sediment and water samples can be collected. Porewaters were generally sampled from aquifer sands at 1-3 meters below the surface while sediments were collected every 3 meters or whenever there was an observable facies change—whichever distance was smaller. Sediments for OSL dating were collected when there was an observable change to sands during drilling, and sand-aquifer samples were then collected for OSL using black-taped or steel AMS probe liners that are inserted into the drill hole during needle-sampling (van Geen et al., 2004). The black tape and steel liners protect the

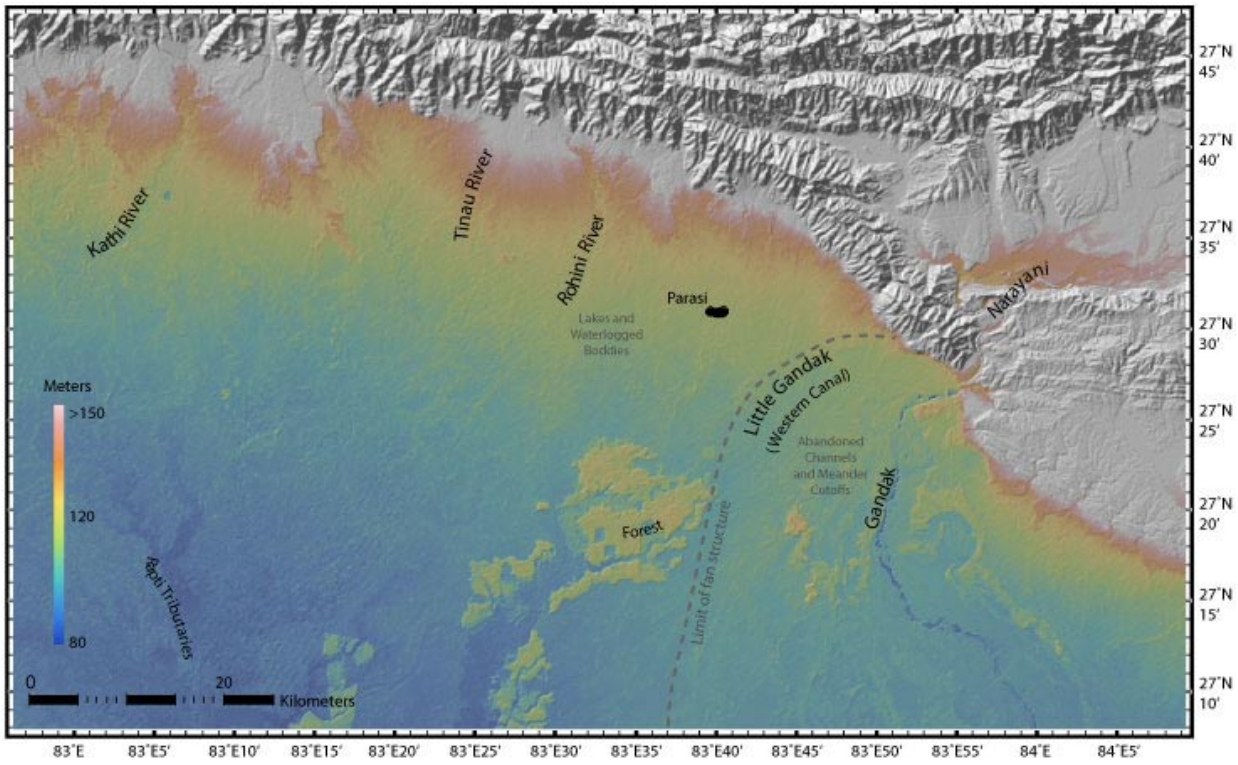

Figure 4. High resolution map of the Rapti and Gandak interfluve made usi MMng Columbia University's GeoMapApp s.s.3 Global Multi-Resolution Topography (GMRT, http://www.marine-geo.org/portals/gmrt/). Map coloring is based on a continuous color GMRT Grid, with a vertical exaggeration of 2 and sun illumination of -45 declination and 35 inclination.

sediment from being "bleached" with sunlight, preserving the sediments for OSL dating. The samples for OSL were then foiled and stored in the dark until they could be processed and measured.

2.2. Aquifer Sedimentology and History

Aquifer sediment type and evolution was reconstructed in Parasi by optical luminescence dating (OSL) of aquifer sands and corroborated, when possible, by ^{14}C on organic matter—retrieved sediment samples are typically organic-poor, with small pieces of preserved terrestrial detritus and shell fragments seen perhaps once in each drill hole. Sediments were classified in the field using a grain-sizing kit and hand lens (GSA 1999) based on our experience of classifying sediments in other locations (i.e., Vietnam, Cambodia, and Bangladesh; Appendix D). The sediment observations were then used in constructing a

cross-sectional stratigraphic profile for comparison with the other sediment properties, such as arsenic and OSL age-dating (Figure 2D).

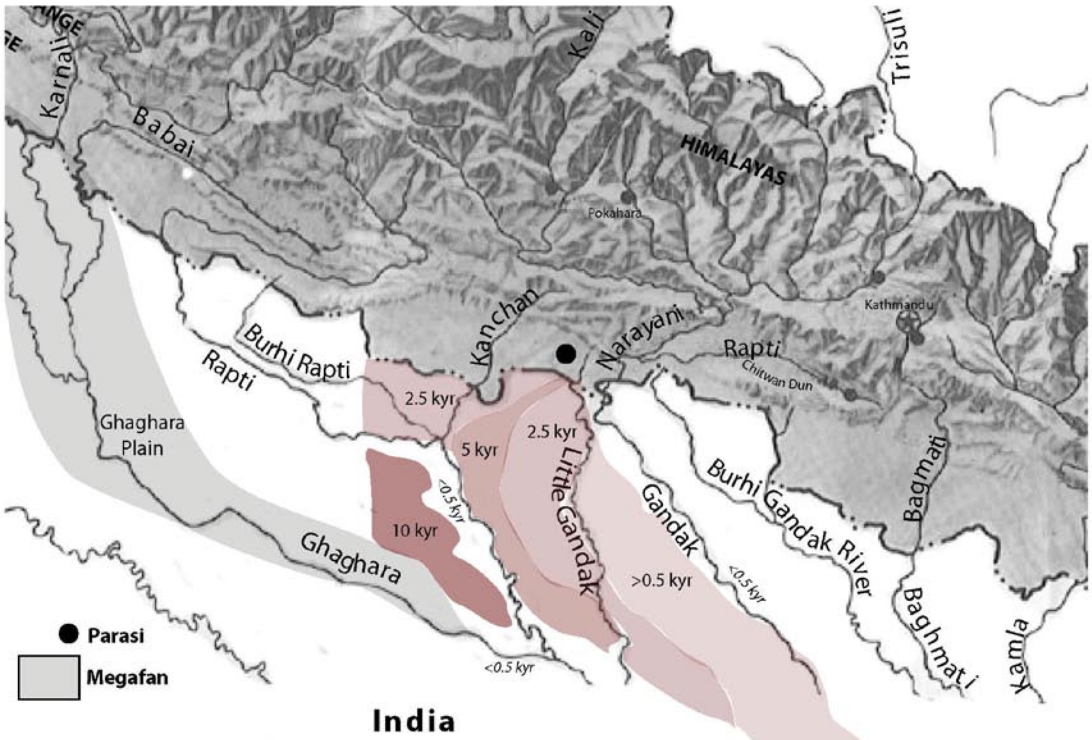

Figure 5. Close-up of Indo-Nepalese rivers draining into the Ganga Basin of northeast India, showing more of the Parasi interfluve region. The Rapti-Gandak interfluve is shaded by soil age-estimates in Mohindra et al., 1992, which indicate more Gandaki and Rapti influence in Parasi's interfluve 2.5 kyr ago. "Burhi" preceding river names indicates the "Old" course of the same river.

For OSL ages, the protected samples were taken to India's National Physical Laboratory (PRL) for determining the depositional ages, while woody fragments retrieved from Nepal were rinsed with distilled water, dried overnight at 60°C and sent to Daniel Weinand at the University of Tennessee's Center for Archaeometry and Geochronology for liquid scintillation counting ^{14}C dating[ii], calibrated with IntCal04/OxCal4.0 for reservoir correction. At PRL, the sediments were separated and processed under

red light conditions[2]. Sediments were removed from the protective steel or taped liners and then treated with 10% HCl to remove carbonate fractions and then a 30% H_2O_2 solution to remove organic matter. Quartz was then separated using sodium polytungstate (ρ = 2.58 g/cm^3) and, if needed, with a magnetic separator, starting at 0.4 amp at 15° slope to 1.5 amp at 5°slope, using increments of 0.2-0.4 amp and 2°. For each sample, a few grains from the sample with the lowest magnetic susceptibility were double-checked under a microscope to affirm a pure sample of quartz. Samples were then sieved into different size fractions, of which a 150-210 μm fraction was etched in 40% HF and used for a single-aliquot OSL method (Aitken, 1998; Jain et al., 2003; Duller, 2004; Wintle and Murray, 2006).

The natural luminescence, or the "paleodose," was measured at PRL using a Risø TL/OSL-DA-12 readers equipped with a 40mCi ^{90}Sr/^{90}Y beta-source, a blue LED stimulation system (470 ± 30 nm) and an IR laser (830 ± 10 nm). For significance, 20-30 aliquots were typically prepared for equivalent dose measurements on each sample, and data from the aliquots were rejected if there was a poor fit of the growth curve or if the recycling ratio fell beyond the range 1.0 ⍰⍰0.1. For some of the Parasi samples, microscopy and initial runs of OSL showed that, despite several separation attempts, the samples were dominated by feldspars, in which case, the "naturally-corrected" single aliquot regenerative dose (SAR) OSL procedure (Nagar 2007) was modified with an infrared bleaching step so the OSL measured was only from quartz ((Zhang and Zhou 2007) Table 2). The final OSL age for each sample was based on a weighted mean of either the minimum 10% of paleodoses or a weighted mean of all the paleodoses, depending on the shape of the age distribution.

External dose rates were measured using thick source ZnS (Ag) alpha counting for U and Th, and gamma counting and XRF[3] for potassium determination. A radioactive equilibrium in the decay chains was assumed, and the cosmic dose rate estimation is based on the muon production models of Prescott

[2] Red light is not energetic enough to penetrate to band gap depths deep enough to stimulate luminescence.
[3] Due to PRL machine demand, some of the K measurements were made post-OSL analysis using Warner Cribb's XRF at Middle Tennessee State University.

and Hutton (Prescott 1988; Prescott 1994). The experimental errors in the OSL ages include errors in paleodose measurements (photon statistics), errors in the measurement of K, U, Th, and errors in source standards and source calibrations.

2.3. Groundwater Arsenic

The number of porewater samples taken from each location depended upon the type of sediments encountered. Typically, porewaters were collected from 7, 10, and 15m intervals in Parasi. Once retrieved, porewaters were immediately filtered out of the needle-sampling device through a 0.45µm Acrodisc® syringe filter. The dripping filtrate was collected within an acid-cleaned 20mL HDPE scintillation vial and acidified on site to 1% HCl (Optima, Fisher Scientific). Water samples were then analyzed for dissolved arsenic and other groundwater constituents at Lamont-Doherty Earth Observatory by HR ICP-MS using a method that can detect arsenic concentrations as low as ~0.1 µg/L with a precision of +2% (Cheng et al., 2004). These concentrations were then compared to the groundwater arsenic measurements made using a Hach arsenic test kit in the field with other concentrations being provided by ongoing monitoring coordinated by Linda Smith of Filters for Families[4] and ENPHO (NASC/ENPHO 2004).

2.4. Provenance

To test for the presence of source-area differences in the aquifer sediments, zircons and other heavy minerals were separated from two aquifer horizons: PNS1-44 (13m) and PNS5-25 (8m). Following a cleaning treatment of 10% HCl and 30% H_2O_2, the samples underwent a mineral separation series using a magnetic separator and liquids of different densities. From the heaviest mineral fraction, >3g/cm^3, zircons were hand separated and mounted into epoxy for ^{238}U-^{206}Pb age dating at Vanderbilt

[4] http://www.filtersforfamilies.org/

University using their Environmental Engineering Laboratory's laser ablation inductively coupled mass spectrometry (LA-ICPMS) with results calibrated to NIST 612, 610, and internal 91500 standard references.

3. Results

3.1. Aquifer Sedimentology – Lithology Results

Overall, the lithology of sediments from the five drill holes shows that they comprise coarse to fine-grained, light-grey to dark-grey sands interbedded with greyish to yellow-brown silts, grey, black to yellow-brown clays, and occasional gravel layers (Figure 2D). Sand, silt and clay sediment of certain depths contain micas and are occasionally massive to laminated, bioturbated, and/or also have root and plant debris. A similar abundance of fine-grained silts and sands is typical of floodplain sediments along the Ganga river system (Singh, 2009). Specifically, the primary sediment facies observed in the subsurface aquifers of Parasi include:

a) interbedded muds and micaceous fine sands from the surface to ~105 m depth;
b) a laterally discontinuous gravel bed with Siwalik alluvium from 100-105 m depth;
c) grey micaceous sands and silts from 95-100 m depth;
d) a prominent 1-5m thick, laterally extensive, organic-rich black clay from 92-97 m depth;
e) a hard, basal gravel unit with sand lenses and yellow-brown muds, typically > 92m depth.

The muddy sediments of the last facies, with angular to sub-angular gravels are interpreted as debris-flow deposits due to the intermixing of grain sizes.

These general facies coincide with previous lithologies described in the Terai/Ganga Plain region (Table 3, Gurung, 2005; Prasad, 2005). The surface interbedded muds and fine sands are equivalent to the Terrace Alluvium of the Rapti-Gandaki based on their similar descriptive lithologies. The grey

micaceous sands and silts recovered in this study interpreted as Rapti-Gandaki Recent Alluvium based on their … characteristics. The black clays correlated with the black mud layer described from the Varanasi Older Alluvium by Gurung (2005) and Prasad (2005). Finally, the Siwalik fragments—identified as rocks similar to the Siwalik outcrops sampled along driving from Kathmandu to Butwal--intermixed with sands and yellow-brown muds are representative of Banda Older Alluvium.

These facies are stacked in a predictable stratigraphic sequence, with the younger alluvial sequences overlying the older, and the contacts between the facies are defined by distinct yellowish-brown or brownish-grey paleosol horizons. These old soil horizons were distinct when sampling, and typically contained calcareous nodules. To compare the lateral extent of our observed facies, we incorporate sedimentological results from work done by Gurung et al. (2005), in a site ~2 to 3 km NNE to NE of our study area. Inasmuch, data coming from the same nearby sedimentological environments will be integrated into our discussion, to better assess the extrapolatability of our findings. In other words, how other arsenic-prone regions may similarly or dissimilarly evolve their aquifers and arsenic.

3.2. Aquifer Age – OSL Results

Here we report detailed results for the luminescent age dating of Parasi's aquifer material. The section is divided into two units: first, we describe the samples' responses to OSL and the suitability of using OSL for age-dating the Parasi samples. Second, we report the age distributions for each aquifer sample, discussing how we went about assigning an age to the unit. Given the large age-spreads in most of the samples, we want to be upfront about the method's uncertainty, and how we went about dealing with the distributions of ages. (most of which we expected, due to fluvial sediment's tendency for partial-bleaching).

3.2.1. Parasi's OSL Suitability and Behavior

The OSL depositional timings of Parasi's shallow aquifer are reported in Table 1. Altogether, three (PNS1-25, PNS1-60, PNS2-25) of the eight processed OSL samples had undetectable IRSL signals, while some IRSL responses were unsuccessfully removed from the remaining samples (PNS1-50, PNS1-50(II), PNS3-45, PNS4-53, and PNS5-33; examples are shown in Figure 6). This was despite repeated attempts at etching and separation. After repeated unsuccessful etchings, the samples that remained responsive to IRSL were "bleached" using an IRSL step prior to OSL reading. This allowed us to remove feldspar contamination to the OSL signal, while simultaneously allowing us to compare ages from dose equivalents (D_e) using both IRSL SAR (single aliquot regeneration) and OSL. An adequately bleached aliquot was one where the IRSL counts fell below 10% of the initial OSL counts, and where the OSL measurements remained bright and well-behaved (negligible depletion in the blue light signals after IR stimulation at 50°C, Figure 6). Besides remnant IRSL, another problem we found for some samples was that the quartz was not that sensitive. This seems to be common for much of the newly weathered and not yet sensitized quartz being shed from the Himalayas (Jaiswal, Srivastava et al. 2008; Jaiswal, Bhat et al. 2009; Juyal, Pant et al. 2009). Similar to behavior exhibited by quartz from river terraces in India's Goting Basin (Juyal, Pant et al. 2009), 1-2 aliquots from PNS1-25, PNS1-50, PNS1-50(II), and a majority of PNS1-60 samples had anomalously small natural OSL signals. This was despite the fact that the samples were able to produce relatively larger laboratory induced regeneration and test doses. Except for PNS1-60, the few anomalously low ages were excluded from the age distributions (Ballarini 2006, Figure 7). We report the age distributions for PNS1-60, which are all anomalously low since it is impossible for PNS1-60 to be younger than PNS1-50, the unit immediately over it. In the future, PNS1-60 will be remeasured using the double-SAR protocol, which was not initially used due to a low IRSL response in the sample, the need to run other samples, and successful age determination from the PNS1-50 sample.

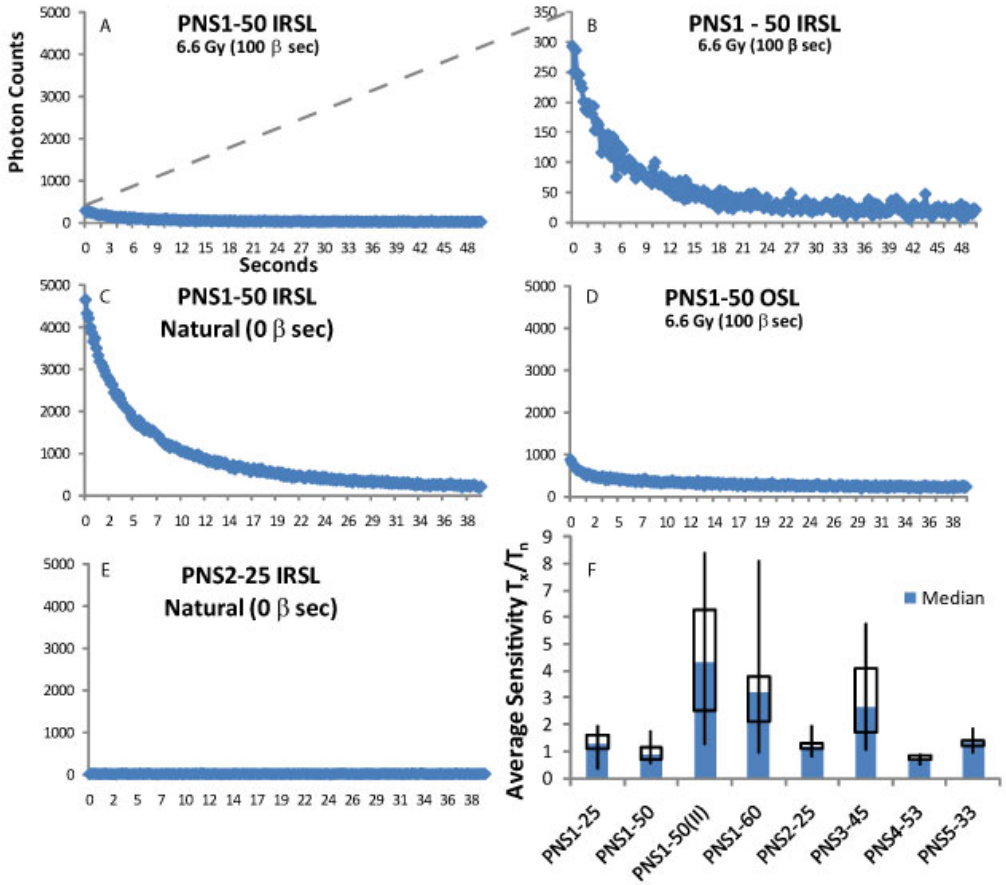

Figure 6. Typical OSL and IRSL shine down and response curves shown for two of Parasi's samples, PNS1-50 and PNS2-25 (A-E). Figure A shows the typical test-response used to test for total removal of feldspars in the samples. Figure B is a zoomed-in graph of A, showing the type of IRSL response we would use to determine which samples required a double-SAR procedure. Figures C and D show the natural and dose point generation response of the same sample, while Figure E shows the absence of IRSL response in PNS2-25, indicating we could use normal OSL-SAR on the sample. Figure F is the average sensitivity change on all of the aliquots run for each sample.

The complete chronology of Parasi's aquifer is summarized in Table 2 and depicted stratigraphically with the sedimentary facies in Figure 2D. With the exception of PNS1-60, all ages are stratigraphically consistent with no age inversions. Again, this inconsistency is probably due to feldspar contamination, which is well known to undergo anomalous fading (Li et al., 2008; Kars and Wallinga, 2009). But, with several of the Parasi samples having quartz with poor sensitivity and dosimetry, the feldspar response is particularly useful when the aliquot is able to regenerate an IRSL dose curve, recycles a regenerative dose, and produces an age that is stratigraphically consistent. While we cannot rule out the possibility of anomalous fading affecting the IRSL determined ages, fading was undetectable in the IRSL ages ascertained before and after 1 year of storage (in the dark, at room temperature). But, with several IRSL ages averaging less than the OSL determined age, some fading does happen—this is

not always the case, though, and we do not see more than a fraction of percent difference that can be attributable to fading. Considering a fading rate on the order of ~0.1 percent per decade (i.e., ascertained from PNS4-53), the overall effect on the calculated ages will be on the order of 1 ka, or less, which will not significantly change our interpretation of Parasi's late Quaternary history.

Given the likelihood of partial-bleaching and the expected variance for the Himalayan fluvial-borne sediments (Puthusserry, Juyal et al. 2007; McArthur 2008), several considerations were taken into account in determining each sample's depositional age. For example, a minimum or "least 10%" age model may not be appropriate for sediments that have experienced post-depositional mixing (Lian and Roberts 2006) or for deposits in which the spread in age is due to something other than partial bleaching (i.e., spatial variations in beta dose rate, which is possible given the range of dose rates observed in Parasi's aquifer: ~1-5 Gy/ka, Table 2). Given the spread in ages, we used a combination of OSL, IRSL, and age distribution results in assigning the aquifer's depositional ages (Figure 7).

3.2.2. Parasi's OSL Aquifer Ages

3.2.2.1. PNS4-53

Going in order from east to west in the transect, our first age at PNS4-53 is the oldest sample. Equivalent doses for PNS4-53 are the highest among the samples and range between 52-152 Gy. In behavior, the OSL and IRSL SAR are both well behaved, with the younger IRSL ages indicating the feldspar in this sample are prone to fading—again, less than half a percent per decade. Altogether, the average OSL age of the aliquots are 23 ± 6 kyr, which is older than the faded ~13 kyr IRSL age. Being the sample with the highest D_e in our transect, and taking into account errors from incomplete bleaching and dose-rate errors[5], we assign PNS4-53 with the mode OSL age of 21.6 ± 0.2 kyr, because it is an actual measurement, it is close to the average age, and because it represents a younger and not overestimated depositional age of the sample (Table 1, Figure 7).

[5] According to Naomi Porat, the dose rate is the least well constrained part of the age calculation.

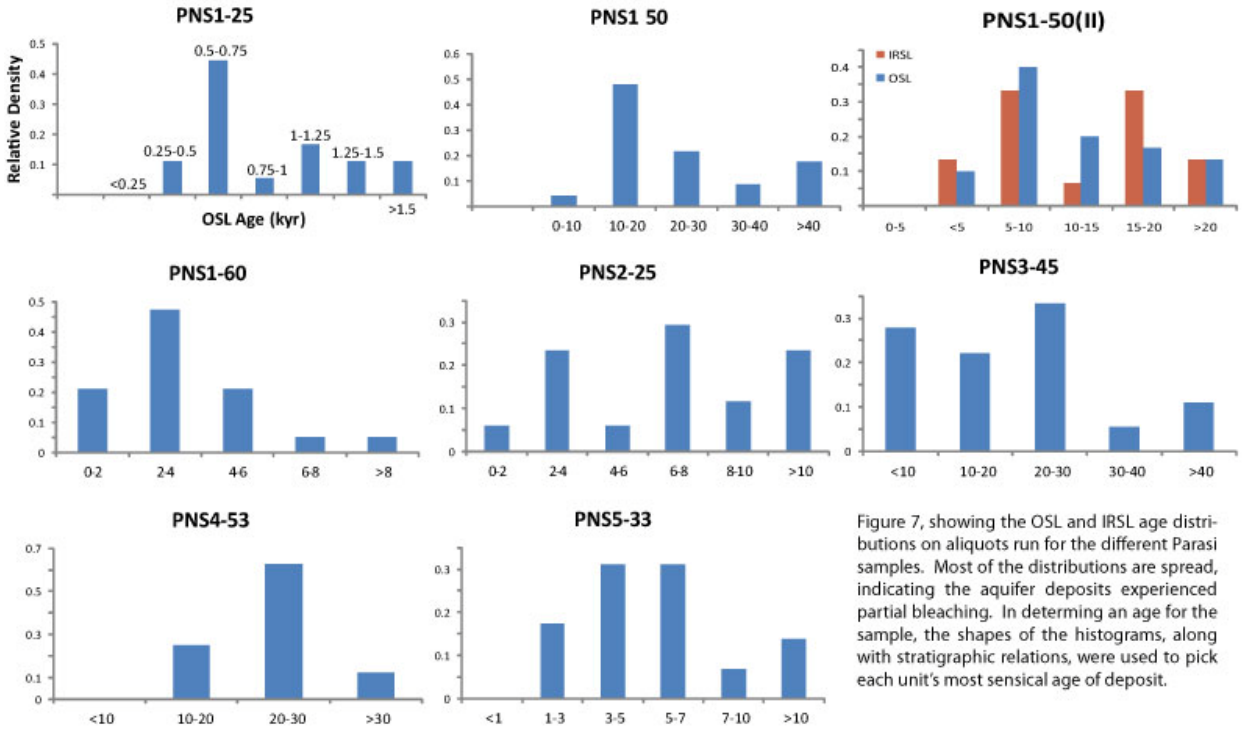

Figure 7, showing the OSL and IRSL age distributions on aliquots run for the different Parasi samples. Most of the distributions are spread, indicating the aquifer deposits experienced partial bleaching. In determing an age for the sample, the shapes of the histograms, along with stratigraphic relations, were used to pick each unit's most sensical age of deposit.

3.2.2.2. PNS5-33

The next sample is PNS5-33, which had an IRSL response in only one of the 29 aliquots. A regular OSL-SAR protocol was therefore used on all but that one sample, along with a corroborative ^{14}C age from a wood fragment retrieved while drilling. The wood is from the same horizon as the sample obtained for OSL, and was radiometrically dated at UTAG (UTAG sample 07-013). With fractionation (-28.1±0.5‰ $\delta^{13}C$) and reservoir (IntCal04/OxCal4.0 with 4465±70calBC) corrections, the wood dates to 3354-2928calBC. In our conventionally reported OSL time, this converts to 5.4-4.9 kyr (95.4% confidence). This 5kyr age is consistent with the age peak in PNS5-33's OSL histogram (Figure 7), so we are comfortable assigning a 5kyr age to this deposit. The one IRSL age obtained amid the aliquots yielded an age of 3.0 kyr, which agrees with the OSL result for the same aliquot: 2.8 kyr. While these ages are a little younger than 5kyr—ages that, by the way, still fall into the sample's Gaussian age spectra—the similar age of IRSL and OSL on the same run indicate that PNS5-33 is suitable for SAR and

capable of producing reliable ages. Combined with the ^{14}C results of the wood, the depositional timing of PNS5-33 occurred at 5kyr.

3.2.2.3. PNS3-45

Toward the transect's midpoint is the arsenic transitional area, where two OSL samples (PNS3-45 and PNS3-55), although only PNS3-45 was able to be processed and measured since it was the coarser sample and more likely reflective of a previous channel deposit that, now buried, serves as a shallow aquifer for Parasi. Although unprocessed, PNS3-55 was taken from silts below a black mud sequence, which is a regional datum that has been dated (Figure 2D) to 12.7kyr black muds described by Gurung et al. (2005). Thus, the silts at PNS3-55 are relatively older than this datum, perhaps 15-20 kyr based on the lack of an unconformable surface. Overlying PNS3-55 and the black muds is PNS3-45, which should be younger than the lower 12.7 kyr black mud unit. Considering PNS3-45's younger position and its OSL and IRSL age distribution, we assign a date of 9±1kyr to the unit. This is because the average OSL age of 21kyr for PNS3-45 is stratigraphically inconsistent—the deposit must be younger than the deeper 12.7kyr black muds. This is probably due to the sample being mostly partially bleached, which is not uncommon and supported by three paleodoses falling into the saturated end of the SAR curve (paleodoses equivalent to 35, 44, and 57kyr, which skews the population). Additionally, the <8kyr ages behave anomalously low in both OSL and IRSL performed on the same samples, so consistent with the stratigraphy and using a least 10% of the leftover distribution, we are most comfortable using an age of 9±1kyr for this part of the aquifer.

3.2.2.4. PNS1-25

Going further east, the next drill hole is PNS1, which is in Sunwach village and noted in the field as being a previous site of the modern-day Jharai River. Today, the river lies ~100m east of the village. Because of the village's higher reported groundwater arsenic (100-300μg/L), four OSL samples were collected to see if there were aquifer age trends that could explain some of the heterogeneity: PNS1-25,

PNS1-50, PNS1-50(II), and PNS1-60. The two PNS1-50 and PNS1-50(II) samples were taken above and below a sand-to-mud unconformity to see if the time span across the depositional change and hiatus could be dated. Starting with the shallowest sample, PNS1-25 had no observable response to IRSL and was able to regenerate and recycle doses using OSL alone. Three ages were rejected, two for being anomalously low (0.08 and 0.1kyr) and one for being in the saturated part of the SAR curve (10kyr). Without those aliquots, the ages for PNS1-25 range from 0.4-2kyr, with an overall average age of 0.9±0.5kyr. It is likely, however, that the deposit is a little younger than this, given the probability for partial bleaching of the samples. Since the convention with this technique tends towards the younger ages to prevent overestimation, we refer to PNS1-25's age distribution and statistics to refine the interpreted age. The histogram of OSL ages shows a 0.5-0.75kyr peak, with ages in this peak-bin averaging 0.6kyr. With the mode of the entire distribution, 0.7kyr, being so close to the peak-bin and overall OSL averages, we have the most confidence in using 0.7kyr as PNS1-25's time of deposition—this is really the age of river abandonment, as it dates not only the aquifer, but also the last time Sunwach was fluvially active.

3.2.2.5. PNS1-50

Below the 700 year old PNS1-25 sands, there is another sand aquifer at PNS1-50. In cross-section (Figure 2D), the sands in this lower, mid-transect layer are chronologically *and* facies-correlative with the sand aquifer at PNS3. They also become similarly 3-4 times more sensitive during the measurement process (Figure 6F). Similar to the IRSL behavior of PNS3, the sands in PNS1-50 remained IRSL responsive and were able to regenerate dose curves using the double SAR method (Figures 6A-D). The IRSL ages from PNS1-50 produced one anomalously low age of 0.3kyr, which was rejected, with the remaining aliquots ranging between 10 and 64kyr—again, similar to PNS3-45's age distribution (Table 1, Figure 7). In choosing an actual age, we are most comfortable in dating the unit towards PNS1-50's minimum ages—the least and actual age for all the aliquots run is 10.0±1kyr (assuming a 10% error),

which is consistent with the unit's least 10% ages: PNS3 sands date to 9±1kyr and the lower PNS1 sands to 11±1kyr. With our ±1kyr OSL resolution (assuming a 10% error[6]), the two aquifers are indeed correlative, being deposited at the same 10kyr time frame. In other words, the lateral movement of the river between PNS3 and PNS1 is not currently resolvable using these particular OSL and IRSL techniques. We argue later, however, that there is an overall eastward migration of the river that deposited these sands. Considering steady-state as a minimum boundary, this means the older river was capable of scouring and processing the landscape *at least* 0.2m/yr, which is quite different than Parasi's current moribund conditions.

3.2.2.6. PNS1-50(II)

In trying to date Parasi's transition into this 10kyr period of high river activity and sandy deposition, we attempted to date the mud unit immediately beneath PNS1-50. In collecting OSL samples, we typically concentrate on being able to retrieve aquifer sands. In Parasi, however, this was difficult because many of our attempts to retrieve sands for OSL were unsuccessful due to the sand deposits being thinly layered within the aquifer. This was different to our experience with the more continuous and homogenous sands we typically find in the shallow aquifers of Araihazar (van Geen, Zheng et al. 2006; Weinman 2008). In Parasi, the sand units are thin, meter-thick interbeds (or lenses) that were often too easily drilled through and missed using the local wash-boring technique and needle-sampling. Given the thinness of sands and our wont to date as much as possible, we retrieved the mud unit immediately below PNS1-50 to test whether the muds could be used for OSL dating. We also thought this would be helpful in not only corroborating our other dates, but also in understanding the 'activity' (or fluvial geomorphic dynamics) of these poorly understood interfan regions (Jain and Sinha 2003; Jain and Sinha 2004). As with the aquifer sands, the muds produced a wide range of OSL and IRSL ages: between 3-23kyr for the OSL ages and 3-38kyr for the IRSL ages (Figure 7). Considering both

[6] Errors from partial bleaching, dose-rate approximations, and 2% instrument error.

distributions, there is a good overall agreement between the IRSL (14±9kyr) and OSL (12±6kyr) results, with the average of the OSL average age best fitting the stratigraphy. Knowing that these muds *must* be older than the 10kyr aquifer sands (PNS1-50) and younger than the 12.7kyr black mud datum, presumably lower in the PNS1 sequence—the drill hole here did not go down enough to penetrate Gurung's correlative unit (2005)—we reject ages younger than 10kyr and older than 12.7kyr, leaving us with an average, 12kyr OSL age that is most suited for PNS1-50(II). This age is further supported by the age histogram (Tables.xlsx) and a rounded estimate of the least 10% of the remaining ages: 12kyr (11.83±0.02kyr).

3.2.2.7. PNS1-60

We also tried sampling once more below PNS1-50(II), capturing coarser silts upon reaching the drill-hole's lowermost facies: PNS1-60. As with PNS1-50(II), this unit is still finer than the typical sands we aim for, but we wanted to see if we could, again, date these finer units. Currently, constraints on lab time—laboratory measurement time is still often *the* limiting factor in these types of studies (Telfer, Bateman et al. 2008)—limited us to completing an OSL SAR sequence on 5 aliquots. The rest of the aliquot's dose-equivalents were gotten from an averaged-standardized growth curve (SGC)(Roberts and Duller 2004). Initially, a typical OSL sequence was used because 1) it takes half the time of the double SAR sequence (1 vs. 2 days per 5 aliquots), 2) because of an insignificant observed IRSL response on natural samples,[7] and 3) due to the lack of observable 270˚C feldspar peaks in any of the TL glow curves. Using only the OSL, the limited results we have on PNS1-60 gives us an entire distribution of anomalously low ages (0.8-8kyr, Table 1). Out of the 19 aliquots, none of the samples dated older than 12kyr. This is a problem since PNS1-60 is stratigraphically constrained by an age between 12 and 12.7kyr. With all the ages anomalously low and with PNS1-60 having sensitivity characteristics similar to

[7] IRSL shine down curve starts at an intensity of 50 counts and stays at 45-35 counts per second thereafter.

the PNS1-50(II) and PNS3-45 samples (Figure 6F), PNS1-60 would probably produce better corroborative results using the double-SAR IRSL method.

3.2.2.8. PNS2-25

The last OSL sample measured, PNS2-25, is from Unwach village, on the eastern bank of today's Jharai River, found by Filters for Families[8] and ENPHO to have some of the highest concentrations of groundwater arsenic (300-500µg/L). This site is considered the contaminated end-member of the transect. The sands processed from this sample sometimes showed a response to IRSL, so aliquots were measured using both the typical and double SAR protocols. The quartz OSL ages range from 2-16kyr with an average age of 7±4kyr, while the older, less bleached IRSL ages range from 9-14kyr with an average age of 10±2kyr (Table 1). Again, since we favor using minimum ages—which is justified due to 1) partial bleaching, 2) using a sampling method that can combine grains of different ages over a 0.3m interval (the length of the AMS soil probe liners we used), and 3) feldspar requiring more time to bleach vs. quartz (i.e., quartz is at least an order of magnitude faster in zeroing the OSL latent signal (Godfrey-Smith, Huntley et al. 1988))—using the younger, OSL age distribution is preferred in assigning PNS2-25's age. With the average and mode of the OSL distribution converging on 7kyr, this is the best age to describe the unit. With two peaks, however, showing in the histogram (Figure 7), it is very likely that there are two main periods of deposition—once at 7kyr followed by another deposit at 3kyr. Between the two times, PNS2 could have experienced a lack of deposition within the sampled interval. This could have been from channel switching and a move to more anastomosing conditions. In any case, despite the different problems we had measuring the OSL of Parasi's aquifer samples, the results still enable us to give a well resolved account of the aquifer's evolutionary history.

[8] http://www.filtersforfamilies.org/index.shtml

3.3. Provenance - Zircon Age Dating

One sediment sample each from the low- and high-arsenic aquifers were analyzed for zircon U/Pb dating, and also include dating results from titanite grains in the same samples (DATA TABLE FOR RESULTS). In the low arsenic, shallower sample of PNS5-25, results were consistent with exclusive zircon minerals (~90000 ppm Zr), while the separates from PNS1-44 showed spikes of Ti indicating that the heavy separates of PNS1-44 comprised predominantly titanite grains (~300000 ppm Ti). Only XX zircons were recovered in PNS1-44 due to differences in heavy mineral abundances between samples, where PNS1-44 is titanite-rich and zircon-poor and PNS5-25 is zircon-rich and titanite-poor. Because these two minerals have the same density are not easily weathered, these differences are not a result of sorting and thus can be used as a provenance indicator. This inference is further supported in the U-Pb concordia diagrams for the two deposits (Figure 8) that show different trends in source-rock ages. Sample PNS5-25 with 26 zircon ages span a broader age-range, from ~0.5-2.5 billion years, while the two zircons from sample PNS1-44 both date to more recently evolved crust ~0.73 billion years. The titanite ages also fall along different trends, further indicative of different source terrains. Sample PNS1-44 with 6 titanite ages is younger, measuring at ~30 million years versus sample PNS5-25 which, with 4 ages measuring at almost 1 billion years. While the ages are discordant, likely due to Pb loss and higher initial Pb incorporation into the titanite structure, the two samples show distinct and different age populations.

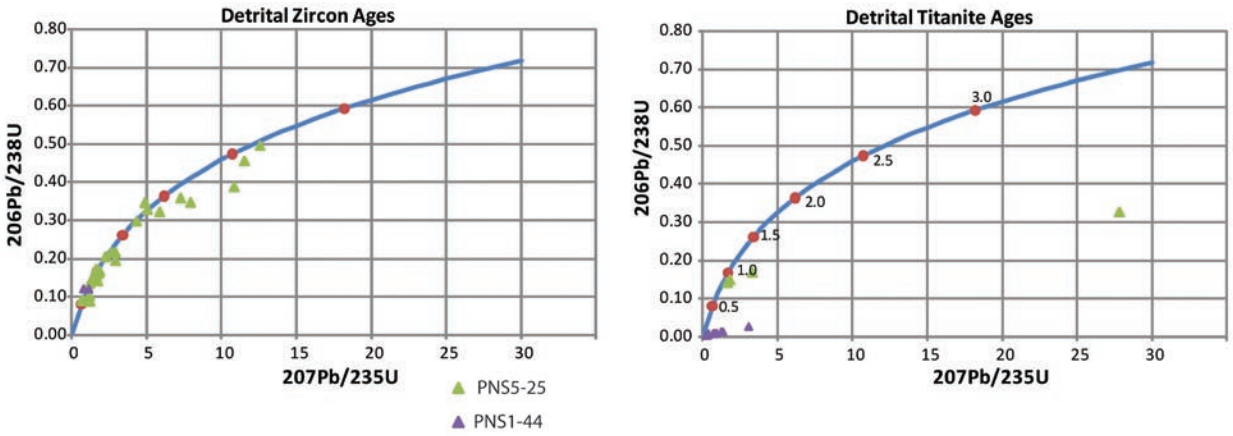

Figure 8. The figures above are U-Pb concordia diagrams with the LA-ICPMS results of the detrital zircon (left) and titantite (right) age dating. In each, the smoothed concordia line defines the idealized decay between the 207Pb/235U and 206Pb/238U isotope systems assuming no Pb loss and no initial daughter after closure. Left panel: Sample PNS5-25 with 26 zircon ages span a broader range, from ~0.5-2.5 billion years, versus sample PNS1-44 with two dates agreeing well at 0.73 billion years. The reason for so few zircon ages for PNS1-44 is due to differences in heavy mineral abundances between samples, i.e., PNS1-44 was titanite rich and zircon poor while PNS5-25 was zircon rich and titanite poor. Right panel: Sample PNS1-44 with 6 titanite ages are younger, measuring at ~30 million years versus sample PNS5-25 which, with 4 ages measures at almost 1 billion years. While the ages are discordant, likely due to Pb loss and higher initial Pb incorporation into the titanite structure, the two samples show distinct and different age populations, indicative of difference provencance sources.

4. Discussion

4.1. Sedimentological Evolution of Parasi

The age and history of development of shallow aquifers around Parasi is complex, even compared with the results of similar work in Araihazar, Bangladesh (Weinman et al., 2008). Determining Parasi's shallow stratigraphic evolution in context of the surrounding hilly source terrains and numerous rivers is challenging in part due to the lack of *absolute* sediment age-dating to draw correlations (Tandon, Sinha et al. 2008). For the most part, the timing of major climatic and geomorphic events documented in the literature are either too old (>1Myr), missing (12-1kyr hiatus; Rao, Bisaria et al. 1997; Yonebayashi and Mutsuhiko 1997), or too relatively dated (Mohindra, Parkash et al. 1992; Mohindra and Parkash 1994; Dwivedi, Sharma et al. 1997; Dill, Khadka et al. 2003; Sakai, Sakai et al. 2006). In contrast to studies on the megafan deposits (Prasad and Khan 2005), southern terraces (Rao, Bisaria et al. 1997), and (paleo)lakes (Yonebayashi and Mutsuhiko 1997; Hayashi, Tanimura et al. 2009), there has not been

much research on these interfan regions. This puts limits on what we can contextually and regionally interpret in terms of aquifer evolution, but our results are still important in that they are among some of the initial findings, outside of the Bagmati (Jain and Sinha 2003), that show the type of dynamic sedimentation occurring in these of interfan regions. This is a considerable advance since earlier belief held that these areas were fluvially inactive, and since our findings also help fill-in events between 12-1kyr—a period missing in the Ganga lake and terrace deposits (Rao, Bisaria et al. 1997; Yonebayashi and Mutsuhiko 1997). And, even more relevant to the problem of arsenic, our findings also give better insight into the local processes of aquifer formation in these highly avulsive regions. So, while there is a limit to what we can synthesize between local happenings in Parasi and the entire Ganga catchment, an effort is still made to contextualize Parasi's aquifer evolution with what is currently thought to have occurred during the Late Quaternary Siwalik and Gangetic evolution.

4.1.1. Parasi in the Late Pleistocene - Last Glacial Maximum, (~21-12 kyr)

The oldest, lower-most units (<90m) in the transect are muddy, with oxidized silts and clays inter-layered with cobble-sized fragments of the Siwaliks and paleosol concretions. These characteristics correlate to descriptions of two different alluvium sequences reported in the basin: the "Banda" sequence, which is supposedly from the Upper Pliocene-Lower Pleistocene (1.6-0.8 Myr, Dwivedi, Sharma et al. 1997) and the Hazipur/Madhabani/Moguraha/Mohanpur/Gobardhana Formations of northern Bihar with speculated ages of Middle to Late Pleistocene (0.8-0.02 Myr, (Prasad and Khan 2005)). Since the deepest (95m), earliest age that we record in the aquifer dates to 21kyr (Figure 2, bottom panel), and since megafan deposits and dun valleys record active sedimentation between 50 to 20 kyr (Kazuo 1999; Suresh, Bagati et al. 2002; Chandra, Rhodes et al. 2007), it is more likely that the lowermost (<90m) deposits also reflect deposition during the Late Pleistocene. This makes the lowermost deposits likely Gobardhana-Varnasi equivalents (Rao, Bisaria et al. 1997; Prasad and Khan 2005), with the presence of older alluvium (i.e., the Banda) still possible taking into account

depositional hiatuses—in fact, muds below 90m show unconformable weathering, meaning that equivalence with earlier units cannot be ruled out.

While the depositional timing of the lowermost units remains uncertain, the oxidized mud unconformity at ~90m likely dates to the Last Glacial Maximum, agreeing with other work showing 20-18 kyr as a time of erosion and depositional hiatus (Dwivedi, Sharma et al. 1997; Suresh, Bagati et al. 2002; McArthur 2008; Clark, Dyke et al. 2009). In general, it is thought that much of the Gangetic basin did not undergo deposition between the LGM and 12kyr, which is supported by our lack in OSL-dates recovered for this timeframe (Figure 2D, Rao, Bisaria et al. 1997; Srivastava, Sharma et al. 2003; Chandra, Rhodes et al. 2007)[9]. In the southern Ganga Plain, the lack of sedimentation before 12kyr is speculated to be due to river confinement within uplifted terraces and possible changes in base-level[10] (Rao, Bisaria et al. 1997; Suresh, Bagati et al. 2002), although an inland response to sea level changes as far inshore as Parasi is unlikely (Jain and Sinha 2003; Tandon, Sinha et al. 2008). A more likely scenario is erosional uplift of the sub-Himalayas and/or sediment sequestration within one of the newly forming piggyback basins during this time. The Chitwan Dun is not too far from Parasi[11] (Figure 5) and is thought to have been actively accumulating sediments by the later Pleistocene (Kazuo 1999). While the synchronicity and affects of dun-development on Parasi is not exactly known, their late Quaternary formation, along with a weakened monsoon, probably led to very little sedimentation: piggyback basin formation shifted sediment accumulation north of Parasi, which probably accounts for the lack of late Pleistocene deposition in the transect (and region).

Despite factors limiting sediment aggradation in the late Pleistocene, there is some deposition of sands in Parasi at 21 kyr (~95m), along the western part of the transect. This timing is coeval with a large scale wet event in Paleolake Kathmandu (Hayashi, Tanimura et al. 2009) and the Bagmati River's

[9] An exception to the typical LGM-12kyr hiatus is found in N. Indian glacial lake deposits by Juyal et al., 2009
[10] This is vague and base-level involvement this far inland is refuted by Jain and Sinh, 2003
[11] Adobe Illustrator "Nepal-Rivers – High Resolution.ai" File

breakthrough into the Terai (Dill, Khadka et al. 2003), which, before this time, drained into the Kathmandu Basin. In breaking through Lake Kathmandu's southern rim, the Bagmati River brought a new source of sediments into the Terai and improved the interconnectivity between Nepal's northern and southern basins. While this is not a direct connection to deposition in Parasi since the Bagmati is one interfan to the east—between the Gandak and Kosi Rivers[12]--the area is prone to impulsive sedimentation (Pratt, Burbank et al. 2002), and a breakthrough of the Seti River through a paleolake at Pokhara is thought to have occurred around the same time-frame (Ross and Gilbert 1999). Whether or not these 21kyr sands are related to the breakthrough of the Bagmati remains a question—i.e., if deglaciation following the LGM increased snowmelt enough to cause a synchronous phase of downcutting and lake-bursting throughout the entire frontal thrust region—but the presence of sands in Parasi at 21kyr suggests that the Rapti-Gandak interfluve also experienced a similar increase in interconnectivity with its upland region around this time.

After a brief increase in river activity at 21kyr, deposition is not recorded again until the Pleistocene-Holocene transition, showing as a layer of unconformable black muds throughout the transect (Figure 2D). These black muds have little-to-no paleosol development, are often varved, and have ~1% higher organic content (LOI) than other muddy sequences[13]. In the literature, similar black muds are described by Gurung et al. (2005) in three boreholes ~2-5km northeast of our transect, with a ^{14}C date of 12.7kyr (Figure 2).[14] A regional correlation of this unit can be made with similar black, swampy-muds, found in India's Sanai Lake, which is ~250km southwest of Parasi, between the Ganga and Ghaghra rivers (Sharma, Joachimski et al. 2004). All three black-mud deposits display a remarkable similarity in both *time* and *facies,* and agree with the "persistent dark clay beds" reported by Dwivedi et al. (1997) in northern Varnasi Alluvium sediments. Despite widespread support for this unit's

[12] Adobe Illustrator "Nepal-Rivers – High Resolution.ai" File
[13] Refer to LOI Chapter
[14] Organic-rich mud and peat were collected from PNS1-53 and PNS1-68 (16 and 21 m), available for ^{14}C dating

Pleistocene-Holocene depositional timing, the origin of these organic-rich clays are poorly understood (Sinha and Sarkar 2009), and it is uncertain how relevant they are to local or regional groundwater problems. Schematic diagrams of Ganga Plain megafan-interfan architecture show organic-rich mud layers, or "tals," in the interfan subsurface (Sinha 1995; Sinha and Sarkar 2009), suggesting that these deposits are the byproducts of rivers: as rivers migrate and avulse within the interfan, abandoned oxbows and "tals" deposit organic-rich muds, which can be preserved in "undynamic" interfan regions. This, however, is genetically different than what we see as an extensive layer of black-clays deposited as a "Pleistocene-Holocene" transition layer. Instead of a "normal" lateral formation, another explanation involves a more vertical movement: enhanced downcutting starting ~13kyr[15] (Rao, Bisaria et al. 1997; Srivastava, Sharma et al. 2003; Chandra, Rhodes et al. 2007; Sinha and Sarkar 2009) caused a vertical disconnection of interfluves from their rivers. While it is still unclear exactly why these interfluves regionally ponded—i.e., why there was such poor drainage—extensive swampy lacustrine environments were created from reinvigorated rainfall and perennial flooding. One possible explanation could be poor recharge in the early Holocene due to hardened, indurated muddy surfaces formed by long-term exposure and weathering during the late Pleistocene. So, rather than ascribing the formation of ponded interfluves to autocyclic fluvial processes, it is more likely that this 12.7kyr unit represents [and can be used as a regional datum for] a regional response to climate change from Pleistocene to Holocene conditions, which promoted extensive ponding and mud deposition throughout the entire northern Ganga-plain (Figure 9A).

4.1.2. Parasi's Late Pleistocene – Early Holocene transition, (~12 – 9 kyr)

Overlying the black muds, and following this 12.7kyr "ponding" transition, there is a brief unit of grey silts and sands, overlain by the first sands deposited after the Holocene transition (Figure 2D). These 10 and 9kyr-old sands are facies that show an increase in fluvial activity across the interfluves, and

[15] In the literature as T2 formation (terrace surface 2)

a transition into the hypsithermal period of strengthened monsoon and increased precipitation (Pratt, Burbank et al. 2002). This timing of enhanced fluvial activity also correlates with the newer, post-glacial alluvium that covers much of the Rapti Basin (Chandra, Rhodes et al. 2007)—the basin in which Parasi lies—as well as the doubling of sediment flux from the entire Ganges catchment (Goodbred 2000). High sediment flux and aggradation during this time is also reported by (Sinha and Sarkar 2009), whereby a newly-strengthened monsoon is thought to have increased sediment flux out of the Himalayas. This, in turn, increased deposition in the foreland (terai) and deltaic basins. Other evidence for high fluvial activity around this time also comes from Sharma et al. (2004), who note a warmer climate and higher rainfall from lake deposits, and Pratt et al. (2002), who show 6.3-7.8 kyr-old bedrock exposure ages along the Marsyandi River,[16] which they interpret as a 'punctuated' and rapid removal of sediment out of Parasi's upstream mountainous region. OSL ages from Rapti-basin-sediments by Chandra et al. (2007) also conclude early Holocene aggradation in the Terai, which is further supported by OSL work by Rao et al. (1997), who show similar timings of deposition in the Ghaghara-Ganga basin. Altogether, this suggests that Parasi's 10 and 9 kyr-old sands are good recorders of the enhanced fluvial and sediment output from the Himalayas during this early Holocene timeframe (Figure 9B).

One of the more important findings from the Parasi transect is that the sediment source from the early Holocene is different than the source of sediment being delivered in the mid-late Holocene. For the late Quaternary, there are two possible source regions for sediments being deposited in the study area: 1) the foothills in the Churia Range-Siwaliks or 2) the higher Himalayan mountains. This is an important distinction because local rivers flowing to the Terai are either foothill-fed or mountain-fed, each posing different source-rock lithology for the sediments comprising Parasi's aquifers, and perhaps for arsenic. U-Pb ages from detrital zircons deposited in the aquifer sands 10kyr ago show that the river feeding Parasi at that time must have drained an area of Higher Himalayan crystalline rocks

[16] Drains into the Narayani-Gandak River

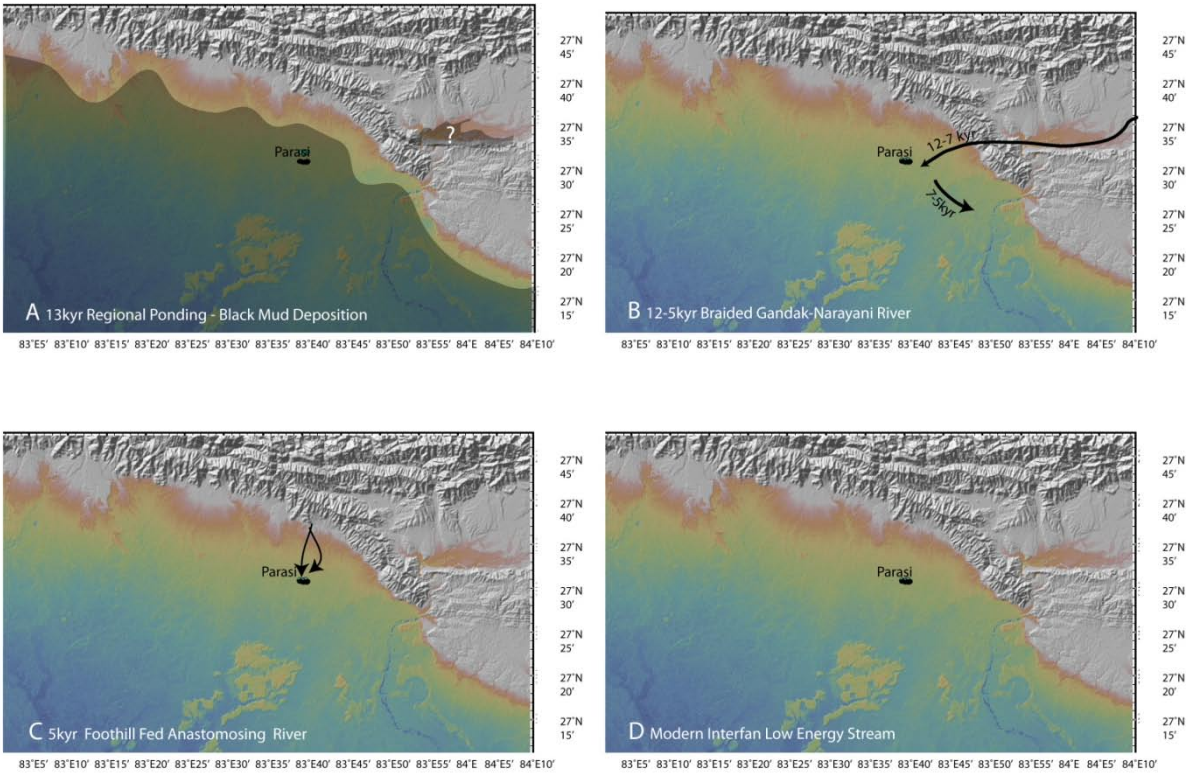

Figure 9. High resolution map of the Rapti and Gandak interfluve made using Columbia University's GeoMapApp s.s.3 Global Multi-Resolution Topography (GMRT, http://www.marine-geo.org/portals/gmrt/). Map coloring is based on a continuous color GMRT Grid, with a vertical exaggeration of 2 and sun illumination of -45 declination and 35 inclination.

owing to the much younger ages compared with those of the shallow sediments[17]. These young zircon ages are similar to ages of zircons from the Tibetan and Greater Himalayas (0.9-0.5Gyr, (DeCelles, Gehrels et al. 2000)[18]. Such young zircon ages are not found in the much older Lesser Himalaya rocks derived from Tethyan sediments (REF), which comprises the dominant source lithology for the modern Parasi rivers. Since the Narayani-Gandak's tributaries[19] incise Tibetan (i.e., Mustang, Nepal) and Greater Himalayan (i.e., HHC from the Marsyandi River) sequences upstream of Parasi, it is likely that the zircons in the 10 kyr deposits are a mixture from both source regions. For these zircons to make it all the way down to the Terai, Parasi had to be the site of a much more active, mountain-fed river. This requires

[17] Refer to Chapter on Provenance
[18] Young titanite ages also imply a metasedimentary source region
[19] Inferred from Figure 1 of DeCelles (2000), Mustang Khola flowing into Kali Gandaki and then into the Narayani

that the active river flowing through Parasi at 10 kyr be one of the large, transverse rivers draining across the orogen (Gupta 1997). Due to its proximity, we think that this river was most likely the Narayani-Gandak river, which today sits only 25 km east of Parasi, and is migrating westward (BBC 2007),[20] towards Parasi, to reoccupy one of its older paleochannels (Figure 9B).

4.1.3. Parasi's mid-Holocene 'stabilization,' (9 – 5 kyr)

Following the early Holocene occupation of the Parasi area by the paleo-Narayani River, there are several lines of evidence supporting the mid-Holocene as a time of 'stable' west-to-east migration of Parasi's paleo-river. First, there is a continuous west-to-east trend in early Holocene depositional ages in the aquifer (Figure 2D), from XX kyr to XX kyr. Second, there is a general increase in the volume of sandy sediments from west to east. Third, this inferred west-to-east movement of the river channels follows a regional trend of river migration and piggyback basin progradation over this same time period (Mohindra and Parkash 1994; Kimura 1999; Jain and Sinha 2003). Lastly, eastward migration of the paleo-Narayani is supported by soil research that suggests a decreasing age of soil formation from 10 to 5 to 2.5kyrs (Figure 5, (Mohindra, Parkash et al. 1992)).

As the paleo-Narayani shifted east, abandoned channel muds filled in older courses of the river. This is seen by the grey silty muds overlying the 10 and 9 kyr sands in the middle of the transect (~101m, Figure 2D). Overall, the stratigraphy suggests a mid-Holocene history of eastward river migration and the burial of older sandy channel deposits by overbank muds. After this period of migration, river courses appear to stabilize between 10 and 7kyr, as shown by the ~7 meter-thick continual aggradation of sands in the eastern part of the transect (97-107m, Figure 2D). These thick, massive sands suggest that the paleo-Narayani course was stable and confined to the eastern part of the transect. We speculate there was adequate muddy overbank deposition to build stable levees and maintain the channel course. In addition, the vertical offset of the black mud facies between PNS4 and PNS3

[20] This is the cause of an ongoing border dispute between Nepal and India

Gurung's 12.7kyr (Figure 2D) suggests possible faulting that helped force the channel eastward, whereby this faulting caused a ~3m lowering of black muds in the aquifer (97-94m, equivalent to a subsidence rate of ~2-3mm/yr), and the muddy slickensides recovered while drilling. Lastly, it gives another reason for river stabilization in the eastern part of the transect: the down-dropping was high enough to keep the channel in the eastern part of the landform (relative to average sedimentation rates in the foreland of ~0.25mm/yr over 10^3 time scale, (Tandon, Sinha et al. 2008).

Another line of evidence indicating that the paleo-Narayani stabilized during the mid-Holocene is in the presence of calcitic paleosol concretions just above the 10kyr and 9kyr channel deposits (Figure 2D). The theory goes that this type of paleosol concretion forms on stabilized surfaces when evaporation of water draws groundwater upwards through the soils. This leaves behind precipitated calcium carbonate nodules in the uppermost soils (Nichols 1999). In Gangetic soils, these concretions are referred to as "kankars" and form over multiple cycles of wetting and drying and from soil leaching in a limited drainage environment (Malek 1967; Zaleha 1997; Heroy, Kuel et al. 2003). Their presence is important in aquifer formation for several reasons: they tell us there is a range of processes involved in aquifer formation, they give an idea about the length scales over which aquifer formative processes operate, and they also tell us something about how wetting-drying can affect arsenic in the region. This is important because it is unclear how and if periodic of wetting and drying affects the evolution of these aquifers—for instance, recent findings from the derelict Woolston Canal in the UK suggests that wetting and drying promotes arsenic availability (Hartley and Dickinson 2009), and collaborative work by (Guillot, Weinman et al. 2009), indicates that arsenic becomes enriched in sediments deposited during dry periods. In the Parasi transect, these wet-dry kankar-soils are laterally discontinuous, which may be one of the reasons behind arsenic's heterogeneity in the aquifer. According to Zaleha et al., (1997), these kankar paleosols form in floodplain areas that experienced little to no sediment input (i.e., floodbasins) and/or abandoned floodplains and channel belts that rarely received sedimentation. This

means that as the paleo-Narayani began stably and perennially aggrading in the east, the western part of the transect became abandoned enough to intermittently wet and dry, promoting kankar soil formation. By capturing the synchronicity of channel aggradation and soil-drying in our transect, we define an important ~100m length-scale of fluvial processes responsible for imparting such high degrees of aquifer heterogeneity: 'dry' kankar-type soils can form ~100 meters away from a 'wet' and fluvially active channel environment. This scaling also has significant implications for sedimentary reconstruction work, in that one core is likely not enough for capturing all of a village's sedimentary history. For instance, a core from the westernmost part of our transect would entirely miss the early Holocene's occupation of the paleo-Narayani River. Thus, when doing reconstruction work, high-resolution lateral drilling, such as our needle-sampling, gives a much more broad and contextual account for an area's depositional history.[21]

4.1.4. Parasi's source and planform change at ~5 kyr

Another line of evidence supporting mid-Holocene stabilization is a channel regime switch from braided to anastomosing planforms by 5kyr. Anastomosing rivers are considered to be more stable than braided regimes, which again supports 5kyr as a time of less stream power and stability. Following the braided, mountain-fed river of the early Holocene, Parasi's river underwent a continuous winnowing as the paleo-Narayani migrated eastward to its present day location: ~30 km east of Parasi, in Bhaisalotan, Nepal. Before reaching its current location, the paleo-Narayani was first captured by the course of today's Little Gandak River, before migrating east to the Burhi-Gandak river, and then starting back westward ~100 years ago its present-day location (Figure 5 and 8B (Mohindra, Parkash et al. 1992; Sinha 1996; Mahadevan 2002; Tandon, Sinha et al. 2008)). In leaving Parasi, the paleo-Narayani was followed by a series of less powerful rivers. These new rivers were fed by the nearby Churia and Mahabharat ranges. This change to less powerful, more proximally sourced rivers is recorded in the aquifer in two

[21] I think I went a little off tangent here, so I might move this to discussion

ways: by changes in our transect's stratigraphy and by a change in detrital zircon ages. In case of the former, the switch from braided to anastomosing conditions is seen by a change in deposition. The earlier braided channels left laterally continuous, uninterrupted sands, which then change into a series of gravelly channels. The two separate and synchronous sandy channel deposits in both the western and eastern part of the transect at 5kyr show this planform switch quite clearly (PNS5 102m and PNS2 105m both have similar 3, 5, and 7kyr modal ages, Figure 7, PNS5-33). Overall, the stratigraphy shows a new, more 'stable' anabranching system—a river with multiple channel threads—in place by 5kyr (Figure 9C).

The stratigraphic evidence of the new anastomosing system is seen in the aquifer profile by a lateral discontinuity of sandy channel facies, separated by thick, continuous muddy floodplain sequences that date 5kyr by both OSL and ^{14}C. In the cross-section of Figure 2D, the change to an anastomosing system is specified by two coarse gravel beds at ~103m, colored blue, in the mid-part of the transect. We interpret these gravels as bed deposits—and not bars or debris flows—due to 1) their large size relative to their paleochannels and 2) the lack of support from a fine-grained matrix ((Nakayama and Ulak 1999; Jain and Sinha 2004; Shukla 2009) and references therein). We envision these gravels similar to the modern fluvial gravels of other northern Ganga piedmont rivers, which are typically described as 'anastomosed, gravelly braided' systems (Nakayama and Ulak 1999; Davies 2007), although we wish to keep a distinction between 'anastomosing' and 'braiding,' since the formation of anabranches causes a reduction in discharge along a stream, which is quite different than the geomorphic destabilization exhibited by braided rivers (Makaske 2001). Anastomosing increases aggradation, stabilization, and the likelihood for abandonment (Jain and Sinha 2004), while braiding is less stable with more sediment transport through the active channels (Nichols 1999). Inasmuch, we wish to keep a braided and anastomosing distinction between the two regimes so that we better capture the differences between them: the paleo- and modern-day Narayani are more classically

braided systems, versus the 3kyr streams that anastomosed through Parasi. This timing and distinction is consistent with other work defining post 5kyr as a time period of less stream-power (Nakayama and Ulak 1999; Tandon, Sinha et al. 2008; Sinha and Sarkar 2009). This is speculated to be due to a temporary cut-off from the upper mountainous catchment and less stream-power after 5kyr due to the post-hypsithermal decrease in rainfall—an event supported by a lack of post-hypsithermal depositional ages in our transect as well as other nearby basins (Yonebayashi and Mutsuhiko 1997; Sharma, Joachimski et al. 2004; Sinha and Sarkar 2009).

Further indication of river-cutoff and reduced stream power in the higher Himalayan catchments is reflected in the zircon provenance shift observed in the 5kyr-old sediments. Unlike the 10kyr detrital zircon ages that are consistent with the Tibetan Tethys and the Greater Himalayas, the 5kyr deposits contain clasts of Siwalik fragments[22] and detrital zircons from Siwalik source regions. This suggests that there was indeed a cutoff to this part of the Terai from upper mountainous regions. While this could be due to hydrologic waning associated with climate or a temporary blockage from upstream damming, a shift to Siwalik sourcing is definitely seen in the 5kyr aquifer sediments. Provenance shifts bracketing this time have also been seen in other alluvial deposits along Srinagar's Alaknanda River (Wasson, Juyal et al. 2008). No longer able to receive sediments from Nepal's mountainous catchment, Parasi's deposits at ~5kyr were sourced from Nepal's foothill-fed rivers. These foothill-fed rivers may have served as minor tributaries to the paleo-Narayani during its earlier Holocene time there. With the lack of stream power from climatic and avulsive controls, the only thing favoring deposition at 5kyr was neotectonic activity occurring along the Siwaliks (i.e., the Piggyback Basin formations, (Kimura 1999)). Altogether, the 5kyr deposits are consistent with:

1) Parasi's river changing from a braided to a more stable anastomosing regime,
2) Parasi's sediments being affected by the Late Quaternary uplift of the Siwaliks,

[22] A week was spent, prior to needle-sampling in Parasi, sampling possible 'source' rocks from upstream catchments in the Lesser Himalayas, while driving south from Kathmandu

3) Parasi undergoing a middle-Holocene change to more arid conditions.

Additional support for fluvial stability around 5kyr is provided by the deposits infilling Parasi's paleo-Narayani—the previously active eastern channel is unconformably overlain with clay chips, dark gray clayey silts, and a shelly/organic mottled gray silt sequence (PNS2 ~105m). This is a classic sequence of channel abandonment, showing a cessation of fluvial activity (sand to silt unconformity) and infilling of a channel (silts). With less stream power after the mid-Holocene, muddy surfaces were stable enough to undergo soil formation. This is preserved in the overlying unit's mottling and presence of organic fragments (paleo-root pieces). According to Zaleha et al (1997), hundreds of years of subaerial exposure and soil formation are required for a sedimentary facies' primary structure to be lost through weathering and mixing, resulting in the formation of typical Siwalik soil. This means *at least* 100 yrs of no river activity in the paleochannel. While the evidence, altogether, supports 5kyr as being stable, Parasi's rivers were still more active than today's moribund, Jharai river. At 5kyr, the conditions were probably very similar to today's Baghmati river— a river in the Gandak-Kosi interfluve that has avulsed 8 times over the past 230 years (Jain and Sinha 2003; Jain and Sinha 2004). While we do not know if the 5kyr rivers in Parasi were as hyperavulsive as the Baghmati, they have dimensionally similar widths: ~30-100m (Figure 2D, (Jain and Sinha 2004; Google, TeleAtlas et al. 2009)). Thus, we suggest that today's Baghmati—or a less dynamic version of it—is a relatively good analogue for Parasi's river at 5kyr.

4.1.5. Parasi's late Holocene: a gradual abandonment of a river, (5 - 0.7 kyr)

The late Holocene marks a moribund, interfan phase for Parasi. After an early to mid Holocene occupation by a major Himalayan river, Parasi's late Holocene fluvial regime weakens to today's minor Jharai River that has a width of only ~7m in the main thalweg and ~35m at bank-full flow. This is in contrast to the ~200m main thalweg and ~1km bank-full flow of today's Gandak-Narayani, making today's Jharai River likely ~4% of its predecessor's flow. With the winnowing of fluvial activity following

the loss of the Narayani, two major rivers bracketed Parasi's interfan: the Rapti to the west and the Narayani-Gandak to the east. Closer to their modern day locations, these major rivers were slowly aggrading their megafan surfaces (Goodbred 2003), leaving Parasi progressively abandoned and limited to catchments from the nearby foothills. As previously mentioned, Parasi's mid-Holocene rivers likely resembled today's Baghmati River. In the transect, the mid-Holocene sands and muds are consistent with deposits of a Baghmati-type system (i.e., avulsive and anastomosing deposits as described by (Makaske 2001)). This is recorded as a river 'jump' away from the paleo-Narayani's relict channel (PNS2) into newer bypasses in the lower-lying floodplain (PNS5 and PNS1). As the new younger channels scoured out muds and channelized the lower floodplain, the trunk of the paleo-Narayani was abandoned—a behavior consistent with a Baghmati-type system. After losing flow to the lower floodplains, the paleochannel was abandoned somewhere on the time span of 100-1000 yrs, which enabled the surface to stabilize and form soils (PNS2 ~103m). Just before 5kyr, the paleochannel experienced a brief re-activation, shown by the 1m-thick deposit of fine sands over the paleosol. This could have been a crevasse splay reconnecting the river's old stem to the new anastomosing system, or a brief reoccupation of the paleochannel. We think, however, that a splay occurred, due to a continued channel connection thereafter—the paludal facies above the splay sands indicate that a bank failure likely "opened" a tie-type connection with the newer anastomosing channels. Regardless of the cause, the sand deposition shows that the previously exposed, stable surface became flooded and buried, precluding further soil formation. Rather, a re-opened connection filled the old channel with water, leading to 100-1000 years of suspended sediment deposition typical of an oxbow lake in which organic-rich, underconsolidated clays accumulate over the clean, coarse sands of the Narayani's paleochannel.

After losing power and aggrading enough elevation in the eastern channel, Parasi's river avulsed into the lower, western portion of the floodplain from the location of PNS2 to PNS5. Abandoned, the main paleochannel infilled with fine-grained sediments (PNS2), while sand deposition continued in

Parasi's new channels at PNS5 and PNS1 and separated by a muddy interfluve (PNS3). The mottling of the mud unit indicates gley-soil formation supports the idea that the interfluve was stable, further indicating the late Holocene (<3kyr) as a less dynamic period. With the stability of an anastomosing river, the interfluve was able to persist long enough to preserve its paleosol that now comprises part of the aquifer. Our findings are similar to Sinha and Sarkar's (2009) descriptions of modern anastomosing channels in the Upper Ganga plains. These anastomosing channels in Parasi lasted from 5-0.7 kyr, a long enough time period to enable the preservation of three depositional environments—the anastomosing channel, the oxbow lake, and the muddy interfluve—within 100's of meters of each other in the aquifer. This gives us important information about the scaling of heterogeneity inherent to this aquifer system: at 5 kyr, different fluvial environments existed ~500 meters from each other. Geologically speaking, this is one of the main reasons why Parasi's shallow aquifer boasts such high degrees of arsenic heterogeneity. Unlike the earlier periods of laterally contiguous deposition, such as Gurung's black muds (12.7 kyr) or the braidbelt sands from the paleo-Narayani (10-9 kyr), the late Holocene deposits, after the hypsithermal, are marked by much more heterogeneity at one time and in one space--at least three different deposits are concurrent within <1 km of our transect. Interestingly, with the end of the 5-0.7kyr anastomosing phase, Parasi's aquifer becomes capped with the silty mud facies typical to today's abandoned, interfan settings: "relatively low energy systems… …[with] interfans made up of muds and sand ribbons in the shallow sub-surface," Figure 9D, Tandon et al., 2008).

4.1.6. Parasi's aquifer in context with Indo-Nepal history (Prehistoric - 0 kyr)

Since the most recent aquifer deposits in Parasi are the interfan silts that are unremarkably and uniformly muddy, an attempt was made to better resolve Parasi's recent history with paleo-environmental work done in areas bordering Parasi. Approximately 40 km west of Parasi is the town of Lumbini (Figure 10), which is situated just southwest of Butwal's alluvial fan.[23] Named as

[23] Tinau River Fan

one of UNESCO's World Heritage sites and as the site of Buddha's birthplace, archeological findings in Lumbini since the 1880's (Rijal 1984; Pandey 1985; Mishra 1996) present an opportunity to better interpret the area's history. While our current attempts to find sedimentological data from Lumbini has been limited,[24] some archeological work on the Mayadevi temple site suggests flooding conditions ~1.8-1.9 kyr (Mishra 1996). While we currently cannot conclude that Lumbini was flooded at this time, or, more precisely, whether the flooding was from a change in river course or from over-bank flooding (Sinha 2009), it would be helpful, in the future, to be able to relate the histories of the two sites to one another—for both the goals of preserving cultural heritage and understanding how locations 40km away from each other, and in the same interfan region, evolve in terms of sediments, rivers, and arsenic.

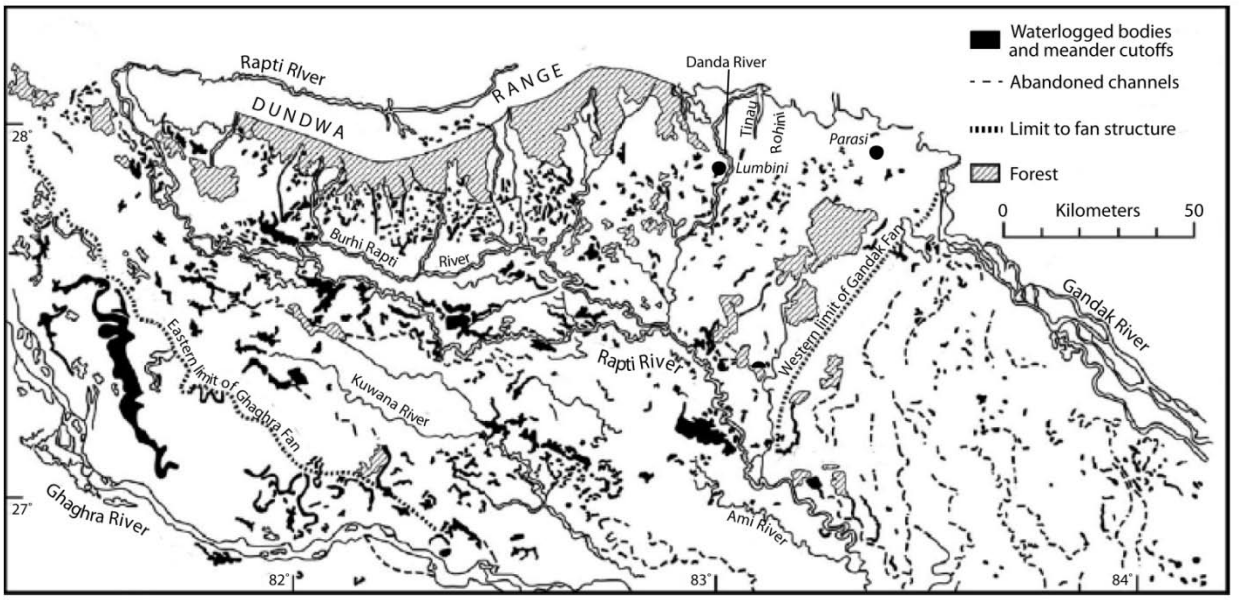

Figure 10, close-up map of the Rapti River Basin, modified from Chandra et al., (2007), who used LandSat imagery to illustrate the main fluvial features of the region. UNESCO's World Heritage site, the birthplace of Buddha at Lumbini and our site in Parasi, are superimposed to show their locations. Proposed damming of the Danda River in 2001 posed an inundation problem for the conservation of Lumbini. The Telar "oil" River was likely part of today's Danda River complex, which is the river in antiquity scripts banking the garden where Buddha was born ~2.5 kyr (Mishra, 1996).

[24] Which is a shame because our stratigraphy is relevant to the prehistoric time of Buddha

4.2. The evolution of Parasi's aquifer in context with arsenic (21 - 0 kyr)

So far, the OSL ages of aquifer sands, as well as their facies, suggest an overall history of aquifer development that can be explained in context of tectonic and climatic changes in the region. The stratigraphy and depositional history of Quaternary sediments in the Himalayan foreland basin have been investigated (Sharma et al., 2004; Gurung et al., 2005; Shah, 2008; Singh, 2009), and most studies converge on the idea that sediment deposition has been affected by Himalayan uplift and climate change during the Pleistocene-Holocene transition (Sinha and Friend, 1994; Sharma et al., 2004). How this relates to arsenic has, until now, been limited to observational (and usually un-groundtruthed) findings that groundwater arsenic occurs in Holocene sands (Acharyya 2000; BGS-DPHE 2001; Smedley 2002; Chakraborti, Mukherjee et al. 2003; Singh 2006; Shah 2008; Selim Reza, Jiin-Shuh Jean et al. 2009). We see this age-trend again in Parasi's, where different aged deposits have different concentrations of arsenic (Figure 11). The Holocene deposits show the typical arsenic enrichment in younger deposits, a phenomenon that is also observed in our Vietnam and Bangladesh study sites, as well as other sites throughout the Bengal basin (McArthur et al., 2001; Ishiga et al., 2000; Charlet and Polya, 2006). One new insight from this study, separating it from previous work, is that Parasi shows arsenic elevation in aquifer portions deposited during a *specific* interval of the Holocene. In overlaying Parasi's stratigraphy with arsenic, we see that elevated arsenic is constrained in units deposited between 10 and 5kyr (Figure 11). This is different from previous findings is that we see for the first time a mud-capped Holocene sand sequence that is not contaminated with arsenic (PNS5-25, Figure 11). From our previous findings in Bangladesh (Weinman 2008), we would expect a 'capped' portion of recent alluvium to be higher in arsenic. Instead, the sands deposited after 5kyr, with a sizable capping (~8m, which would translate into high arsenic in Araihazar) are able to maintain low groundwater arsenic. This gives a time constraint on arsenic contamination in Parasi occurring between 10-5kyr in portions of the aquifer formed during the Holocene's wet hypsithermal.

From the zircon age dating, the sands of the 10-5kyr deposits were being sourced out of the mountainous higher Himalayas. This is different than the period following the wetter hypsithermal, when the decreasing monsoon along with abandonment of the Narayani River left Parasi receiving sands from the nearby foothills. These findings are markedly different from previous studies in the Ganga plains, which suggest that Higher Himalayan Crystallines are the major source of all sediments (Galy and France-Lanord, 2001). In addition, other studies using REE's (Tripathi et al. 2007; Bibi, Ahmed et al. 2006) infer that Ganga Plain sedimentation is highly homogenous. Our work supports neither of these for Parasi, where the sedimentary source has changed within the aquifer. After the hypsithermal, the sands were no longer being sourced from the upper Himalayan's newer and "more weatherable" crust, (i.e., White 2003); instead the youngest Holocene sands are from the Siwalik rocks, which have already undergone *at least* one full weathering cycle—another reason why the late Holocene deposits support such low concentrations of arsenic; they are weathered and already "flushed." So, not only do our results show a distinction between Pleistocene and Holocene deposits, we also show, for the first time, a likely pre-depositional and provincial affect contributing to Parasi's heterogeneity of arsenic—not all Holocene sands are necessarily high in groundwater arsenic.

Overall, our work here is important because, along with only a handful of other *contextual* and *high-resolution* sedimentological studies (i.e., Beckie's UBC site[25] and McArthur 2008), it represents one of the first attempts of understanding how these aquifers evolve as an entire process. This is a considerable step in managing and modeling groundwater and understanding geomorphic surfaces, as it enables us to link current hydrological processes with current and previous Earth surface processes—the areas these aquifers are in are some of the most sedimentologically and geomorphically active places on the planet. So, we contend that understanding arsenic using traditional biogeochemical cycling is not

[25] I can't find any publications on their site, but they presented their work at the 2009 AGU Chapman Conference

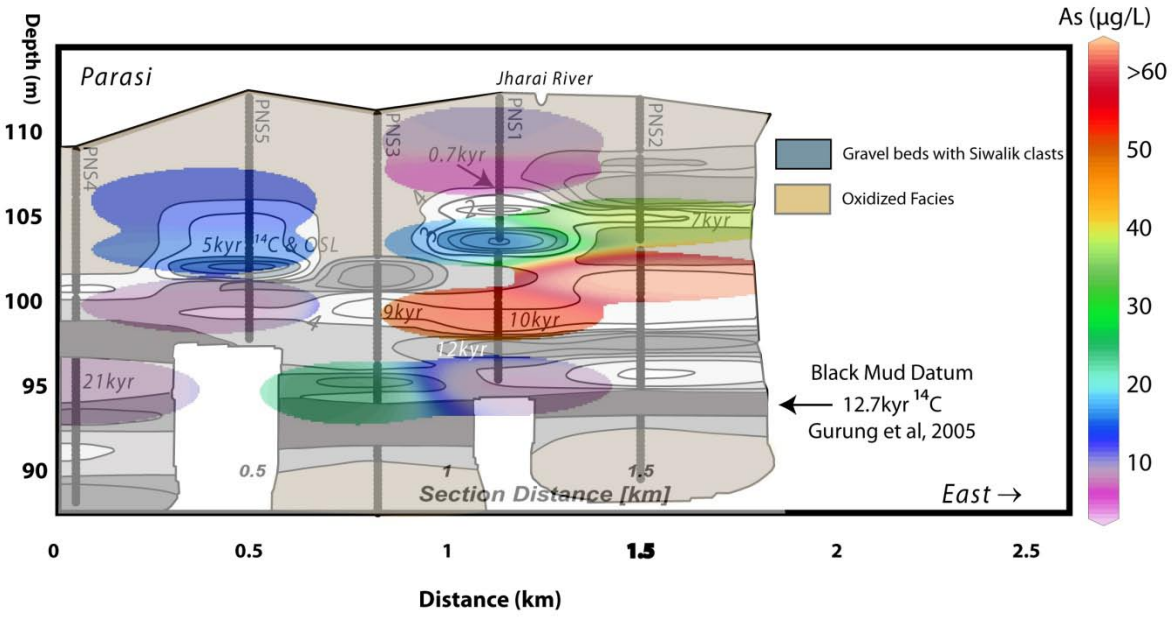

Figure 11, high resolution ICP-MS arsenic results of needle-sampled groundwater. The concentrations range from 3-150µg/L arsenic, which are shaded using OceanDataView and overlain on Parasi's aquifer stratigraphy. Similar to the Hach field test results by ENPHO and Filters for Families, the needle-sampling distributions corroborate the arsenic concentrations observed in the preliminary monitoring data. Combined with the dated aquifer stratigraphy, the results show that higher arsenic concentrations are found in younger, more recently deposited aquifer sediments.

enough for managing Asia's arsenic-prone groundwater. In Asia's highly dynamic fluvial and deltaic regions, we need to incorporate fluvial geomorphology (i.e., aquifer forming rates) and sedimentology (i.e., aquifer facies) for the best efforts of preventive groundwater mitigation. This is non-trivial since most biogeochemistry studies to date in these aquifers are not *sedimentologically* contextual; they are limited to considering only microbial activity (i.e., carbon fixation and remineralization) into their hydrological models (Dowling 2002; Harvey, Ashfaque et al. 2006). In these models, the aquifer sediments are static features, approximated by porosity and hydraulic conductivity values. Outside of considering aquifer sediments as passive matrixes that can surface-complex and/or reactively transport arsenic (i.e., through models using SCM and adsorptive constants like K_d), there is little to no account of how these aquifers sedimentologically *and* geochemically form. This is not only an important interaction, it is especially nontrivial since the SCM and reactive transport models (to date) neglect the

fact that local, tube-well and village-sized heterogeneity—both sedimentologically and geochemically—form over comparable time and length scales. While the models are good at predicting current conditions, they lack the long-term understanding necessary for managing water resources in these numerous sedimentologically dynamic regions.

New approaches by Datta et al. 2009 and Jung et al. 2009 find permeable reactive-barrier type transport along the hyporheic zones of rivers. The premise of their work focuses on understanding the arsenic adsorptive and desorptive behavior in deposits that exchange water between aquifers and rivers. While the Asian aquifers typically have ubiquitously reducing waters, the zones where the aquifers interface with oxygenic river water precipitate Mn and Fe oxides that trap and remove arsenic from the groundwater. In this vein, the water discharging from the aquifer into the river is naturally filtered. The aquifer and channel deposits that experiencing this exchange have the potential for becoming future sources of arsenic *within the aquifer*—once the river moves and/or experiences waning, the old river course fills-in with muds, leaving a new capped portion of aquifer. While we do not currently know if this is a process relevant to Parasi's 10-5kyr, we see it as an important inclusion of landscape dynamics in understanding groundwater heterogeneity—especially in areas where rivers avulse and move as they do in many of the affected regions of Asia. Incorporating a more dynamic and coupled view of the surface processes leading to the co-evolution of arsenic and aquifers is needed to best make use of the land and the water within it. With the study here showing an aquifer vulnerability in response Holocene hypsithermal deposition, other areas of the Terai and Ganga plain undergoing punctuated deposition during the early Holocene may also have similar deposits.

5. Conclusion

Overall, our findings show Parasi's predominant *post-glacial* deposition consistent with other young ages of deposition in the region (Chandra, Rhodes et al. 2007). The oldest aquifer sands

encountered in our transect date to the glacial maximum of the late Pleistocene, ~21kyr, which serves as a good groundwater source with low arsenic for the overlying village. With the onset of the Holocene, the next aquifer deposited in Parasi were from a braided river between 10-5kyr that was likely an older course of today's Narayani-Gandak River. Post-hypsithermal conditions along with eastward Narayani migration left Parasi with some pockets of anastomosing channel sands dating between 5-3kyr, followed by a continually waning river until 0.7kyr, when Parasi became a fully moribund system. One of the important findings of this work shows that 10-5kyr deposits are particularly vulnerable to arsenic, meaning that this may be a deposit to avoid in other Terai and Ganga Plain regions. It is important to stress however that instead of necessarily looking for a specific layer or datum—such as the hypsithermal units, black muds, or LGMP paleosols—it is our view that the sediment facies themselves, in each location, are quite different, and that is important to understand local aquifer formative processes in managing Asia's water.

References

Acharyya, S. K., S. Lahiri, B.C. Raymahashay, and A. Bhowmik (2000). "Arsenic toxicity of groundwater in parts of the Bengal basin in India and Bangladesh: the role of Quaternary stratigraphy and Holocene sea-level fluctuation." Environmental Geology **39**(10): 1127-1137.

Ballarini, M. (2006). Optical dating of quartz from young deposits; from single-aliquot to single-grain. Fairfax VA, IOS Press.

BBC (2007). Nepal government to probe border area encroachment by India. BBC Monitoring South Asia - Political. UK, British Broadcasting Corporation.

BGS-DPHE, Ed. (2001). Arsenic contamination of groundwater in Bangladesh. British Geological Survey Technical report, WC/00/19, Keyworth.

Bibi, M. H., F. Ahmed, et al. (2006). "Distribution of arsenic and other trace elements in the Holocene sediments of the Meghna River Delta, Bangladesh." Environmental Geology **50**(8): 1243-1253.

Chakraborti, D., S. C. Mukherjee, et al. (2003). "Arsenic groundwater contamination in Middle Ganga Plain, Bihar, India: A future danger?" Environmental Health Perspectives **111**(9): 1194-1201.

Chandra, S., E. Rhodes, et al. (2007). "Luminescence dating of late Quaternary fluvial sediments in the Rapti Basin, north-central Gangetic plains." Quaternary International **159**(1): 47-56.

Clark, P. U., A. S. Dyke, et al. (2009). "The Last Glacial Maximum." Science **325**(5941): 710-714.

Datta, S., B. Mailloux, et al. (2009). "Redox trapping of arsenic during groundwater discharge in sediments from the Meghna riverbank in Bangladesh." Proceedings of the National Academy of Sciences of the United States of America **106**(40): 16930-16935.

Davies, R. J. (2007). Seismic geomorphology: applications to hydrocarbon exploration and production. Bath, UK, The Geological Society Publishing House.

DeCelles, P. G., G. E. Gehrels, et al. (2000). "Tectonic Implications of U-Pb Zircon Ages of the Himalayan Orogenic Belt in Nepal." Science **288**(5465): 497-499.

Dill, H. G., D. R. Khadka, et al. (2003). "Infilling of the Younger Kathmandu-Banepa intermontane lake basin during the Late Quaternary (Lesser Himalaya, Nepal): a sedimentological study." Journal of Quaternary Science **18**(1): 41-60.

Dixit, A., M. Upadhya, et al. (2007). Flood Disaster Impact and Responses in Nepal Tarai's Marginalized Basins. Working with Winds of Change. Towards Strategies for Responding to the Risk Associated with Climate Change and other Hazards. M. Moench and A. Dixit. Kathmandu, Institute for Social and Environmental Transition**:** 119-157.

Dowling, C. B., R.J. Poreda, A.R. Basu, and S.L. Peters (2002). "Geochemical study of arsenic release mechanisms in the Bengal Basin groundwater." Water Resources Research **38**(9): 1173.

Dwivedi, G. N., S. K. Sharma, et al. (1997). "Quaternary geology and geomorphology of a part of Ghaghara-Rapti-Gandak sub-basins of Indogangetic Plain, Uttar Pradesh." Journal Geological Society of India **49**: 193-202.

Godfrey-Smith, D. I., D. J. Huntley, et al. (1988). "Optical dating studies of quartz and feldspar sediment extracts." Quaternary Science Reviews **7**(3-4): 373-380.

Goodbred, S. L., and S.A. Kuehl (2000). "The significance of large sediment supply, active tectonism, and eustasy on margin sequence development: Late Quaternary stratigraphy and evolution of the Ganges-Brahmaputra delta." Sedimentary Geology **133**: 227-248.

Goodbred, S. L., Steven A. Kuehl, Michael S. Steckler, and Maminul H. Sarker (2003). "Controls on facies distribution and stratigraphic preservation in the Ganges-Brahmaputra delta sequence." Sedimentary Geology **155**(3-4): 301-316.

Google, TeleAtlas, et al. (2009). Google Earth 5.1.3533.1731, Google.

GSA (1999). Pocket-Size Sand Grain Sizing Folder. GRN001, Geological Society of America.

Guillot, S., B. Weinman, et al. (2009). "Tracing the origin of arsenic anomaly in Nawalparasi (Terai, Nepal)." Journal of Environmental Science and Health Part A **in prep**.

Gupta, S. (1997). "Himalayan drainage patterns and the origin of fluvial megafans in the Ganges foreland basin." Geology **25**(1): 11-14.

Hartley, W. and N. M. Dickinson (2009). "Exposure of an anoxic and contaminated canal sediment: Mobility of metal(loid)s." Environmental Pollution **in press**: 1-9.

Harvey, C. F., K. N. Ashfaque, et al. (2006). "Groundwater dynamics and arsenic contamination in Bangladesh." Chemical Geology **228**(1-3): 112-136.

Heroy, D. C., S. A. Kuel, et al. (2003). "Mineralogy of the Ganges and Brahmaputra Rivers: implications for river switching and Late Quaternary climate change." Sedimentary Geology **155**: 343-359.

Jain, V. and R. Sinha (2003). "Hyperavulsive-anabranching Baghmati river system, north Bihar plains, eastern India." Z. Geomorph. N.F. **47**(1): 101-116.

Jain, V. and R. Sinha (2003). "River systems in the Gangetic plains and their comparison with the Siwaliks: a review." Current Science **84**(8): 1025-1033.

Jain, V. and R. Sinha (2004). "Fluvial dynamics of an anabranching river system in Himalayan foreland basin, Baghmati river, north Bihar plains, India." Geomorphology **60**(1-2): 147-170.

Jaiswal, M. K., M. I. Bhat, et al. (2009). "Luminescence characteristics of quartz and feldspar from tectonically uplifted terraces in Kashmir Basin, Jammu and Kashmir, India." Radiation Measurements **44**(5-6): 523-528.

Jaiswal, M. K., P. Srivastava, et al. (2008). "Feasibility of the SAR technique on quartz sand of terraces of NW Himalaya: A case study from Devprayag." Geochronometria **31**: 45-52.

Jung, H. B., M. A. Charette, et al. (2009). "Field, Laboratory, and Modeling Study of Reactive Transport of Groundwater Arsenic in a Coastal Aquifer." Environmental Science & Technology **43**(14): 5333-5338.

Juyal, N., R. K. Pant, et al. (2009). "Reconstruction of Last Glacial to early Holocene monsoon variability from relict lake sediments of the Higher Central Himalaya, Uttrakhand, India." Journal of Asian Earth Sciences **34**: 437-449.

Kars, R. H. and J. Wallinga (2009). "IRSL dating of K-feldspars: Modeling natural dose response curves to deal with anomalous fading and trap competition." Radiation Measurements 44(5-6): 594-599.

Kazuo, K. (1999). "Diachronous evolution of sub-Himalayan piggyback basins, Nepal." The Island Arc **8**(1): 99-113.

Kimura, K. (1999). "Diachronous evolution of sub-Himalayan piggyback basins, Nepal." The Island Arc **8**(1): 99-113.

Li, B., S. H. Li, et al. (2008). "Isochron dating of sediments using luminescence of K-feldspar grains." Journal of Geophysical Research-Earth Surface 113(F2).

Lian, O. B. and R. G. Roberts (2006). "Dating the Quaternary: progress in luminescence dating of sediments." Quaternary Science Reviews **25**(19-20): 2449-2468.

Mahadevan, T. M. (2002). Geology of Bihar and Jharkhand. India, Geological Society of India, Dept. of Science and Technology.

Makaske, B. (2001). "Anastomosing rivers: a review of their classification, origin and sedimentary products." Earth-Science Reviews **53**(3-4): 149-196.

Malek, K. T. (1967). "Land form and use and characteristics of some soils in Nepal." Soil Science **104**(5): 350-357.

McArthur, J. M., P. Ravenscroft, D.M. Banerjee, J. Milsom, K.A. Hudson-Edwards, S. Sengupta, C. Bristow, A. Sarkar, S. Tonkin, and R. Purohit (2008). "How paleosols influence groundwater flow and arsenic pollution: A model from the Bengal Basin and its worldwide implication." Water Resources Research **44**(11): W11411.

Mishra, T. N. (1996). "The archaeological activities in Lumbini." Ancient Nepal **139**: 36-48.

Mohindra, R. and B. Parkash (1994). "Geomorphology and Neotectonic Activity of the Gandak Mega-Fan and Adjoining Areas, Middle Gangetic Plains." Journal of the Geological Society of India **43**(2): 149-157.

Mohindra, R., B. Parkash, et al. (1992). "Historical Geomorphology and Pedology of the Gandak Megafan, Middle Gangetic Plains, India." Earth Surface Processes and Landforms **17**(7): 643-662.

Nagar, Y. C. (2007). Methodological aspects of radiation dosimetry of natural radiation environment using luminescence techniques: New minerals and applications. Physical Research Laboratory. Ahmedabad, India, Gujurat University. **Ph.D. Thesis:** 162.

Nakayama, K. and P. D. Ulak (1999). "Evolution of fluvial style in the Siwalik Group in the foothills of the Nepal Himalaya." Sedimentary Geology **125**(3-4): 205-224.

NASC/ENPHO (2004). The State of Arsenic in Nepal - 2003. B. R. Shrestha, J.W. Whitney, and K.B. Shrestha, (Editors), USGS**:** 100 pages.

Nichols, G. (1999). Sedimentology and stratigraphy. Malden, MA, Wiley-Blackwell.

Pandey, R. N. (1985). "Archaeological Remains of Lumbini: The Birth-place of Lord Buddha." Contributions to Nepalese Studies **12**(3): 51-62.

Prasad, S. and E. A. Khan (2005). "Gandak fan - A macro quaternary feature of middle Ganga plain, Uttar Pradesh and Bihar." Journal of the Geological Society of India **65**(5): 597-608.

Pratt, B., D. W. Burbank, et al. (2002). "Impulsive alluviation during early Holocene strengthened monsoons, central Nepal Himalaya." Geology **30**(10): 911-914.

Prescott, J. R., and J.T. Hutton (1988). "Cosmic ray and gamma ray dosimetry for TL and ESR." Nuclear Tracks and Radiation Measurements **14**: 223-227.

Prescott, J. R., and J.T. Hutton (1994). "Cosmic ray contributions to dose rates for luminescence and ESR dating: large depths and long-term variations." Radiation Measurements **23**(2/3): 497-500.

Puthusserry, J. T., N. Juyal, et al. (2007). "Luminescence chronology of late Holocene extreme hydrological events in the upper Penner River basin, South India." Journal of Quaternary Science **22**(8): 747-753.

Rao, M. S., B. K. Bisaria, et al. (1997). "A feasibility study towards absolute dating of Indo-Gangetic alluvium using thermoluminescence and infrared-stimulated luminescence techniques." Current Science **72**(9): 663-669.

Rijal, B. K. (1984). "The Birth Place of Lord Buddha." Ancient Nepal **82**: 10-18.

Roberts, H. M. and G. A. T. Duller (2004). "Standardized growth curves for optical dating of sediment using multiple-grain aliquots." Radiation Measurements **38**(2): 241-252.

Ross, J. and R. Gilbert (1999). "Lacustrine sedimentation in a monsoon environment: the record from Phewa Tal, middle mountain region of Nepal." Geomorphology **27**(3-4): 307-323.

Sakai, H., H. Sakai, et al. (2006). "Pleistocene rapid uplift of the Himalayan frontal ranges recorded in the Kathmandu and Siwalik basins." Palaeogeography, Palaeoclimatology, Palaeoecology **241**: 16-27.

Selim Reza, A. H. M., J. S. Jiin-Shuh Jean, et al. (2009). "Occurrence of Arsenic in Core Sediments and Groundwater in the Chapai-Nawabganj District, Northwestern Bangladesh." Water Research **in press**.

Shah, B. A. (2008). "Role of Quaternary stratigraphy on arsenic-contaminated groundwater from parts of Middle Ganga Plain, UP-Bihar, India." Environmental Geology **53**(7): 1553-1561.

Sharma, S., M. Joachimski, et al. (2004). "Late glacial and Holocene environment changes in Ganga plain, Northern India." Quaternary Science Reviews **23**: 145-159.

Shukla, U. K. (2009). "Sedimentation model of gravel-dominated alluvial piedmont fan, Ganga Plain, India." International Journal of Earth Science **98**: 443-459.

Singh, A. K. (2006). "Chemistry of arsenic in groundwater of Ganges-Brahmaputra river basin." Current Science **91**(5): 599-606.

Sinha, R. (1995). "Sedimentology of Quaternary Alluvial Deposits of the Gandak-Kosi Interfan, North Bihar Plains." Journal of the Geological Society of India **46**(5): 521-532.

Sinha, R. (1996). "Channel avulsion and floodplain structure in the Gandak-Kosi interfan, north Bihar plains, India." Z. Geomorph. N.F. **Suppl.-Bd. 103**: 249-268.

Sinha, R. (2009). "The Great avulsion of Kosi on 18 August 2008." Current Science **97**(3): 429-433.

Sinha, R. and S. Sarkar (2009). "Climate-induced variability in the Late Pleistocene-Holocene fluvial and fluvio-deltaic successions in the Ganga plains, India: A synthesis." Geomorphology **in press**.

Smedley, P. L., H.B. Nicolli, D.M.J. Macdonald, A.J. Barros, and J.O. Tullio (2002). "Hydrogeochemistry of arsenic and other inorganic constituents in groundwaters from La Pampa, Argentina." Applied Geochemistry **17**(259-284).

Srivastava, P., M. Sharma, et al. (2003). "Luminescence chronology of incision and channel pattern changes in the River Ganga, India." Geomorphology **51**: 259-268.

Suresh, N., T. N. Bagati, et al. (2002). "Optically stimulated luminescence dating of alluvial fan deposits of Pinjaur Dun, NW Sub Himalaya." Current Science **82**(10): 1267-1274.

Tandon, S. K., R. Sinha, et al. (2008). "Late Quaternary evolution of the Ganga Plains: Myths and misconceptions, recent developments and future directions." Golden Jubilee Memoir of the Geological Society of India **66**: 259-299.

Telfer, M. W., M. D. Bateman, et al. (2008). "Testing the applicability of a standardized growth curve (SGC) for quartz OSL dating: Kalahari dunes, South African coastal dunes and Florida dune cordons." Quaternary Geochronology **3**(1-2): 137-142.

van Geen, A., T. Protus, Z. Cheng, A. Horneman, A.A. Seddique, M.A. Hoque, and .M. Ahmed (2004). "Testing groundwater for arsenic in Bangladesh before installing a well." Environmental Science & Technology **38**(24): 6783-6789.

van Geen, A., Y. Zheng, et al. (2006). "A transect of groundwater and sediment properties in Araihazar, Bangladesh: Further evidence of decoupling between As and Fe mobilization." Chemical Geology **228**(1-3): 85-96.

Wasson, R. J., N. Juyal, et al. (2008). "The mountain-lowland debate: Deforestation and sediment transport in the upper Ganga catchment." Journal of Environmental Management **88**: 53-61.

Weinman, B., S.L. Goodbred, Y. Zheng, A. van Geen, Z. Aziz, A. Singhvi, and M. Steckler (2008). "Controls of Floodplain Evolution on Shallow Aquifer Development and the Resulting Distribution of Groundwater Arsenic: Araihazar, Bangladesh." GSA Bulletin **120**(11/12): 1567-1580.

White, A. F., and S.L. Brantley (2003). "The effect of time on the weathering of silicate minerals: why do weathering rates differ in the laboratory and the field?" Chemical Geology **202**: 479-506.

Yonebayashi, C. and M. Mutsuhiko (1997). "Late Quaternary vegetation and climatic history of eastern Nepal." Journal of Biogeography **24**: 837-843.

Zaleha, M. J. (1997). "Siwalik paleosols (Miocene, Northern Pakistan): genesis and controls on their formation." Journal of Sedimentary Research **67**(5): 821-839.

Zhang, J. F. and L. P. Zhou (2007). "Optimization of the 'double SAR' procedure for polymineral fine grains." Radiation Measurements **42**: 1475-1482.

Table 1. Needle Sample Locations and OSL Results for SAR and Double SAR on Parasi Aquifer Sands

Sample	Location, Setting, and Sample Comments	Lattitude	Longitude	Depth (m)	SAR-NCF OSL Aliqouts (n)	Dose rate (Gy/ka)	±	Mean Age (ka)	±	Least 10% Age (ka)	±	Least sed rate (cm/yr)	Mean sed rate (cm/yr)
[OSL]PNS1-25	Sunwach village, along a possible older course of the Jharai River, an area with high groundwater arsenic (100-300ug/L).	27.51512	83.67187	7.6	21	2.4	0.1	0.9	1	0.44	0.01	1.74	0.83
[IRSL]PNS1-50		27.51512	83.67187	15.1	23	2.3	0.1	23	12	11	1	0.14	0.07
[OSL,IRSL,SGC]PNS1-50(II)	IRSL age average of 14 ± 8 kyr (n=15)	27.51512	83.67187	15.2	30	3.8	0.2	12	6	4	1	0.4	0.1
[OSL,SGC]PNS1-60	Anomalously low OSL, small IRSL counts, redo with DoubleSAR during future OSL measurements	27.51512	83.67187	18.3	19	4.4	0.3	4	2	0.8	0.1	2.3	0.5
[OSL,IRSL]PNS2-25	Unwach village, on the east bank of the Jharai River, with the highest concentrations of groundwater arsenic (300-500ug/L). IRSL response in roughly half of the samples, with an average age of 10± 2 kyr (n=9)	27.51706	83.6749	7.6	17	1.65	0.06	7	4	2.1	0.3	0.4	0.1
[OSL,IRSL,SGC]PNS3-45	Transitional area between Santapur and Unwach villages, sited on an older course of the Jharai River (10-100ug/L arsenic).	27.51594	83.66876	13.7	19	3.6	0.2	21	14	9.3	0.6	0.1	0.07
PNS3-55		27.51594	83.66876	16.8	Sample Not Opened								
PNS4-35	Western-most part of transect, with the lowest concentrations of groundwater arsenic (<10ug/L).	27.51648	83.66119	10.7	Waiting Measurement	4.2	0.3						
[OSL,IRSL]PNS4-53	High IRSL counts depsite separations. Even with feldspar contamination, the OSL and IRSL was well-behaved, with IRSL average age a little lower at 13± 2 kyr (n=6)	27.51648	83.66119	16.2	14	4.6	0.2	23	6	17	1	0.1	0.07
PNS5-25		27.51528	83.66772	7.6	Waiting Measurement	1.6	0.1						
[OSL, IRSL, SGC]PNS5-33	One IRSL age of 1.75 kyr, ^{14}C age 5kyr	27.51528	83.66772	10.1	29	1.56	0.04	6	3	2	0.4	0.5	0.2
PNS5-45		27.51528	83.66772	13.7	Waiting Measurement	4.4	0.1						

[OSL]OSL based on regular SAR protocol

[IRSL]OSL based on Double IRSL-OSL for removing luminescence due to felspar

[SGC]OSL based on Single Growth Curve SAR

Table 2. OSL Protocols for the SAR and Double SAR Methods

OSL Step	Quartz SAR	OSL Step	Feldspar Double SAR
	□		□
	TL (200°C, 2°C/sec)		TL (200°C, 2°C/sec)
	Preheat (240°C, 2°C/sec)		Preheat (240°C, 2°C/sec)
	□		□
	TL (200°C, 2°C/sec)		TL (200°C, 2°C/sec)
$L_n + T_x$	Blue OSL, 60-70% power, 125°C		IRSL, 60% power, 50°C
	TL (200°C, 2°C/sec)	$L_n + T_x$	Blue OSL, 60-70% power, 125°C
	□		TL (200°C, 2°C/sec)
	TL (200°C, 2°C/sec)		□
	□		TL (200°C, 2°C/sec)
	Preheat (240°C, 2°C/sec)		□
T_x	Blue OSL, 60-70% power, 125°C		Preheat (240°C, 2°C/sec)
	Blue Bleach, 90% power, 260°C		IRSL, 60% power, 50°C
	□	T_x	Blue OSL, 60-70% power, 125°C
	Preheat (240°C, 2°C/sec)		Blue Bleach, 90% power, 260°C
L_1	Blue OSL, 60-70% power, 125°C		□
	□ (		Preheat (240°C, 2°C/sec)
	Preheat (240°C, 2°C/sec)		IRSL, 60% power, 50°C
T_x	Blue OSL, 60-70% power, 125°C	L_1	Blue OSL, 60-70% power, 125°C
	Blue Bleach, 90% power, 260°C		□ (
	□		Preheat (240°C, 2°C/sec)
	Preheat (240°C, 2°C/sec)		IRSL, 60% power, 50°C
L_2	Blue OSL, 60-70% power, 125°C	T_x	Blue OSL, 60-70% power, 125°C
	□ (		Blue Bleach, 90% power, 260°C
	Preheat (240°C, 2°C/sec)		□
T_x	Blue OSL, 60-70% power, 125°C		Preheat (240°C, 2°C/sec)
	Blue Bleach, 90% power, 260°C		IRSL, 60% power, 50°C
	□	L_2	Blue OSL, 60-70% power, 125°C
	Preheat (240°C, 2°C/sec)		□ (
L_3	Blue OSL, 60-70% power, 125°C		Preheat (240°C, 2°C/sec)
	□ (		IRSL, 60% power, 50°C
	Preheat (240°C, 2°C/sec)	T_x	Blue OSL, 60-70% power, 125°C
T_x	Blue OSL, 60-70% power, 125°C		Blue Bleach, 90% power, 260°C
	Blue Bleach, 90% power, 260°C		□
	□		Preheat (240°C, 2°C/sec)
	Preheat (240°C, 2°C/sec)		IRSL, 60% power, 50°C
L_0	Blue OSL, 60-70% power, 125°C	L_3	Blue OSL, 60-70% power, 125°C
	□ (		□ (
	Preheat (240°C, 2°C/sec)		Preheat (240°C, 2°C/sec)
T_x	Blue OSL, 60-70% power, 125°C		IRSL, 60% power, 50°C
	Blue Bleach, 90% power, 260°C	T_x	Blue OSL, 60-70% power, 125°C
	□		Blue Bleach, 90% power, 260°C
	Preheat (240°C, 2°C/sec)		□
L_1	Blue OSL, 60-70% power, 125°C		Preheat (240°C, 2°C/sec)
	□ (		IRSL, 60% power, 50°C
	Preheat (240°C, 2°C/sec)	L_0	Blue OSL, 60-70% power, 125°C
T_x	Blue OSL, 60-70% power, 125°C		□ (
			Preheat (240°C, 2°C/sec)
			IRSL, 60% power, 50°C
		T_x	Blue OSL, 60-70% power, 125°C
			Blue Bleach, 90% power, 260°C
			□
			Preheat (240°C, 2°C/sec)
			IRSL, 60% power, 50°C
		L_1	Blue OSL, 60-70% power, 125°C
			□ (
			Preheat (240°C, 2°C/sec)
			IRSL, 60% power, 50°C
		T_x	Blue OSL, 60-70% power, 125°C

L_x = "Regenerative Dose," with L_1, L_2, and L_3 being increasingly dosed by the $^{90}Sr/^{90}Y$ beta-source

T_x = "Test Dose," the same dosing by the $^{90}Sr/^{90}Y$ beta-source after each L_x for sensitivity correction (L_x/T_x)

TL = Thermoluminescence

L_0 = Measurement with zero dose, for determining if any charges are left in the traps

NCF = ratio of TL 110°C peaks from TL measurements before and after the natural L_n measurement

L_1/L_1 = Recycling Ratio, with samples rejected if not in the 1.00 ± 0.1 limit

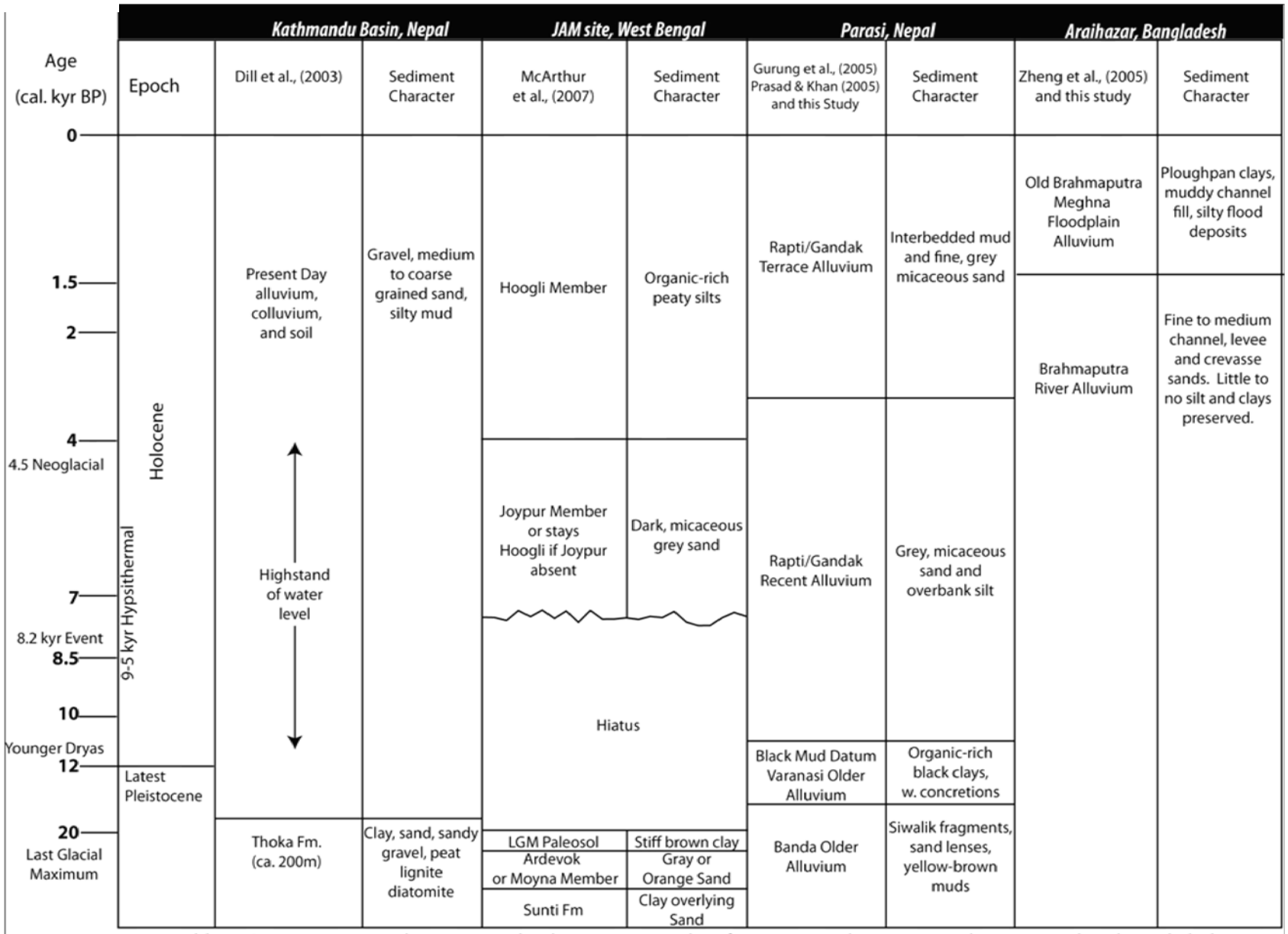

Table 3. Comparative Late Pleistocene and Holocene stratigraphies for arsenic-study sites in Nepal, West Bengal, and Bangladesh. References for the compliation are listed in the first row of the table.

CHAPTER III

LINKING SHALLOW GROUNDWATER ARSENIC HETEROGENEITY WITH SEDIMENT AGE AND SEDIMENTARY ORGANIC MATTER: LEACHING RESULTS FROM COLUMNS WITH SEDIMENTS OF DIFFERENT AGES.

Abstract

In trying to understand how aquifer sediment ages can account for some of the heterogeneous distributions of arsenic in Asia, a series of field and lab geochemical experiments were combined to help infer how sediment age impacts groundwater arsenic. We particularly wanted to test if older-aged aquifer material had lower laboratory weathering rates or less in-situ natural organics. To assess the relative roles of aquifer age and/or the natural organic content in the release of arsenic in some of Asia's arsenic-prone deltaic aquifer systems, the type of organic content was characterized in the different aquifer facies of Parasi, Nepal and Araihazar, Bangladesh. A volumetric comparison of organic content in the facies comprising the aquifers show that there is just as much sedimentary organic stored in the sand and fine mud facies. C:N analysis on the Araihazar sediments shows that there is no C:N difference between facies, and more of an overall diagenetic terrestrial $\rightarrow$ microbial $\rightarrow$ denitrification trend with depth in the aquifer. Combined with the results of flow-through column experiments using several sand facies, we infer the release of arsenic into Araihazar and Parasi's groundwater is a product of natural weathering, fueled by natural organics associated with the sediments. The column experiments indicate that aquifer sands—the facies with the highest amounts of combustible organics—released the highest amounts of arsenic, regardless of the depositional age of the aquifer.

1. Introduction

When thinking and reading about the arsenic problem in Asia, one of the questions a sedimentologist asks herself[26] is whether the organic matter fueling the release of arsenic in the Himalayan aquifer system is from a sedimentary source. Knowing whether the 'primary' organic matter involved in arsenic's release is a young, labile source infiltrating from the surface (Harvey, 2002; Sengputa, 2008; Polizzotto, 2005), or whether it is from another, more recalcitrant source, 'co-deposited' within the aquifer deposits themselves (Meharg, 2006; McArthur, 2004; McArthur, 2008) is important, because it will help us understand how these aquifers actually become vulnerable to arsenic. Are the reductants responsible for arsenic's release found naturally in the aquifer? Or, is the organic matter something being loaded through human activity? This is an important distinction because we still do not know whether or not these aquifers were always affected.

In looking more closely into the work that is being done to answer this question, it appears that we are far from a consensus on *exactly* how long arsenic has been in the groundwaters of Asia (van Geen, 2009). We only became aware of the problem in Bangladesh's post-tube well years, meaning that we still do not know what pre-irrigative and pre-pumping conditions resemble for arsenic. In Bangladesh, observed steady-state arsenic concentrations $\left(\frac{d[As]}{dt} = 0\right)$ in thousands of tube-wells despite variations in other dissolved elements (Cheng, 2005) gives a notion that arsenic may have always been there, staying at the same concentration since the aquifer's formation. And, since most of the affected Himalayan shallow deposits are found to be Holocene-aged (Saunders, 2005; Ahmed, 2004; Weinman, 2008; McArthur, 2008), we can extrapolate that the arsenic conditions seen today could possibly date back to the formation of the Himalayan deltas (Dowling, 2002; Goodbred, 2000; Guillot, 2007; Guillot, 2007; Hori, 2004). At a maximum, this gives us an arsenic and aquifer co-evolutionary process that occurs over a 10,000 year time span, with little insight as to whether or not human activity

[26] or, himself

has or can worsen the problem. To put this in perspective, this is similar to trying to understand how humans can affect climate with the lone observation that atmospheric CO_2 has increased within the past 10,000 years. In other words, we want to know *when* and *how fast* an aquifer becomes vulnerable to arsenic.

On the other end of the time-spectrum, we know that dissolved arsenic can accumulate quickly in the pore-waters of the new [re-]deposited muds in the "mobile mud-belt" of the Amazon delta—a buildup of ~ 75 to 225 μg/L in one year (Sullivan, 1996). Opposite to our 10,000 year vulnerability bracket, this type of fast ingrowth indicates that natural contamination can occur within a year. A compilation of arsenic "release" from OSL, $^3He/^3H$, and time-series studies in Araihazar, Bangladesh and now Van Phuc, Vietnam indicate a common, zero order ~4-20 μg/L release rate of arsenic into the aquifers (Cheng, 2005; Stute, 2007; Weinman, 2005; Larsen, 2008), meaning that within a year of capping and/or inhibited flushing, arsenic contamination can occur in a newly mud-capped location (Weinman, 2005). With other aquifers becoming contaminated with arsenic through human activity (Aksoy, 2009; Lawrence, 2000), it is unclear how "sensitive" Asia's aquifers are to damming, irrigating, and organic[27] infiltration—i.e., anthropogenically changing flow through the existing aquifer facies (Polizzotto, 2008; Silbergeld, 2008).

As sedimentologists, we know that there is a range of natural organic content associated with different types of sedimentary deposits. Productive lacustrine deposits have higher organic contents versus dune sand deposits, and older sedimentary units typically contain less labile organics than younger deposits (Tyson, 1995; Kilops, 2005). In the case of Asian aquifers, it is similarly intuitive to think that surface soils have higher and more labile organic contents than the "clean" sandy paleo-river deposits located several meters below a mud-capped surface. This supports the idea that much of the organic matter responsible for these aquifers' reducing conditions is coming from the surface. But, how

[27] Fertilizer, landfill, and/or sewage

much of the reductant is young, organic matter infiltrating the aquifer from the surface (Kocar, 2008; Harvey, 2002; Lawrence, 2000; Neumann, 2010) and how much is from older organic matter sourced within the sedimentary deposits themselves (McArthur, 2008; Meharg, 2006)? If the organics are coming mainly from the surface, then it has different implications for how these groundwaters evolve than if the arsenic is driven from organics being co-deposited as the aquifer forms. In considering the question as to where the reductant(s) for arsenic release is (or are) being sourced, we can look at the organic contents of the aquifer sediments to see if there is enough organic carbon to drive reductive-dissolution. We can also start to assess if older deposits are less prone to arsenic because they have exhausted their supply of sedimentary organics.

To assess the types of sedimentary organic facies and if there is enough natural sedimentary organic matter to drive the release of arsenic in these aquifers, estimates of organic matter were made on sediment samples from ~1km high-resolution sampling transects in sites with well-established and ongoing arsenic and aquifer age-dating studies in Nepal and Bangladesh (Shrestha, 2004; van Geen, 2003; Zheng, 2005; Stute, 2007; van Geen, 2008; NASC/ENPHO, 2004; Maharjan, 2006; Gurung, 2005; Weinman, 2008). Column experiments were also performed on young and old OSL-dated aquifer sediments ascertained from the field sites to test the importance of sediment age and/or the amount of sedimentary organic matter on the release rate of arsenic. Distinguishing the relative roles of the aquifer age and the availability of a labile organic has important implications for how we use, treat, and maintain groundwater resources. For instance, if older aquifer units naturally have lower release-rates arsenic, they can be preferentially targeted for sources of low-arsenic water. Here we explore how important the organics naturally associated with an aquifer facies is in mediating arsenic. Results indicate that the sands with higher amounts of organic matter have accelerated release of arsenic, despite being depositionally older. Considered with sediment properties, the results indicate that

reductive dissolution in these aquifer systems is the prime weathering pathway of arsenic release in all of the sand facies.

1.1. Study Areas

In the regional maps used to understand the spatial heterogeneity of Asia's groundwater arsenic, the southern fluvial- and floodplains of Nepal and Bangladesh both typically have tube-wells with higher arsenic concentrations (Figure 1). This regional "enrichment" of arsenic to the south in the Nepalese "Terai"—which is Nepal's depositional lowland region just south of the Himalayas—and the enrichment that extends from Bangladesh's mid-areal delta-plain to the Bay of Bengal, has been observed in several studies, with elevated groundwater arsenic concentrated in the finer-grained lithologies in the foreland basin (Shrestha, 2004; Hoque, 2009; Ahmed, 2004). These modern lowlands, in areas like the Atrai and Sylhet Basins, are naturally prone to recent deposition (Goodbred, 1998; Goodbred, 2003), with the accumulation and preservation of sedimentary organic matter preferred in these types of areas (Tyson, 1995).

From the continual uplift and monsoonal rains that yield high sediment loads into and through the Himalayan catchments, vast siliclastic sedimentary sequences, from 5.5 km to 200 km thick have been left in Nepal and Bangladesh since the Quaternary (Guillot, 2007; Saunders, 2005; Goodbred, 2000; Steckler, 2008; Robinson, 2001). In both countries, the topography of the southern plains are remarkably flat (Gurung, 2005; Tandon, 2008; Steckler, 2008; BGS-DPHE, 2001; Harvey, 2005; Ravenscroft, 2004; Smedley, 2002; NASC/ENPHO, 2004; Maharjan, 2006; Stanger, 2005), giving little clue to the complexity of deposits comprising the aquifers below the surface (Stute, 2007; Coleman, 1969). With the avulsive and meandering-prone rivers in the Terai and Bengal (Tandon, 2008), the landscape is surprisingly un-telling of the aquifers' sedimentary and groundwater heterogeneity.

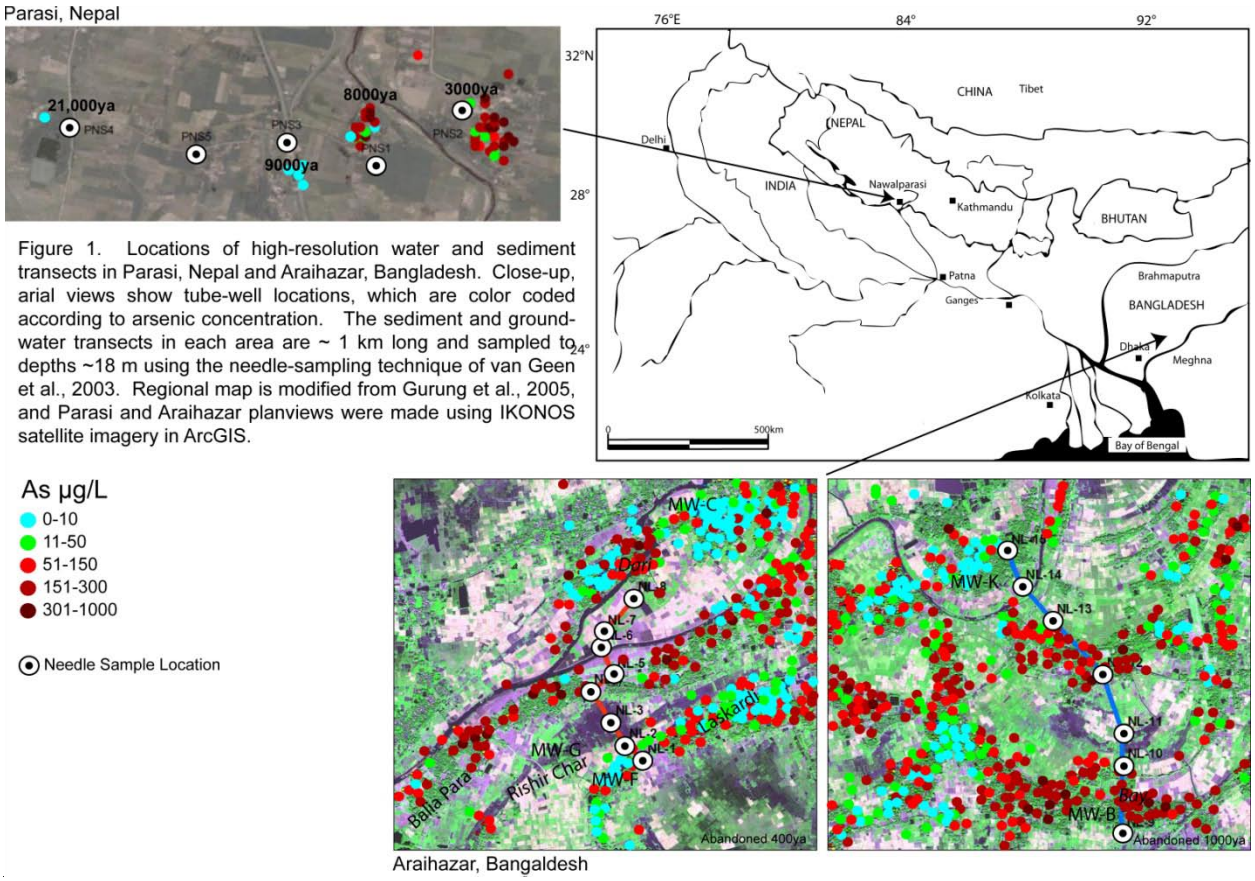

Figure 1. Locations of high-resolution water and sediment transects in Parasi, Nepal and Araihazar, Bangladesh. Close-up, arial views show tube-well locations, which are color coded according to arsenic concentration. The sediment and groundwater transects in each area are ~ 1 km long and sampled to depths ~18 m using the needle-sampling technique of van Geen et al., 2003. Regional map is modified from Gurung et al., 2005, and Parasi and Araihazar planviews were made using IKONOS satellite imagery in ArcGIS.

A high-resolution, sedimentological study of aquifer sediments in Araihazar, Bangladesh showed that groundwater arsenic distributions are explainable by a change in facies and depositional processes occurring over the past 1000 years (Weinman, 2008). In this time, the 25km^2 area of Araihazar has undergone a series of dynamic fluvial phases, leaving behind a shallow aquifer with a complex sedimentological architecture (i.e., Sharp Jr., 2003). As concentrations of arsenic are found to change laterally over 10's of meters, so too, does the thickness of sediment "capping" the aquifer, accounting for differences in recharge and the accumulation of arsenic in the shallow groundwater below (up to about 25m, van Geen, 2008). Located ~20 km northeast of Dhaka, Araihazar is just south of the uplifted

Madhupur Tract[28] (150 kyr old sediments, personal communication John Whitney, USGS), a moribund modern floodplain, with a shallow aquifer sequence primarily affected by the fluvial activity of the Old Brahmaputra River. From a comprehensive 6000 tube-well survey of Araihazar, half of the wells exceed 50μg/L arsenic (van Geen, 2002). Tube-wells emplaced in areas of out-cropped aquifer sands—i.e., channel bars and levees dating to a time when Araihazar was occupied by the Old Brahmaputra—are characterized by low groundwater arsenic, while aquifer sands underlying muddy infill from the Brahmaputra's neotectonic abandonment typically have higher concentrations of groundwater arsenic. While the studies to date in Araihazar have served to answer aquifer and arsenic evolution in terms of aquifer history, there is more work that can be done in quantifying mineralization rates—the rate at which the aquifer is "weathering"—from looking at organic inventories in aquifer sequences of different ages.

Parasi is a town located in the Nawalparasi district of the Nepalese Terai, which is a low-lying region on the southern border of Nepal. Comprised mainly of Holocene alluvium from India's collision into Asia, the Terai runs east to west along the Indian-Nepal border, and it is bound to the north by the main frontal thrust of the Lesser Himalayas (NASC/ENPHO, 2004). To the south of the Terai is India's Gangetic Plains, where Nawalparasi's main river, the Narayani, becomes India's Gandaki River. The Jharai river, a smaller river in the Terai's Rapti- and Gandaki interfan region (Gupta, 1997), bisects Parasi in a divisional area between the spring-fed stable-incised rivers of the eastern Terai and the hyperavulsive, glacially- and monsoonal-driven rivers of the west. Being amid the Gandaki's dynamic instability, Parasi is prone to frequent flooding and river shifting (Dixit, 2007). Wells in Nawalparasi found that ~25% had >50 μg/L arsenic (NASC/ENPHO, 2004), and further work by Gurung et al. (2005), Shrestha et al. (2004), indicate that village-scaled arsenic heterogeneity is likely controlled by differences in grainsize, sediment facies, and organic content.

[28] This is in contrast to Bangladesh's other Pleistocene uplands, the Barind Tract, which, according to Whitney, dated to 25-43kya.

1.1.1 Site Transects: F to A (Araihazar, Bangladesh)

For the F to A transect, which bisects the low-arsenic area by Laskardi village, north to the higher-groundwater arsenic village of Dari, aquifer ages range from 47 kyr to the most recent sands left ~400 ya. Taking the ^{14}C ages as times of deposition presumes F to A's deeper, 47 kyr deposit (~20 mbgl) was emplaced during the Upper Pleistocene. During this time, sea-level was in steady decline, with slow erosion and valley-side retreat propagating through older alluvium (BGS-DPHE, 2001). Erosive conditions were further favored by a more punctuated fall in base-level at 28 kyr, which was then followed by the Last Glacial Maximum's lowstand at 21-18 kyr. This caused even more rejuvenation of old alluvium surfaces and lateritic uplands, resulting in little to no sediment preservation. In the absence of deposition, there is paucity in ^{14}C ages until after the LGM, which is why the next ^{14}C age in the aquifer dates to 14 kyr (~10 mbgl). Prior to 14 kyr, sea-level fall and ~40kyr of erosive-exposure accounts for the lack of sands and weathered silts in the 10m between the 47kyr and 14kyr deposits.

With the onset of the Holocene's rise in base-level, and early onset of Ganges-Brahmaputra delta formation, the F to A area in-filled with fine- and medium-sands, as large sediment discharge and more active rivers interacted with the land surface (Goodbred, 2000). This discharge and high-degree of fluvial reworking preserved little to no muds in the shallow Holocene sandy aquifer (top panel, Figure 2). Combined with the high river activity, the Holocene's eastward migration of the delta's rivers stabilized sandy aquifer deposition here until ~400 ya, when the Old Brahmaputra River switched its course, capturing the Meghna north, no longer bisecting through the Madhupur Terrace. This, followed with the Brahmaputra's avulsion to its western corridor ~175 ya (Fergusson, 1863), left behind the final capping of abandoned muds and muddy in-fillings. These muds are the channel fill and mud cap north of MW-F towards Dari (Figure 2), which are, today, sustained by winnowed flow from an 'un-fit' flood-channel anabranching from the Meghna River.

1.1.2. Site Transects: BNNW (Araihazar, Bangladesh)

The depositional history for BNNW is very similar to that of F to A, in that they share much of the same Pleistocene and Holocene history. The beginning of the BNNW transect starts with a 16 kyr ^{14}C deposit, ~10 m below the Bay village (Zheng, 2005), which is similar to the ^{14}C age beneath Dari. The key difference between the two transects is the causality of their surface morphology. Unlike the Meghna muds of F to A, BNNW's cap is from a lessening regime of the Old Brahmaputra. In other words, BNNW's mud cap is not a product of punctuated abandonment—its lateral uniformity is the sedimentological signature of the gradual meandering of an offshoot of the Brahmaputra River. The OSL date at the mud-sand disconformity underneath Bay at 1kyr predates the Brahmaputra's recent avulsion, meaning that at ~1kyr the Brahmaputra held a stable channel in Araihazar. This type of stable flow and landform development is less than what would typically be associated with the full power of the Brahmaputra, meaning that the river flowing through Araihazar was likely a bifurcation. The main channel was probably bifurcated around the remaining piece of Pleistocene terrace just north of Araihazar. Saved from the full brunt of the Brahmaputra, a scroll-plain developed, producing BNNW's layer-cake uniformity (middle panel, Figure 2). This phase of gradual meandering persisted for several hundred years until the channel form was unstabilized by higher inflow from the Brahmaputra. OSL dates this event at ~600-400 ya, when in response to the additional infow, Araihazar's channel widened, forming a sequence of sandy bars and levees. This anastomosed sandy planform was then filled in with muds with the avulsion event 175 ya, which left behind today's Meghna-fed, moribund river.

1.1.3. Site Transects: *Parasi, Nepal*

Parasi's aquifer sequencing and history is more complex than Araihazar, and putting its evolution in context with the formation of the surrounding hills and rivers is challenging due to not enough *absolute* sediment age-dating in the literature (Tandon, 2008). For the most part, the timing of

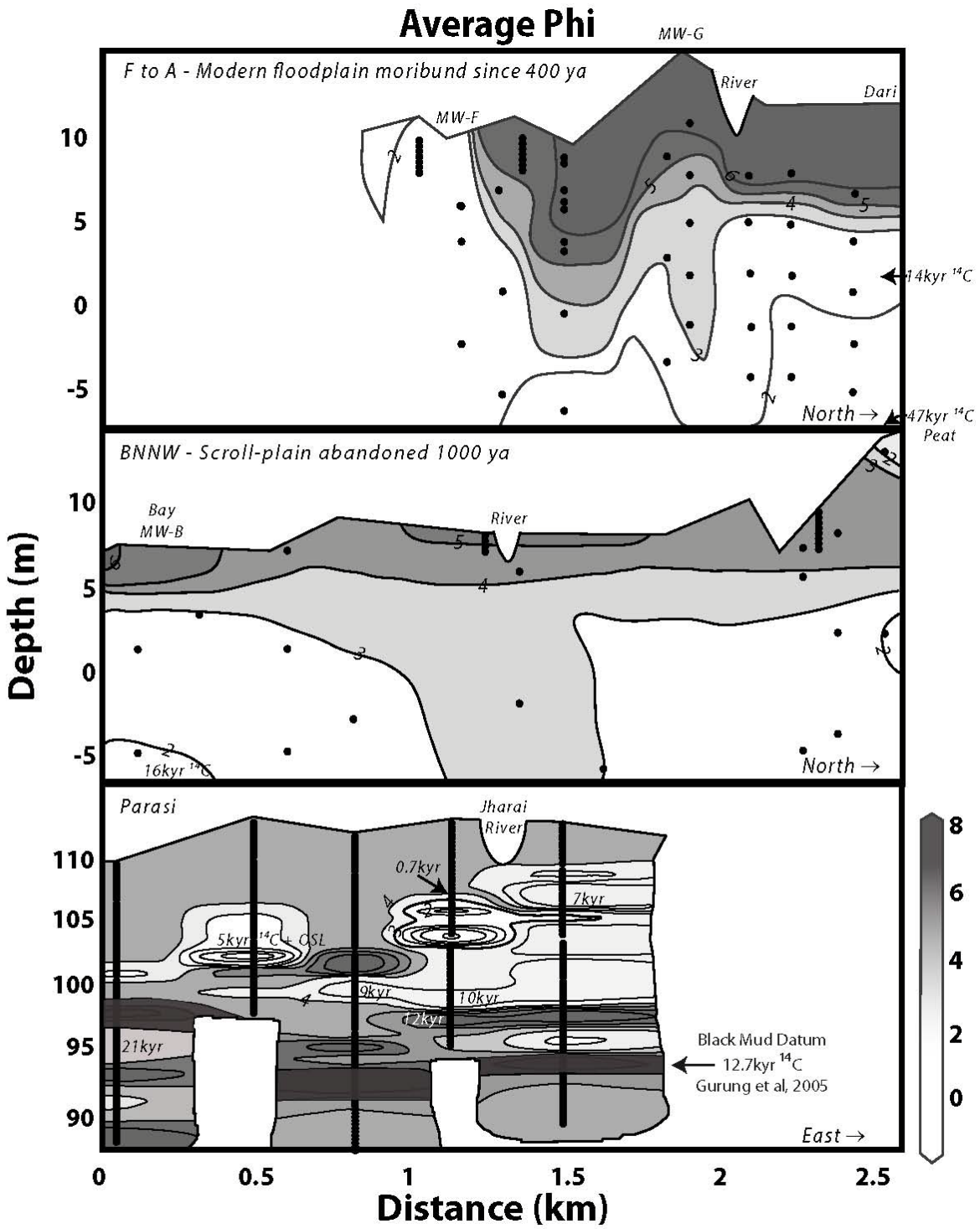

Figure 2. Grainsize profiles of aquifer sediments from Araihazar, Bangladesh (top and middle, F to A and BNNW, respectively) and Parasi, Nepal (bottom). The elevation and sampling depths in Araihazar are adjusted to USGS DTED data and to Google Earth elevations for Parasi, Nepal. Sediment sampling locations are depicted with black dots, and Araihazar ^{14}C ages are from Zheng et al., 2005. The Parasi ^{14}C date was done at UTAG on a wood piece retrieved while drilling, and all other dates are the aquifer OSL dates measured for this study. Aquifer sediments comprised of clays and muds (aquitards) are darkly shaded, while sandier units (aquifers) are shaded light grey and white.

events recorded are either too old (>1Myr), missing (12-1kyr hiatus, i.e., Yonebayashi, 1997 and Rao, 1997), or too relatively dated (Dwivedi, 1997; Mohindra, 1992; Mohindra, 1994; Dill, 2003; Sakai, 2006). In addition, contrary to megafan deposits (Prasad, 2005), southern terraces (Rao, 1997), and (paleo)lakes (Yonebayashi, 1997), there has not been too much work done on these interfan regions. This puts limits on what we can contextually and regionally interpret in terms of aquifer evolution, but our results are still important in that they are among some of the initial findings, outside of the Bagmati (Jain, 2003), that show the type of dynamic sedimentation occurring in these of interfan regions. This is a considerable advance since earlier belief held that these areas were fluvially inactive, and since our findings also help fill-in events between 12-1kyr—a period missing in the Ganga lake and terrace deposits (Yonebayashi, 1997; Rao, 1997). And, even more relevant to the problem of arsenic, our findings also give better insight into the local processes of aquifer formation in these highly avulsive regions. So, while there is a limit to what we can synthesize between local happenings in Parasi and the entire Ganga catchment, an effort is still made to contextualize Parasi's aquifer evolution with what is currently thought to have occurred during the Late Quaternary Siwalik and Gangetic evolution.

2. Methods

To resolve how organic matter affects the accumulation of arsenic in a hyper-avulsive portion of the Terai and an abandoned floodplain of the Old Brahmaputra, a needle-sampling device (van Geen, 2004) was used to obtain depth transects of both sediment and pore-water samples. Transects were taken in March 2004 in Araihazar, Bangladesh (Google Earth Coordinates 23°46'31.38"N, 90°37'17.44"E) and in May 2007 in Parasi, Nepal (Google Earth Coordinates 27°31'60.0"N, 83°40'0.0" E, Figure 1). In Araihazar and Parasi, a total of 20 depth transects were sampled in three different floodplains—1) an 21,000-3000ya sequence from a tributary of the Gandaki River, 2) a 1000ya Scroll Plain in Araihazar, and 3) a 400ya sequence from the abandonment of Bangladesh's Old Brahmaputra River—with each

transect bisecting between sites with opposing trends in tube-well arsenic, e.g. from a low As cluster by [29]MW-F (average As = 17 ± 17 μg/L) to a high As cluster in north Araihazar (average As = 127 ± 127 μg/L, Figure 1, Table 1). Separation distances along each transect average ~200 to 300m between sampling sites, while at each location, sediments and groundwater samples were retrieved at ~1-3 m intervals to a final depth ~20 m below the surface, depending on observed transitions in sediment texture and facies. Labile sediment properties for mobilizable arsenic and aquifer redox conditions, including phosphate-extractable As, Fe(II)/Fe ratios as extracted by 1.2M HCl, and diffuse spectral reflectance (ΔR) were obtained in the field. After fieldwork, filtered pore-water samples from the needle-samples were analyzed by HR ICP-MS for dissolved arsenic, and sediments were further evaluated for their bulk organic C (e.g. loss upon ignition) and grainsize characteristics.

2.1 Sediment and Water Sampling

Samples of groundwater and aquifer sediments were collected using a drilling and needle-sampling method developed by van Geen et al. (2004). Briefly, the method obtains sediment and water via a needle-capped, evacuated tube that is plunged to a known depth within a drill hole. Porewaters were generally sampled from aquifer sands at 1-3 meters below the surface while sediments were collected every 3 meters or whenever there was an observable facies change—whichever distance was smaller. Immediately upon retrieval, 0.8-1.2g and 3.5-4.5g of sediment were respectively measured into scintillation vials for Fe(II)/Fe-total and phosphate extractable arsenic from each interval. Sediments for Fe(II)/Fe ratios were immediately preserved in 10mL trace-metal grade 1.2N HCl to inhibit iron oxidation while the sediments for the phosphate extraction were covered with 10ml of 1M Na_2HPO_4 (pH=5) containing 0.1 M ascorbic acid to begin the 24 hour leaching and separation process (Zheng, 2005; Keon,

[29] MW is an acronym for "multi-well," which are sites where multiple wells have been drilled and cased at different depths to monitor geochemical profiles of the groundwater. The multi-well locations are labeled A, B, C, etc., by ongoing investigations in Araihazar since 2001, with the most recent compilation of MW locations and references included in Appendix B.

2001). A remaining sediment fraction was also preserved in a Twirl-Pak bag for diffuse spectral reflectance performed later that day, as well as for future lab measurements (i.e., loss upon ignition and grainsize).

2.2. Sediment Redox Conditions: Iron Leaching, Speciation, and ΔR

To infer the local redox condition for each needle sample, sediments from each interval were subjected to color and iron speciation analyses. Both methods are described in more detail in (Horneman, 2004), which starts with placing the acid preserved, sediment-filled vials for Fe(II)/Fe ratio determination into a hot bath at ~80°C for 30 minutes. After heating, the vials were shaken for an hour and then left to settle. Following settling, a 10µL aliquot of each leachate was added to 10mL of a 1% HCl solution containing 0.1g ferrozine/L and buffered to pH~5 with acetic acid and ammonia for the sediment Fe(II) fraction. For total Fe, another 10µL aliquot of leachate was added to a similar ferrozine solution containing an additional 2g/L hydroxylamine hydrochloride. Fe speciation was then determined by comparing blank-corrected absorbance readings at 560nm using a Hach 890 portable spectrophotometer. The redox state of the sediment was also inferred from each interval's diffuse spectral reflectance—or color—by folding ~50g of sediment from the center of each Twirl-Pak within a sheet of cellophane wrap and measuring the diffuse reflectance spectrum from each sample relative to a disk of white barium sulfate with a CM 2002 spectrophotometer (Minolta Corp., USA). A first derivative transform of each reflectance spectrum at 520 nm was then calculated, producing ΔR, a value that increases with the abundance of tan, brown, and orange colored sediments in the sample (Horneman et al, 2004)[30].

[30] ΔR correlations to Munsell soil color chips are included in Appendix C.

2.3. Mobile Fraction of Sediment As

For the analysis of the more labile portion of arsenic on the aquifer particles, the sediments were leached in the phosphate extraction solution, shaken overnight, then left to settle, and filtered through a 0.45μm filter after a total leaching time of 24 hours. Within a week of returning from the field, the amount of arsenic extracted from the sediments was determined by high resolution inductively coupled plasma mass spectrometry (HR ICP-MS) at Lamont-Doherty Earth Observatory using a detection method similar to the one developed by (Cheng, 2004) and described by (Zheng, 2004) on samples diluted 100 fold.

2.4. Sediment Size

Grainsize analysis was performed on 33 of the recovered Araihazar sediment samples (n=58) and Parasi sediment used in the columns. Araihazar sediments underwent x-ray analysis at Stony Brook using a Micromeritics Sedigraph, and grainsize on the column sediments was done using a Malvern laser particle-size analyzer at Vanderbilt University. Results from both analyses were used to validate the accuracy of our grainsize estimates made during drilling, and applied to characterize sediment sequences observed while drilling in Nepal using a grain-sizing kit and hand lens (GSA, 1999, and Appendix D). The observations and measurements were then used in constructing two cross-sectional stratigraphic profiles for comparison with the other sediment properties.

2.5. Organic Carbon and C:N

The organic fraction associated with each sample of sediment was determined within 2-3 weeks of returning by loss on ignition (LOI) on refrigerated Parasi and Araihazar sediments (10-15g wet weight) already pre-dried for 24 hours in a drying oven at 60°C. Sediments were weighed within 10 minutes of removal of the drying oven to prevent rehydration and reweighed a day later to confirm that the

sediments had reached a stable dry weight (±0.003g). The dehydrated sediments were then placed in a Thermolyne 62700 furnace set for 6 hours at 450°C. After combusting, the crucibles were cooled for 10 minutes and weighed again for the LOI determination of each sample. The organic carbon was then estimated from LOI using the interpolation method of (Santisteban, 2004) and checked for linearity against %C measurements made during C and N analysis (Appendix D).

For more information on the organic type and remineralization process(es) in the aquifers (i.e., remineralization and weathering efficiencies, pg. 47 (Fenchel, 1988), bulk sediment samples (~10 g) from Araihazar were dried overnight at 60°C and ground with a ceramic mortar and pestle to pass through a 63 micron sieve and for H, C, N analysis. Approximately 5cc of the ground, homogenized samples were put into a 50cc acid-cleaned Falcon centrifuge tube, and covered to 25cc with 10% HCl. After the initial effervescence ceased, the tubes were placed in a 40°C oven for five hours, mixing each hour. The samples were centrifuged, supernatant discarded, and rinsed three times with 25cc of distilled water. The rinsed sediment was then dried at 70°C overnight, and then measured by D. Hirschberg at Stony Brook University's School of Marine and Atmospheric Sciences (SoMAS) for %C and %N using a Carlo Erba 1602 CNS analyzer. Due to the low amounts of organic expected in the aquifer—especially in the better sorted channel facies that comprise the "true" aquifer sands—the analytical lab at SoMAS was chosen because of their experience measuring low concentrations of particulate organic carbon and nitrogen from ocean waters (Liu, 2005). Data were corrected for instrument blank, with the typical uncertainty at this level of analyte at ± 5% and 2% for N and C, respectively. Chromatographs of the samples are available for inspection at SoMAS as CN runs GV (1/9/09) and GY (1/29/09).

Since the C and N analysis was performed on archived samples 5 years following the initial LOI determination (LOI 4/04 and C:N 1/09), possible C:N ratio changes due to storage can be approximated using a theoretical batch treatment with coupled differential equations (David Furbish, personal communication). The premise of the model is that C:N in the sample is altered due to bacterial

breakdown of the sediment's original organic content, which would cause a likely decrease in C:N over time (Yan Zheng, personal communication). Since the organic content of sediment from combustion is a bulk entity—i.e., we cannot say how much of organic carbon is from carbohydrates, waxes, lipids, etc.—we can refer to the organic content as a "bulk substrate" with an initial C:N of "C_0/N_0." For most sediments undergoing the deposition and burial process, the C:N is typically found to be ~10 due to humification (Ehrlich, 2009; Stevenson, 1994). Assuming remineralization rates of C observed from a range of sediment environments, (~0.01 - 20 mol C/m/yr, Table 2., and references in Stahl, 2004; Ullman, 2003; Aller, 2006; and Baisden, 2002), and assuming the loss of N in proportion to bacterial biomass C:N so that 0.2 units of N is lost for each loss of C, the change of C and N, and thus the change in C:N can be modeled from a batch reaction with the following stoichiometry:

$$C + 0.2N \rightarrow \text{bacterial biomass}$$

The rate of the reaction can then be expressed as $R = kC_CC_N$, where R is the rate of the reaction, k is the rate constant, C_C is the amount of carbon, and C_N is the amount of nitrogen in the bulk substrate.

Coupling the equations:

$$\frac{dC_C}{dt} = -R \qquad \text{eq. 1}$$

$$\frac{dC_N}{dt} = -0.2R \qquad \text{eq. 2}$$

and summing equation 2 with -0.2 times equation 1 gives $\frac{d(C_N - 0.2C_C)}{dt} = 0$. Assuming a change of C:N in the substrate (C:N = 10) on the same order as C:N assimilation into bacteria (C:N = 5:1), $0.2C_C = C_{No} - 0.2C_{Co}$, so that $C_N = 0.2C_C - 1$ and

$$\frac{dC_C}{dt} = -kC_c\ (0.2C_c - 1) \qquad \text{eq.3}$$

Separating variables and integrating between C_0 and C_t gives carbon loss from the substrate with time as:

$$C_C(t) = \frac{1}{0.2-\left(e^{-kt}\times\frac{0.2C_{Co}-1}{C_{Co}}\right)} \qquad C_0 = 10, \text{ eq. 4}$$

$$C_C(t) = \frac{1}{0.2-\left(e^{-kt}\times\frac{0.2C_{Co}-3}{C_{Co}}\right)} \qquad C_0 = 20, \text{ eq. 5}$$

$$C_C(t) = \frac{1}{0.2-\left(e^{-kt}\times\frac{0.2C_{Co}-5}{C_{Co}}\right)} \qquad C_0 = 30, \text{ eq. 6}$$

From this solution, the change of C:N from storage can be modeled and then compared to the losses observed to validate the model and evaluate the C:N of the initial samples and compare several remineralization rate constants from the literature (Table 2). Since it is unlikely that N loss occurs as much as C since mineral product C:N ratios tend to be an order higher than the C:N of the substrate (Fenchel, 1988), the fractionation allows for the assumption of N net immobilization, yielding a solution to eq. 4-6 that approximates the change in *both* C *and* C:N from the initial substrate condition. In other words, without high C:N ratios that favor N-loss via denitrification (Hu, 2009), most of the N should stay in the organic fraction of the sediment despite loss of C during storage. This means that, for our purposes, results of $C_C(t) \approx C_{C/_N}(t)$ and can be used to approximate changes in C:N over the 5 years of storage.

2.6. Dissolved Arsenic

The number of porewater samples taken from each location depended upon the type of sediments encountered. Locations where aquifer sands were more at depth and covered by meters of aquiclude-like mud resulted in the retrieval of one or two water samples, whereas locations with shoaling sands yielded more. Typically, porewaters were collected from the 3, 9, and 15m intervals in

Araihazar, and 7, 10, 15m in Parasi, with other intervals sampled when mud prevented sampling. Once retrieved, porewaters were immediately filtered out of the needle-sampling device through a 0.45µm Acrodisc® syringe filter. The dripping filtrate was collected within an acid-cleaned 20mL HDPE scintillation vial and acidified on site to 1% HCl (Optima, Fisher Scientific). In both Araihazar and Nepal, samples were analyzed for dissolved arsenic and other groundwater constituents within three weeks of collection at Lamont-Doherty Earth Observatory by HR ICP-MS using a method that can detect arsenic concentrations as low as ~0.1 µg/L with a precision of +2% (Cheng et al., 2004). In Nepal, groundwater arsenic measurements were also corroborated using a Hach arsenic test kit in the field, as well as concentrations gotten via the monitoring efforts of Linda Smith and Filters for Families[31] and ENPHO (NASC/ENPHO, 2004).

2.7. Sediment Dating

Aquifer evolution was reconstructed in Parasi and Araihazar by optical luminescence dating (OSL) of aquifer sands and corroborated, when possible, by ^{14}C on organic matter—retrieved sediment samples are typically organic-poor, with small pieces of preserved terrestrial detritus and shell fragments seen perhaps once in each drill hole. In Araihazar, sediments were collected by horizontally coring shallow sequences of sands, as described in Weinman et al., 2008. Collected in 2004, the timing of facies sampling in Araihazar was prior to the development of our simultaneous sediment and water-needle-sampling technique, which was deployed in Parasi: aquifer deposits were vertically cored and collected in steel liners using an AMS soil probe inserted into the drill hole during needle-sampling (van Geen et al., 2004) for optical luminescence dating. The steel liners protect the sediment from being "bleached" with sunlight, preserving the sediments for OSL dating. OSL samples were taken to India's National Physical Laboratory (PRL) for determining the depositional ages, while woody fragments

[31] http://www.filtersforfamilies.org/

retrieved from Nepal were rinsed with distilled water, dried overnight at 60°C and sent to Daniel Weinand at the University of Tennessee's Center for Archaeometry and Geochronology for liquid scintillation counting ^{14}C dating[32], calibrated with IntCal04/OxCal4.0 for reservoir correction.

For OSL ages, sediments were separated and processed under red light conditions[33]. Sediments were removed from the protective steel liners and then treated with 10% HCl to remove carbonate fractions and then a 30% H_2O_2 solution to remove organic matter. Quartz was then separated using sodium polytungstate (ρ = 2.58 g/cm^3) and, if needed, with a magnetic separator, starting at 0.4 amp@15° slope to 1.5 amp@5°slope, using increments of 0.2-0.4 amp and 2°. For each sample, a few grains from the sample with the lowest magnetic susceptibility were double-checked under a microscope to affirm a pure sample of quartz. Samples were then sieved into different size fractions, of which a 150-210 μm fraction was etched in 40% HF and used for a single-aliquot OSL method (Aitken, 1998; Jain et al., 2003; Duller, 2004; Wintle and Murray, 2006).

The natural luminescence, or the "paleodose," was measured at PRL using a Risø TL/OSL-DA-12 readers equipped with a 40mCi $^{90}Sr/^{90}Y$ beta-source, a blue LED stimulation system (470 ± 30 nm) and an IR laser (830 ± 10 nm). For significance, 20-30 aliquots were prepared for equivalent dose measurements on each sample, and data from the aliquots were rejected if there was a poor fit of the growth curve or if the recycling ratio fell beyond the range 1.0 ± 0.1. For some of the Parasi samples, microscopy and initial runs of OSL showed that, despite several separation attempts, the samples were dominated by feldspars, in which case, the "naturally-corrected" single aliquot regenerative dose (SAR) OSL procedure (Nagar, 2007) was modified with an infrared bleaching step so the OSL measured was only from quartz (Zhang, 2007, and Table 2 of Nepal's Chapter). The final OSL age for each sample was based on a weighted mean of either the minimum 10% of paleodoses or a weighted mean of all the paleodoses, depending on the shape of the age distribution.

[32] http://web.utk.edu/~anthrop/utcag/14c_dating.html
[33] Red light is not energetic enough to penetrate to band gap depths deep enough to stimulate luminescence.

External dose rates were measured using thick source ZnS (Ag) alpha counting for U and Th, and gamma counting and XRF[34] for potassium determination. A radioactive equilibrium in the decay chains was assumed, and the cosmic dose rate estimation is based on the muon production models of Prescott and Hutton (Prescott, 1988; Prescott, 1994). The experimental errors in the OSL ages include errors in paleodose measurements (photon statistics), errors in the measurement of K, U, Th, and errors in source standards and source calibrations.

2.8. Column Experiments

Different aged-aquifer sands were used in five column experiments. Three of the sands were OSL dated from Parasi, Nepal, and two of the sands are relatively aged from the northwestern, low-arsenic area of Birganj, Bangladesh (Table 3). Relatively, the deeper sands are older than the shallow ones. From preliminary luminescence, the Birganj sands date mid to late Holocene (~2ka-6ka), with the sands chosen to test whether even low-arsenic sands of different ages can differentially weather and leach different rates of arsenic—i.e., if sediment age does play a role in Asia's arsenic distributions, the deeper, older Birganj sands should weather and leach less arsenic.

To make the columns, the aquifer material was wet packed into 31.4cm^3 ID core liners, and run in upflow mode at 2-3mL/d using a multi-channel manostat and deionized water. The flow rate was chosen based on annual rainfall for the study regions: 1427 mm for Kathmandu Nepal and 1920 mm for Dhaka Bangladesh (Met Office, www.metoffice.gov.uk). An average of these annual rainfalls yields ~1670 mm, which approximates a daily rainfall of ~5 mm, converting to a 2-3mL/d flow rate for the column specifications. Deionized water was chosen as the leaching agent because it allows us to compare the leachate results with other weathering work (White, 2003) and because it is a suitable laboratory analogue for infiltrating rainwater.

[34] Due to PRL machine demand, some of the K measurements were made post-OSL analysis using Warner Cribb's XRF at Middle Tennessee State University.

Over the course of the flow-through experiment (8/4-12/27/07), effluent samples were collected monthly for trace metals (and REE's for future studies). Clean methods were used in preparing all of the columns and sampling containers (Shannon, 2005). Since cheaper containers made from HDPE are found to be as sufficient as Teflon as long as the samples are adequately acidified, 20 mL HDPE scintillation vials were used for effluent collection. Prior to collection, the bottles were filled with >5% ACS grades HNO3 and HCl for at least 24 hours and kept in a low traffic area of the clean lab and covered with plastic wrap. After cleaning, the bottles were rinsed 2-3 times with deionized water, with excess water shaken out vigorously before sampling. Column effluent was then collected by filtering the effluent into the HDPE containers using a 0.45 um filter and acidifying the sample to 1% ultrapure HNO_3. All syringes and filters were "conditioned" first by pre-filtering and disposing ~10-20 mL of sample. After collection, concentrations of the analytes were sent to Actlabs.[35] Concentrations of Na, Mg, Al, Si, K, and Ca were be measured for weathering results comparable to those reported in White and Brantley (2003); P, S, Ti, Cr, Mn, Fe, Ni, Cu, Zn, As, Cd, Cs, Pb, and U for release rates of arsenic, as well as other elements that can affect water quality and that are currently being monitored in Araihazar (Cheng et al., 2004); and La, Ce, Pr, Nd, Sm, Eu, Gd, Tb, Dy, Ho, Er, Tm, Yb, and Lu for an exploratory study of rare earth elements—i.e., to see if aquifer sediments from different deltas can be traced back to a common source terrain in the Himalayas (see final chapter and summary for how this relates to my future work).

3. Results

3.1. Profiles of Aquifer Sediments - Stratigraphic Patterns

Overall, the three aquifer profiles display differing layouts of sedimentary architecture. Since there has yet to be a standard on how to best characterize an aquifer, we use profiles of 1) cross-

[35] http://www.actlabs.com/gg_hydro_usa.htm

sectional facies, 2) the organic content of the different facies, 3) the arsenic and redox geochemistry of the facies, and 4) each transect's ^{14}C and OSL alluvial history to characterize each setting. This characterization of the sediments and their patterns provides a basis for the interpretation of the type of deposits and depositional history (or histories) important for dealing with arsenic and other groundwater problems. It also allows for better assessment of whether a village's arsenic is coming from a surface soil source, being weathered from a buried unit, or coming from a more complex, process involving reactive-transport—i.e., arsenic once weathered from soils, immobilized in the subsurface, and now undergoing re-mobilization, as the case of arsenic coming from sands that once experienced hyporheic exchange between ground- and river-water (Jung, 2008). In this interest, the time is taken here to describe stratigraphy and profile patterns without too much interpretation of aquifer bio- and hydro- geochemical processing, so that the results can more easily be assessed with other and future work seeking to understand the dynamics between landforms and groundwater (i.e., the quantification of spatial patterns and processes, and the coupling of stratigraphy and water chemistry with models of geomorphology). Thus, our interpretation of the observed patterns of sedimentary organic matter with the availability of groundwater arsenic is highlighted in our discussion.

3.1.1. Aquifer Architecture – Dimensions of Sedimentary Facies

In looking at the layering of sedimentary facies within each transect (Figure 2), the profiles show three general aquifer facies common to the three settings: a surface muddy facies, a buried muddy facies, and a sandy aquifer facies—the facies that is most often tapped into for drinking water. The surficial muds are typical floodplain overbank and infill deposits, comprised of fine suspended load material that either keep floodplain elevations steady with channel aggradation, or during transient phases, acts to infill abandoned portions of the land (Bridge, 2003). Along these transects, the thickness of the muds range from zero to depths of 12 m, with over-bank deposits thinner than the cappings made from those of in-filled channels. This is shown by the comparable average mud-cap depths

between the Parasi transect and the F to A transect in Araihazar: 6 - 7 meters mean mud depths with the same standard deviation (±3 m, Table 4). The thickest of the cappings, ~10-12 m, correspond to places that were previously occupied by river channels, producing a typical concave-upward basal contact in the subsurface. Compared with the F to A and the Parasi transects, the surficial mud capping along BNNW is thinner and more laterally continuous, with a mean capping depth of 3 m and smaller, ±1 m standard deviation. This lateral uniformity along BNNW is less from a punctuated type of deposition (i.e., avulsion) and more from a gradual geomorphic process, such as the deposition left from the longer-term lateral migration of a meandering river (Figure 3).

Immediately, and often sharply, underlying the surface muds is a sandy facies comprised of coarser grained levee, crevasse splay and channel sands (Bridge, 2003). These sands comprise ~65 – 80 percent of the upper ~20 m of aquifer, and display differing degrees of interconnectivity between the transects (Table 4, Figures 2 and 3). This is seen in the sandy facies of Araihazar, which are more interconnected and laterally continuous than the Parasi transect. The connectivity of the shallow aquifer in both Araihazar transects (F to A and BNNW) is consistent with previously described mid-Holocene sand units (Goodbred, 2003). During the time of Araihazar's sandy deposition, there was little accommodation and enough erosional reworking to prevent mud accumulation within the aquifer—in other words, Araihazar was not subsided enough and too far north of the delta front to preserve muds. More complex and less interconnected than the Araihazar sands is the Parasi transect, which has a lot more isolation of sands in the subsurface. The sandy facies in Parasi becomes isolated by the presence of subsurface muds, which surprisingly comprise a larger portion of muds than those at the surface, (20 vs. 14 percent, respectively, Table 4). Unlike Araihazar's mud-poor sandy facies, the interfan location of Parasi between the Rapti-Ghaghra Plain and the Gandaki River (Gupta, 1997) explains this difference in muddy substrata. In the interfan region, muddy sequences are the main deposits left by the interfan rivers, because they carry exceptionally high loads of fine material (Sinha, 1995). So, while Araihazar

preserved a bedload-dominated, sandy aquifer sequence from limited accommodation and frequent river reworking, the development of megafans in the Ganges Basin sequestered bedload, (Sinha, 1995), leaving interfan regions, like Parasi, with more muds in their aquifer sequence.

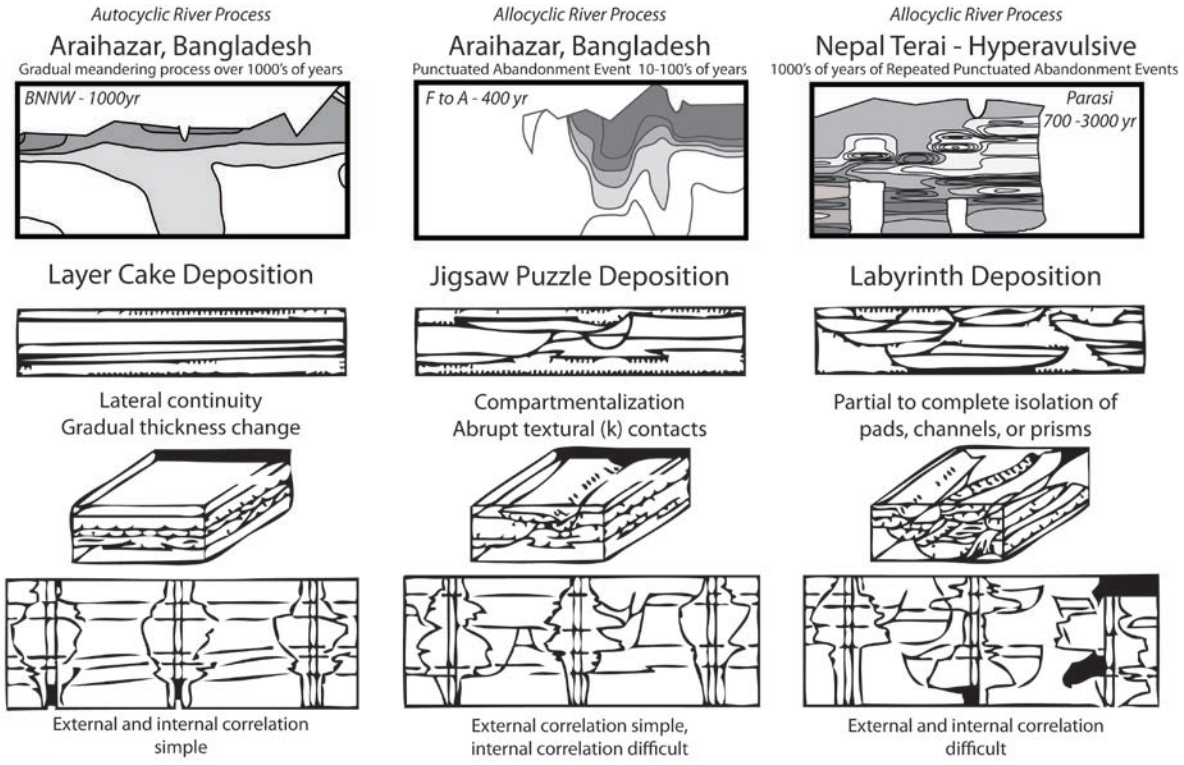

Figure 3. Giving context to concept: grainsize profiles of aquifer sediments from Araihazar, Bangladesh and Parasi, Nepal compared with the idealized principal styles of facies and hydrostratigraphic complexity reported in Sharp and Galloway (2003). From left to right, the depositional styles of the three profiles at ~20m vertical and 2.5km horizontal scales. Transect BNNW, a scrollplain dating back 1000 yrs, resembles a basic layer-cake architecture, presumably due to a gradual ≥1000 yr autocyclic meandering process that deposits laterally continuous sequences of alluvial facies. F to A and Parasi are increasingly complex in stratigraphy, as tectonic events create lateral discontinuities and isolation of facies. Transect F to A has an abrupt lateral change in facies due to a tectonic event that caused an avulsion and infilling of a river, while Parasi exhibits more lateral and vertical complexity due to repeated avulsions and tectonic downdropping that offsets the continuity of internal facies.

In terms of overall architecture, the differing degrees of lateral variation give each transect a unique structural characterization (Figure 3). They each have a different profile and they each resemble a different style of architectural complexity (Sharp Jr., 2003). Transect BNNW, with its laterally continuous profile, resembles a basic “layer-cake” aquifer architecture, while F to A and Parasi show

increasingly complex, lateral discontinuities and isolation of facies. These transects show that aquifer styles are highly variable in space, even when they are located within the same district, as the case of F to A and BNNW in Araihazar. Presumably, these dimensional differences are imbued by the different evolutionary history of each setting, giving context and genesis to Sharp et al.'s three styles of hydrostratigraphy. Transect BNNW's simplicity and lateral homogeneity stems from the gradual, 1000 yr autocyclic meandering of a river along its scroll-plain, while F to A and Parasi are allocyclically more complex: transect F to A has an abrupt lateral change in facies due to a recent tectonic event that caused an avulsion and infilling of a river (Weinman, 2008), while Parasi exhibits more lateral and vertical complexity due to repeated avulsions and tectonic downdropping[36] that offsets the continuity of internal facies. This is a "groundtruthing" for the concepts of Sharp et al., (2003) as well as other studies seeking to better understand and quantify aquifer continuity (i.e., Hodgkinson, 2008; de Marsily, 1998).

3.2. Sedimentary Organic Matter

3.2.1. %C and %N

In seeking to better understand the nature of sedimentary organic matter in the aquifers, a "bulk" sedimentary organic content was determined by combustion along with CHN analysis. The results of combustion are reported in a "percent lost on ignition," or %LOI (Tables 4 and 5), which when compared to the CHN results, show the expected linear trends of increased C/N with the amounts of sedimentary organic matter (Figures 4A and 4B, i.e., Santisteban, 2004; Tyson, 1995; Konen, 2002). Furthermore, the ~0.4 slope conversion between %LOI and %C agrees well with other LOI-sedimentary carbon equations (0.5-0.6, in Konen, 2002 and Santisteban, 2004). And, despite the nice linearity between %C and %N in all the measured samples (R^2 = 0.93, Figure 4B), F to A and BNNW samples plot on slightly different trend-lines (Figure 4C). F to A, which is a more recent portion of Araihazar's

[36] Refer to Chapter II, Part 2, Nepal Stratigraphy

floodplain complex than BNNW—F to A was abandoned 600 yrs after BNNW (Weinman, 2008)—has more nitrogen preservation than deposits in the older BNNW scroll-plain. Two-sample T-tests using the C/N ratios from F to A and BNNW support the idea that F to A's sedimentary organic matter is significantly more nitrogen-rich than BNNW. Critical t values show that differences in C/N values from the two areas are greater than differences from chance alone: the critical t-value is 1.7, which is greater than the calculated probability difference (0.19). This makes sense given the previously known age sequencing of the deposits, with F to A being more recent, and hence having more N-enriched organic matter than BNNW.

Since differences in C/N have been used to infer differences in the source of sedimentary organic matter, a question arises as to how we know that the differences in sedimentary organics are simply diagenetic. Since the transects lack any signs of marine sedimentation, and since Araihazar's shallow deposits show signs of fluvial reworking (Weinman, 2008; Goodbred, 1998; Goodbred, 2003), it is expected that the C/N ratios are—and have continually been—from a well-mixed terrestrial source that, over the past thousand or so years, have not altogether too much varied. Instead, any difference in C/N comes from diagenetic organic degradation and weathering (Hartog, 2002; Hartog, 2005). This is a fair assumption given that C:N does show a general increasing with depth, which is another way of considering C:N changes with the aging of the deposits (Figures 4D-G). In Araihazar, older deposits are at deeper depths, which show continuous depletions of %C and %N (Figure 4D) and higher C/N ratios than younger, shallow deposits (Figure 4G).

Profiles of percent LOI and C:N ratios were also plotted to see if there were any distinguishing sedimentary patterns, such as an overall higher organic content in the finer, muddier facies. In Araihazar, profiles of organic content (%LOI) along the two transects conform to patterns in facies, with higher organic fractions coinciding with the finer muddy caps and muddy infillings (Figures 2 and 5). In F to A, there's a higher organic association with the infilled channel muds (~1.5km), and the mud cap

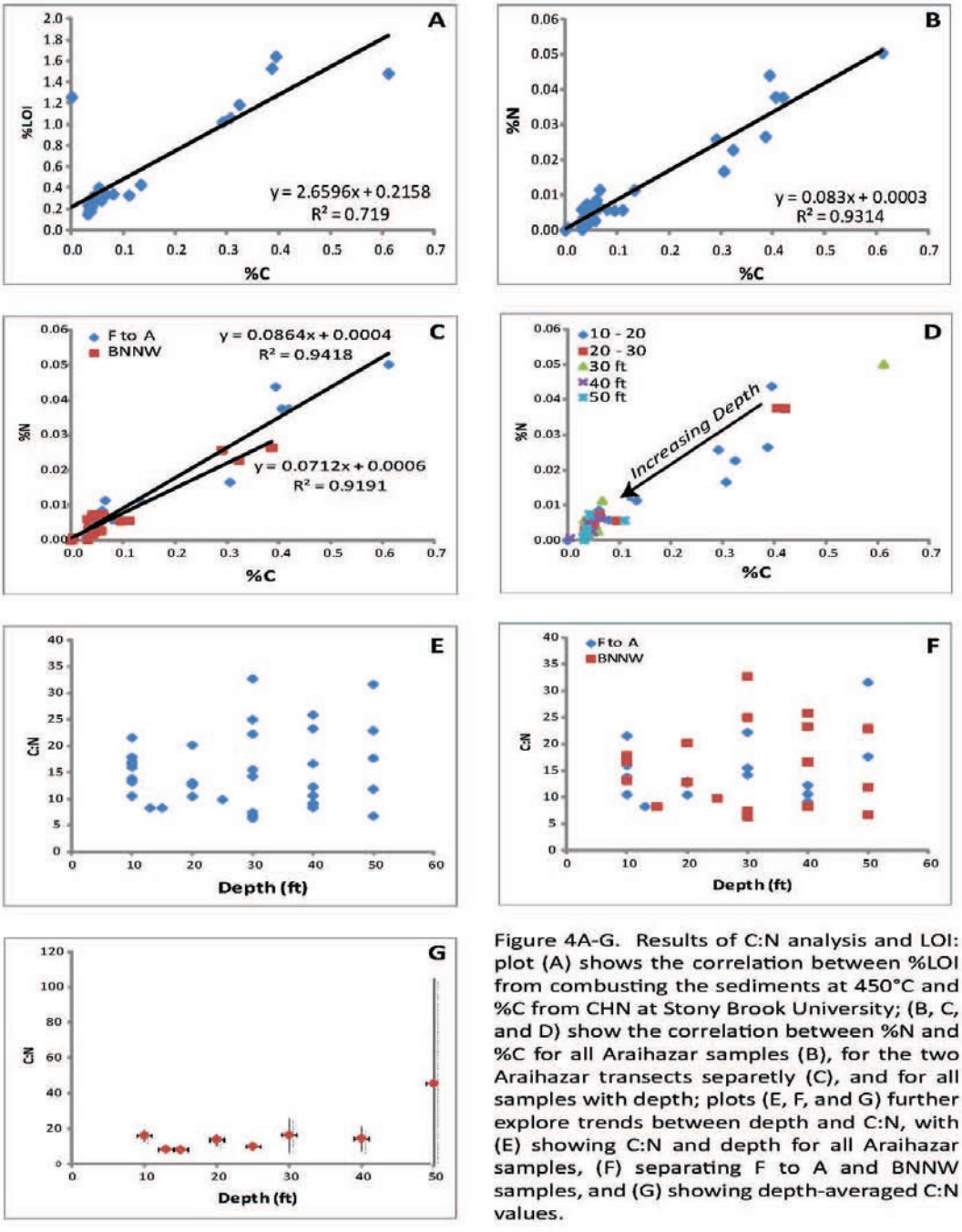

Figure 4A-G. Results of C:N analysis and LOI: plot (A) shows the correlation between %LOI from combusting the sediments at 450°C and %C from CHN at Stony Brook University; (B, C, and D) show the correlation between %N and %C for all Araihazar samples (B), for the two Araihazar transects separetly (C), and for all samples with depth; plots (E, F, and G) further explore trends between depth and C:N, with (E) showing C:N and depth for all Araihazar samples, (F) separating F to A and BNNW samples, and (G) showing depth-averaged C:N values.

along BNNW shows a similar enrichment (2-3% LOI). Despite this first-order correlation between organic content and muddier fractions, higher amounts of sedimentary organics are also found in the sandier facies. Parasi's transect has the highest %LOI occurring in a sandy unit (~100m depth to the below left of the Jharai River at a coarse-to-finer sand disconformity in PNS1-41, Figure 5; patterns in agreement with profiles made by Stephane Gulliot and Laurent Charlet at the University of Grenoble). In fact, a comparison of the %LOI data between muds and aquifer sands show that the sands can not only have higher amounts of organic matter (Table 4), they can also have more sedimentary organic on a volumetric[37] basis. By multiplying each facies' average %LOI by the percent-area of facies in the aquifer profile,[38] both the BNNW and Parasi transects have aquifer sands as the largest LOI reservoirs. They hold 60% and 50%, respectively, of the cross-sections' organic matter. The mud caps in BNNW serve as the remaining reservoir (40%), which is a smaller volume, while the mud cap (20%) *and* interstitial muds (30%) in Parasi store its remainder. Thus, from a reservoir perspective, there is an *equal* portioning of organics between the different facies.

Unlike the more observable conformity between facies and organic matter, the nature of the organic matter—or the sediment's C:N—plot more randomly (Figure 6). There is no apparent similarity between C:N and the sand or mud facies. Upon closer observation, however, there is a depth-trend in the C:N distributions, with an overall pattern of terrestrial organic dominating the surface (C:N ~20), and then grading into microbial processes (C:N ~5) and denitrification in the subsurface (C:N $\geq$30; Tyson, 1995). In both F to A and BNNW, the surface sediments typically have terrestrial values of C:N (~20), which grade to lower, bacterial C:N values at depth (~5). Furthermore, the highest values of C:N ($\geq$30) are typically deepest, likely representing denitrification in the lowermost unit (Hartog, 2005; Solaiman, 2009). Since it is typically difficult to infer biogeochemistry in aquifers based on profiles of water geochemistry, (Fendorf, 2009), this tractable patterning of sediment C:N downward is a good indicator

[37] This is a relative volume, given that the calculations are done on profile cross-sections.
[38] Done by highlighting areas and taking pixel counts using Adobe Illustrator.

of the biogeochemical reactions occurring in the aquifer: F to A is a younger transect with more of its original terrestrial organic, while BNNW is older, with more microbial alteration.

3.2.2. C/N Changes from Storage

To address how sample storage could have affected the fidelity of Araihazar's C:N data, changes in sediment-C:N over the 5-yr storage were approximated by modeling the aerobic and anaerobic reprocessing of the sedimentary organic matter. Plotting measured sedimentary C:N values with mineralized-C:N estimates from:

$$C/N_{mineralized} = \frac{1-E}{\frac{N}{C}-0.2E} \qquad \text{eq. 7}$$

where $\frac{N}{C}$ is the N:C measured, 0.2 the N:C of bacterial biomass, and *E* the aerobic or anaerobic efficiency, C:N(s) of the initial substrate(s) were inversely determined, double-checking the applicability of the C_0/N_0 assumptions in equations 4-6 (Figure 7). The measured sediment-C:N and the C:N-mineral estimates well-fit a remineralization curve for sedimentary organic matter with an initial C_0/N_0 = 20, undergoing microbial anaerobic degradation (almost an exact fit with E = 0.2). Taking this fit together with the average C:N for all of our measurements—which is also 20—indicates that the C:N ratios can remain robust despite storage. The solution to changes in C and N over time (eq. 5, Figure 8) supports a conservation of N in the sedimentary organic matter. Furthermore, the ratio's decrease, which is a conservative maximum at 13% for C:N = 20 and k=0.01, is small enough to conserve differences over the five years of storage. At this high rate of mineralization, which is unlikely to persist beyond a few months due to rate law and surface reactivity changes (Washton, 2008; White, 2003; Maher, 2006; Casey, 1993), it would take ~50 years for samples with C_0/N_0 ranging from 10-50 to become indistinguishably similar.[39] Along with reports of N-immobilization when organic C:N≈20 (Howlader,

[39] C:N≈9 ± 2 for four samples with C_0/N_0 equaling 10, 20, 30, and 50

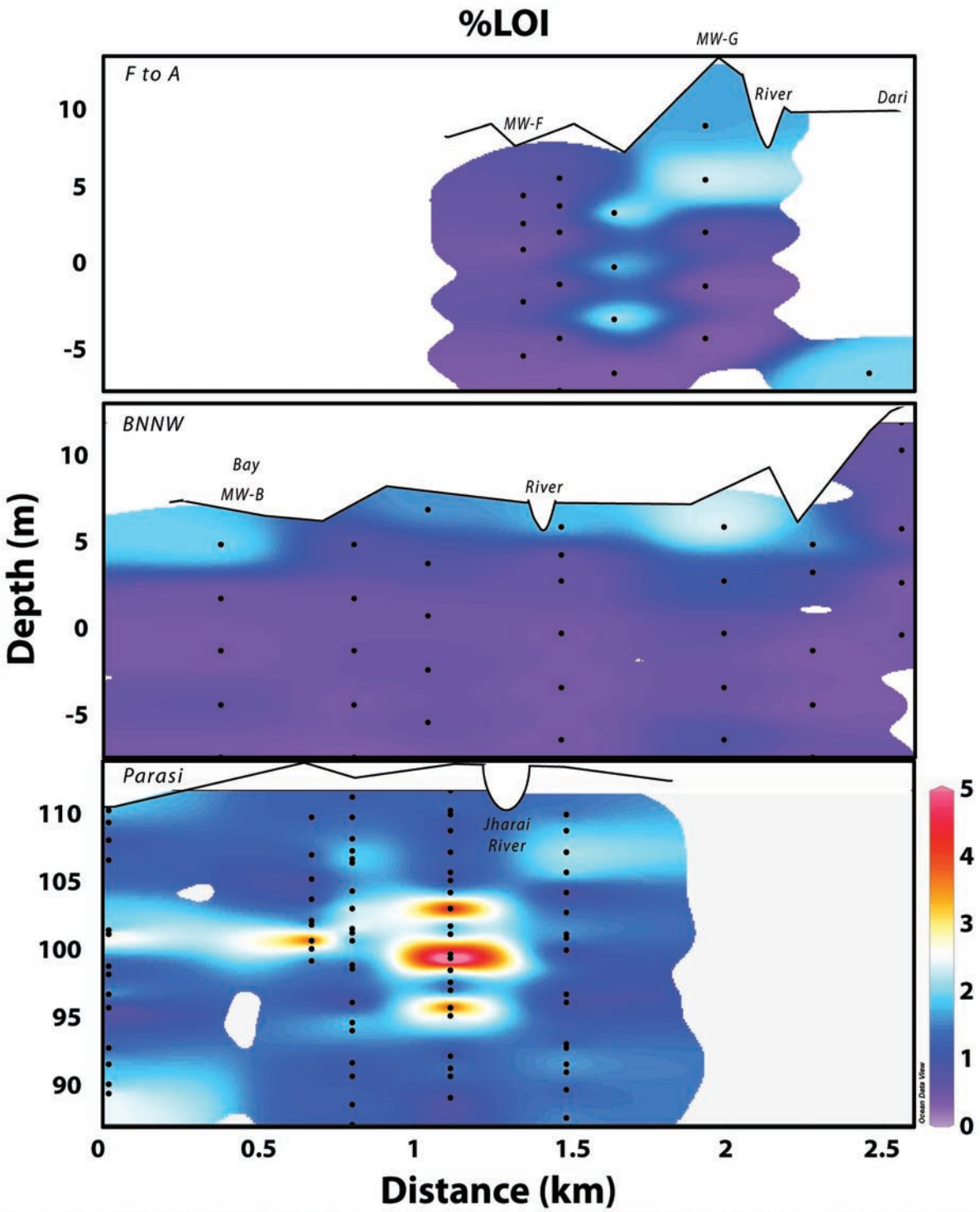

Figure 5. Loss-on-ignition profiles for the three transects, used to infer the distribution of organic matter in the aquifers of Parasi, Nepal and Araihazar, Bangladesh. The transects from Araihazar, F to A and BNNW, show patterns of higher LOI typically conformable with finer, mud facies (Figure 2). An exception occurs in a needle-sample collected at depth under village of Dari (top most pannel and Zheng et al., 2005) and in the aquifer sands a little over 1 km into the Parasi profile. These distributions suggest that organic matter in these aquifers are not only sourced in surface soils or in finer facies preserved at depth. They can occur in the sandier facies of the aquifer sediments.

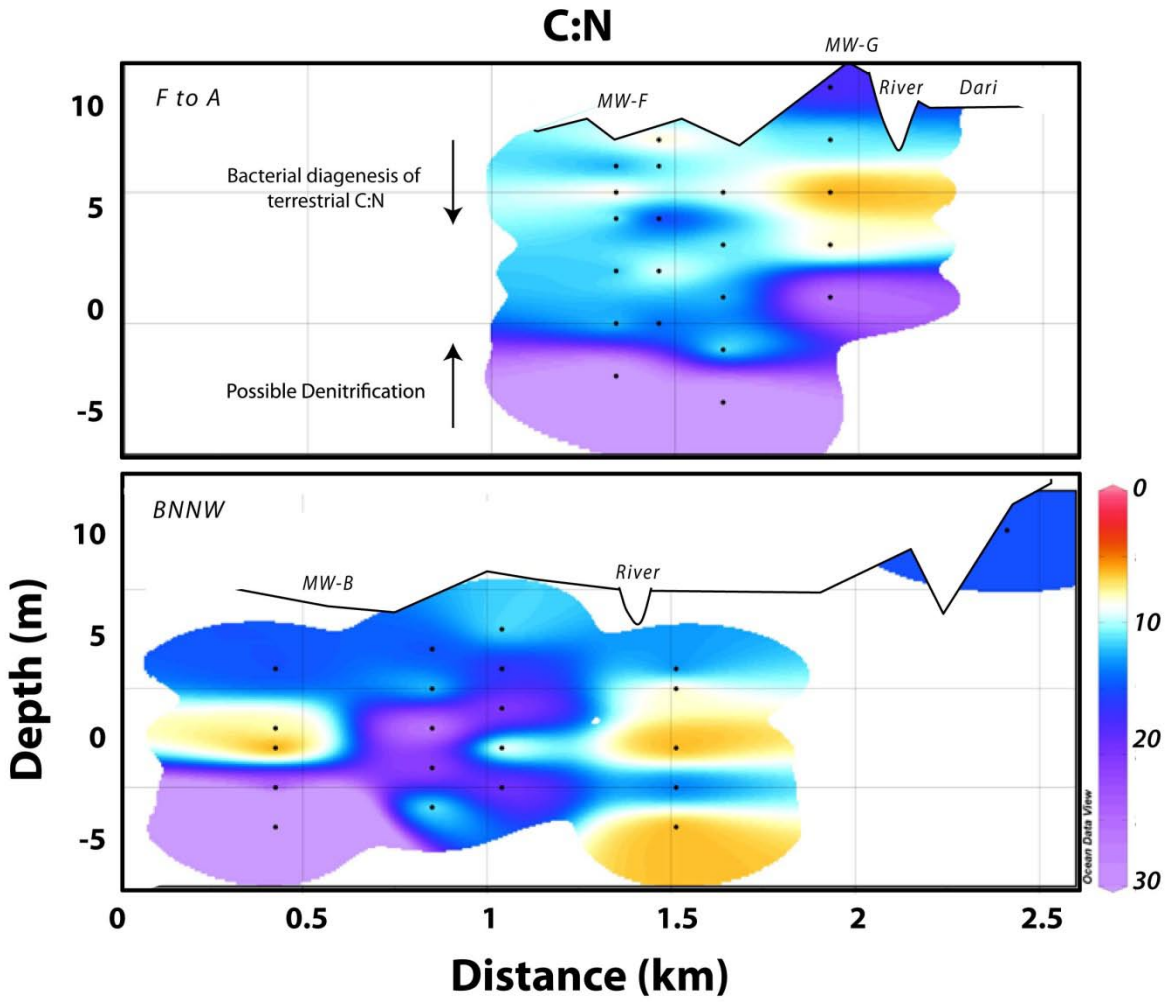

Figure 6. C:N ratios from CHN results on a select number of decarbonated Araihazar sediments and the biogeochemical processing they represent. Unlike %LOI, patterns of C:N do not conform to patterns of mud cappings and aquifer sands. Instead, they conform to likely biogeochemical reactions of terrestrial organic matter diagenesis in the aquifer. Along both transects, surface sediments typically have terrestrial values of C:N (~20), which grade to lower, bacterial C:N values at depth (~5) (ref. Tyson, 1995). Furthermore, highest values of C:N are typically deepest (>30), likely representing denitrification from the lower unit.

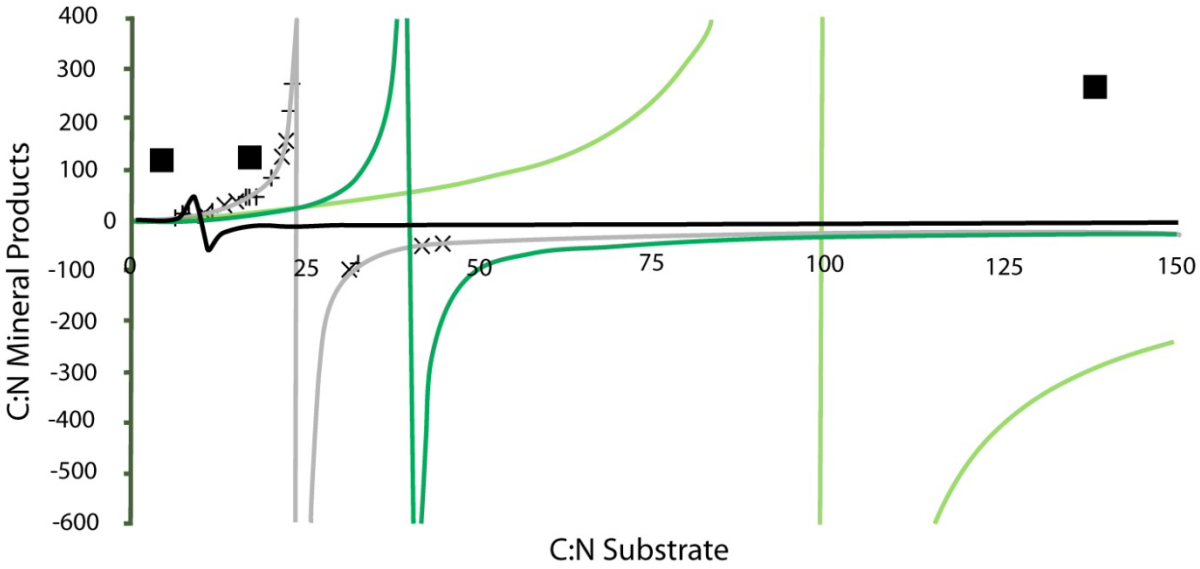

Figure 7 (above): Plot of C:N in different substrates versus C:N in mineral products with different efficiencies of metabolic processes (E), after Figure 2.1 in Fenchel et al., (2000). Higher efficiencies (0.5) apporximate remineralization under aerobic conditions, while lower efficiencies (0.2) approximate an anaerobic setting. The C:N of mineral products is calculated from C:N = (1-E)/(Ns-ENc), where Ns is the sediment N:C and Nc is the typical N:C of bacteria (0.2). The C:N of the "bulk" substrate in Araihazar fits C:N ~20. For comparison, C:N calculated from thermodynamic equilibria with groundwater temperature, pH, ammonium and nitrate measurements from Zheng et al., (2005) ($\Sigma[CO_2]/\Sigma[N_2]+[NH_4]+[NO_3]$) are plotted to evaluate the theoretical C:N of the model and aquifer equilibria

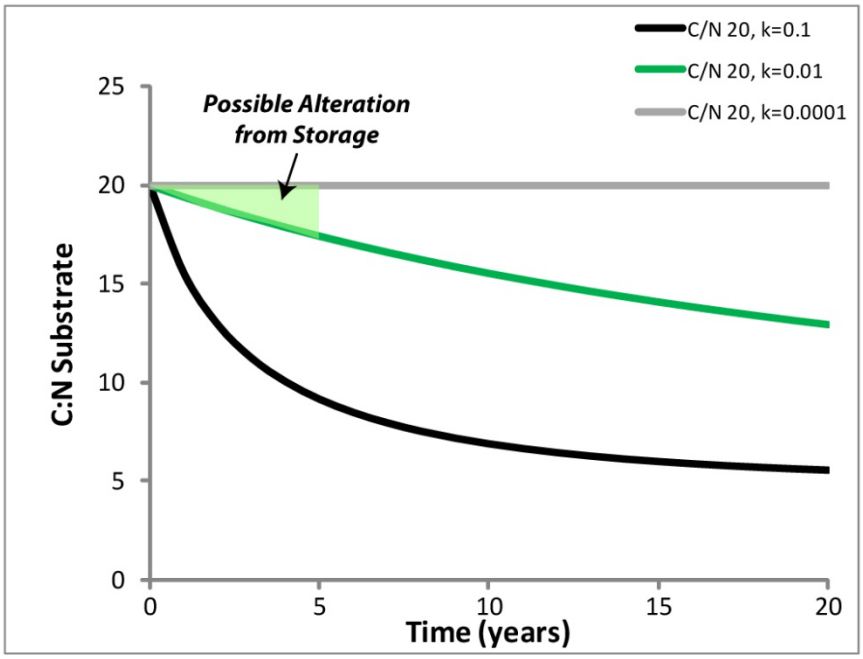

Figure 8 (left): Model of possible C:N changes over time using a theoretical batch treatment with coupled differential reactions. Conditional rate constants spanning several orders of magnitude, were used from this and other studies (Table 2). From FIgure 7, the initital substrate for the model best-fit a remineralization curve where C_0/N_0 = 20. Following the model's analytical solutions, conditional constants up to 0.01 likely express the degree of degredation of the sedimentary organic matter.

2004; Solaiman, 2009), and impeded denitrification due to arsenic (S.R., 2008), the values of C:N reported here are valid representations of their original values. Inasmuch, the spatial differences of C:N in the profiles are useful for interpreting aquifer processes, and translating picture-patterns into more meaningful biogeochemistry (i.e., seeing the terrestrial $\rightarrow$ microbial $\rightarrow$ denitrification process in Araihazar).

3.3. Transect Arsenic and Redox Geochemistry

In deploying the needle-sampler, we are able to produce unprecedented, high-resolution arsenic and redox aquifer imagery, which is important for understanding how aquifer deposits, and their three dimensional architecture, affect groundwater quality. In particular, we use the profiles to let us know how similar aquifers are, not only between villages, but between study sites as well—a highly relevant issue in determining how relatable results are from one site to another (McArthur, 2004; van Geen, 2009; Kocar, 2008; Berg, 2008).

As previously observed along a 0.5 km pilot transect ~25m away from the beginning of F to A, (van Geen, 2006), there is no simple, consistent relationship between groundwater arsenic concentrations and the different sediment properties. The organic, reducing, and mobilizable arsenic ranges vary for each transect (Table 6). From subsets of cuttings and needle-samples, sediments from the same horizon were analyzed for reflectance, Fe(II)/Fe ratios, PO_4-extractable arsenic, and groundwater arsenic via methods outlined in Cheng et al., (2004), Horneman et al., (2004), van Geen et al., (2004) and Zheng et al., (2005). As reported by Horneman et al., (2004), there is a significant correspondence between the first derivative transform of the reflectance at 520 nm and the sediments' leachable Fe(II)/Fe ratios (Tables 7a-d and Figure 9). Pearson correlations performed using Minitab® indicate strong, negative correlations that are highly significant ($R = 0.6\text{-}0.8$, $p \leq 0.003$), which is

consistent with previous findings of low reflectance from reducing, gray sediments and higher reflectance from less reduced, more orange and brown sediments (van Geen, 2006).

3.3.1. Fe(II)/Fe-total Ratios

Amid the three transects, it is noteworthy that the patternings of the aquifer's sediment redox potential are different for each transect. In comparing the three profiles, the Fe(II)/Fe ratios and reflectance do not follow a uniform subsurface patterning between sites with different groundwater arsenic (Figures 9 and 10). This is despite the similar averages and standard deviations for Fe(II)/Fe in the transects (0.6 ± 0.2 for Bangladesh and 0.8 ± 0.1 for Nepal, Table 6), which is important because it indicates that the visual profiles add another level of understanding to these aquifers than geochemical correlations alone—and they also show a geochemical conformity with each aquifer's sediment faces (Figures 2 and 3). Key features of the redox profiles show more reducing-Fe(II) conditions conforming to the mud caps and infillings of the Bangladesh transects. The infilled channel muds of F-to-A and the mud capping along BNNW have the highest Fe(II)/Fe ratios, ~0.8, with lower ratios generally in the sandier units (Figures 2 and 9). Alternatively, there is a less discernable patterning between Fe(II)/Fe and the sediments in the Parasi facies. Despite a more obvious conformity in Parasi, the three transects, overall, agree with previous findings where sediments with Fe(II)/Fe <0.4 typically are associated with low groundwater arsenic (van Geen, 2006; van Geen, 2008, and Figures 9 and 10).

3.3.2. Reflectance (ΔR)

The reflectance, similar to Fe(II)/Fe ratios, follow no one tractable patterning between the transects. Again, there is a nice conformity to facies in Bangladesh's F-to-A transect, where lower reflectance, more reducing sediments coincide with the muds of the infilled channel (Figure 10, top panel). And, where Fe(II)/Fe ratios conformed to BNNW's facies, reflectance measurements for the same transect display a lower sensitivity for facies. The dynamic range in reflectance is less over the 2.5 km transect (BNNW's 0.1-0.5 vs. F-to-A's 0.1-0.8), with ubiquitously low measure-

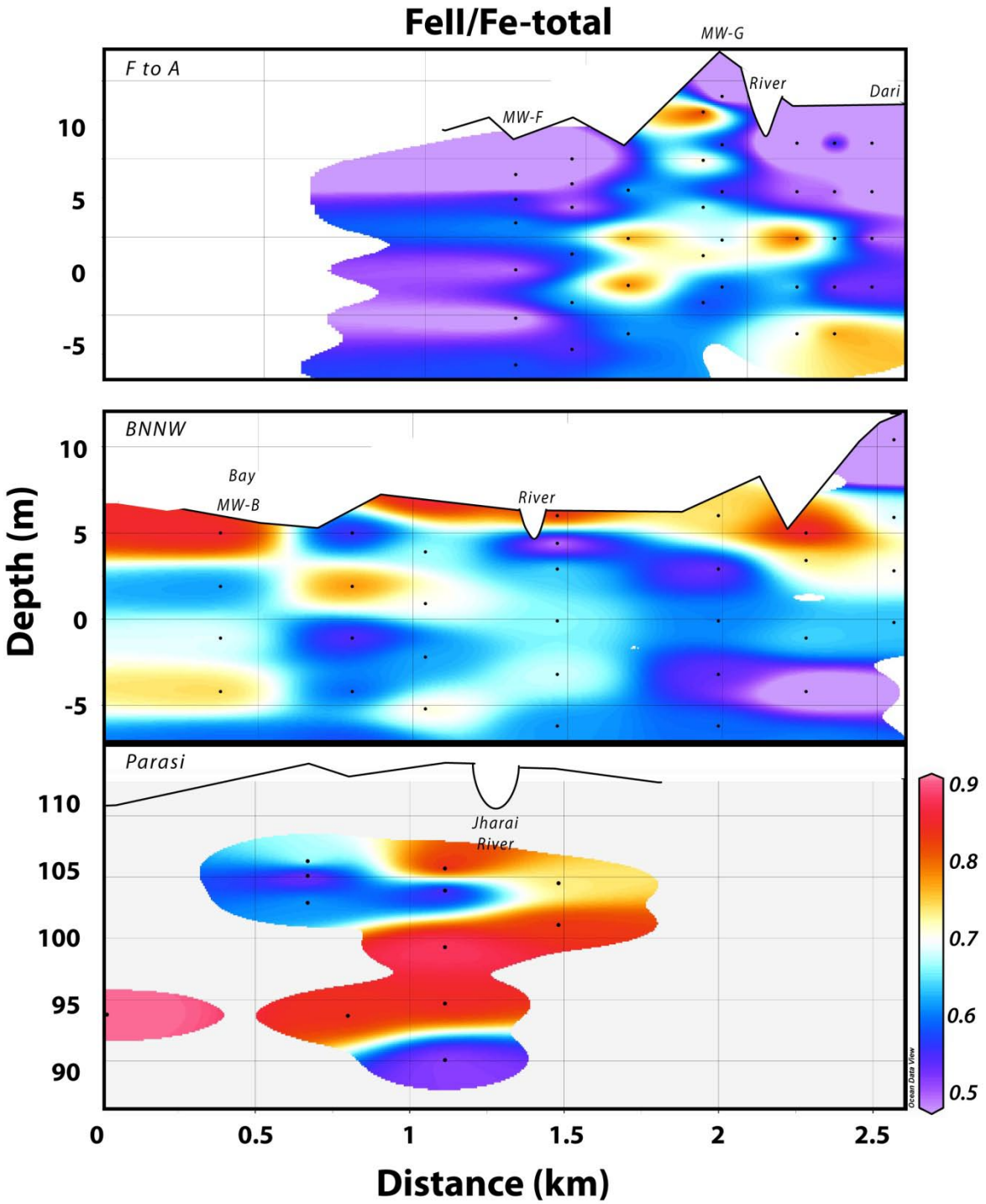

Figure 9. Iron ratios of leached aquifer sediments. Higher ratios are indicative of more reducing conditions sediment surface conditions, while lower ratios are more conducive to FeOOH coatings on sediments. Previous work by van Geen et al., (2004) shows ratios in excess of 0.6 to be, overall, reducing, with little or no surface Fe-oxyhydroxide phases present.

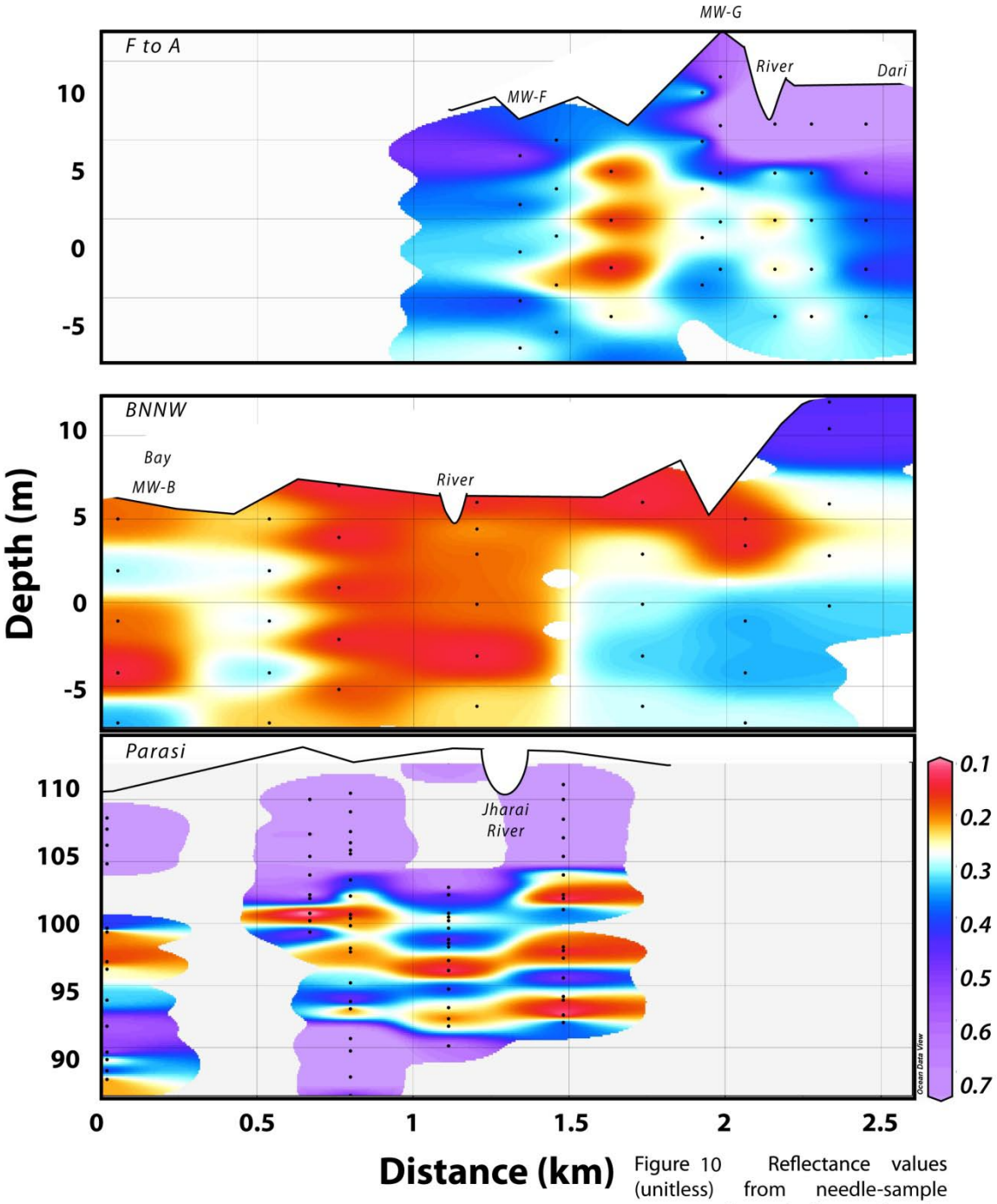

Figure 10 Reflectance values (unitless) from needle-sample transects from Araihazar, Bangladesh (top & middle), and Parasi, Nepal (bottom).

ments throughout BNNW's profile (~0.2, Table 6). In comparison, the dynamic range and average reflectance for sediments along Parasi's profile are both higher than those of Araihazar (Table 6), with patterns conforming to muds in the subsurface. This is different to reflectance-conformity with surface muds and infillings in Araihazar, in that Parasi's surface muds appear uniform and continuously reflective (>0.7 to depths of ~102 m, Figure 10). Buried mud units, which are typically more fine-grained than those at the surface (Figure 2), conform to less reflective, ~0.2 measurements in the subsurface. These buried muds, like F-to-A's muds, are those of old infilled channels, which since abandonment, have been deposited over by newer channel and floodplain facies. This means that there may be a general conformation between low-reflectance measurements and infilled facies, with reflectance preserved through burial. Overall, while there appears to be no systematic profile-trend for reflectance, and with surprisingly high reflectance significantly correlating only with low arsenic in BNNW's "least sensitive" transect (Table 7c), there is a good regional correlation between reflectance and groundwater arsenic from the cumulated profiles ($R = -0.6$, $p < 0.001$, Figure 8E).

3.3.3. Phosphate Extractable Arsenic

The association between groundwater arsenic concentrations and another property of the sediment, the concentration of P-extractable arsenic, also appear somewhat systematically in the profiles, (Figure 12), with "hot spots" of mobilizable arsenic tending towards localized, high-groundwater arsenic areas. Along F-to-A, P-extractable arsenic increases from the low-arsenic MW-F village towards Dari, the village with higher concentrations of groundwater arsenic (Figure 11). Similarly along BNNW, higher P-extractable arsenic occurs northwest of Bay, where higher amounts of arsenic are also found in the groundwater. In Parasi, higher P-extractable arsenic is also in close vicinity to where groundwater arsenic concentrations start elevating, at the ~95m depth-interval by the Jharai River (Figure 11). This tendency for finding higher groundwater arsenic coinciding with sediments that have

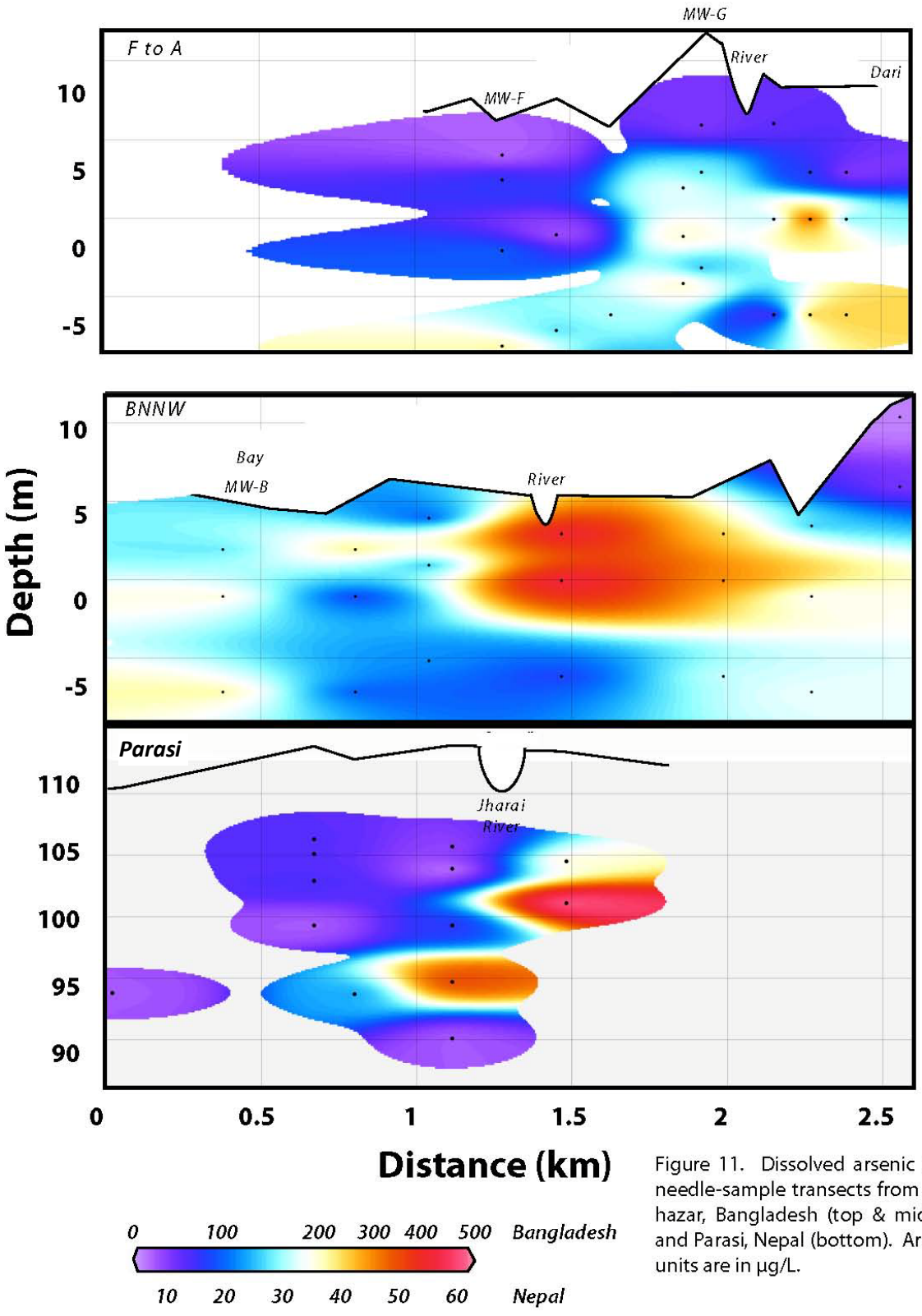

Figure 11. Dissolved arsenic in the needle-sample transects from Araihazar, Bangladesh (top & middle), and Parasi, Nepal (bottom). Arsenic units are in µg/L.

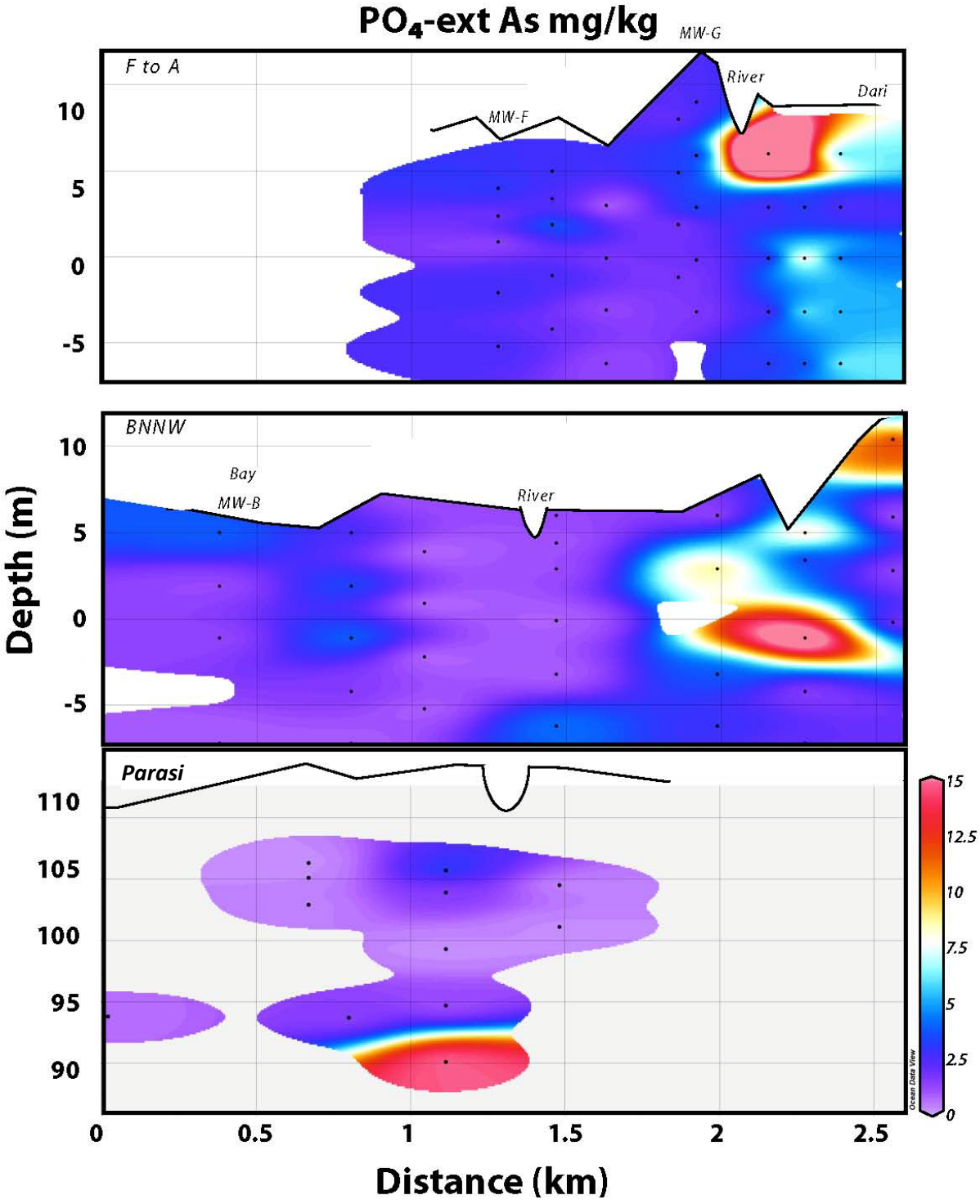

Figure 12. Phosphate extractable arsenic in ppm leached from aquifer sediments after Zheng et al., 2005. This fraction of extractable arsenic is significantly correlated to dissolved arsenic concentrations in Bangladesh, Vietnam, West Bengal, and Nepal. (van Geen et al., 2008 and Metral et al., 2008), with the solid extractable fraction on par with crustal values of arsenic in Earth's upper crust (~1.5-5.1) and riverine particulates (15 & 27 ppm, EarthRef.org, 2009).

higher P-extractable arsenic is consistent with previous needle-sampling results in other regions (van Geen, 2008).

3.4. Column Experiments

3.4.1. Major Cations

In the column experiments, Na, Mg, Si, Ca, Al, and K dominate the effluents of the different aquifer material. Higher effluent concentrations for most elements were released during the initial stages for all of the aquifer material (usually starting ~5 pore volumes, and then dwindle). Typical ranges for Na, Mg, Si, Ca, Al, and K were between 100-990 µg/L (4-43 µM), 228-4010 µg/L (9-165 µM), 600-6400 µg/L (21-228 µM), 700->20000 µg/L (17->500 µM), 10->2000 µg/L (0.4->75 µM), and 370-1690 µg/L (9-43 µM), respectively (Figures 13 and 14, top panel), with the higher concentrations relating to the early effluent and the lower concentrations being the tailed-off, converged, and typically steady concentrations in the final effluents. Initial unsteady-state conditions is supported by the removal of the initial effluent concentrations from the molar ratio graphs—without the initial effluent, there is much more correlation between the elements (Figure 13, 14, and 15). A comparison of plots with and without the ~5 pore-volume concentrations show better fits without the presumably less "equilibrated"[40] initial effluent data (Figure 13 vs. Figure 15). Only Fe, Mn, and Al show trends in weathering using all of the data (Figure 13), whereas K, Na, Fe, Mn, and Al correlate when we exclude data from the initial effluent (Figure 15). Most likely, the better correlations we get from discounting the initial effluent chemistries

[40] I use the word "equilibrate" loosely here, since it is a term we use when "equilibrating" pH, Eh, etc. flow-through cells with groundwater samples in the field. Similar to the flow-through cells and the sampling of tubewells, the columns required time to adjust to new conditions, and for mineral phases to equilibrate with the influent water. While the columns may never reach a chemical equilibrium over the duration of the experiment, they will be closer to chemical equilibrium conditions over time (here after ~5PV), reaching more steady-state conditions.

are due to the removal of data from less “equilibrated” waters—it probably took several pore-volume exchanges to flush the columns and achieve new steady-state conditions.

In addition to the better trend lines for more “equilibrated” waters, even better trends are seen when the data is presented in a way that can differentiate columns (Figures 14 and 16). Magnesium is perhaps the most striking example for this, with a Si and Mg relationship that appears trendless until the columns are plotted separately (Figure 14). With all of the data, Mg shows no strong trend with Si (Figure 14, top panel). Removing disequilibrated early effluent only worsens the scatter (Figure 14, middle panel. A trend is not seen until the data is marked and color-coded to highlight data from the different columns (Figure 14, bottom panel). Distinguished by marker and color, continuous stoichiometries of Si:Mg are seen being released out of the columns. This column-distinction can be seen for the other elements as well (Figure 16), with Si correlations supportive of silicate weathering. Thus, it appears that the weathering and dissolution of silicates is likely going on in the columns. Linear trend lines with good fits for Si with Mg, K, Na, Ca, Fe, Mn, Al, and Mg all support alumina-silicate weathering (Figures 13-16): some good ratio fits include mica (Si:K), hornblende (Si:Na and Si:Fe), and calcic plagioclase (Si:Ca), (Schroeder, 2000; Velbel, 1989).

The presence of these elements and their availability for weathering were confirmed by Cu$K\alpha_1$ XRD scanning (Wellons, 2007). Scans of Nepal’s aquifer material show diagnostic 2-theta (crystal d-spacing) peaks for mica, quartz, plagioclase, and hornblende for all three aquifer samples (Figure 17, top panel). The XRD peaks show the same mineralogy for both shallow and deep PNS5 samples (both 5 and 12kyr show the same mineralogy). The PNS1 sample show the same peaks as the PNS5 samples, with additional peaks for clay and titanite, which are absent in the PNS5 samples. The mineral separates for the Zr-age dating confirm titanite in PNS1-44, (Nepal’s Chapter Figure 8). Interestingly, despite evidence for different mineralogies, stoichiometry and the convergence of K, Na, Fe, Mn, and Al concentrations in the last two samplings—this is seen in Figures 15 and 16, where the lowest y-values trend along

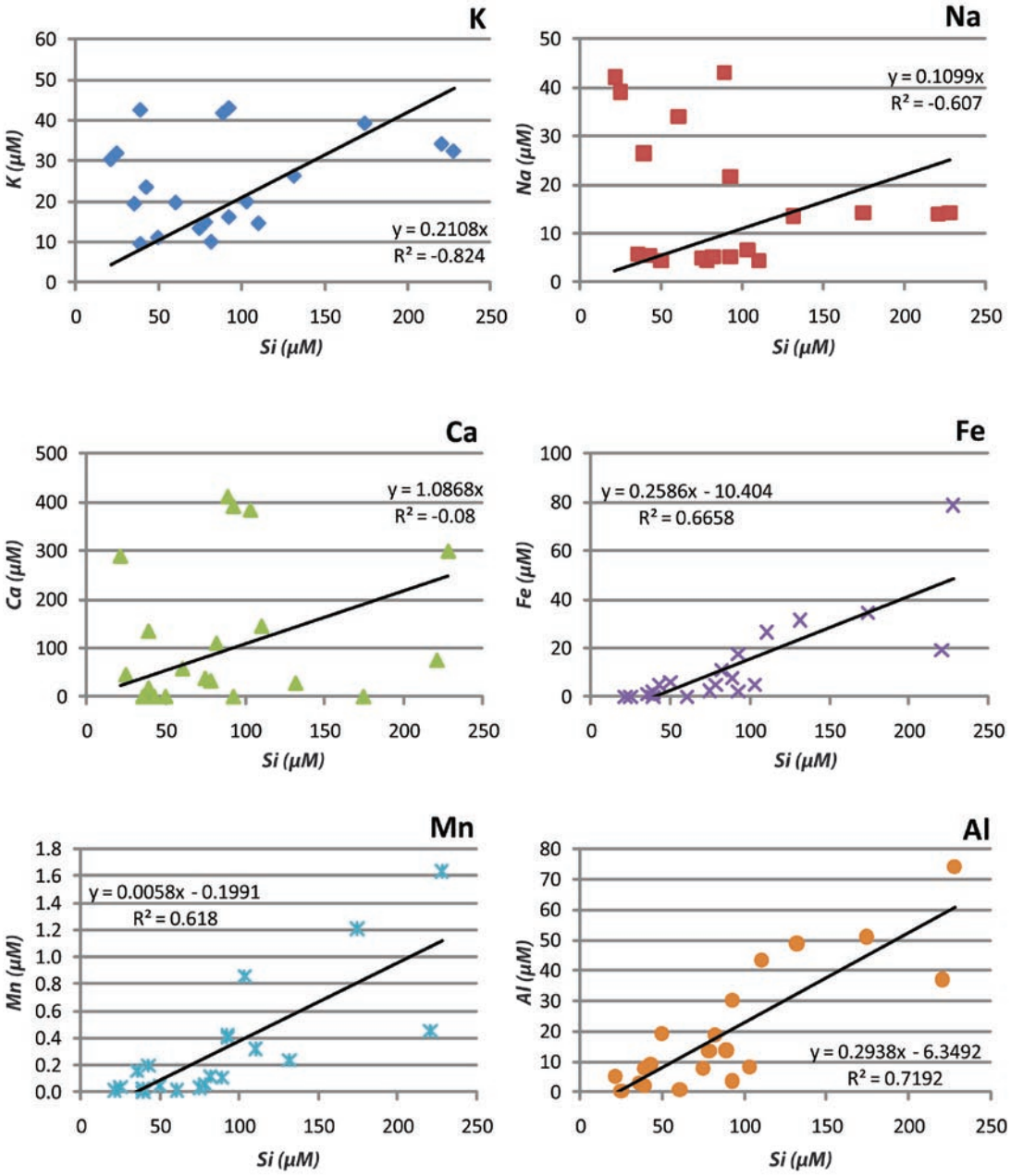

Figure 13. Results of column experiments, plotting dissolved silicon concentrations (µM, x-axis) versus other major cations in the column effluents (y-axis). Between all of the cations, Fe, Mn, and Al have the highest correlations with Si, indicating the preferential weathering of Fe-Mn aluminosilicate minerals within the columns. Molar ratios for each element is given in the slopes of linear regressions: Si:Fe and Si:Al ~ 4, and Si:Mn ~ 167

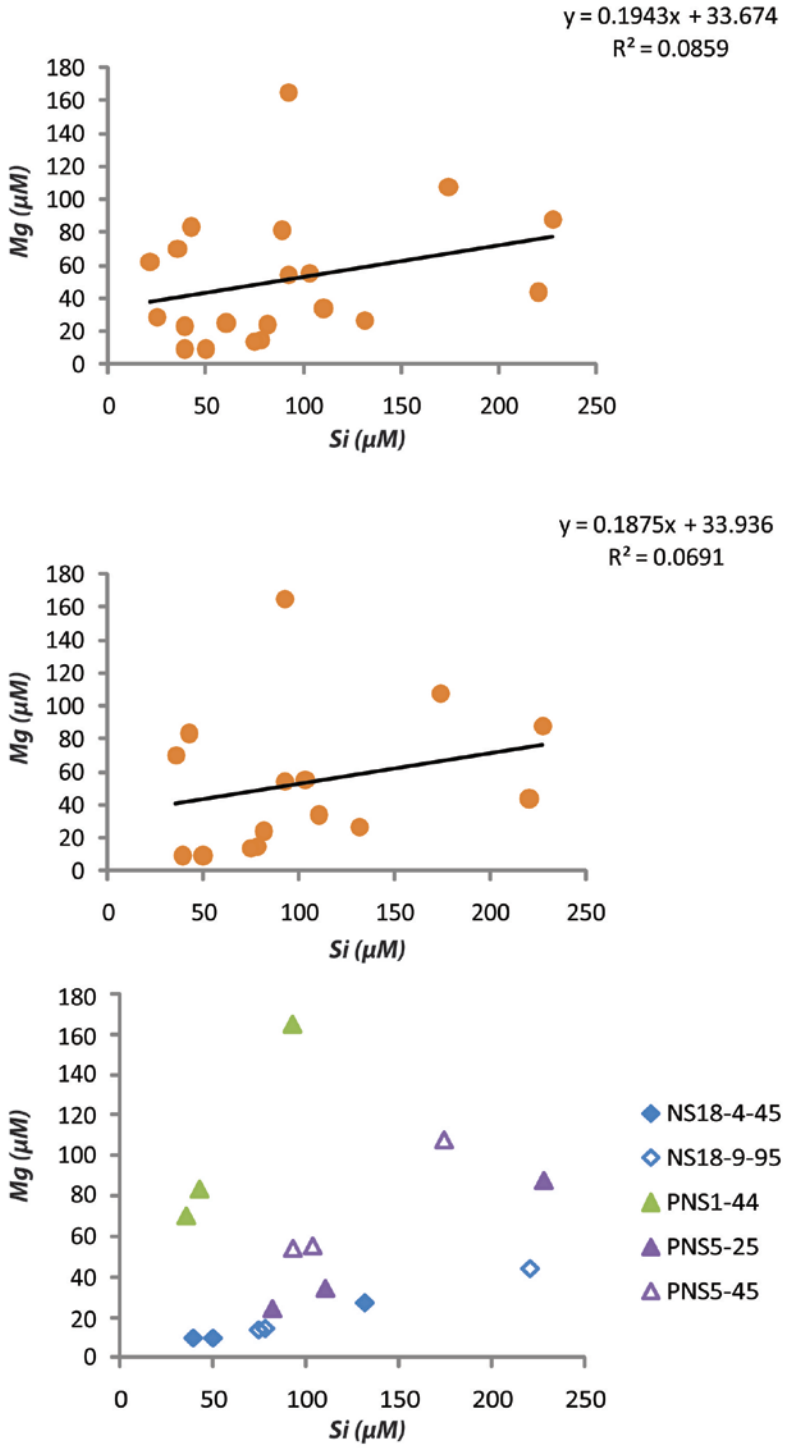

Figure 14. Results of effluent Mg concentrations in column experiments. Silicon concentrations (µM, x-axis)) versus other major cations in the column effluents (µM, y-axis). The top graph plots all effluent values, the middle graph plots Mg effluents after 5 pore volumes, and the bottom graph shows Mg concentrations distinguished for each column. The bottom graph shows how distinction between the columns gives more of a trend pattern to the data. The Si:Mg molar ratios are the same for both Bangladesh, NS18 samples (Si:Mg ~ 5, R^2 >0.99) and both Nepal PNS5 samples (Si:Mg ~ 2), with Nepal's PNS1-44 weathering the most Mg (Si:Mg ~ 0.6).

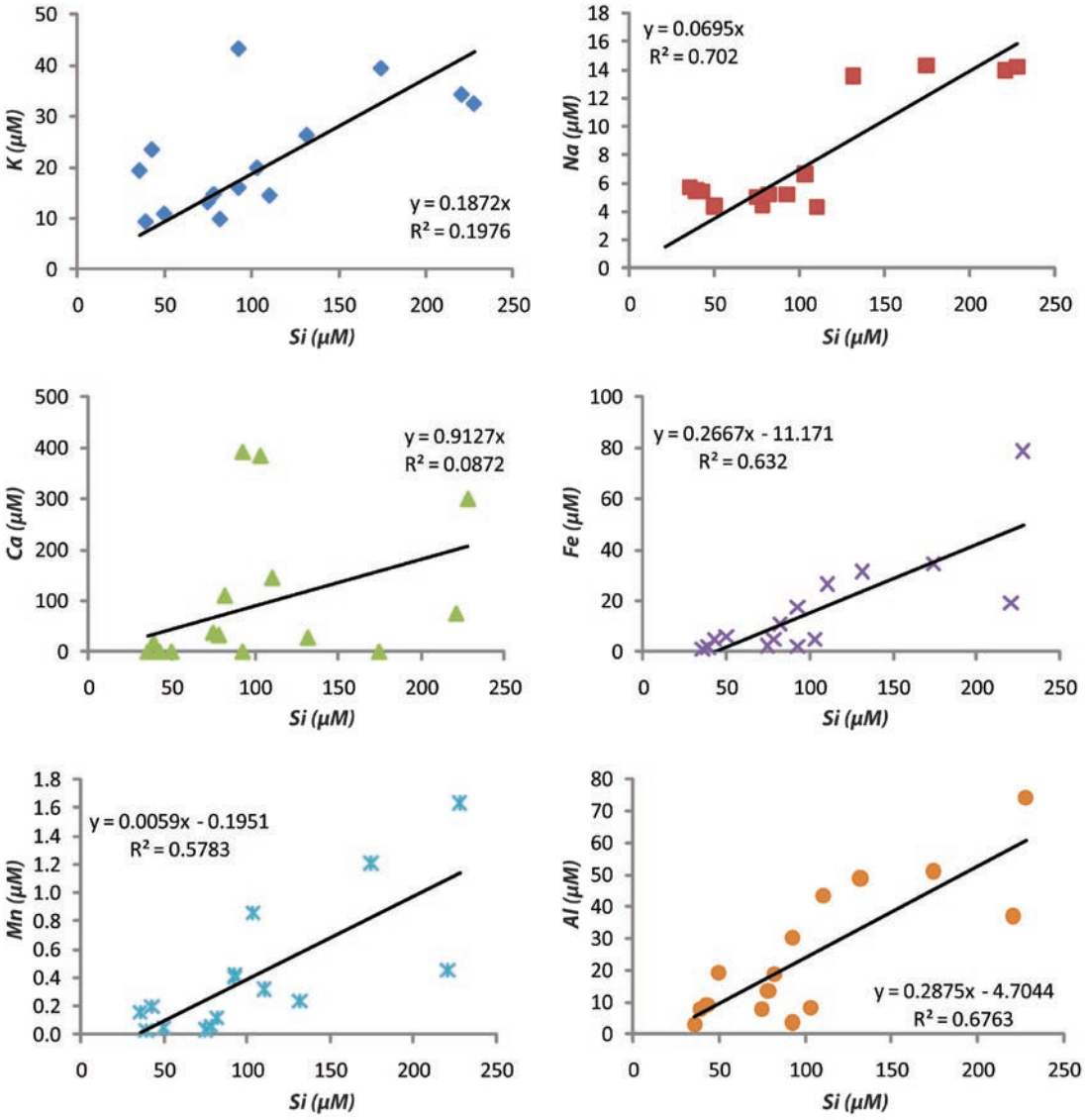

Figure 15. Results of column experiments, plotting dissolved silicon concentrations (µM) versus other major cations in the column effluents, without the first five pore-volumes of effluent (which are included in Figure 13). Without concentrations in the inital effluent, all cations correlate with Si, with Na, Fe, Mn, and Al having the highest correlations with Si. This suggests plagioclase and Fe-Mn aluminosilicate weathering within the stabilized columns. Molar ratios for each element is given in the slopes of linear regressions: Si:K ~5, Si:Na ~14, Si:Ca ~1, Si:Fe and Si:Al ~ 4, and Si:Mn ~ 167.

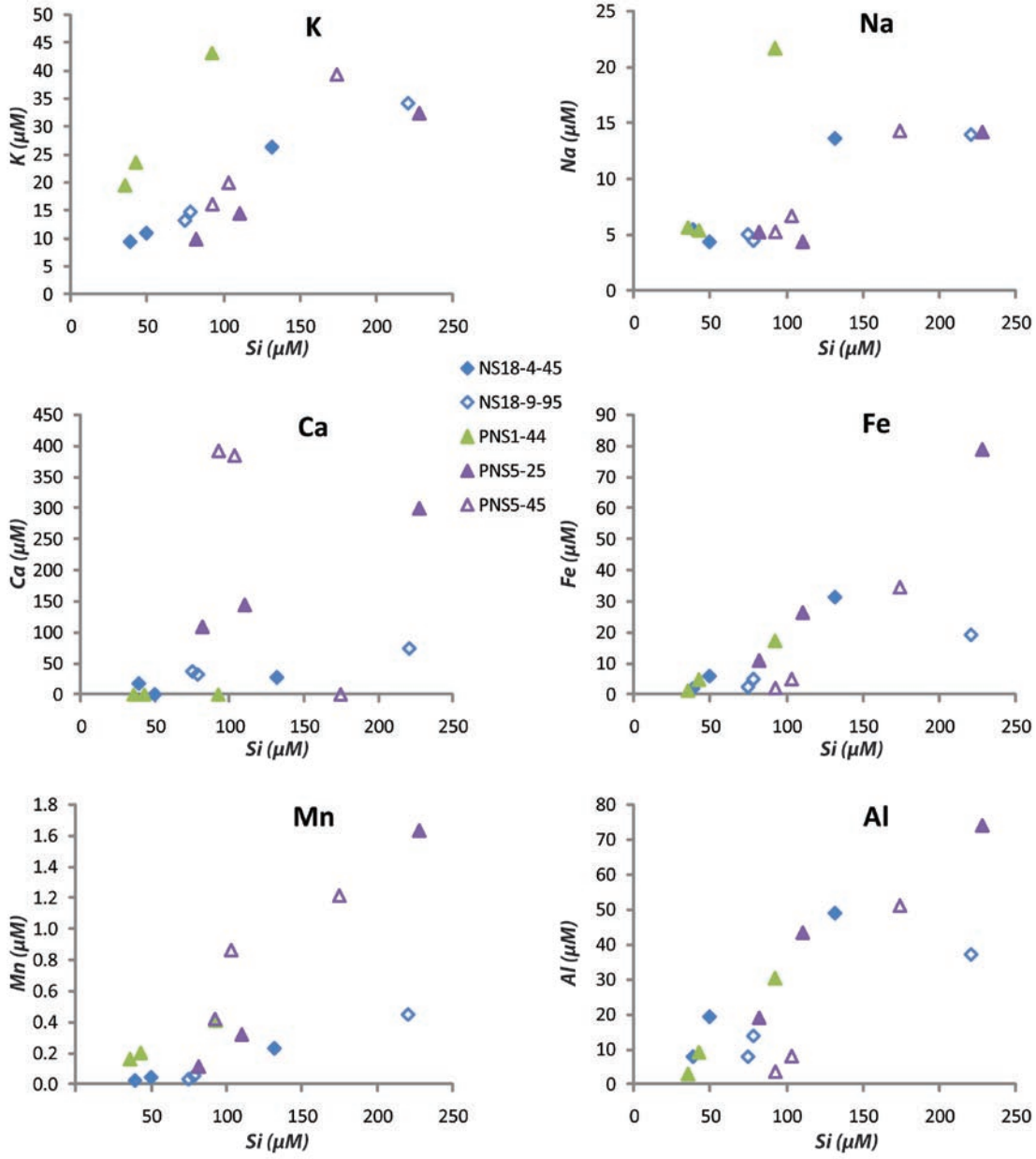

Figure 16. Column effluents, plotting dissolved silicon concentrations (μM) versus other major cations in the column effluents, without the first five pore-volumes of effluent and colored to show differences between the different columns (a recoloring of Figure 14). Using a different type of marker for each column, K and Na concentrations show a different, more K and Na enriched weathering trend for PNS1-44, the 12ky-old aquifer deposits in Parasi, Nepal. PNS5 weathers more Ca then the other columns, and the deeper samples (which are unfilled-markers) weather lower amounts of Fe and Al than shallower, younger samples.

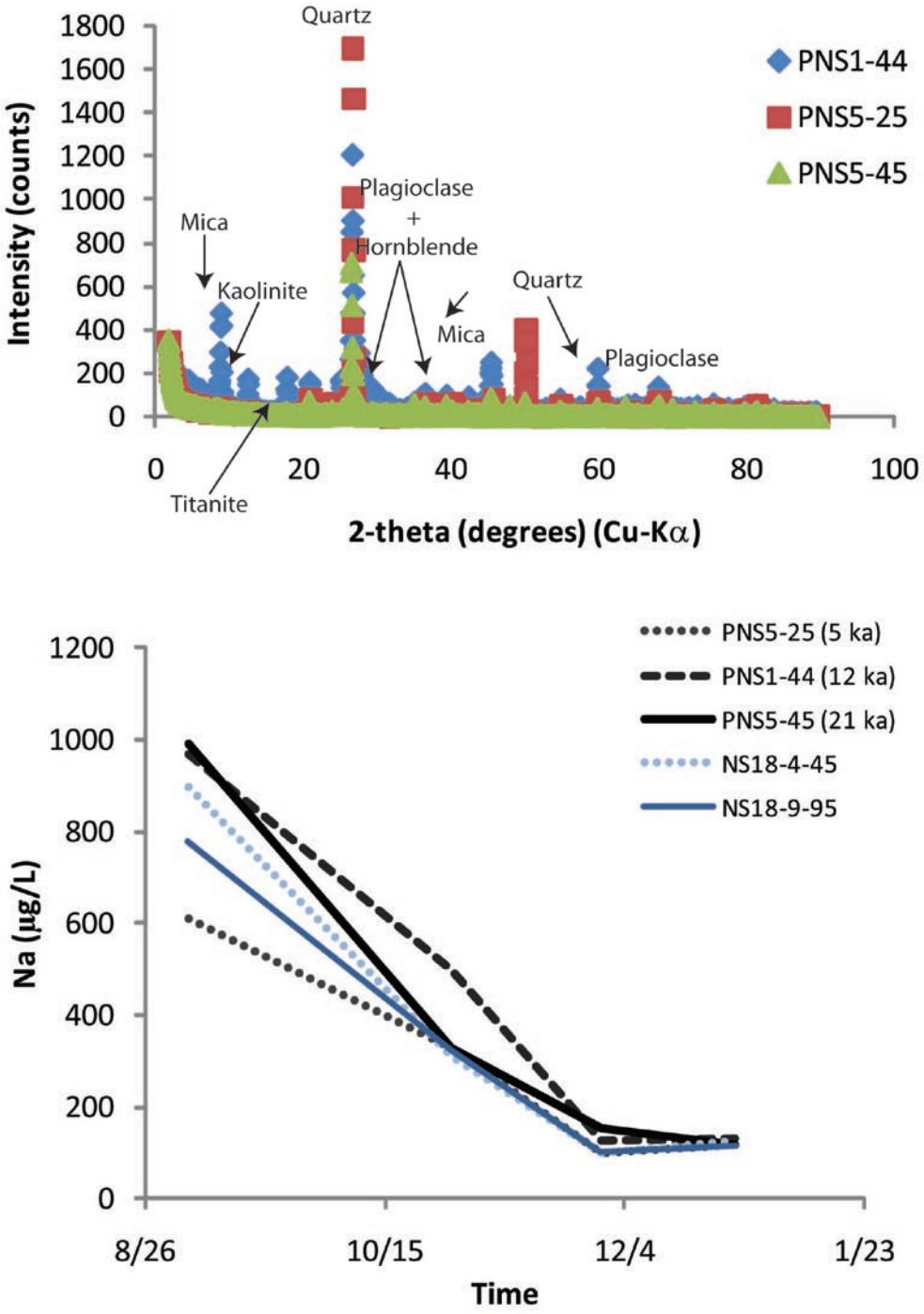

Figure 17. Top: Qualitative XRD results of Parasi column sediments, with mineral peaks identified using the RRUFF database (http://rruff.info/). Bottom: Na concentrations were monitored for aquifer weathering rates (after White and Brantley, 2003) .

horizontally, showing the concentrations converging—indicate that the sediments in all of the columns ultimately weather to similar steady-state conditions (Figure 17, bottom).

3.4.2. Arsenic

Not following the same trends as the major elements, effluent arsenic concentrations behave more erratically. Effluent arsenic concentrations ranged between <0.03-2.11 µg/L, (5E-4-0.03 µM, detection limit 0.03 µg/L), with the different aquifer materials releasing arsenic at different initial rates (Figure 18, top panel). The highest concentrations of arsenic were leached from Parasi (Figure 18, top and bottom left), with [surprisingly] the oldest deposits (21kyr, PNS5-45) leaching the most arsenic (1.5 - 2.1 µg/L). The second highest arsenic concentrations were leached by Parasi's youngest deposits (5kyr, PNS5-25), followed by the 12kyr sands at PNS1-44. Leaching less that the Parasi samples, the "younger" Birganj sands (thought to be 2-6kyr), ended the flow through experiment with non-detectable levels of arsenic, (Figure 18, top and bottom left).

4. Discussion

4.1. Arsenic Mobilization from the Columns

In pursuing this work, the goal was to shed light on why different deposits have different concentrations of arsenic. By investigating the sedimentological history of heterogeneously affected villages in Nepal, Vietnam, and Bangladesh, we, along with others (i.e., McArthur, 2008; Papacostas, 2008) show consistent trends between aquifer age and arsenic, helping to explain the local heterogeneity (i.e., more than 100 µg/L change over a distance of 10-100 meters). To get at why older deposits tend to host lower concentrations of groundwater arsenic, we conducted column experiments to test whether we would see differential weathering from the columns. In beginning the experiment, we hypothesized that the older sediments would weather slower, and result in the lower leached rates

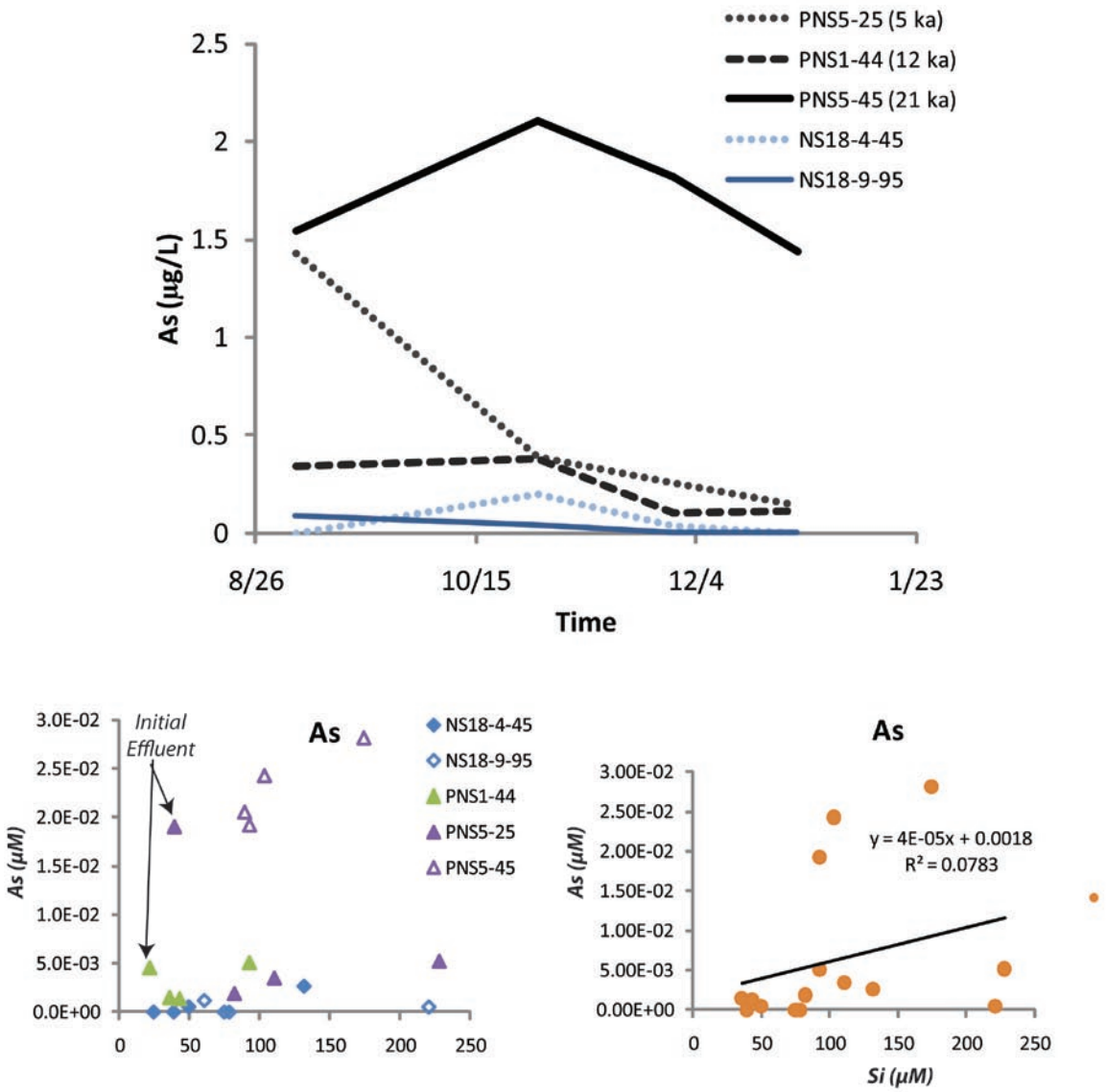

Figure 18. Results of column experiments - the upper graph plots arsenic concentrations leached at different times from the columns and the bottom graph plots As (y-axis, µM) versus Si (x-axis, µM). The times are reported in month/day format from August 2007 - January 2008. The concentrations shown are after the first five pore-volumes of effluent. The left graph is colored to show differences between the different columns, while the right graph shows the trend for al of the data. The high As leaching is from the deeper, PNS5 samples, which have an OSL age of 12kyr.

of dissolved arsenic. This is based on the hypothetical reactivity decline of older, more weathered sediment (White, 2003), meaning that we should have seen an age-progression in the effluent concentrations. Correcting for differences in grainsize, Figure 19 (top panel) shows the type of results differential weathering would produce, with the oldest sediments (PNS5-45 and NS18-9) being less reactive and steadily leaching low concentrations along the graph's bottom (i.e., the solid lines with little or no curvature). Above this, younger deposits would plot, showing an increasing progression of reactivity (curvature) and arsenic—the youngest deposit, PNS5-25 should have the steepest slope (highest initial weathering rate) and leach the highest concentrations of arsenic (i.e., the finest dotted black line).

While the deeper Birganj (NS18-9) and youngest Parasi (PNS5-25) samples behaved as we expected, the older Parasi samples (PNS1-44 and PNS5-45) unexpectedly leached more arsenic (Figure 19, bottom). Surprisingly, these older materials kept leaching ~0.1 μg L^{-1} m^{-2} of arsenic throughout the duration of the experiment. This is an order of magnitude higher than the converged release rates in the rest of the columns: ~0.04 μg L^{-1} m^{-2}. The preferential weathering of arsenic from the oldest sediments is also shown in Figure 18's plot of As:Si, with the 21kyr old sands (PNS5-45) with the highest As:Si slope line ($9x10^{-5}$, R^2 of 0.8 for datasets plotted with and without initial, disequilibrated effluents). Given that the columns' individual As:Si trend lines suggest arsenic is being leached via silicate weathering, initial effluent concentrations for two Nepal samples (PNS1-44 and PNS5-25) show arsenic mobilized through something other than silicate weathering (Figure 18, bottom left panel). Basically, this means that the dissolved arsenic in the initial effluent from these columns was translocated from another source area, and/or the arsenic is from some other weathering process—i.e., the reductive dissolution of FeOOH phases (Nickson, 2000). The oldest Parasi sands at PNS5 show a good correlation with Fe (R^2 0.74), as well as the later effluents from the younger, PNS5-25 column (Figure 20, top panel). These two aquifer sands had the highest amounts of organic, determined by loss-on-ignition (LOI, Table

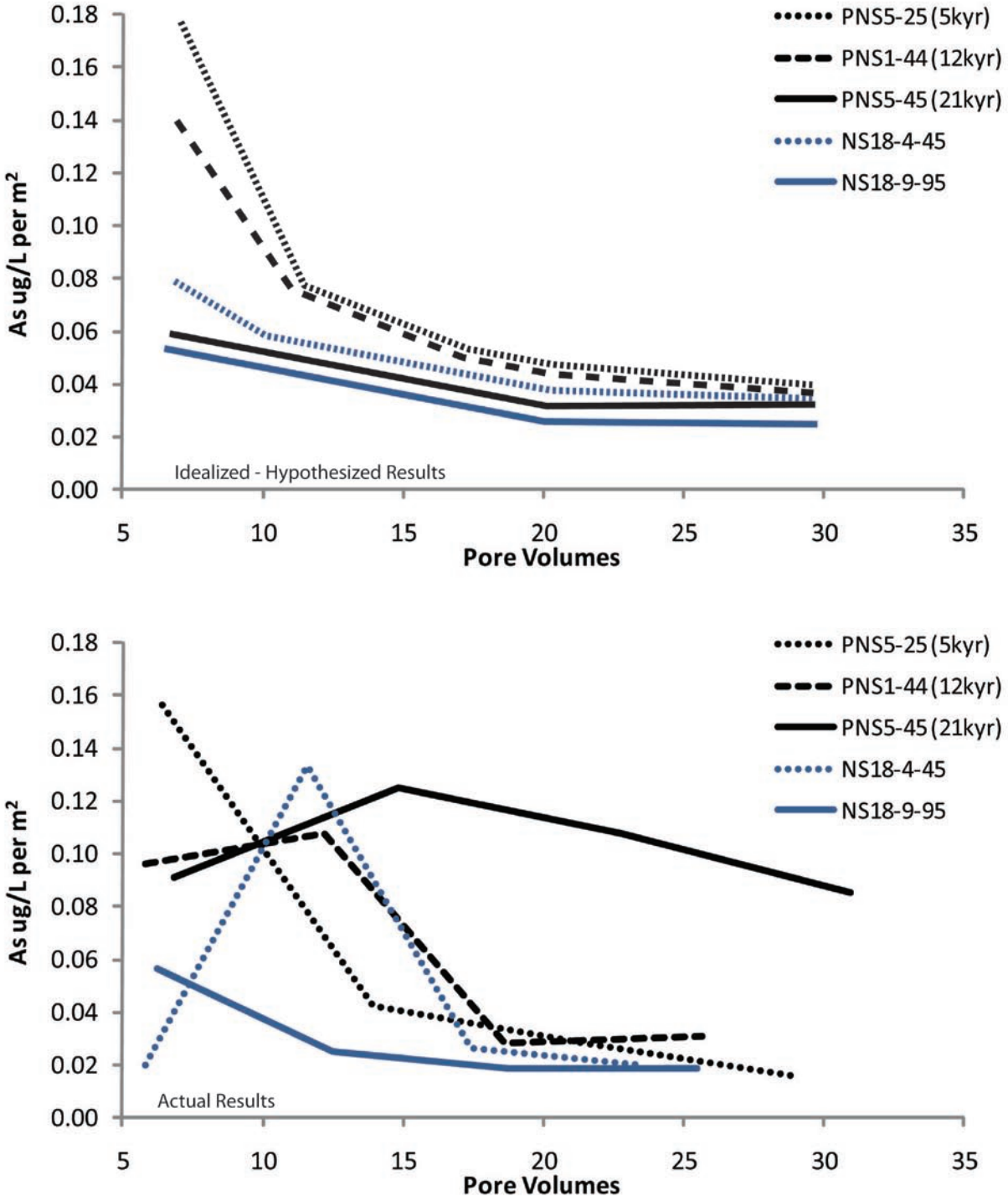

Figure 19. Results of column experiments (column information is in Table 3). The upper graph is the expected results for comparison with the actual flow-through results between 8/4 and 12/27/2007. If depositional age impacted the rate of release of arsenic, young deposits should have higher release rates.

3), meaning that reductive weathering of FeOOH, as well as some silicate phases, is likely the cause of the highest amount of arsenic coming from the oldest aquifer material. This is supported by the better agreement with the expected results (Figure 19) upon normalizing the effluent to surface area as well as the amount of sedimentary organic (Figure 20, bottom panel).

4.2. Arsenic Mobilization in the Field

At the field scale, correlations between groundwater arsenic and aquifer sediment properties (%LOI, Fe(II)/Fe-total, reflectance and P-extractable As, Tables7a-d) also support the idea that the Araihazar and Parasi aquifers are undergoing reductive dissolution. An overall comparison of the different sediment properties with groundwater arsenic shows good correlations between the amounts of sedimentary organic and sediment iron ratios, which is a good indication that there is enough sedimentary organic already within the aquifer, to naturally weather and leach arsenic. This is shown by the distribution of sedimentary organic in Figure 5, where sediments with higher organics are not just restricted to surface soils/deposits (i.e., the profile for BNNW; Polizzotto, 2008). Aquifer units and sands at depth can also be a source for high amounts of organics (i.e., buried organics in F to A and Parasi, (McArthur, 2004; Meharg, 2006). This may bean that despite aquifer age, the availability of a reductant from buried deposits may be more important in controlling arsenic. Hence, knowing the depositional history and facies within a local aquifer is particularly important for developing and using water. Importantly, two findings emerge from the column and transect data. The first is that despite higher arsenic being leached from sediments with higher sedimentary organics in the columns, the redox properties for each transect show no significant direct correlations between LOI and arsenic (Tables 7b-d). Considering that these correlations do not consider the openness of the system—i.e., organics and/or arsenic coming from upstream flow, a direct link between the solid and fluid concentrations are not reflected in these correlations. While there might not be a direct correlation between the

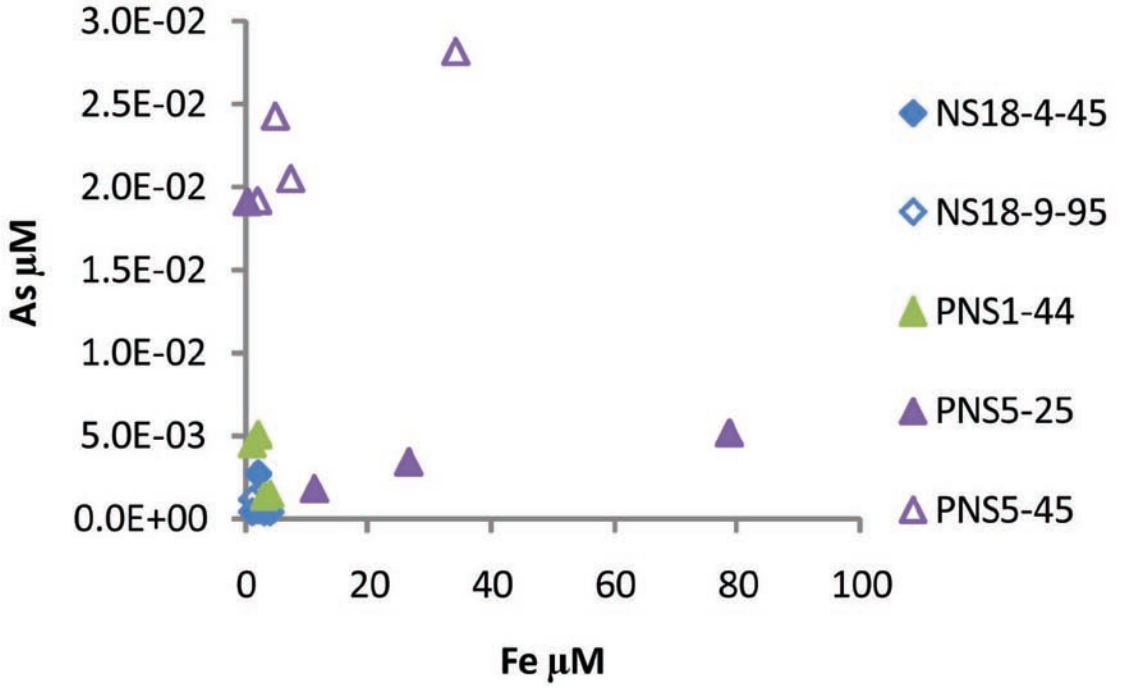

Figure 20. Top: column effluents, plotting dissolved Fe concentrations (µM) versus As, colored to show differences between the different columns. All effluent data, including initial concentrations are included. Bottom: arsenic in the column effluent normalized to surface area and loss-on-ignition, which is a proxy for sedimentary organic carbon.

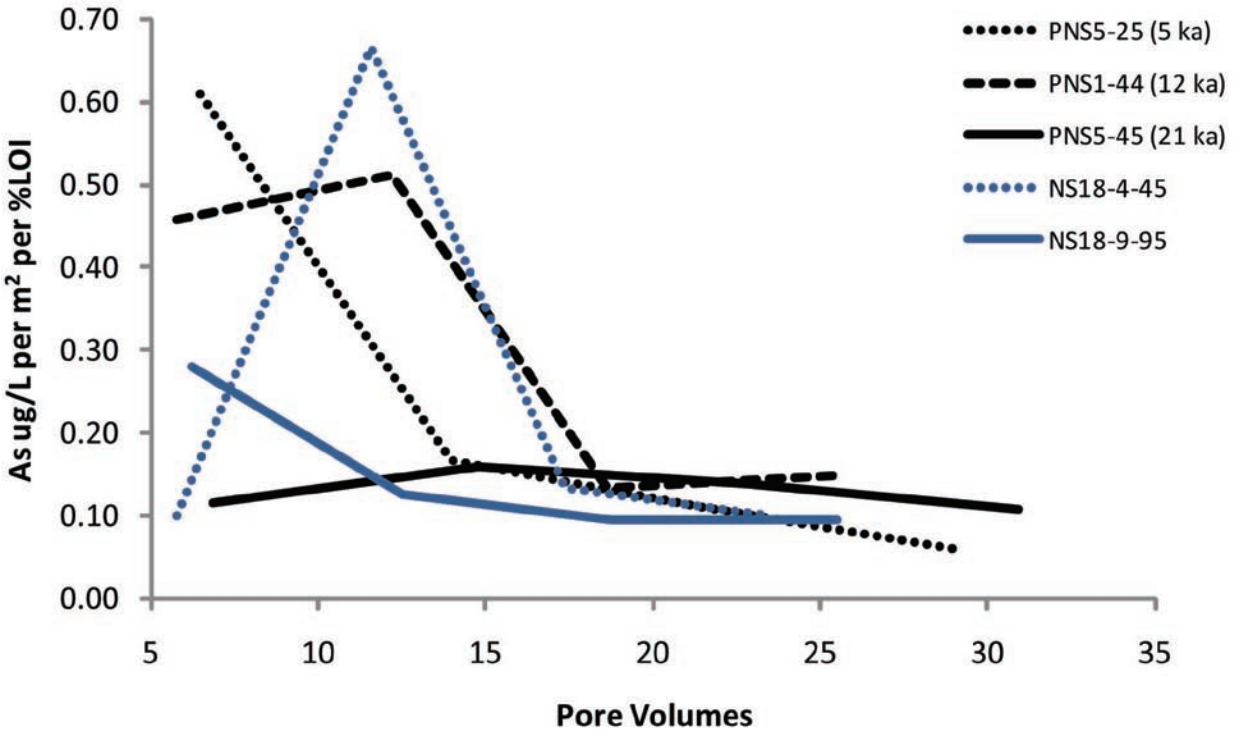

sedimentary organic and redox and arsenic-mobility at a particular depth, this column-to-field discrepancy can be due to fluid flow and translocation: sedimentary organics from an infilled deposit a few meters away can interact with an altogether different sedimentary unit—this could be why areas of highest microbial activity (lowest C:N, Figure 6) are offset from source areas of sedimentary organic—the surface muds of BNNW and F to A's infilled channel. It is also supported by the difference in actual C:N values dissolved in the water versus the values predicted from equilibration with the sediment (Figure 7). Finally, p-values for LOI correlations are just shy of significance, (p 0.07 for F to A's arsenic, and 0.06 for Parasi's reflectance, Tables 7b and d). This likely means that the sedimentary organic responsible for releasing arsenic may not necessarily be co-deposited in the deposit from where the arsenic is being sourced—hence an offset of significance in the data. This has important implications for villages located near Pleistocene outcroppings or where deep Pleistocene units can be invaded by non-native organics, (i.e., increased abstraction and the drawdown of sewage into deep Pleistocene deposits). As the arsenic release from the columns shows, the highest amount came from the Pleistocene sediments with the highest amount of sedimentary organic.

4.3. Regional Comparison of Aquifer Weathering

Estimations of the rate in which sedimentary organic is being depleted from the transects can be made by dividing mass differences in the amount of sedimentary organic by the difference between the age of the deposit. For Parasi, this results in C-losses approximating 0.03-.99 mol C m^{-2} yr^{-1}, and for Araihazar, 0.2-6.8 mol C m^{-2} yr^{-1}. If these approximations are correct and assuming that different aged deposits had the same initial mass of sedimentary organic, these are considerably high rates of remineralization compared to the rates of C-diagenesis in sediments that are conceptually thought of as being more reactive (Table 2). If these aquifer remineralization rates are correct, then the weathering in these aquifers is comparable to the weathering in soils and margin sediments (Baisden, 2002; Aller,

2006; Stahl, 2004). Furthermore, the weathering rates in the columns also supersede the weathering reported for fresh granite (White, 2003). Taking into account differences in flow and surface area, the final Na weathering rates from our columns are 0.0025 - 0.05 mol m^{-2} hr^{-1}, while the fresh Panola granite ranges from $5x10^{-5}$ – 0.0004 mol m^{-2} hr^{-1}. Because of the faster flow-through used in the granite experiments (10-15mL/hr vs. 0.08mL/hr), the Panola granite weathering should favor less retention and higher release rates (Gao, 2010). Therefore, the difference in flow-rate should favor higher weathering from the granite, meaning that the aquifer sediments are more "reactive" than fresh granite. This is probably because due to the higher supply of aquifer materials' sedimentary organics. Overall, these aquifers have sufficient organics to mobilize and weather arsenic, which is supported by the much smaller magnitude of organics needed to explain groundwater arsenic in a site along the Red River: 10^{-5} mol C m^{-2} yr^{-1}, (Postma, 2007).

A final important finding is that no one relationship or pattern appears for the different transects. The sedimentology of each transect is entirely different (Figures 2 and 3), despite displaying a similar heterogeneous arsenic trend when tube-well concentrations are plotted in map-view along the surface (Figure 1). Since it is important to know how findings can or should be extrapolated to other field sites, the column and transect results can be used to infer regional similarities and differences. One significant similarity between the different transects is the conformity of aquifer geochemistry to aquifer sedimentology. This highlights the utility of ascertaining the local deposits comprising an aquifer system. Another similarity is the overarching natural reductive process governing weathering and arsenic release in these systems. Correlations using a compilation of data from all of the transects show statistically significant relationships between %LOI, iron-ratios, leachable, and dissolved arsenic (Table 7a). Better correlations between the proxies come from combining the data, which may indicate the need for combining and adding more datasets for understanding regional/crustal-scaled processing of arsenic.

5. Conclusion

Our work in previous arsenic-prone sites in Asia shows a relationship between aquifer depositional age and groundwater arsenic. In trying to understand how aquifer sediment ages can account for some of the heterogeneous distributions of arsenic in Asia, a series of field and lab geochemical experiments were combined to help infer how sediment age impacts arsenic. A volumetric comparison of organic content in the facies comprising the aquifers show that there is just as much sedimentary organic stored in the sand and fine mud facies. C:N analysis on the Araihazar sediments shows that there is no C:N difference between facies, and more of an overall diagenetic terrestrial $\rightarrow$ microbial $\rightarrow$ denitrification processing with depth in the aquifer. Combined with the results of flow-through column experiments using several sand facies, the release of arsenic into Araihazar and Parasi's groundwater is a product of natural weathering, fueled by natural organics associated with the sediments. The column experiments indicate that aquifer sands—the facies with the highest amounts of combustible organics—released the highest amounts of arsenic, regardless of the depositional age of the aquifer.

References

Ahmed, K. M., Prosun Bhattacharya, M. Aziz Hasan, S. Humayun Akhter, S.M. Mahbub Alam, M.A. Hossain Bhuyian, M. Badrul Imam, Aftab A. Khan, and Ondra Sracek (2004). "Arsenic enrichment in groundwater of the alluvial aquifers in Bangladesh: an overview." Applied Geochemistry **19**: 181-200.

Aksoy, N., C. Simsek, et al. (2009). "Groundwater contamination mechanism in a geothermal field: A case study of Balcova, Turkey." Journal of Contaminant Hydrology **103**(1-2): 13-28.

Aller, R. C. and N. E. Blair (2006). "Carbon remineralization in the Amazon-Guianas tropical mobile mudbelt: A sedimentary incinerator." Continental Shelf Research **26**(17-18): 2241-2259.

Baisden, W. T., R. Amundson, et al. (2002). "Turnover and storage of C and N in five density fractions from California annual grassland surface soils." Global Biogeochemical Cycles **16**(4): 1117, doi:10.1029/2001GB001822.

Berg, M., Caroline Stegel, Pham Thi Kim Trang, Phan Hung Viet, Mickey L. Sampson, Moniphea Leng, Sopheap Samreth, and David Fredericks (2008). "Magnitude of arsenic pollution in the Mekong and Red River Deltas--Cambodia and Vietnam." Science of the Total Environment **in press**.

BGS-DPHE, Ed. (2001). Arsenic contamination of groundwater in Bangladesh. British Geological Survey Technical report, WC/00/19, Keyworth.

Bridge, J. S. (2003). Rivers and floodplains: forms, processes, and sedimentary record. Oxford, UK, Wiley-Blackwell.

Casey, W. H., J. F. Banfield, et al. (1993). "What Do Dissolution Experiments Tell Us About Natural Weathering." Chemical Geology **105**(1-3): 1-15.

Cheng, Z., A. van Geen, A.A. Seddique., and K.M. Ahmed (2005). "Limited temporal variability of arsenic concentrations in 20 wells monitored for 3 years in Araihazar, Bangladesh " ENVIRONMENTAL SCIENCE & TECHNOLOGY **39**(13): 4759-4766.

Cheng, Z., Y. Zheng, R. Mortlock, and A. van Geen (2004). "Rapid multi-element analysis of groundwater by high-resolution inductively coupled plasma mass spectrometry." Analytical and Bioanalytical Chemistry **379**(3): 512-518.

Coleman, J. M. (1969). "Brahmaputra river: Channel processes and sedimentation." Sedimentary Geology **3**(2-3): 129-239.

de Marsily, G., F. Delay, et al. (1998). "Some current methods to represent the heterogeneity of natural media in hydrogeology." Hydrogeology Journal **6**(1): 115-130.

Dill, H. G., D. R. Khadka, et al. (2003). "Infilling of the Younger Kathmandu-Banepa intermontane lake basin during the Late Quaternary (Lesser Himalaya, Nepal): a sedimentological study." Journal of Quaternary Science **18**(1): 41-60.

Dixit, A., M. Upadhya, et al. (2007). Flood Disaster Impact and Responses in Nepal Tarai's Marginalised Basins. Working with Winds of Change. Towards Strategies for Responding to the Risk Associated with Climate Change and other Hazards. M. Moench and A. Dixit. Kathmandu, Institute for Social and Environmental Transition**:** 119-157.

Dowling, C. B., R.J. Poreda, A.R. Basu, and S.L. Peters (2002). "Geochemical study of arsenic release mechanisms in the Bengal Basin groundwater." Water Resources Research **38**(9): 1173.

Dwivedi, G. N., S. K. Sharma, et al. (1997). "Quaternary geology and geomorphology of a part of Ghaghara-Rapti-Gandak sub-basins of Indogangetic Plain, Uttar Pradesh." Journal Geological Society of India **49**: 193-202.

Ehrlich, H. L. and D. K. Newman (2009). Geomicrobiology. Boca Raton, FL, CRC Press.

Fenchel, T., G. M. King, et al. (1988). Bacterial Biogeochemistry, The Ecophysiology of Mineral Cycling. San Diego, Academic Press.

Fendorf, S. and B. D. Kocar (2009). "Biogeochemical processes controlling the fate and transport of arsenic: implications for South and Southeast Asia." Advances in Agronomy **104**: 137-164.

Fergusson, J. (1863). "On recent changes in the delta of the Ganges." Quarterly Journal of the Geological Society of London **19**: 321-354.

Gao, H., C. Q. Qiu, et al. (2010). "Three-dimensional microscale flow simulation and colloid transport modeling in saturated soil porous media." Computers & Mathematics with Applications **59**(7): 2271-2289.

Goodbred, S. L., and S.A. Kuehl (2000). "The significance of large sediment supply, active tectonism, and eustasy on margin sequence development: Late Quaternary stratigraphy and evolution of the Ganges-Brahmaputra delta." Sedimentary Geology **133**: 227-248.

Goodbred, S. L. and S. A. Kuel (1998). "Floodplain processes in the Bengal Basin and the storage of Ganges-Brahmaputra river sediment: an accretion study using ^{137}Cs and ^{210}Pb geochronology." Sedimentary Geology **121**: 239-258.

Goodbred, S. L., Steven A. Kuehl, Michael S. Steckler, and Maminul H. Sarker (2003). "Controls on facies distribution and stratigraphic preservation in the Ganges-Brahmaputra delta sequence." Sedimentary Geology **155**(3-4): 301-316.

GSA (1999). Pocket-Size Sand Grain Sizing Folder. GRN001, Geological Society of America.

Guillot, S., and L. Charlet (2007). "Bengal arsenic, an archive of Himalaya orogeny and paleohydrology." Journal of Environmental Science and Health Part A **42**: 1785-1794.

Gupta, S. (1997). "Himalayan drainage patterns and the origin of fluvial megafans in the Ganges foreland basin." Geology **25**(1): 11-14.

Gurung, J. K., H. Ishiga, and M.S. Khadka (2005). "Geological and geochemical examination of arsenic contamination in groundwater in the Holocene Terai Basin, Nepal." Environmental Geology **49**: 98-113.

Hartog, N., J. Griffioen, et al. (2005). "Depositional and paleohydrogeological controls on the distribution of organic matter and other reactive reductants in aquifer sediments." Chemical Geology **216**(1-2): 113-131.

Hartog, N., J. Griffioen, et al. (2002). "Distribution and reactivity of O-2-reducing components in sediments from a layered aquifer." Environmental Science & Technology **36**(11): 2338-2344.

Harvey, C. F., C.H. Swartz, A.B.M. Badruzzaman, N. Keon-Blute, W. Yu, M.A. Ali, J. Jay, R. Beckie, V. Niedan, D. Brabander, P.M. Oates, K.N. Ashfaque, S. Islam, H.F. Hemond, M.F. Ahmed (2005). "Groundwater arsenic contamination on the Ganges Delta: biogeochemistry, hydrology, human perturbations, and human suffering on a large scale " Comptes Rendus Geoscience **337**(1-2): 285-296

Harvey, C. F., Christopher H. Swartz, A.B.M. Badruzzaman, Nicole Keon-Blute, Winston Yu, A. Ashraf Ali, Jenny Jay, Roger Beckie, Volker Niedan, Daniel Brabander, Peter M. Oates, Khandaker N. Ashfaque,

Shariqul Islam, Harold F. Hemond, and M. Feroze Ahmed (2002). "Arsenic mobility and groundwater extraction in Bangladesh." Science **298**: 1602-1606.

Hodgkinson, J., M.E. Cox, S. McLoughlin, and G.J. Huftile (2008). "Lithological heterogeneity in a back-barrier sand island: Implications for modeling hydrogeological frameworks." Sedimentary Geology **203**: 64-86.

Hoque, M. A., A. A. Khan, et al. (2009). "Near surface lithology and spatial variation of arsenic in the shallow groundwater: southeastern Bangladesh." Environmental Geology **56**(8): 1687-1695.

Hori, K., S. Tanabe, et al. (2004). "Delta initiation and Holocene sea-level change: example from the Song Hong (Red River) delta, Vietnam." Sedimentary Geology **164**: 237-249.

Horneman, A., A. van Geen, D. Kent, P.E. Mathe, Y. Zheng, R.K. Dhar, S. O'Connell, M.Hoque, Z. Aziz, M. Shamsudduha, A. Seddique, and K.M. Ahmed (2004). "Decoupling of arsenic and iron release to Bangladesh groundwater under reducing conditions. Part I: Evidence from sediment profiles." Geochim. Cosmochim. Acta. **68**(17): 3459-3473.

Howlader, M. A. R., A. R. M. Solaiman, et al. (2004). "Biodynamics of microbial biomass nitrogen in organic matter amended lowland paddy soil of Bangladesh." Bulletin of the Institute of Tropical Agriculture Kyushu University **27**: 11-17.

Hu, J., D. Li, et al. (2009). "Effect of organic carbon on nitrification efficiency and community composition of nitrifying biofilms." Journal of Environmental Sciences **21**(3): 387-394.

Jain, V. and R. Sinha (2003). "Hyperavulsive-anabranching Baghmati river system, north Bihar plains, eastern India." Z. Geomorph. N.F. **47**(1): 101-116.

Jung, H. B., M. Charette, and Y. Zheng (2008). A Field, Laboratory and Modeling Study on Reactive Transport of Arsenic in a Coastal Aquifer. GSA 2008 Joint Annual Meeting, George R. Brown Convention Center, Houston TX, Geological Society of America.

Keon, N. E., C.H. Swartz, D.J. Brabander, C. Harvey, and H.F. Hemond (2001). "Validation of an arsenic sequential extraction method for evaluating mobility in sediments." Environmental Science and Technology **35**: 2778-2784.

Kilops, S. and V. J. Kilops (2005). Introduction to Organic Geochemistry, Wiley-Blackwell.

Kocar, B. D., M. L. Polizzotto, et al. (2008). "Integrated biogeochemical and hydrologic processes driving arsenic release from shallow sediments to groundwaters of the Mekong delta." Applied Geochemistry **23**(11): 3059-3071.

Konen, M. E., P. M. Jacobs, et al. (2002). "Equations for Predicting Soil Organic Carbon Using Loss-on-Ignition for North Central U.S. Soils." Soil Sci Soc Am J **66**(6): 1878-1881.

Larsen, F., N. Q. Pham, et al. (2008). "Controlling geological and hydrogeological processes in an arsenic contaminated aquifer on the Red River flood plain, Vietnam." Applied Geochemistry **23**: 3099-3115.

Lawrence, A. R., D.C. Gooddy, P. Kanatharana, W. Meesilp, and V. Ramnarong (2000). "Groundwater evolution beneath Hat Yai, a rapidly developing city in Thailand." Hydrogeology Journal **8**: 564-575.

Liu, Z. F., G. Stewart, et al. (2005). "Why do POC concentrations measured using Niskin bottle collections sometimes differ from those using in-situ pumps?" Deep-Sea Research Part I-Oceanographic Research Papers **52**(7): 1324-1344.

Maharjan, M., R.R. Shrestha, Sk.A. Ahmad, C. Watanabe, and R. Ohtsuka (2006). "Prevalence of Arsenicosis in *Terai*, Nepal." Journal of Health, Population, and Nutrition **24**(2): 246-252.

Maher, K., C. I. Steefel, et al. (2006). "The mineral dissolution rate conundrum: Insights from reactive transport modeling of U isotopes and pore fluid chemistry in marine sediments." Geochimica Et Cosmochimica Acta **70**(2): 337-363.

McArthur, J. M., D.M. Banerjee, K.A. Hudson-Edwards, R. Mishra, R. Purohit, P. Ravenscroft, A. Cronin, R.J. Howarth, A. Chatterjee, T. Talukder, D. Lowry, S. Houghton, D.K. Chadha (2004). "Natural organic matter in sedimentary basins and its relation to arsenic in anoxic ground water: the example of West Bengal and its worldwide implications." Applied Geochemistry **19**: 1255-1293.

McArthur, J. M., P. Ravenscroft, D.M. Banerjee, J. Milsom, K.A. Hudson-Edwards, S. Sengupta, C. Bristow, A. Sarkar, S. Tonkin, and R. Purohit (2008). "How paleosols influence groundwater flow and arsenic pollution: A model from the Bengal Basin and its worldwide implication." Water Resources Research **44**(11): W11411.

Meharg, A. A., C. Scrimgeour, S.A. Hossin, K. Fuller, K. Cruickshank, P.N. Williams, and D.G. Kinniburgh (2006). "Codeposition of organic carbon and arsenic in Bengal Delta Aquifers." Environ. Sci. Technol. **40**: 4928-4935.

Mohindra, R. and B. Parkash (1994). "Geomorphology and Neotectonic Activity of the Gandak Mega-Fan and Adjoining Areas, Middle Gangetic Plains." Journal of the Geological Society of India **43**(2): 149-157.

Mohindra, R., B. Parkash, et al. (1992). "Historical Geomorphology and Pedology of the Gandak Megafan, Middle Gangetic Plains, India." Earth Surface Processes and Landforms **17**(7): 643-662.

Nagar, Y. C. (2007). Methodological aspects of radiation dosimetry of natural radiation environment using luminescence techniques: New minerals and applications. Physical Research Laboratory. Ahmedabad, India, Gujurat University. **Ph.D. Thesis:** 162.

NASC/ENPHO (2004). The State of Arsenic in Nepal - 2003. B. R. Shrestha, J.W. Whitney, and K.B. Shrestha, (Editors), USGS**:** 100 pages.

Neumann, R. B., K. N. Ashfaque, et al. (2010). "Anthropogenic influences on groundwater arsenic concentrations in Bangladesh." Nature Geosci **3**(1): 46-52.

Nickson, R. T., J.M. McArthur, P. Ravenscroft, W.G. Burgess and K.M. Ahmed (2000). "Mechanism of arsenic release to groundwater, Bangladesh and West Bengal." Applied Geochemistry **15**: 403-413.

Panthi, S. R. and D. G. Wareham (2008). "The affect of arsenite on denitrification using volatile fatty acids as a carbon source." Journal of Environmental Science and Health Part A **43**(10): 1192-1197.

Papacostas, N. C., B. C. Bostick, et al. (2008). "Geomorphic controls on groundwater arsenic distribution in the Mekong River Delta, Cambodia." Geology **36**(11): 891-894.

Polizzotto, M. L., C.F. Harvey, S.R. Sutton, and S. Fendorf (2005). "Processes conducive to the release and transport of arsenic into aquifers of Bangladesh." PNAS **102**(52).

Polizzotto, M. L., B. D. Kocar, et al. (2008). "Near-surface wetland sediments as a source of arsenic release to ground water in Asia." Nature **454**(7203): 505-U5.

Postma, D., F. Larsen, et al. (2007). "Arsenic in groundwater of the Red River floodplain, Vietnam: Controlling geochemical processes and reactive transport modeling." Geochimica Et Cosmochimica Acta **71**(21): 5054-5071.

Prasad, S. and E. A. Khan (2005). "Gandak fan - A macro quaternary feature of middle Ganga plain, Uttar Pradesh and Bihar." Journal of the Geological Society of India **65**(5): 597-608.

Prescott, J. R., and J.T. Hutton (1988). "Cosmic ray and gamma ray dosimetry for TL and ESR." Nuclear Tracks and Radiation Measurements **14**: 223-227.

Prescott, J. R., and J.T. Hutton (1994). "Cosmic ray contributions to dose rates for luminescence and ESR dating: large depths and long-term variations." Radiation Measurements **23**(2/3): 497-500.

Rao, M. S., B. K. Bisaria, et al. (1997). "A feasibility study towards absolute dating of Indo-Gangetic alluvium using thermoluminescence and infrared-stimulated luminescence techniques." Current Science **72**(9): 663-669.

Ravenscroft, P., W. G. Burgess, et al. (2004). "Arsenic in groundwater of the Bengal Basin, Bangladesh: Distribution, field relations, and hydrogeological setting." Hydrogeology Journal **13**: 727-751.

Robinson, D. M., P. G. DeCelles, et al. (2001). "The kinematic evolution of the Nepalese Himalaya interpreted from Nd isotopes." Earth and Planetary Science Letters **192**: 507-521.

Sakai, H., H. Sakai, et al. (2006). "Pleistocene rapid uplift of the Himalayan frontal ranges recorded in the Kathmandu and Siwalik basins." Palaeogeography, Palaeoclimatology, Palaeoecology **241**: 16-27.

Santisteban, J. I., R. Mediavilla, et al. (2004). "Loss on ignition: a qualitative or quantitative method for organic matter and carbonate mineral content in sediments?" Journal of Paleolimnology **32**(3): 287-299.

Saunders, J. A., M.K. Lee, A. Uddin, S. Mohammad, Richard T. Wilkin, Mostafa Fayek, and Nic E. Korte (2005). "Natural arsenic contamination of Holocene alluvial aquifers by linked tectonic, weathering, and microbial processes." Geochemistry Geophysics Geosystems **6**(4): 1-7.

Schroeder, P. A., N. D. Melear, et al. (2000). "Meta-gabbro weathering in the Georgia Piedmont, USA: implications for global silicate weathering rates." Chemical Geology **163**(1-4): 235-245.

Sengputa, S., J.M. Mcarthur, A. Sarkar, M.J. Leng, P. Ravenscroft, R.J. Howarth, and D.M. Banerjee (2008). "Do ponds cause arsenic-pollution of groundwater in the Bengal Basin? An answer from West Bengal." Environ. Sci. Technol. **42**: 5156-5164.

Shannon, W. M. a. S. A. W. (2005). "The analysis of picogram quantities of rare earth elements in natural waters." In Rare Earth Elements in Groundwater Flow Systems, K.H. Johannesson, ed: 1-37.

Sharp Jr., J. M., Mingjuan Shi, and William E. Galloway (2003). "Heterogeneity of fluvial systems--control on density-driven flow and transport." Environmental Engineering and Geoscience **IX**(1): 5-17.

Shrestha, S. D., T. Brikowski, et al. (2004). "Grain size contraints on arsenic concentration in shallow wells of Nawalparasi, Nepal." Journal of Nepal Geological Society **30**: 93-98.

Silbergeld, E. K. and K. Nachman (2008). "The Environmental and Public Health Risks Associated with Arsenical Use in Animal Feeds." Environmental Challenges in the Pacific Basin **1140**: 346-357.

Sinha, R. (1995). "Sedimentology of Quaternary Alluvial Deposits of the Gandak-Kosi Interfan, North Bihar Plains." Journal of the Geological Society of India **46**(5): 521-532.

Smedley, P. L. and D. G. Kinniburgh (2002). "A review of the source, behavior and distribution of arsenic in natural waters." Applied Geochemistry **17**: 517-568.

Solaiman, A. R. M., A. A. Meharg, et al. (2009). "Arsenic mobilization from iron oxyhydroxides is regulated by organic matter carbon to nitrogen (C:N) ratio." Environment International **35**(3): 480-484.

Stahl, H., A. Tengberg, et al. (2004). "Factors influencing organic carbon recycling and burial in Skagerrak sediments." Journal of Marine Research **62**(6): 867-907.

Stanger, G. (2005). "A palaeo-hydrogeological model for arsenic contamination in southern and south-east Asia." Environmental Geochemistry and Health **27**: 359-367.

Steckler, M. S., S. H. Akhter, et al. (2008). "Collision of the Ganges-Brahmaputra Delta with the Burma Arc: Implications for earthquake hazard." Earth and Planetary Science Letters **273**(3-4): 367-378.

Stevenson, F. J. (1994). Humus chemistry: genesis, composition, reactions. New York, John Wiley and Sons.

Stute, M., Y. Zheng, P. Schlosser, A. Horneman, R.K. Dhar, M. A. Hoque, A. A. Seddique, M. Shamsudduha, K. M. Ahmed, and A. van Geen (2007). "Hydrological control of As concentrations in Bangladesh groundwater." Water Resources Research **43**: W09417.

Sullivan, K. A. a. R. C. A. (1996). "Diagenetic cycling of arsenic in Amazon shelf sediments." Geochem. Cosmochim. Acta **60**: 1465-1477.

Tandon, S. K., R. Sinha, et al. (2008). "Late Quaternary evolution of the Ganga Plains: Myths and misconceptions, recent developments and future directions." Golden Jubilee Memoir of the Geological Society of India **66**: 259-299.

Tyson, R. V. (1995). Sedimentary Organic Matter. London, Chapman & Hall.

Ullman, W. J., B. Chang, et al. (2003). "Groundwater mixing, nutrient diagenesis, and discharges across a sandy beachface, Cape Henlopen, Delaware (USA)." Estuarine Coastal and Shelf Science **57**(3): 539-552.

van Geen, A., H. Ahsan, et al. (2002). "Promotion of well-switching to mitigate the current arsenic crisis in Bangladesh." Bulletin of the World Health Organization **80**(9): 732-737.

van Geen, A. and S. Fendorf (2009). AGU Chapman Conference on Arsenic in Groundwater of Southern Asia, Siem Reap, Cambodia, American Geophysical Union.

van Geen, A., K. Radloff, Z. Aziz, Z. Cheng, M.R. Huq, K.M. Ahmed, B. Weinman, S. Goodbred, M. Berg, P.T.K. Trang, L Charlet, J. Metral, D. Tisserand, S. Guillot, S. Chakraborty, A.P. Gajurel, and B.N. Upreti (2008). "Comparison of arsenic concentrations in simultaneously-collected groundwater and aquifer particles from Bangladesh, India, Vietnam, and Nepal." Applied Geochemistry **23**: 3244-3251.

van Geen, A., T. Protus, Z. Cheng, A. Horneman, A.A. Seddique, M.A. Hoque, and .M. Ahmed (2004). "Testing groundwater for arsenic in Bangladesh before installing a well." Environmental Science & Technology **38**(24): 6783-6789.

van Geen, A., Y. Zheng, R. Versteeg, M. Stute, A. Horneman, R. Dhar, M. Steckler, A. Gelman, C. Small, H. Ahsan, J. H. Graziano, I. Hussain, and K. M. Ahmed (2003). "Spatial variability of arsenic in 6000 tube wells in a 25 km^2 area of Bangladesh." Water Resources Research **39**(5): 1140.

van Geen, A., Y. Zheng, S. Goodbred, A. Horneman, Z. Aziz, Z. Cheng, M. Stute, B. Mailloux, B. Weinman, S.H. Chowdhury, and K. M. Ahmed (2008). "Flushing history as a hydrogeological control on the regional distribution of arsenic in shallow groundwater of the Bengal Basin." Environ. Sci. Technol. **42**(7): 2283-2288.

van Geen, A., Y. Zheng, et al. (2006). "A transect of groundwater and sediment properties in Araihazar, Bangladesh: Further evidence of decoupling between As and Fe mobilization." Chemical Geology **228**(1-3): 85-96.

Velbel, M. A. (1989). "Weathering of hornblende to ferruginous products by a dissolution-precipitation mechanism: Petrography and stoichiometry." Clays and Clay Minerals **37**(6): 515-524.

Washton, N. M., S. L. Brantley, et al. (2008). "Probing the molecular-level control of aluminosilicate dissolution: A sensitive solid-state NMR proxy for reactive surface area." Geochimica Et Cosmochimica Acta **72**(24): 5949-5961.

Weinman, B. (2005). Controls of Floodplain Sediments and Evolution on Shallow Aquifer Development and the Distribution of Groundwater Arsenic: Araihazar, Bangladesh. Marine and Atmospheric Sciences. Stony Brook, Stony Brook University. **M.S. Thesis:** 73.

Weinman, B. (2005). Modeling arsenic heterogeneity in recent Holocene alluvium: simplifying the complex behavior of arsenic in the Ganges-Brahmaputra Delta., Vanderbilt University**:** *unpublished report for D. Furbish's Transport, 10* pages.

Weinman, B., S.L. Goodbred, Y. Zheng, A. van Geen, Z. Aziz, A. Singhvi, and M. Steckler (2008). "Controls of Floodplain Evolution on Shallow Aquifer Development and the Resulting Distribution of Groundwater Arsenic: Araihazar, Bangladesh." GSA Bulletin **120**(11/12): 1567-1580.

Wellons, M. S., W. H. Morris, et al. (2007). "Direct Synthesis and Size Selection of Ferromagnetic FePt Nanoparticles." Chemistry of Materials **19**(10): 2483-2488.

White, A. F., and S.L. Brantley (2003). "The effect of time on the weathering of silicate minerals: why do weathering rates differ in the laboratory and the field?" Chemical Geology **202**: 479-506.

Yonebayashi, C. and M. Mutsuhiko (1997). "Late Quaternary vegetation and climatic history of eastern Nepal." Journal of Biogeography **24**: 837-843.

Zhang, J. F. and L. P. Zhou (2007). "Optimization of the 'double SAR' procedure for polymineral fine grains." Radiation Measurements **42**: 1475-1482.

Zheng, Y., A. van Geen, M. Stute, R. Dhar, Z. Mo, Z. Cheng, A. Horneman, I. Gavrieli, H.J. Simpson, R. Versteeg, M. Steckler, A. Grazioli-Venier, S. Goodbred, M. Shahnewaz, M. Shamsudduha, M. Hoque and K. M. Ahmed (2005). "Geochemical and hydrogeological contrasts between shallow and deeper aquifers in two villages of Araihazar, Bangladesh: Implications for deeper aquifers as drinking water sources." Geochim. Cosmochim. Acta. **69**(22): 5203-5218.

Zheng, Y., M. Stute, A. van Geen, I. Gavrieli, R. Dhar, J.H. Simpson, P. Schlosser, and K.M. Ahmed (2004). "Redox control of arsenic mobilization in Bangladesh groundwater." Applied Geochemistry **19**(2): 201-214.

Table 1. Field Site Locations

Parasi, Nepal - 18,000-3,000 ya		
Site	Latitude (N)	Longitude (E)
PNS1	27.51512	83.67187
PNS2	27.51706	83.6749
PNS3	27.51594	83.66876
PNS4	27.51648	83.66119
PNS5	27.51528	83.66772

Araihazar, Bangladesh - 400 ya Abandoned Channel		
Site	Latitude (N)	Longitude (E)
NL1	23.77290	90.60564
NL2	23.77389	90.60437
NL3	23.77537	90.60341
NL4	23.77733	90.60196
NL5	23.77838	90.60354
NL6	23.78015	90.60272
NL7	23.78113	90.60293
NL8	23.78324	90.60503
Site	Latitude (N)	Longitude (E)
NL9	23.77819	90.63885
NL10	23.78252	90.63894
NL11	23.78454	90.63894
NL12	23.78832	90.63756
NL13	23.79177	90.63407
NL14	23.79395	90.63196
NL15	23.79618	90.63093

Table 1. Locations of ~1km needle-samping transects between villages with different groundwater arsenic concentrations in Parasi,

Table 2. A comparison of carbon processing rates in different sedimentary environments

C Rate	Process	Environment	Source
0.01 mol C/m^2/yr	Remineralization	California grassland soils	[1]Baidsen, 2002
0.03 mol C/m^2/yr	Remineralization	California grassland soils	[2]Baidsen, 2002
10^{-5} yr^{-1} C_{org}	Remineralization	California grassland soils	[3]Baidsen, 2003
0.03 - 0.99 mol C/m^2/yr	Remineralization	Outer Terai alluvium, Parasi	This study
10^{-5} yr^{-1} C_{org}	Remineralization	Outer Terai alluvium, Parasi	[3]This study
0.8-6.6 mol C/m^2/yr	Remineralization	Skagerrak margin sediments	Stahl, 2004
0.2-6.8 mol C/m^2/yr	Remineralization	Araihazar distal floodplain	This study
10^{-4} yr^{-1} C_{org}	Remineralization	Araihazar distal floodplain	[3]This study
4.4-5.5 mol C/m^2/yr	Remineralization	Amazon mud belt	[4]Aller, 2007
0.2-0.6 yr^{-1} C_{org}	Remineralization	Amazon mud belt	[3]Aller, 2006
6x10^{-5}mol C/m^2/yr	Remineralization	Red River meander sediment	[5]Postma, 2007
4-17 mol C/m/yr	Fixation	Delaware beachface	Ullman, 2003

[1]Rate caculated from an exponential fit of soil age vs. kg/m^2 C_{org} (R^2= 0.91)

[2]Rate caculated from a linear fit of Baisden's Figure 2 data, soil age vs. kg/m^2 C_{org} (R^2= 0.96)

[3]Conditional rate constant

[4]Rate converted from 12-15 mmol ΣCO_2/m^2/day - exceeds mineralization in organic rich estuaries

[5]Rate converted assuming ~0.4 porosity, for 1 meter of sediment

Table 3. Column Sediment Age, Porosity, and Grainsize Information

Sample	Depth (m)	Age	Column sediment (wet) g	%LOI	%$CaCO_3$	Sediment Type	**Sediment Volume cm^3	Liquid/ Solid ratio (mL/g)	Pore Volume	Porosity	Avg Specific Surface Area (m^2/g)	Avg % Clay	Avg Mean Grainsize (μm)
PNS5-45	14	21kyr (OSL)	48.3658	0.78	4.37	silty sand	18.25	0.27	13.16	0.42	0.43	6.7	113
PNS5-25	8	5kyr (OSL)	46.2198	0.26	0.39	sand	17.44	0.30	13.97	0.44	0.24	3.5	219
PNS1-44	13	12kyr (OSL)	42.0243	0.21	1.70	sand	15.86	0.37	15.56	0.50	0.10	1.4	288
NS18-4-45	14	Relative Young	42.1059	0.20	-*	coarse sand	15.89	0.37	15.53	0.49	0.04	0.4	568
NS18-9-95	29	Relative Old	45.0837	0.20	-*	coarse sand	17.01	0.32	14.40	0.46	0.04	0.3	483

*Not measured

□□□$_{qtz}$=2.65g/cm^3

Table 4. Summary of Araihazar and Parasi Stratigraphic Data

	Bangladesh		*Nepal*
	F to A	BNNW	Parasi
Maximum Mud Depth (m)	11	6	12
Minimum Mud Depth	0	0	3
Mean Mud Depth	6	3	7
n	18	28	17
Variance (m^2)	12	1	10
Std. dev. (m)	3	1	3
[1]Transect Mud Cap (m^2)	2516	1890	2759
Aquifer Sands (m^2)	5627	7835	12834
[2]Aquifer Muds (m^2)	-	-	3946
[3]Transect Mud Cap (%)	31	19	14
Aquifer Sands (%)	69	81	66
Aquifer Muds (%)	-	-	20
%LOI in Mud Cap	1.7 - 2.6	0.4 - 2.4	0.3 - 4
%LOI in Aquifer Sands	0.2 - 2.3	0.3 - 1.1	0.2 - 16
%LOI in Aquifer Muds	-	-	0.4 - 9
[4]Mud Cap %LOI μ,σ, and n	2.2, 0.5, 3	1.4, 0.8, 8	2, 1, 25
Aquifer Sands %LOI μ,σ, and n	0.6, 0.6, 20	0.5, 0.2, 28	1, 3, 27
Aquifer Muds %LOI μ,σ, and n	-	-	2, 2, 30

[1]Mud cap is the profile areal thickness of Figure 2's 4-phi contour surface

[1]Buried, hydrological confining units

[3]Percentages are based on the upper ~20m of aquifer deposits

[4]μ is mean, σ is standard deviation, and n is the number of samples

Sample	%LOI	N (%)	C (%)	C:N	Elevation	Depth (m)	Elev-Depth (m)
NL-1-1-10	0.53	0.006	0.080	16	8	2.0	6
NL-1-2-15		0.009	0.061	8	8	3.1	5
NL-1-3-20	0.34	0.004	0.039	10	8	4.1	4
NL-1-4-30		0.003	0.042	16	8	6.1	2
NL-1-5-40		0.006	0.065	12	8	8.2	0
NL-1-6-50		0.001	0.038	42	8	10.2	-2
NL-2-1-10	0.67	0.011	0.134	14	10	2.0	8
NL-2-2-13		0.007	0.047	8	10	2.7	7
NL-2-3-20		0.004	0.050	13	10	4.1	6
NL-2-4-30	0.43	0.002	0.040	22	10	6.1	4
NL-2-5-40		0.006	0.048	9	10	8.2	2
NL-2-6-50	0.27	0.002	0.037	18	10	10.2	0
NL-3-1-10	2.59	0.044	0.395	11	7	2.0	5
NL-3-2-20		0.038	0.420	13	7	4.1	3
NL-3-3-30	2.34	0.050	0.612	14	7	6.1	1
NL-3-4-40		0.006	0.057	11	7	8.2	-1
NL-3-5-50	0.24	0.001	0.032	45	7	10.2	-3
NL-4-1-10	1.67	0.017	0.306	22	11	2.0	9
NL-4-2-20		0.038	0.406	13	11	4.1	7
NL-4-3-30	0.53	0.011	0.067	7	11	6.1	5
NL-4-4-40		0.005	0.039	9	11	8.2	3
NL-4-5-50	0.24	0.001	0.032	32	11	10.2	1
NL-9-1-10	1.99	0.000	0.000	18	8	2.0	6
NL-9-2-25		0.007	0.061	10	8	5.1	3
NL-9-3-30	0.37	0.006	0.032	6	8	6.1	2
NL-9-4-40		0.002	0.048	23	8	8.2	0
NL-9-5-50	0.37	0.000	0.032	188	8	10.2	-2
NL-10-1-10	0.63	0.003	0.053	18	9	2.0	7
NL-10-2-20		0.003	0.034	13	9	4.1	5
NL-10-3-30	0.46	0.001	0.041	33	9	6.1	3
NL-10-4-40		0.002	0.037	26	9	8.2	1
NL-10-5-50	0.30	0.003	0.035	12	9	10.2	-1
NL-11-1-10	1.61	0.026	0.292	13	10	2.0	8
NL-11-2-20		0.006	0.096	20	10	4.1	6
NL-11-3-30	0.44	0.003	0.057	25	10	6.1	4
NL-11-4-40		0.001	0.005	8	10	8.2	2
NL-11-5-50	0.51	0.006	0.111	23	10	10.2	0
NL-12-1-10	1.87	0.023	0.324	17	8	2.0	6
NL-12-2-15		0.007	0.050	8	8	3.1	5
NL-12-3-30	0.50	0.007	0.043	7	8	6.1	2
NL-12-5-40		0.003	0.039	17	8	8.2	0
NL-12-6-50	0.39	0.007	0.042	7	8	10.2	-2
NL-13-1-10	2.41	0.026	0.387	17	15	2.0	13

Table 5. Results of LOI and CHN analysis on a selection of Araihazar needle-samples from the 400 and the 1000 year-old aquifer transects. C/N is the percent ratio multiplied by 14.01/12.01 for the end results being reported as molar C/N ratios, but due to the small difference in molar mass, the weight and molar ratios do not differ that greatly. The average C/N for all the samples is 20 ± 28, and 16 ± 9 with NL-9-50's omission. The elevations are from digital terraine elevation data provided by USGS.

Table 6. Arsenic and Sediment Redox Concentration Ranges

F to A					
	Min	*Max*	*Avg*	*Std-Dev*	*n*
%LOI	0.2	2.6	0.8	0.8	22
FeII/Fe-total	0.1	1.0	0.6	0.2	41
dR	0.1	0.8	0.3	0.1	41
PO_4ext-As (mg/kg)	0.2	33	3	5	40
As (μg/L)	12	332	124	84	23
C:N	7	45	16	10	23
BNNW					
%LOI	0.3	2.4	0.7	0.5	36
FeII/Fe-total	0.2	0.9	0.6	0.2	36
dR	0.1	0.5	0.2	0.1	36
PO_4ext-As (mg/kg)	0.2	18	3	4	34
As (μg/L)	3	479	168	134	20
C:N	6	188	24	38	21
Parasi					
%LOI	0.2	15.6	1.6	2.1	78
FeII/Fe-total	0.5	0.9	0.8	0.1	17
dR	0.0	2	0.6	0.4	81
PO_4ext-As (mg/kg)	0.2	1	0.5	0.2	17
As (μg/L)[1]	0	25	11	8	14

[1]Hach kit determination

Tables 7a-d. Correlations of As, organic, and redox-properties for Parasi and Araihazar sediment samples.
Emboldened values are coefficients with p-values <0.05.

7a. Correlation for F to A, BNNW, and Parasi needle-samples

	%LOI	*FeII/Fe-total*	*dR*	*Log PO_4 ext-As (mg/kg)*	*Log As (ug/L)*	*C/N*
%LOI	1					
FeII/Fe-total	***0.461***	1				
dR	-0.097	***-0.423***	1			
Log PO_4 ext-As (mg/kg)	-0.052	***-0.493***	0.056	1		
Log As (ug/L)	***-0.339***	-0.058	***-0.565***	***0.346***	1	
C/N	-0.118	-0.047	0.220	-0.105	0.12	1

7b. Correlation for F to A needle-samples, Laskardi north to Satyabandi, Araihazar (n= 43)

	%LOI	*FeII/Fe-total*	*dR*	*Log PO_4 ext-As (mg/kg)*	*Log As (ug/L)*	*C:N*
%LOI	1					
FeII/Fe-total	***0.595***	1				
dR	***-0.696***	***-0.866***	1			
Log PO_4 ext-As (mg/kg)	-0.360	***-0.495***	0.248	1		
Log As (ug/L)	-0.563	***0.491***	-0.393	-0.051	1	
C:N	-0.193	-0.024	0.249	-0.044	-0.065	1

7c. Correlation for BNNW needle-samples, northwest of Bay, Araihazar (n= 32)

	%LOI	*FeII/Fe-total*	*dR*	*Log PO_4 ext-As (mg/kg)*	*Log As (ug/L)*	*C:N*
%LOI	1					
FeII/Fe-total	***0.473***	1				
dR	***-0.383***	***-0.804***	1			
Log PO_4 ext-As (mg/kg)	0.114	-0.262	***0.476***	1		
Log As (ug/L)	0.017	***0.697***	***-0.521***	-0.214	1	
C:N	-0.120	-0.082	0.294	-0.099	0.199	1

7d. Correlation for Parasi cuttings and needle-samples, from Sunwach east to Unwach village (n= 81)

	%LOI	*FeII/Fe-total*	*dR*	*Log PO_4 ext-As (mg/kg)*	*Log As (ug/L)*
%LOI	1				
FeII/Fe-total	0.227	1			
dR	-0.212	***-0.671***	1		
Log PO_4 ext-As (mg/kg)	0.131	-0.321	***0.488***	1	
Log As (ug/L)	-0.470	-0.045	-0.165	0.523	1

CHAPTER IV

CONCLUSIONS AND FUTURE WORK

The three manuscripts that make up this thesis have two components that constitute important advances in understanding the 10-100m heterogeneous patterns of groundwater arsenic in Asian aquifers. In Parts 1 and 2 of Chapter II, I have shown how aquifer depositional age explains 1km differences in groundwater arsenic. Initially, upon entering these field sites, the possibility of different-aged aquifer material accounting for the arsenic differences was not considered. The prevailing view at the time I started this work was from a geochemical perspective, where differences in arsenic were thought to be explainable purely by geochemistry. The aquifers were envisioned to be more or less sedimentologically undifferentiated, other than identifying deposits as sands, silts, or clays.

The main contributions of this thesis is that it shows, for the first time, the importance of sedimentology in understanding Asia's arsenic. In investigating the evolution of several arsenic-prone villages in Nepal, Bangladesh, and Vietnam using traditional sedimentology and newer optical luminescence dating techniques, I show how aquifer geochemistry consistently conforms to aquifer sedimentology. This sedimentological perspective is an advance in that it defines an important interaction between the water and sediment. Furthermore, it also gives insight into how these aquifers develop—arsenic prone areas are underlain by Holocene deposits, while areas free of contamination are Pleistocene units.

To investigate why younger deposits tend to have higher concentrations of arsenic, Chapter 3 sought to see if the different-aged sediments weathered differently. Previous weathering work showed that older, more weathered granite weathers slower than freshly exposed granite, which could help explain the different concentrations of arsenic in our study areas. Surprisingly, however, the results of the column experiments showed the highest amount of arsenic weathered from the oldest-aged

sediment deposit. This leaves questions that will direct my future work, as it raises concerns about how vulnerable Pleistocene sediments are to ingrowing dissolved arsenic.

An additional avenue of research will be continuing to look into how sediments sourced from different provenance terrains may impact aquifer geochemistry. Zircon-dating two samples from Nepal showed that the aquifer was not comprised of sediments from the same source region. This is quite different than findings where researchers use rare-earth element patterns to infer a similar source for all the aquifer material. Exploratory work using changes in luminescence sensitivity and cathodoluminescence are mounting more and more evidence for a pre-depositional impact on the distribution of arsenic. With people being more and more of a geomorphic factor, and with more recoverable benefit available from preventative and sustainable development in these regions, understanding these aquifer systems is becoming increasingly important.

APPENDIX A

Summary of Arsenic Chemistry in Natural Groundwaters

Included here is a brief summary page, overviewing the general chemistry of arsenic in natural groundwaters. Information is taken from several sources which are good reference works compiling and describing the known characteristics of arsenic in the environment (Kumaresan and Riyazuddin 2001; Smedley and Kinniburgh 2002; EPA 2004). The works by Kumaresan and Smedley focus on the occurrence of natural arsenic, its speciation and where groundwater arsenic is a problem, while the EPA document is a compilation of known arsenic K_d values.

Arsenic concentrations in natural waters: <0.5 μg -L to >5000 μg L^{-1}

Valence states: -3, 0, +3 and +5

Natural aqueous species: usually as the inorganic oxyanions arsenite [As(III)] and/or arsenate [As(V)]

Other species are the natural organic forms produced by biologic activity, which are typically not quantitatively important. When they are significant, it is usually due to industrial pollution. These varieties include monomethylarsenic (MMA), dimethylarsenic (DMA), arsenobetain and arsenocholine (the last two are from seafood and are without known toxicities).

Toxicity: As(III)>As(V)>MMA>DMA

Speciation:
In reducing groundwaters: at pH <9.2, uncharged As(III) as $H_2AsO_3^-$ predominates.
In oxidizing groundwaters: $H_2AsO_4^-$ is dominant at pH <6.9, while at higher pH, $HAsO_4^{-2}$ dominates.

Sorption studies of arsenic Kd values:
1.9-18 ml/g for As(V) in agricultural soils and clays, pH 4.5-9.0
1-10 ml/g for arsenic in the DOE's Savannah River Plant soils

References

EPA (2004). Review of Geochemistry and Available Kd Values for Americium, Arsenic, Curium, Iodine, Neptunium, Radium, and Technetium. Understanding Variation in Partition Coefficient, Kd, Values. R. G. Wilhelm, EPA**:** 188.

Kumaresan, M. and P. Riyazuddin (2001). "Overview of speciation chemistry of arsenic." Current Science **80**(7): 837-846.

Smedley, P. L. and D. G. Kinniburgh (2002). "A review of the source, behavior and distribution of arsenic in natural waters." Applied Geochemistry **17**: 517-568.

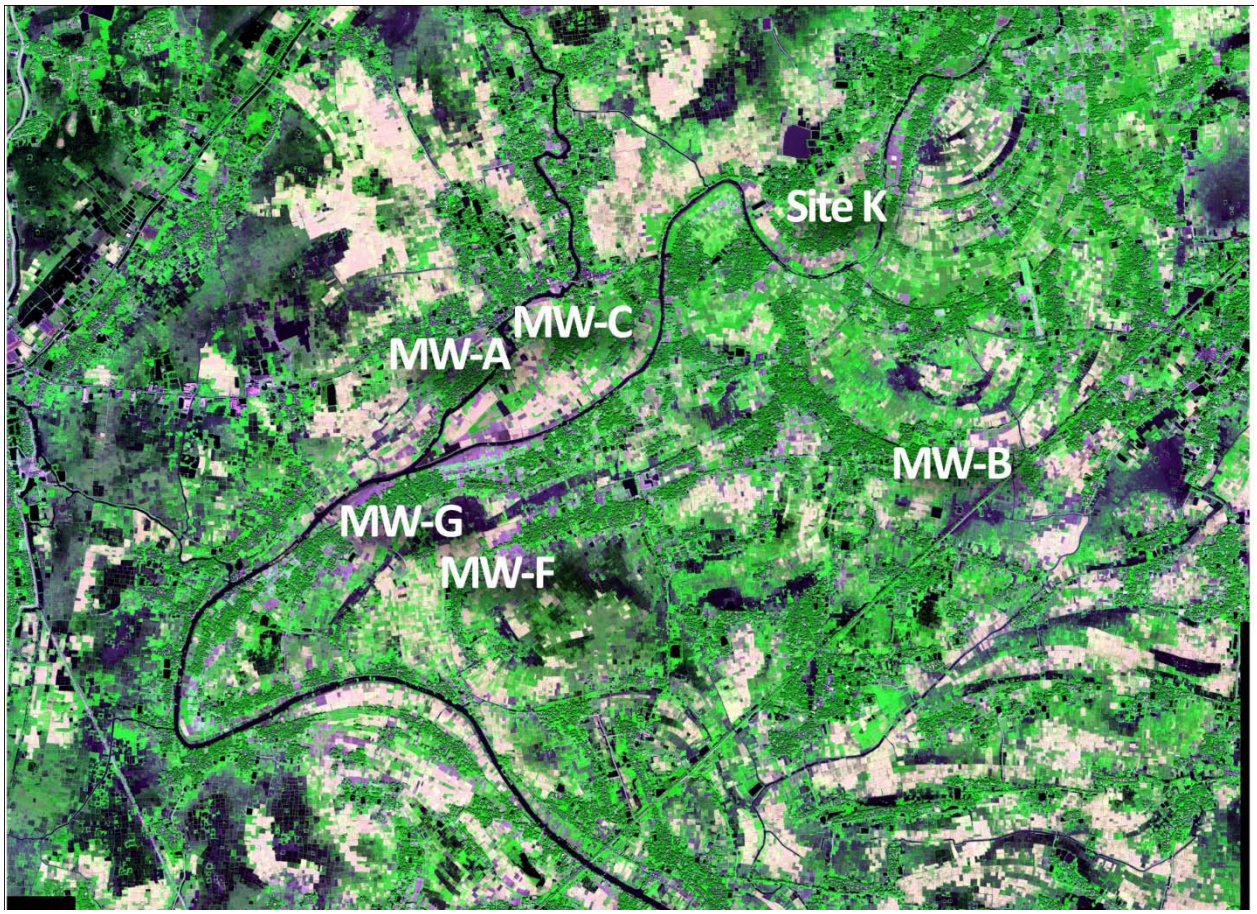

APPENDIX B. Map of Araihazar, Bangladesh showing the locations of multi-level wells monitored for geochemical profiles of the groundwater. The wells have been successively installed since ongoing studies by Lamont-Doherty Earth Observatory in collaboration with the University of Dhaka beginning in 2001, which has since then amassed some of the highest-resolution and comprehensive geochemical, epidemiological, and sociological studies to date on the state of arsenic in the region. The above figure was made using IKONOS satellite imagery, and studies highlighting the findings from MW-F and MW-G can be found in van Geen et al., Chemical Geology 2006; MW-A and MW-B in Zheng et al., Geochim. Cosmochim. Acta 2005; Site K in Radloff et al., Environ. Sci. Technol. 2007, and other multi-well data in Dhar et al., J. of Contaminant Hydrology, 2008 and Cheng et al., Environ. Sci. Technol. 2005.

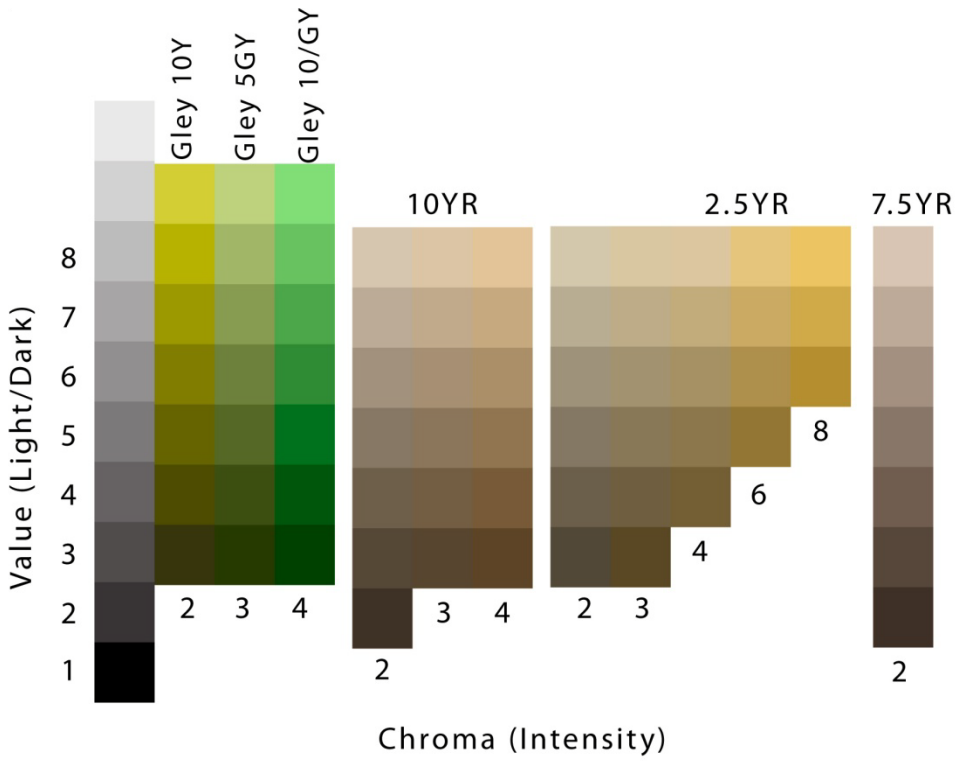

	520 nm	*530 nm*	*ΔR*	*Red*	*Green*	*Blue*
520 nm	1.00					
530 nm	0.99	1.00				
ΔR	0.29	0.42	1.00			
R	0.76	0.81	0.66	1.00		
G	0.96	0.98	0.49	0.81	1.00	
B	0.72	0.72	0.33	0.74	0.71	1.00

Appendix C. An RBG color conversion of Munsell Soil colors used to characterize aquifer sediments during bore and rotary drillings in Nepal and Vietnam. Colors, values and chromas were converted into RGB color space using WallkillColor conversion tables. The correlation table shows higher values of ΔR corresponding to the "redness" of sediments, which can be used to infer aquifer redox conditions--the more red and reflective, the more the sediment is oxic. Further information about sediments, mineralogy, and Munsell colors can be found at http://urbanext.illinois.edu/soil/less_pln/color/color.htm and http://pubs.usgs.gov/of/2006/1195/htmldocs/munsellcode.htm

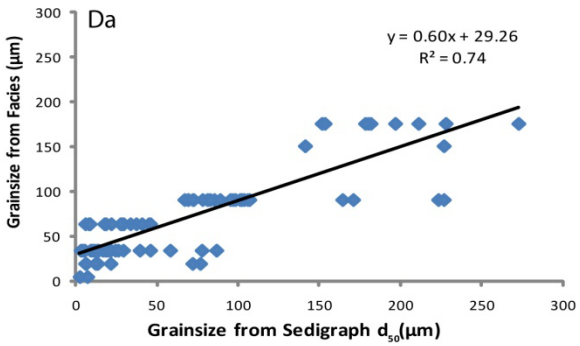

Supplemental Da (left). Plot showing how bulk grainsize estimates from Araihazar surface sediment augers (Weinman et al., 2008) correspond to measurements on the same samples using a Sedigraph particle size analyzer. Facies observations were listed while augering as "clay, fine silt, silt, course silt, very fine sand, and fine sand," and converted to an average grainsize using the Wentworth size scale: 4, 18.75, 33.5, 63, 90, and 175 mm," respectively. The grainsizes observed in the field correspond well to the quantitative measurents, with a bias towards qualifying facies finer than the analytical measurements.

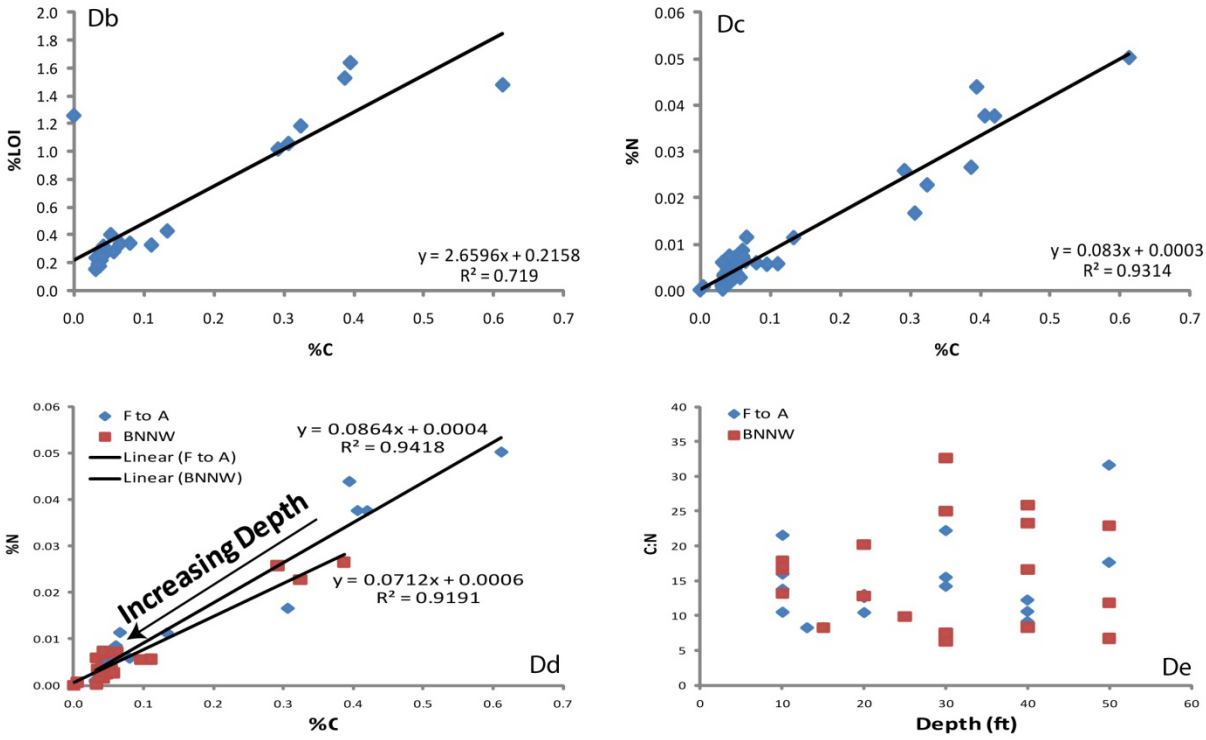

Supplemental 4Db-e (above): graphs showing results from the C and N analysis on aquifer sediment from two high-resolution needle-sample transects in Araihazar, Bangladesh. Figure Db shows the linear relation between organic carbon content measured by combustion (LOI) and CHN analysis. Figure Dc is the relation of weight percent C versus N for all the samples. Figure Dd plots C versus N for the two separate needle-sample transects: F to A are samples from the 400 yr. old modern river area, while BNNW are samples from the 1000 yr. old meander. Samples from deeper depths tend to have less C and N (Dd), and more a range in C:N ratio (De).

APPENDIX E

Comparison of As with Cr and Na in the Column Experiments

Arsenic and Chromium

Here, I was asked to compare arsenic with chromium in the weathering columns because, like arsenic, chromium is another 2 valence-state trace element of natural waters [Cr(III) and Cr(VI)]. The presence of Cr in the sediment was found in several, but not all of the Parasi (Nepal) samples, measured by x-ray fluorescence at Middle Tennessee State University. Aquifer samples with solid Cr had concentrations between 10-400 ppm, while some of the meta-siliclastic "source" rocks sampled from the Siwaliks while driving from Kathmandu to Butwal had Cr ranging from 100-850 ppm. The shales and slates typically had the highest Cr (i.e., Benigat shales and fossiliferous shale varieties). The higher concentrations of Cr in these more reducing Siwalik rocks sense, since the reduced form of Cr is less typically less chemically mobile.

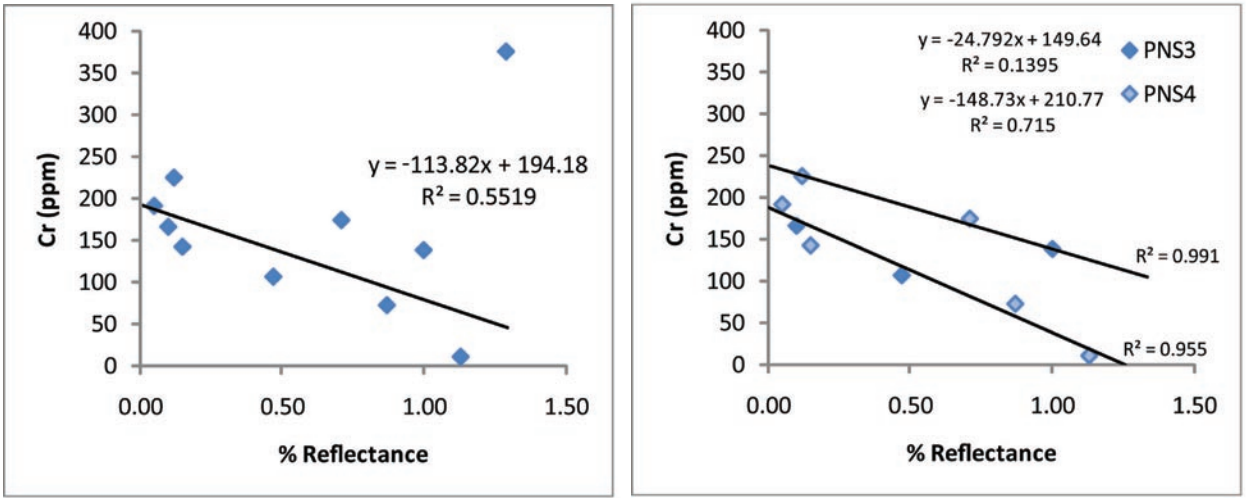

Figure 1. Graphs of chromium as a function of percent reflectance in the aquifer sediments of Parasi, Nepal. The left graph plots all of the Cr-reflectance data, and the right graph distinguishes the data by needle-sample (PNS3 or PNS4). While there is less of a trend when grouped as a whole or grouped by needle-sample, the data groups into two trend lines with a highly significant correlation (R^2 0.955, p=0.0008) for the lower trend line. Despite the good correlation of the upper trend line (R^2 0.991), the relationship is just shy of being significant, with a p-value of 0.06 on the x-variable. The one outlier of the group, with high reflectance and Cr is the only surface soil sample, indicating a Cr content possibly higher than expected due to human pollution.

Higher solid-Cr in more reductive environments is also supported by higher Cr in less reflective aquifer sediments (see Figure 1, above). The graphs plot the Cr results with percent reflectance, with reflectance being a proxy for the sedimentary redox condition—the more reflective and the more

orange/red, the more oxic the sediment. With the graphs showing Cr decreasing as reflectance increases, the trend line supports a scenario where Cr(III) is probably mobilized as Cr(VI) and lost under more oxidizing conditions.

With chromium being more mobile in its oxidized form [Cr(VI)], and arsenic more mobile in its reducing form [As(III)], concentrations in the column effluent should tend towards a negative correlation. Plots of effluent arsenic and chromium concentrations show no clear trend (Figure 2a), however, until the scatter is considered in regard to sampling time (Figure 2b) and column (Figure 2c).

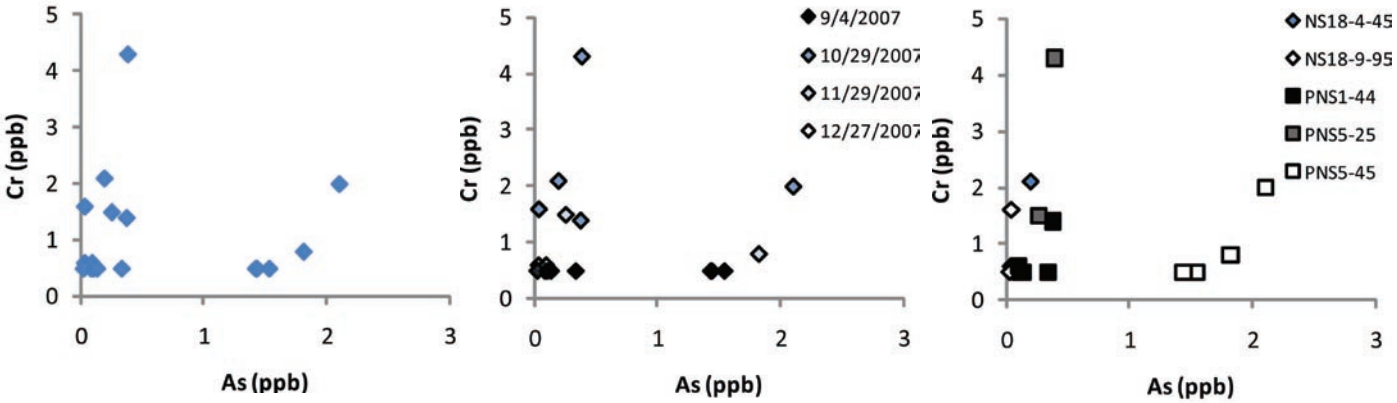

Figures 2a-c, graphs plotting chromium and arsenic concentrations from the column effluents. Graph 2a, (the rightmost graph), plots all the data; 2b (the middle graph), plots the data by sampling time; and 2c (the leftmost graph), plots the data by column.

Looking at the release of arsenic and chromium with regard to sampling time (Figure 2b), there is a peak release of Cr during the mid-sampling time of the experiment. Initial Cr concentrations start low, measuring below the detection limit (<0.5 ppm), and then increase over the next two months of sampling (1-4 ppm at 60-90 days of flow). At the end of the sampling period, Cr concentrations returned to non-detectable levels in the effluent. This lag-peak-lag behavior of Cr could suggest liberation of Cr from certain, more labile phases within the sediments that are prone to oxidization—currently, it is unclear, however, the exact phase Cr is in (perhaps future XAFS work could be done here).

Graphed by column, the relationship between As and Cr amid the scatter is a little more apparent, with more of a proportional relationship than expected—the slopes of Cr:As are all positive, which is in contrast to the inverse trend hypothesized from redox-sensitive mobilization. Again, this is because arsenic is typically released when the environment is reducing, while chromium favors more highly oxic mobilization. The fact that Cr and As release follows positive trend lines for each column is surprising in this regard, and most likely explainable by some Cr in the sediment's labile FeOOH structure. Studies have shown that Cr can coexist in the Fe-oxide structure as $FeCrO_3$ (or possibly some other Fe-Cr-oxyhydroxide), with Cr(III) having similar a coordination and charge/radius ratio as Fe(III) ($q/r \approx 0.4$). Like FeOOH, $FeCrO_3$ is similarly reducible (Massoth and Scarpiello 1971), meaning that, like iron-oxyhydroxides, which are agreed to be the major phase controlling the release of arsenic (Nickson,

Sengupta et al. 2007), iron-chromium oxides can undergo reductive dissolution. This means that the Cr behavior observed in the columns can likely be explained by the destabilization of labile Fe-oxyhydroxide phases at the two-three month-mark of leaching. So, rather than Cr having an inverse relationship, Cr release initially follows a similar reductive dissolution of labile Fe-phases in the aquifer sediment.

Arsenic and Sodium

A comment was made to plot sodium and arsenic together to see if a Na-based weathering proxy (like (White 2003)) is an appropriate assessor for As release in the column experiments. Before comparing the data, it's important to point out that the use of Na as a weathering proxy was not (and should not be) expected to be stoichiometric with the release arsenic. In other words, the geochemical behaviors of the Na and As pretty much preclude an a priori assumption that the two elements will weather similarly. Unlike sodium's aqueous form and activity, arsenic is redox-sensitive oxyanion,

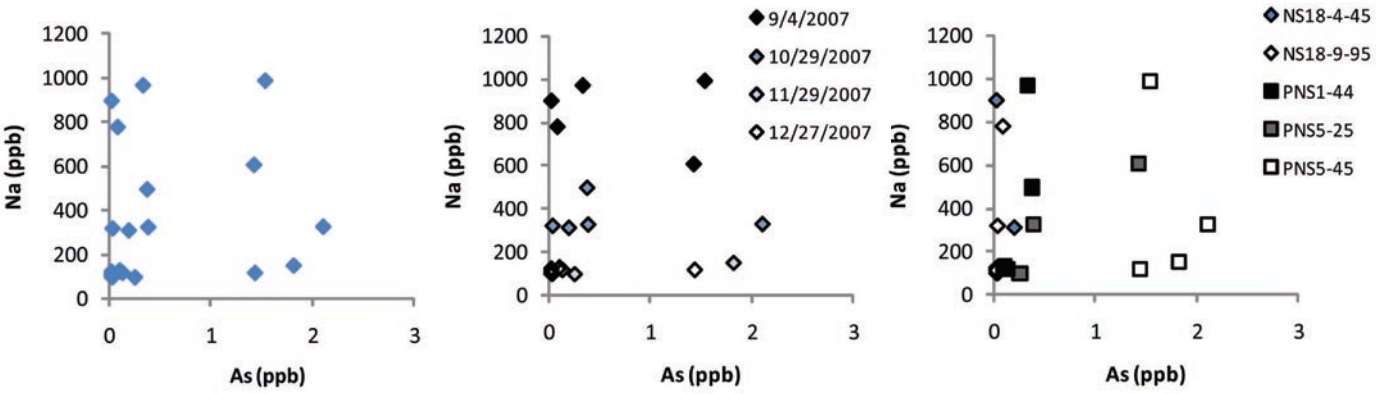

Figure 3, correlations of arsenic and sodium in the column effluents. The left panel, 3a, shows all the data, while the middle (3b) and rightmost panel (3c) show the data differentiated by sampling time (3b) and individual columns (3c).

which does not necessarily behave conservatively (Smedley and Kinniburgh 2002). So, while we can use a Na-based weathering proxy to infer weathering, the idea of the column experiments was to test whether different aged sediments had different rates of weathering. The weathering rates from Na could then be used to infer something about weathering in the field, particularly if older sands weathered slower than newer portions of the aquifer. If so, then future work could be designed to confirm if this is true and better target the exact release mechanisms of As in the field—for instance, in situ measurements of Sr and U isotopes (Maher, DePaolo et al. 2006) could be used to infer very local conditions of weathering and flow, which would help confirm or disprove if a difference of in-situ weathering rates contributes to the heterogeneity of arsenic.

So, again, Na was not chosen to specifically target the release of arsenic, per se, as much as it was chosen as an assessor of over-all aquifer weathering—these could be two different things. In looking at the correlations in Figure 3 above, Na diminishes in the effluent over time, while there is no

obvious decreasing trend in arsenic (3b). There is a little bit more of a correlation when plotted by column (3c), especially for effluent collected on and after October (3c). The individual columns have a bit more linearity between Na and As, indicating a possibility for arsenic weathering. This is further supported by the good correlations between Si and As in the effluent, which also suggests that arsenic accumulation and heterogeneity is controlled by different sedimentological potentials for aquifer weathering. Again, this is how and why arsenic heterogeneity can be primarily controlled by aquifer sedimentology.

References

Maher, K., D. J. DePaolo, et al. (2006). "U-Sr isotopic speedometer: Fluid flow and chemical weathering rates in aquifers." Geochimica Et Cosmochimica Acta 70(17): 4417-4435.

Massoth, F. E. and D. A. Scarpiello (1971). "Catalyst characterization studies on the Zn---Cr---Fe oxide system." Journal of Catalysis 21(3): 294-302.

Nickson, R., C. Sengupta, et al. (2007). "Current knowledge on the distribution of arsenic in groundwater in five states of India." Journal of Environmental Science and Health Part a-Toxic/Hazardous Substances & Environmental Engineering 42: 1707-1718.

Smedley, P. L. and D. G. Kinniburgh (2002). "A review of the source, behavior and distribution of arsenic in natural waters." Applied Geochemistry 17: 517-568.

White, A. F., and S.L. Brantley (2003). "The effect of time on the weathering of silicate minerals: why do weathering rates differ in the laboratory and the field?" Chemical Geology 202: 479-506.

[i] This work is in concert with LDEO, EAWAG, PRL, and Univ.'s of Karlsruhe and Grenoble collaborators

[ii] http://web.utk.edu/~anthrop/utcag/14c_dating.html